STUDIA UNIVERSITATIS
BABEŞ-BOLYAI

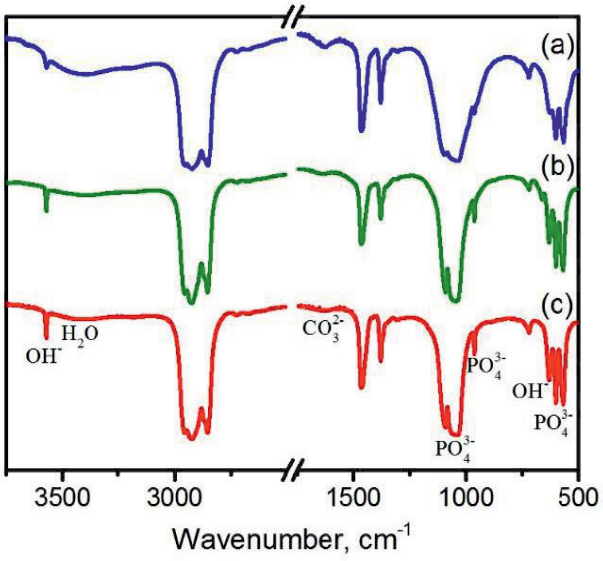

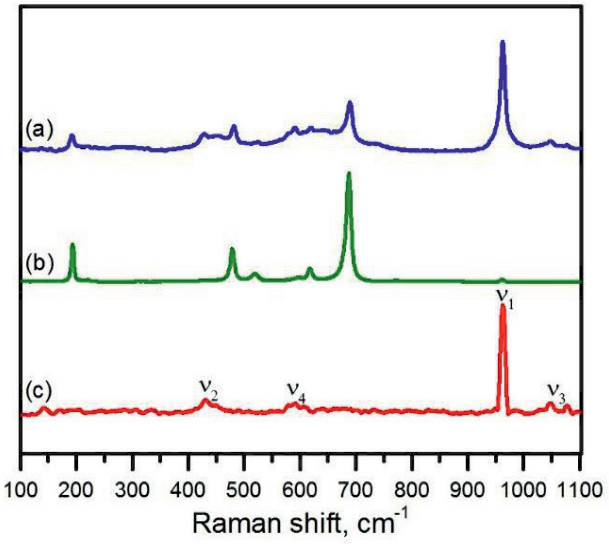

CHEMIA

1/2018

STUDIA
UNIVERSITATIS BABEŞ-BOLYAI

CHEMIA

1/2018

http://chem.ubbcluj.ro/~studiachemia/; studiachemia@chem.ubbcluj.ro
http://www.studia.ubbcluj.ro/serii/chemia/index_en.html

YEAR **Volume 63 (LXIII) 2018**
MONTH **MARCH**
ISSUE **1**

S T U D I A
UNIVERSITATIS BABEŞ–BOLYAI
CHEMIA

1

ISSUE DOI:10.24193/subbchem.2018.1

STUDIA UBB EDITORIAL OFFICE: B.P. Hasdeu no. 51, 400371 Cluj-Napoca, Romania, Phone + 40 264 405352

CUPRINS – CONTENT – SOMMAIRE – INHALT

Studia Universitatis Babes-Bolyai Chemia has been selected for coverage in Thomson Reuters products and custom information services. Beginning with V. 53 (1) 2008, this publication is indexed and abstracted in the following:

- Science Citation Index Expanded (also known as SciSearch®)
- Chemistry Citation Index®
- Journal Citation Reports/Science Edition

STUDIA UBB CHEMIA, LXIII, 1, 2018 (p. 7-20)
(RECOMMENDED CITATION)
DOI:10.24193/subbchem.2018.1.01

HETEROLOGOUS EXPRESSION AND PURIFICATION OF RECOMBINANT CROTOXIN B, THE PHOSPHOLIPASE A2 SUBUNIT OF CROTOXIN

FRANCISC-ANDREI BODA[a], PÁL SALAMON[b], CSONGOR ORBÁN[b], LAVINIA BERTA[a], AUGUSTIN CURTICĂPEAN[a], ȘERBAN-ANDREI GÂZ[a*], MARIA DOGARU[a]

ABSTRACT. Crotoxin is a heterodimeric β-neurotoxin isolated from the venom of *Crotalus durissus terrificus*, consisting of two, non-covalently bound subunits, crotapotin (CA) and crotoxin B (CB). Both subunits present four different isoforms, consequently there are up to 16 different crotoxin complexes, each with different activity levels. The biological activities usually associated with crotoxin include neurotoxicity, myotoxicity and cardiotoxicity, however several other important biochemical and pharmacological effects of crotoxin have been observed, such as the antibacterial, antiviral, anti-inflammatory, antitumoral and analgesic activity. In this study we present the production of recombinant crotoxin B (isoform C). Expression of the protein was carried out using *E. coli Rosetta^{TM} (DE3)pLysS* strain, and the obtained protein was separated and purified using Ni^{2+}-affinity chromatography. To the best of our knowledge the developed method represents the first reported method for obtaining the crotoxin B (isoform C) through heterologous expression using an efficient and cost-effective procedure.

Keywords: *Crotoxin, neurotoxin, phospholipase A2, heterologous expression*

INTRODUCTION

Crotoxin (CTX) is a highly potent β-neurotoxin representing the main toxic component of *Crotalus durissus terrificus* (South American rattlesnake) venom. Crotoxin was the first protein isolated and crystallized from animal venom [1,2].

[a] *University of Medicine and Pharmacy Tirgu Mureș, Faculty of Pharmacy, 38 Gh. Marinescu str. RO-540139, Tîrgu Mureș, Romania.*
[b] *Sapientia Hungarian University of Transylvania, Faculty of Economics, Socio-Human Sciences and Engineering, Department of Bioengineering, 1 Libertatii Square, RO-530104, Miercurea Ciuc, Romania.*
[*] *Corresponding author: andrei.gaz@umftgm.ro*

Crotoxin is a heterodimeric protein that consists of a non-toxic, non-enzymatic, acidic subunit (crotapotin, crotoxin A, CA) non-covalently associated with a weakly toxic, basic subunit (crotoxin B, CB) that expresses phospholipase A_2 activity. The CA subunit acts as a chaperone protein, potentiating the toxicity of the CB subunit [1,3]. Four different isoforms have been identified for each subunit, consequently the venom of *Crotalus durissus terrificus* contains up to 16 different crotoxin complexes, each presenting different activity levels [4,5].

The main biological activities associated with CTX include neurotoxicity, myotoxicity and cardiotoxicity. Along with these well-known activities, several other biochemical and pharmacological effects have been reported, some of them highlighting the potential pharmaceutical use of this protein. These effects include the antibacterial, antiviral, anti-inflammatory, antitumoral, and analgesic activities of CTX and its subunits (CA and CB) [1,2].

The neurotoxic effect of CTX is exerted mainly at the presynaptic level of the neuromuscular junctions, and is caused by inhibition of acetylcholine release [6]. Furthermore, a postsynaptic effect exerted on acetylcholine receptors which are stabilised in a desensitized form by CTX has also been observed [1,7]. The myotoxicity of CTX can be characterized as a systematic and generally irreversible damage caused to skeletal muscles. The systemic myotoxicity caused by CTX is accompanied by an increase in plasma creatine-kinase and myoglobinuria, which often leads to acute renal failure [8–10]. Studies regarding the cardiotoxic effect of CTX showed that it induces a significant decrease in the contractile force of the heart, and causes an increase in creatine-kinase activity [11]. Later studies demonstrated that CTX potentiates L-type Ca^{2+} currents in cardiomyocytes, and also alters significantly the ultrastructure of the cardiac autonomic nervous system [12,13].

The antibacterial effect of CTX and its CB subunit has been demonstrated against several bacterial strains, such as *Burkholderia pseudomallei, Enterobacter aerogenes, Escherichia coli, Pseudomonas aeruginosa, Staphylococcus aureus,* and *Xanthomonas axonopodis pv. passiflorae* [14–16]. The chemical modification of the CB subunit did not influence its antibacterial activity on *E. coli*, suggesting that this effect is not linked with the enzymatic activity of the protein, as other molecular mechanisms might be involved in the bacterial membrane disruption [17]. In a different study, CTX and the CB subunit showed antiviral activity against dengue and yellow fever viruses, possibly by disrupting the virus lipid bilayer envelope [18,19].

Another study has shown that the CTX is able to influence the immune and inflammatory responses by inhibiting macrophage spreading and phagocytic activities [20], by reducing the number of lymphocytes in blood and lymph and promoting leukocyte adherence to endothelial cells,

possibly through the involvement of lipoxygenase-derived mediators [21]. Similar effects have been observed with the CB subunit, but not with the CA subunit [22].

The antitumoral activity of CTX has been demonstrated in both *in vitro* and *in vivo* studies. CTX was found to be effective *in vitro* against mammary ductal carcinoma, glioblastoma and lung adenocarcinoma cells [23], but also showed promising results when used *in vivo* against different forms of advanced cancer [24,25]. A more recent study suggests that autophagy and apoptotic mechanisms might be involved in the cytotoxic effects of crotoxin [26].

Several studies have been conducted to demonstrate the analgesic effect of CTX. The results of these studies showed that CTX induces analgesia by a direct action, presumably by activating the central muscarinic receptors, along with central serotonergic and noradrenergic receptors. Eicosanoids derived from the lipoxygenase pathway have also been observed to mediate the analgesic effect of CTX, which indicates that the PLA_2 activity of the protein is also important in the exertion of this effect [27,28].

Considering the various pharmacological effects and possible therapeutic applications of CTX and its CB subunit, our aim was the development of a simple and cost-effective method for obtaining the pure CB subunit. The first step consisted of the heterologous expression of the recombinant CB (isoform C), followed by the separation and purification of the obtained protein.

RESULTS AND DISCUSSION

Assembly of the CB_pET-30b(+) vector

The expression vector was obtained by inserting the coding sequence of CB (isoform C) into the pET-30b(+) vector using the NotI and HindIII restriction sites resulting in the restriction map of the designed vector (Figure 1).

The CB_pET-30b(+) vector was designed and assembled to be compatible with the chosen prokaryotic host cells (*E. coli Rosetta™ (DE3)pLysS*) and the methods used for protein separation. The selection of host cells was based on experiments in which these cells proved to be adequate for synthesis of proteins of vegetal [29], animal [30] or human origin [31]. The planned separation method for the recombinant protein was based on Ni^{2+}-affinity, thus a 6xHis-tag was added to the coding sequence of CB (isoform C).

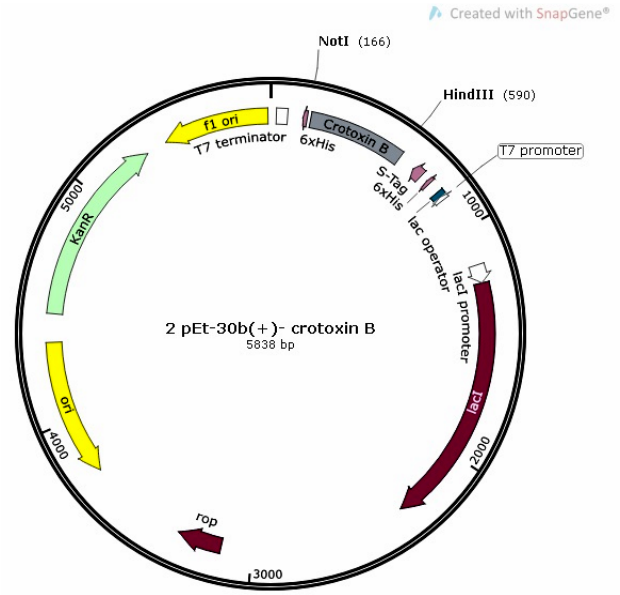

Figure 1. Restriction map of CB_pET- 30b(+) expression plasmid, outlining the significant elements of the vector (Map created in SnapGene® 1.1.3.)

Transformation of competent cells and colony PCR

The CB_pET-30b(+) vector was transformed into chemically competent *Rosetta™ (DE3)pLysS* cells, plated on Luria-Bertani (LB) agar plates containing 50 µg/ml kanamycin and incubated overnight at 37°C. After colony formation, the presence of the plasmid and plasmid insert in the selected bacterial colony was confirmed by colony PCR (Figure 2).

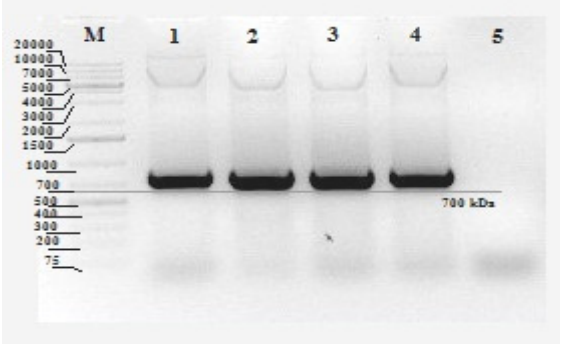

Figure 2. Agarose gel showing the DNA fragments obtained after colony PCR of samples taken from four individual bacterial colony. (M) – 1 kb Plus DNA Ladder (Thermo Scientific); (1-4) – PCR product of transformed *E. coli Rosetta*™ bacterial colonies; (5) – Reaction mixture without added sample (negative control)

Method optimisation for protein expression

The effect of incubation temperature and isopropyl β-D-1-thiogalactopyranoside (IPTG) concentration on protein expression has been determined using transformed bacterial strains inoculated in LB broth containing kanamycin at a concentration of 50 μg/ml. The protein expression has been observed at 30 °C, respectively at 37 °C. For induction we have used 0.01 mM, 0.5 mM or 1.0 mM IPTG.

Biomass levels have been determined during incubation, by measuring the optical density at 600 nm (OD_{600}). The bacterial growth curves for each condition used are presented in Figure 3.

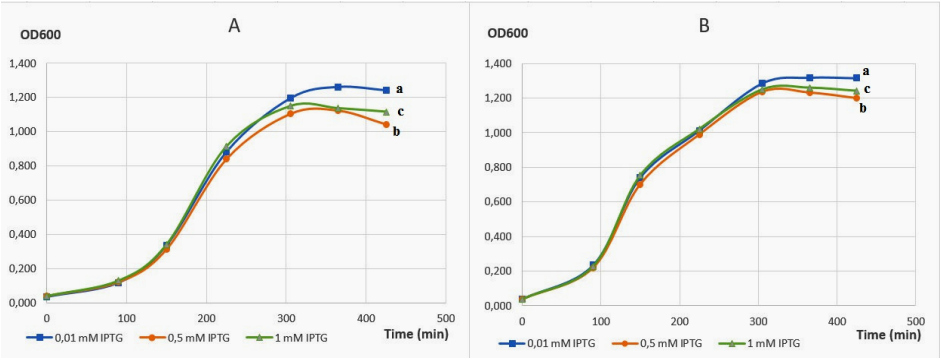

Figure 3. Bacterial growth curves obtained during method optimisation. (A) - Samples incubated at 30 °C, (B) – Samples incubated at 37 °C. (a) – 0.01 mM IPTG, (b) – 0.5 mM IPTG, (c) – 1.0 mM IPTG used for induction.

Protein expression has been assessed by SDS-PAGE analysis of samples taken hourly after induction, for each experimental condition (Figure 4 and Figure 5). The presence of CB (isoform C, 15.9 kDa) was confirmed by visible bands at approximately 16 kDa. Based on the visual examination of these bands, it was concluded that neither the temperature, nor the IPTG concentration have a significant influence on the yield of the protein expression. However, the distortion of the bands corresponding to CB (isoform C) at 3 hours post-induction, suggested that an additional conformational change might take place in the structure of the protein after a prolonged induction.

Based on the obtained results, it was concluded that an optimal biomass level can be obtained at 37°C when the protein expression was induced with 0.5 mM IPTG, and induction time was limited to two hours to prevent possible modifications in the protein structure. Using these parameters, an optimised expression process was conducted, and the presence of the protein confirmed through SDS-PAGE analysis (Figure 6). The obtained cell culture was subsequently used for the optimization of the purification method.

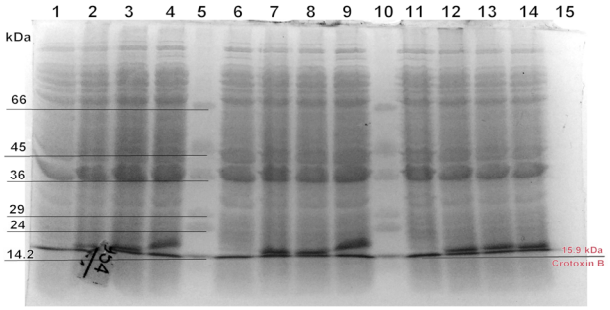

Figure 4. SDS-PAGE gel analysis of samples taken from cell cultures incubated at 30 °C, before and after induction with different concentrations of IPTG. (1) – Before induction, (2-4) – 60, 120, 180 min after induction with 0.01 mM IPTG; (6) – Before induction, (7-9) – 60, 120, 180 min after induction with 0.5 mM IPTG; (11) – Before induction, (12-14) – 60, 120, 180 min after induction with 1.0 mM IPTG; (5),(10) – Molecular Weight Marker 14-66 kDa (Sigma-Aldrich).

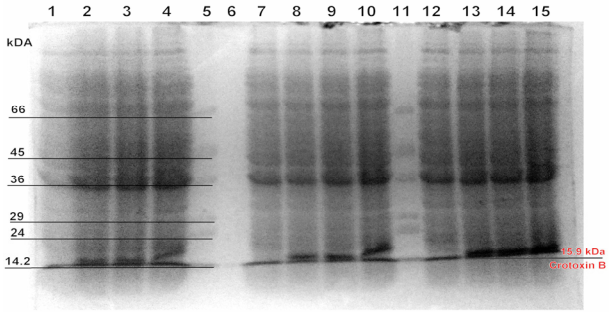

Figure 5. SDS-PAGE gel analysis of samples taken from cell cultures incubated at 37 °C, before and after induction with different concentrations of IPTG. (1) – Before induction, (2-4) – 60, 120, 180 min after induction with 0.01 mM IPTG; (7) – Before induction, (8-10) – 60, 120, 180 min after induction with 0.5 mM IPTG; (12) – Before induction, (13-15) – 60, 120, 180 min after induction with 1.0 mM IPTG; (5), (10) – Molecular Weight Marker 14-66 kDa (Sigma-Aldrich).

Batch purification of recombinant Crotoxin B

To obtain a purified CB (isoform C) solution a single-step separation approach was used, using Ni-affinity chromatography. Separation of the protein was accomplished using two different buffer systems (tris(hydroxymethyl)aminomethane (Tris) and 4-(2-hydroxyethyl)-1-piperazineethanesulfonic acid (HEPES)). Theoretical isoelectric point (pI) of the protein was computed using *Expasy ProtParam* and determined to be 8.74. The purification was carried out at pH=7.6 to allow at least one pH unit difference between the pI of CB and the pH of the solutions. After the Ni-NTA chromatographic step, the protein purity has been verified by SDS-PAGE analysis (Figure 6 and Figure 7).

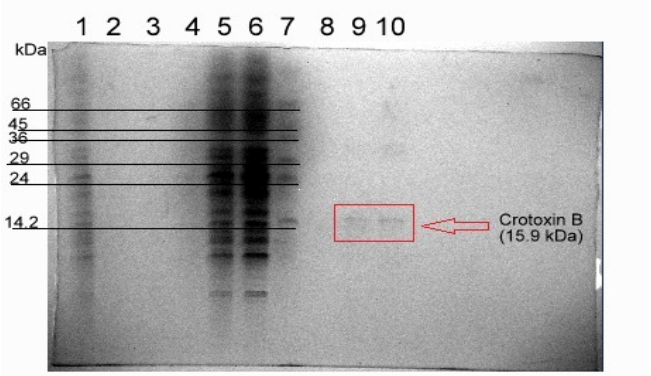

Figure 6. SDS-PAGE gel analysis of samples taken from cell cultures incubated using the optimal conditions (37°C, 0.5 mM IPTG concentration) and the affinity chromatography purification of the recombinant protein using Tris-HCl buffer (pH=7.6). (1) – 120 min after induction; (2) – 60 min after induction; (3) – before induction; (4) - Molecular Weight Marker 14-66 kDa (Sigma-Aldrich), (5) – elution fraction 1, (6) – elution fraction 2, (7) – elution fraction 3.

Using Tris-HCl the desired protein was not selectively separated on Ni-NTA resin column (it was bonded on the stationary phase along with other proteins). On the other hand, changing the Tris-HCl with HEPES buffer a better selectivity for the separation of the protein was achieved. However, we have noticed that the CB (isoform C) was eluted in two separated fractions (2 and 3) increasing the total volume and decreasing the concentration of the final solution.

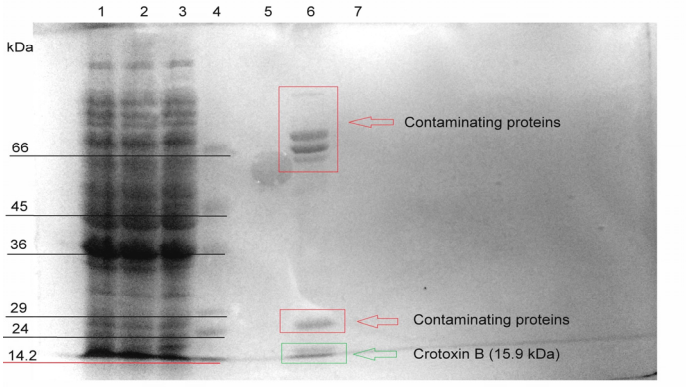

Figure 7. Tricine-SDS-PAGE gel analysis of affinity chromatography purification of the recombinant protein using HEPES buffer (pH=7.6). (1-4) – washing (I) fraction 1-4; (5-6) – washing (II) fraction 1-2; (7) - Molecular Weight Marker 14-66 kDa (Sigma-Aldrich); (8) – elution fraction 1; (9) – elution fraction 2; (10) – elution fraction 3.

The separation method was further optimized by using a HEPES buffer at pH=8.0, purification results are shown in Figure 8. As our results confirm, the target protein was specifically bound by the Ni-NTA resin. Furthermore, the complete amount of CB was eluted in a single fraction, thus slightly increasing the concentration of the solution.

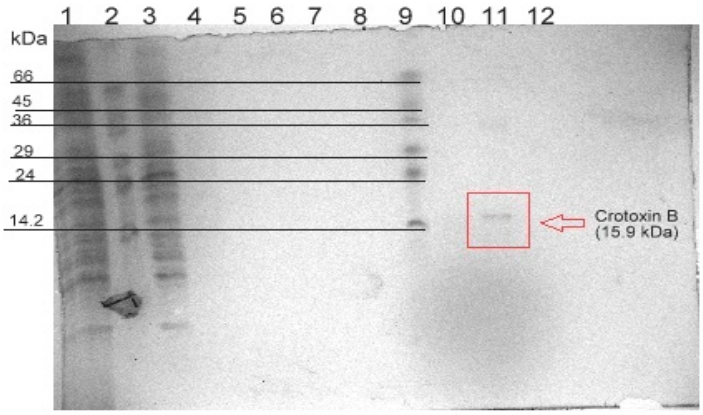

Figure 8. Tricine-SDS-PAGE gel analysis of affinity chromatography purification of the recombinant protein using HEPES buffer (pH=8.0). (1) – flow-through; (2)(9) – Molecular Weight Marker 14-66 kDa (Sigma-Aldrich); (3-6) – washing (I) fraction 1-4; (7)(8) -empty lanes; (10) – elution fraction 1; (11) – elution fraction 2; (12) – elution fraction 3.

CONCLUSIONS

Based on the available coding sequence of CB (isoform C), we have successfully managed to design an experimental protocol for expressing, separation and purification of Crotoxin B using CB_pET-30b(+) vector. The recombinant vector was used to transform the *Rosetta™ (DE3)pLysS* expression cells, and the recombinant protein was successfully obtained in the following optimized conditions: incubation at 37 °C and 250 rpm until optimal optical density of the cell culture was reached, and induction with 0.5 mM IPTG concentration, followed by two hours of effective protein expression.

Using different buffer systems and optimized pH conditions, the purification of the target recombinant protein was achieved through a single-step Ni^{2+}-affinity chromatographic method.

To the best of our knowledge this is the first literature reported method for heterologous expression of the crotoxin B. Furthermore, the protein can be used as positive control for further pharmacological studies being an elegant method for expressing large-scale quantities of crotoxin B.

EXPERIMENTAL SECTION

Plasmids and bacterial strains

The coding sequence of CB (isoform C) obtained from the National Center for Biotechnology Information (NCBI) database (GenBank: X12603.1) was used as a reference. The cloning and expression of the recombinant CB (isoform C) was carried out using a pET-30b(+) vector, which contains and operates using the bacteriophage T7 promoter. The cloning of the coding sequence and the subcloning of the sequence in the pET-30b(+) vector was performed by Genscript USA Inc, using the NotI-HindIII restriction sites.

Protein expression was conducted using *Rosetta™ (DE3)pLysS* cells, genotype F^- *ompT hsdS*$_B$(r_B^- m_B^-) *gal dcm* (DE3) pLysSRARE (Cam^R), which work as a protease deficient expression host.

Transformation of competent cells

The lyophilised CB_pET-30b(+) plasmid was dissolved in nuclease-free water to obtain a solution with a final concentration of 100 ng/µl. 5 µl of the plasmid solution was added to 100 µl *Rosetta™ (DE3)pLysS* competent cells. The resulting suspension was placed on ice for 15 minutes, heat shocked for two minutes at 42 °C, then put again on ice for 5 minutes. LB broth was added to the suspension up to a final volume of 1000 µl, followed by incubation at 37°C and 250 rpm for one hour (Biosan TS-100 Thermo Shaker). The obtained cell cultures were plated on LB agar plates containing 50 µg/ml kanamycin and incubated overnight at 37 °C.

A single colony was selected and inoculated in 3 ml LB broth containing kanamycin 50 µg/ml and incubated at 37 °C and 250 rpm (Biosan Orbital Shaker-Incubator ES-20), until OD_{600} reached a value of 0.5-0.6, which indicated the logarithmic growth phase of the cells. Glycerol stock was prepared from the cell culture and stored at -80 °C for subsequent use.

Colony PCR

The composition of the PCR reaction mixture used for colony PCR is presented in Table 1. To each cold PCR tube containing the reaction mixture a small amount of the selected bacterial colony was added.

Amplification of the DNA was accomplished using a SureCycler 8800 PCR (Agilent Technologies) and the PCR program shown in Table 2. The obtained DNA fragments were separated using a 1 % agarose gel, and the bands were visualised using a Bio-Rad Gel Doc XR System under UV light (λ = 312 nm).

Table 1. Composition of the PCR reaction mixture

Component	Volume
Sterile distilled water	28 µl
10X PCR buffer (500 mM KCl, 100 mM Tris-HCl (pH=9,0), 1.0 % Triton X-100)	5 µl
$MgCl_2$ (25 mM)	3 µl
dNTPs (10 mM each dATP, dTTP, dGTP, dCTP)	3 µl
Forward primer (T7 promoter) (20 µM)	5 µl
Reverse primer (T7 terminator) (20 µM)	5 µl
Taq polymerase	1 µl
Total volume	50 µl

Table 2. Program used for colony PCR

Step	Temperature	Time	Number of cycles
Initial denaturation	95 °C	5 min	1
Denaturation	95 °C	1 min	35
Primer annealing	54 °C	1 min 30 sec	
Extension	72 °C	1 min	
Final extension	72 °C	5 min	1

Method optimisation

A cell culture with an approximate OD_{600} value of 0.04 was prepared and equally divided in flasks. The flasks, each containing 100 ml cell culture, were incubated at 30 °C or 37 °C and 250 rpm. OD_{600} value was measured (Zuzi spectrophotometer 4201/50) from samples taken from each flask until the target value of 0.8-1.0 was reached.

Protein expression was induced using 0.01 mM, 0.5 mM or 1.0 mM IPTG solution in both temperature ranges (Table 3). The cultures were incubated for three more hours at 30 °C or 37 °C and 250 rpm. Samples for measuring OD_{600} and electrophoretic analysis were taken before induction and hourly after induction from each flask. Protein expression was halted three hours after induction by centrifuging the cell culture at 4500 rpm for 10 minutes (Hettich Mikro 22R Centrifuge).

Table 3. Distribution of samples based on conditions used for method optimisation

Samples*	IPTG concentration	Temperature
I	0.01 mM	30 °C
II	0.5 mM	
III	1.0 mM	
IV	0.01 mM	37 °C
V	0.5 mM	
VI	1.0 mM	

* All samples have been prepared in duplicate

Expression of recombinant Crotoxin B

100 µl of transformed cell culture containing the CB_pET-30b(+) vector was added to 10 ml LB broth containing 50 µg/ml kanamycin and incubated for four hours at 37 °C and 250 rpm. The obtained cell culture was then added to 1000 ml LB broth solution containing kanamycin 50 µg/ml and incubated at 37 °C and 250 rpm (Sartorius Certomat BS-T). OD_{600} was measured hourly, and the protein expression inducted with 0.5 mM IPTG when OD_{600} value was in the range of 0.9-1.1.

For measuring OD_{600} and SDS-PAGE analysis samples were taken before induction at 1 h and 2 h after induction. Two hours after the induction with IPTG, the protein expression was stopped, separating the cell culture by centrifugation at 4500 rpm and 4 °C for 10 minutes. The obtained pellets were stored at -80 °C until further processing.

Cell lysis was performed by thawing the pellets and resuspending the cells in 25 ml lysis buffer (Table 4). In order to disrupt the cell structures and obtain a homogeneous solution the cell suspensions were sonicated (Dr. Hielscher UP200H sonicator) at 70 % amplitude for 12 minutes, in three-minute cycles with one-minute pause between the cycles, keeping the suspension on ice in order to prevent overheating and denaturation of proteins. The resulting cell extracts were centrifuged (Beckman Coulter Allegra 64R Centrifuge) at 19000 rpm and 4 °C for 50 minutes.

Table 4. Composition of lysis buffers used

Component	Tris buffer	HEPES buffer	
Tris	50 mM	-	
HEPES	-	50 mM	
NaCl	300 mM	300 mM	
DTT	2.0 mM	2.0 mM	
PMSF	1.0 mM	1.0 mM	
Triton X-100	1.0 %	1.0 %	
Imidazole	20 mM	20 mM	
Protease inhibitor	1 tablet	1 tablet	
pH	7.6	7.6	8.0

Batch purification of recombinant CB protein

Based on the 6xHis tag added to the protein, the purification was performed manually using Ni^{2+}-affinity chromatography at 4 °C. Separation and purification was carried out using Tris-HCl buffer (pH=7.6) and HEPES buffer (pH=7.6 and pH=8.0). The composition of buffer solutions is presented in Table 5.

Table 5. Composition of the washing and elution buffers used

Component	Tris-HCl buffer			HEPES buffer		
	Washing buffer (I)	Washing buffer (II)	Elution buffer	Washing buffer (I)	Washing buffer (II)	Elution buffer
Tris	-	50 mM	50 mM	-	-	-
HEPES	-	-	-	-	50 mM	50 mM
Na_2HPO_4	50 mM	-	-	50 mM	-	-
NaCl	500 mM	1 M	500 mM	500 mM	1 M	500 mM
DTT	2 mM	2 mM	2 mM	2 mM	2 mM	2 mM
Imidazole	40 mM	20 mM	400 mM	40 mM	20 mM	400 mM
Glycerol	-	-	5 %	-	-	5 %
pH	7.6			7.6 / 8.0		

The stationary phase (Ni-NTA resin) was equilibrated with washing buffer (I). Supernatant and 2 ml of HisPur Ni-NTA resin (Thermo Scientific) were mixed (Premiere Roll Mixer) for 60 minutes to allow the binding of the His-tag to the resin.

The suspension was added to an empty column, and the flow-through collected. The Ni^{2+}-NTA resin was washed with 4 x 2 ml washing buffer (I), 4 x 2 ml washing buffer (II) then eluted with 6 x 1.5 ml elution buffer. Each fraction from the washing and elution process was collected separately and analysed using SDS-PAGE for protein content.

SDS-PAGE analysis

Samples for SDS-PAGE analysis was prepared according to Laemmli [32]. Proteins were separated on either 15 % SDS-PAGE gels or 10 % tricine SDS-PAGE gels. SDS-PAGE gels were run using 90 V voltage for 15 minutes, followed by 120 V for 90 minutes (Bio-Rad PowerPac Basic). Tricine SDS-PAGE gels were run using 120 V for 90 minutes, on ice. The separated proteins were stained using Coomassie Brilliant Blue.

ACKNOWLEDGMENTS

The first author would like to thank to the Collegium Talentum 2017 Programme of Hungary for the scholarship support. This work was supported by the joint project of the Studium Prospero Foundation and the Hungarian Academy of Sciences (Contract No. 139/26.01.2017).

REFERENCES

1. G. Faure, D. Porowinska, F. Saul “Toxins and Drug Discovery”, Springer Nature, Dordrecht, **2017**, Part I, Chapter 1, p. 3.
2. S.C. Sampaio, S. Hyslop, M.R.M. Fontes, J. Prado-Franceschi, V.O. Zambelli, A.J. Magro, P. Brigatte, V.P. Gutierrez, Y. Cury, *Toxicon*, **2010**, *55*, 1045.
3. C.A.H. Fernandes, W.M. Pazin, M.R.M. Fontes *et al.*, *Scientific Reports,* **2017**, *7*, 43885.
4. L.A. Ponce-Soto, B. Lomonte, L. Rodriques-Simioni, J.C. Novello, S. Marangoni, *The Protein Journal,* **2007***, 26*, 221.
5. D.P. Marchi-Salvador, L.C. Corrêa, A.J. Magro, C.Z. Oliveira, A.M. Soares, M.R. Fontes, *Proteins*, **2008***, 72*, 883.
6. W. Cavalcante, E. Santos-Diz-Filho, M. Gallacci *et al.*, *Toxicology Letters***, 2007***, 172*, S226.
7. O.V. Brazil, M.D. Fontana, N.F. Heluany, *Journal of Natural Toxins,* **2000***, 9*, 33.
8. C. Montecucco, J.M. Gutierrez, B. Lomonte, *Cellular and Molecular Life Sciences*, **2008***, 65,* 2897.
9. T.F. Salvini, A.C. Amaral, E.H. Miyabara, J.A.O. Turri, P.M. Danella, H.S. Selistre de Araujo, *Toxicon,* **2001***, 39*, 1141.
10. J.M. Gutierrez, L.A. Ponce-Soto, S. Marangoni, B. Lomonte, *Toxicon,* **2008***, 51*, 80.
11. E.H. Myiabara, I.L. Baptista, B. Lomonte, H.S. Selistre-de-Araujo, J.M. Gutierrez, A.S. Moriscot, *Comparative Biochemistry and Physiology, Part C,* **2006***, 143*, 284.
12. M. Hernandez, H. Scannone, H.J. Finol, M.E. Pineda, I. Fernandez, A.M. Vargas, M.E. Giron, I. Aguilar, A. Rodriguez-Acosta, *Experimental and Toxicologic Pathology*, **2007***, 59*, 129.
13. P. Zhang, A.S. Lader, M.A. Etcheverry, H.F. Cantiello. *Toxicon*, **2010***, 55,* 1236.
14. D.G. Oliveira, M.H. Toyama, J.C. Novello, L.O.S. Beriam, S. Marangoni, *Journal of Protein Chemistry*, **2002***, 21*, 161.
15. R. Perumal Samy, A. Pachiappan, P. Gopalakrishnakone, M.M. Thwin, Y.E. Hian, V.T.K. Chow, H. Bow, J.T. Weng, *BMC Infectious Diseases*, **2006***, 6*, 100.
16. R. Perumal Samy, P. Gopalakrishnakone, M.M. Thwin, T.K.V. Chow, H. Bow, E.H. Yap, T.W.J. Thong, *Journal of Applied Microbiology*, **2007***, 102*, 650.
17. A.M. Soares, A.C. Mancin, A.L. Cecchini, E.C. Arantes, S.C. Franca, J.M. Gutierrez, J.R. Giglio, *International Journal of Biochemistry and Cell Biology*, **2001***, 33*, 877.
18. V.D.M. Muller, R.R. Russo, A.C.O. Cintra, M.A. Sartim, R.M. Alves-Paiva, L.T.M. Figueiredo, S.V. Sampaio, V.H. Aquino, *Toxicon,* **2012***, 59*, 507.
19. V.D. Muller, R.O. Soares, N.N. dos Santos-Junior, A.C. Trabuco, A.C. Cintra, L.T. Figueiredo, A. Caliri, S.V. Sampaio, V.H. Aquino, *PLoS ONE,* **2014***, 9*, e112351, 1.
20. S.C. Sampaio, A.C. Rangel-Santos, C.M. Peres, R. Curi, Y. Curi, *Toxicon,* **2005***, 45*, 671.
21. D.F. Cardoso, M. Lopes-Ferreira, E.L. Faquim-Mauro, M.S. Macedo, S.H.P. Farsky, *Mediators of Inflammation,* **2001***, 10*, 125.

22. V.O. Zambelli, S.C. Sampaio, L.S. Sudo-Hayashi, K. Greco, L.R.G. Britto, A.S. Alves, B.C. Zychar, L.R.C. Goncalves, D.D. Spaddaci-Morena, R. Otton, M.S. Della-Casa, R. Curi, Y. Cury, *Toxicon*, **2008***, 51*, 1357.
23. J. Wang, X. Qin, Z. Zhang, M. Chen, Y. Wang, B. Gao, *Molecular Medicine Report,* **2014***, 10*, 3009.
24. L.A. Calderon, J.C. Sobrinho, A.M. Soares *et al.*, *BioMed Research Internationl*, **2014***, 2014*, 203639, 1.
25. J.E. Cura, D.P. Blanzaco, C. Brisson, M.A. Cura, R. Cabrol, L. Larrateguy, C. Mendez, J.C. Sechi, J.S. Silveira, E. Theiller, A.R. de Roodt, J.C. Vidal, *Clinical Cancer Research*, **2002***, 8*, 1033.
26. C. Yan, Y. Yang, Z. Qin, Z. Gu, P. Reid, Z. Liang, *Acta Pharmacologica Sinica*, **2007***, 28*, 540.
27. F.S. Nogueira-Neto, R.L. Amorim, P. Brigatte, G. Picolo, W.A. Ferreira Jr., V.P. Gutierrez, I.M. Conceicao, M.S. Della-Casa, R.K. Takahira, J.L.M. Nicoletti, Y. Cury, *Pharmacology, Biochemistry and Behavior*, **2008***, 91*, 252.
28. Q. Zhu, D.C. Wu, X.P. Zhou, S. Gong, B.C. Cheng, Z.H. Qin, P.F. Reid, Q.Z. Yin, X.H. Jiang, *Toxicon,* **2008**, *51*, 102.
29. S. Wang, Y. Zhang, H. Liu, Y. He, J. Yan, Z. Wu, Y. Ding, *Applied Microbiology and Biotechnology*, **2012**, *96*, 939.
30. F. Bugli, R. Graffeo, F.P. Sterbini, R. Torelli, L. Masucci, M. Sali, A. Grasso, S. Rufini, E. Ricci, G. Fadda, M. Pescatori, *Toxicon,* **2008***, 51,* 547.
31. P. Salamon, I. Miklossy, B. Albert, M. Korodi, K. Nagy, I. Bakos, Sz. Lanyi, Cs. Orban, *Studia UBB Chemia*, **2017***, 62*, 333.
32. U.K. Laemmli, *Nature*, **1970***, 227*, 680.

STUDIA UBB CHEMIA, LXIII, 1, 2018 (p. 21-35)
(RECOMMENDED CITATION)
DOI:10.24193/subbchem.2018.1.02

SCREENING OF BIOACTIVE COMPOUNDS SYNTHESIZED BY MICROALGAE: A PROGRESS OVERVIEW ON EXTRACTION AND CHEMICAL ANALYSIS

D. PATRAS[a,b], C.V. MORARU[b], C. SOCACIU[a,b*]

ABSTRACT. Considering the high biodiversity of microalgae and their important impact on economy and ecological balance, new screening techniques are needed for their phenotypic characterization and efficient valorization of bioactive components. This represents one the key purpose of the emerging bioeconomy concept, involving new biorefinery technologies coupled with advanced analytical tools. The article presents an overview of the recent extraction and chemical techniques used to recover, separate and characterize the main bioactive molecules (lipids and fatty acids, carbohydrates, proteins and mycosporine-like amino acids chlorophylls and carotenoid pigments) syntesized by microalgae, considering their interesting applications in food, pharmaceutical and cosmetic industries. Special focuses will be directed towards the cell disintegration and extraction procedures, identification and quantification of main metabolites by advanced analytical techniques.

Keywords: *microalgae, bioactive compounds, cell disruption, extraction, spectrometry, chromatography*

INTRODUCTION

The green microalgae and cyanobacteria (blue-green microalgae), typically found in freshwater and marine systems are an important group of unicellular (3–10 μm), photosynthetic microorganisms with great economic and ecologic impact. They are dwelling in different

[a] *Faculty of Food Science and Technology, University of Agricultural Sciences and Veterinary Medicine Cluj-Napoca, 3-5, str. Manastur, 400372 Cluj-Napoca, Romania*
[b] *R & D Center for Applied Biotechnology, Proplanta SRL Cluj-Napoca, Romania, 12G str. Trifoiului, 400478 Cluj-Napoca, Romania*
[*] *Corresponding author: carmen.socaciu@usamvcluj.ro*

environments such as freshwater, marine water or surface of moist rocks, growing rapidly, living in harsh conditions and withstanding environmental stressors, such as heat, cold, anaerobiosis, salinity, photooxidation, osmotic pressure and exposure to ultra-violet radiation. Being capable of converting solar energy to chemical substances via photosynthesis, such organisms are able to synthesize interesring, unique bioactive molecules with multiple applications. The large biodiversity of microalgae includes approximately 200,000-800,000 species in many different genera, of which about 50,000 species are described and around 15,000 novel compounds originating from algal biomass have been identfied. The most studied microalgae until now, *Haematococcus pluvialis, Spirulina, Chlorella vulgaris, Nannochloropsis oculata, Arthrospira platensis*, are an important source of aminoacids-peptides-proteins, vitamins, minerals, polyunsaturated fatty acids, secondary metabolites (sterols, pigments) and minerals [1]. A large variety of functional ingredients isolated from such species can be extracted and used to produce food or cosmetic supplements or functional foods with multiple health benefits [2,3].

This overview presents an updated screening of the literature regarding the extraction and chemical analysis of bioactive compounds found in microalgae, aiming the present and future possible applications in food, pharmacy and cosmetics areas.

The overview include a first part dedicated to the extraction of active microalgae ingredients, followed by new data on the main metabolites of scientific and applicative interests, their identification and quantification by advanced analytical techniques.

BIOACTIVE METABOLITES FOUND IN MICROALGAE SPECIES

The microalgal metabolism is very versatile, reacting fast to changes in the external environment and this aspect is valorized technologically, since the environmental stress induces modifications of the biosynthetic pathways. Both primary and secondary metabolites from microalgae are considered promising natural sources of bioactive compounds since approx. 40% of global photosynthesis being due to these microorganisms [4]. Figure 1 presents a simplified scheme of the primary and secondary metabolism of microalgae.

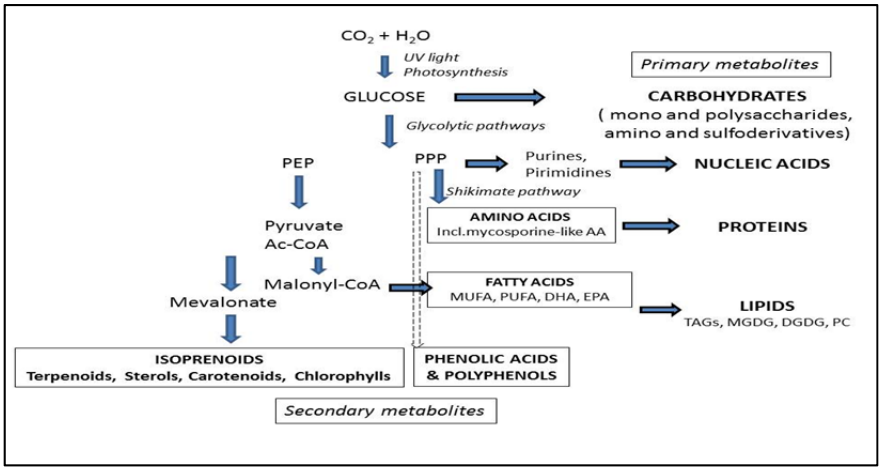

Figure 1. Main biosynthetic pathways which are producing primary and secondary metabolites in microalgae.

Table 1. Carbohydrates and proteins extracted and analysed from different species of microalgae. Relevant references are added.

Species	**Extraction protocols/analysis**	**Compounds identified, ref.**
Nannochloropsis sp.	Freeze-dried algal mass extracted in methanol followed by saponification.	Proteins [8,9]
Chlorella pyrenoidosa	Cell lysed biomass mixed with ammonium sulphate, followed by delipidation with t-butanol. Proteins precipitated and after acidic hydrolysis, the amino acid analysis was done by HPLC	Proteins Amino acids Starch,Cellulose [7]
Haematococcus pluvialis *Nannochloropsis ocul.* (see water algae) *Arthrospira platensis and Chlorella vulgaris* (sweet water algae)	Pre-treatment by freeze-drying, High-pressure cell disruption, ultrasonication Manual grinding and chemical treatment in basic and acid sol.	Water-soluble proteins [10]
BTM 11	Dried biomass on liquid nitrogen, sonication and centrifugation. Supernatant precipitated with ammoniumn sulfate and purified by Sephadex G-50 gel filtration. Separation of proteins by SDS-PAGE electrophoresis.	Lectins [11]
47 microalgae strains (incl. green /red algae, and diatoms)	The algal biomass was hydrolyzed in acid media and analysed by ninhydrin method with absorption of amino acids at 575 nm.	Total proteins [12]
Chlorella pyrenoidosa (sweet water microalgae)	Cell lysed biomass mixed with ammonium sulphate, delipidation with *t*-butanol. Proteins precipitated by acidic hydrolysis, carbohydrates determined by spectrometry	Total carbohydrates Starch Cellulose [11]
Forty-seven microalgae strains, including green algae, red algae, and diatoms	Defatted biomass was hydrolyzed in acidic media. Glucans were determined by the modified thymol-sulfuric acid method	β-α- glucans [12]

The secondary metabolism shows a limited distribution, while the primary metabolism furnishes intermediates for the synthesis of essential macromolecules [5]. The microalgal carbohydrates are complex and include mixtures of neutral sugars, amino sugars and uronic- or sulfo-acids, depending on the species and environmental factors [6], as presented in Table 1. Microalgae are considered an alternative high-value protein source since they contain all essential amino acids [7] (Table 1). There are many methods for proteins extraction from microalgae: ultrafiltration, precipitation, chromatography, dialysis and centrifugation. Precipitation seems to be scalable for industrial processes but it has also its limitation. Precipitation by salting out has low recovery, while precipitation by isoelectric focusing and solvent can cause irreversible denaturation of proteins.

Mycrosporine-like amino acids (MAAs), a specific class of metabolites have important roles in the protection of aquatic organisms against solar radiation. This can be a reason for using MAAs extracts as ingredients for skin protection in suncare products [5]. Microsporine-like aminoacids (MAAs) were extracted and analysed from different species of microalgae, as presented in Table 2.

Table 2. Microsporine-like aminoacids (MAAs) extracted and analysed from different species of microalgae. Relevant references are added.

Species	**Extraction protocols/Analysis**	**MAAs identified, ref.**
33 species of microalgae	Freeze dried microalgae extracted by ultrasonication in acetonitrile and centrifuged to remove cellular debris. Separation of amino acids by HPLC-UV on Luna Amino column and identification at 330 and 310 nm	More than 20 MAAs mycosporine-glycine-valine, -taurine, palythenic acid, mycosporine-methylamine, mycosporine-glycine [13]
	Dried or water suspended cells sonicated and extracted in methanol. The extract was evaporated and and the residue re-dissolved in trifluoroacetic acid and ammonium hydroxide. HPLC-UV analysis on C_{18} column.	More than 15 MAAs: Palythine-serine sulphate, Mycosporinesulfate ester, Mycosporine-2-glycine, Mycosporine-methylamine-serine, -glycine, -taurine [14]
Chlamydomonas hedleyi	Classical extraction in methanol, evaporation of the extract, residue resuspended in H_2O: chloroform with gentle vortexing for delipidation. The water phase was resuspended in methanol for HPLC-ESI^+-MS/MS analysis.	Porphyra-334, shinorine, and mycosporine-Gly [15]

The protocols used to extract mycosporine-like aminoacids varies among studies, every species having a different protocol, using ethanol or methanol, with or without cell wall disruption by sonication or in the presence of chemicals, at different temperatures and for different duration [16].

Table 3. Lipids, fatty acids and pigments extracted and analysed from different species of microalgae. Relevant references are added.

Microalgae	Cell wall disruption/Extraction protocols/analysis	Active compounds extracted, ref.
Nannochloropsis gaditana	Mechanical/ vortex ultrasounds assisted disruption/centrifugation, freezing/unfreezing. Use of methanol, acetone, ethanol.	Pigments [17]
Scenedesmus obliquus *	Freeze-drying, quartz grinding, ultrasounds. Extraction at low temperature and successive extraction with acetone.	Pigments and fatty acids [18]
*Chlorella** *Chroococcus**	Osmosis, grinding with glass powder. Lyophilisation. Extraction with cold/ preheated/ boiling acetone.	Pigments [4]
Chlamydomonas variabills, Chlorella vulgaris Haematococcus pluvialis, Scenedesmus * Chroococcus turgidus, etc.*	Liophilisation of algae followed by classical extraction using chloroform and methanol. Alternative extraction of algae powder or paste, mixed with *n*-hexane and isopropanol, centrifuged at 800 rpm at ambient conditions for 7.5 h, and filtred.	Total lipids [19], [20]
Chlorococcum sp*	Supercritical CO_2 extraction at pressures 10 to 50 MPa and 60 or 80°C. Extraction time: 80 - 120 min. Dynamic Soxhlet extraction in *n*-hexane, 7.5 h	PUFAs [20]
Pavlova viridis	Classical Chloroform/methanol extraction (method Bligh 1959), chloroform extract analysed GC-MS.	MUFAs, EPA, DHA [20]
Nannochloropsis sp.	Lipid transmethylation of freeze-dried samples treated with methanol/acetyl chloride. The final hexane extract was analysed	EPA [8], [9]
	Fatty acid methyl esters (FAMEs) were prepared by trans-methylation with methanol-acetyl chloride	Fatty acids (C14:0, C16:0, C22:5 n-6, DHA/DPA, C22:6 *n*-3), Squalene [21]
Tetraselmis chuii	Fatty acid methyl esters (FAMEs) were prepared by trans-methylation with methanol-acetyl chloride	Fatty acids C16:0, DHA, methylated C16:1, 1,2- benzene-dicarboxylic acid [22]
Pavlova lutheri	Direct transesterification with acetyl chloride. The Fatty Acid Methyl Esters (FAMEs) were analysed by GC-MS.	Fatty acids C16:0, C16:1, C18:2, C18:4, EPA, DHA [23]
*Chlorella kessleri**	Chloroform/methanol extraction, and subsequent fractionation by two-dimensional TLC on precoated silica	MGDG, DGDG, PC, PE [24]
*Nannochloropsis salina Chlorella vulgaris * Arthrospira platensis Scenedesmus obliquus **	Extraction in different solvent mixtures. Chloroform–methanol (1:1) gave the highest lipid content.	Total and non-polar lipids [25]
Dunaliella tertiolecta and	Extraction in different solvent mixtures.	Vitamin E [26]
Tetraselmis suecica	Extraction in different solvent mixtures. 2-propanol substituted methanol	TAGs [27]
Review on microalgae species	Comparison of 5 different methods of extraction (under pressure) 2-ethoxyethanol was shown to provide superior lipid recovery	Linoleic acid 18:2n-6 ARA 20:4n-6 ALA 18:3n-3, EPA, DHA [28]
Tetraselmis sp.	Classical lipid extraction using different solvents and sonication, direct saponification and supercritical CO_2 extraction, compared with Soxhlet-based extraction.	Total lipids [29]
47 microalgae strains, incl.green red algae, diatoms	Direct extraction in n-hexane, sonication and GC-MS analysis	Total lipids [12]

*Sweet water microalgae Abbreviations: Arahidonic acid - ARA; a-linolenic acid – ALA; Monounsaturated fatty acids- MUFAs; Poly unsaturated fatty acids - PUFAs; Monogalactosyl

diacylglycerol – MGDG; Digalactosyl diacylglycerol – DGDG; Phosphatidylcholine-PC, Phosphatidylethanolamine – PE; Eicosapentanoic acid – EPA; Docosahexaenoic acid –DHA; Triacylglycerides –TAGs

The polyunsaturated fatty acids (PUFAs) play a key role in the microalgae biosynthesis, being key-molecules for the regulation of membrane fluidity, electron and oxygen transport, as well as thermal adaptation. Marine microalgae have been targeted as potential candidates for industrial production of *n*-3 LC-PUFAs such as eicosapentaenoic acid (EPA, 20:5*n*-3) and docosahexaenoic acid (DHA, 22:6*n*-3). EPA has been found in a wide variety of marine microalgal classes but only several species showed high production capacity (Table 3).

By the mevalonate pathway (Figure 1), many secondary metabolites are synthesized, mainly isoprenoids having specific roles in survival, adaptation to the environmental stress and defence against predators. Beside some terpenes and chlorophylls (a, b and c), carotenoids, are the most important as main and accessory pigments for photosynthesis, as well sterols, as growing factors. The main carotenoids are β-carotene, lutein, astaxanthin and their esters (liposoluble) and apo-carotenoids or phycobilins (hydrosoluble). Such pigments exhibit colours from green, yellow, brown or red. Production of microalgal pigments may significantly vary dependent on many factors such as temperature, irradiation intensity, photoperiods, colour absorption wavelength, pH, nutrient limitation, nitrogen supplements, salinity, presence of pesticides or heavy metals [30]. Table 4 presents the reference data related to the extraction, isolation and characterization of some isoprenoids, especially pigments

Table 4. Secondary metabolites (isoprenoids) identified and analysed from different species of microalgae. Relevant references are added.

Microalgae species	**Isoprenoids identified**	**References**
Nannochloropsis oculata/granulata *Nannochloropsis salina* *Dunaliella sp.*	Violaxanthin/neoxanthin, astaxanthin, vaucheriaxanthin, lutein/zeaxanthin, canthaxanthin, fucoxanthin, β-cryptoxanthin, β-carotene, α-carotene, Chlorophyll a, Fatty acids	[31], [32], [33]
Chlamydomonas sp.	phenolics, flavonoids, saponins, glycosides, alkaloids, tannins, terpenoids, chlorophyll a, chlorophyll b, astaxanthin	[33], [34]
Chlorella sp. * *Spirulina sp.*	phenolics, flavonoids, saponins, glycosides, alkaloids, tannins, terpenoids, chlorophyll a, chlorophyll b, astaxanthin, canthaxanthin, zeaxanthin, violaxanthin, lutein	[2], [33], [34]

*Sweet water microalgae

Among other secondary metabolites, it is important to mention also phytosterols, found in high quantities in some microalgae (*Chlorella vulgaris*,

Tetraselmis suecica). The main sterols are ergosterol and fungisterol, useful as nutritional ingredients for aquaculture. Phytosterols are also effective as chemotaxonomic biomarker for distinguishing different algal species. Phytosterols extraction can be done by classical methods applied for lipids, using organic solvents or by green extraction technology through supercritical CO_2 extraction [5], [34], [35].

Halogenated derivatives are found in several classes of primary and secondary metabolites, like indoles, terpenes, acetogenins, phenols, fatty acids and volatile halogenated hydrocarbons. They are present mainly in red and brown algae, such as cyanobacteria *Anabaena cylindrica* and *Anabaena variabilis*, found in river waters [19]. The extraction protocols for halogenated compounds may vary from classical extraction with conventional solvents (hexane, ethanol) to supercritical fluid extraction [31].

EXTRACTION OF BIOACTIVE INGREDIENTS: CHALLENGES AND NEW TECHNIQUES

The recovery of functional ingredients from microalgae is challenging and represents a critical step of extraction efficiency, mainly due to their thick and strong cell walls, the localization of products of interest into to cell membranes or in globules [36].

Cell disruption is a first challenge, considered a crucial step for the extraction of active ingredients from microalgae. Several methods, divided into two main groups, are currently available for cell disruption: mechanical (1) and (bio)chemical methods (2).

By mechanical stress (1) the cell wall is disrupted using solid-shear forces (e.g. bead mill, high speed homogenization), liquid-shear forces (high pressure homogenization, microfluidization), energy transfer through waves (e.g. ultrasonication, microwave), electric pulses or heat (e.g. thermolysis, autoclave procedures) [36]. Previous studies showed that *high pressure homogenization* it highly effective in disrupting the cell walls of different microalgae *Chloroccum* species, the rate disruption being maximal after five passes of homogenization [20]. *High speed homogenization* uses high rotation rates (around 8500 rpm/min) to disrupt the cell wall by hydrodynamic cavitations, generated by the shear forces at the solid-liquid interphase, a simple, effective, but aggressive cell disruption method [36]. By *ultrasonication,* the microalgal biomass forms microbubble cavities which impart kinetic energy into the surface of the cells, causing ruptures of wall structure. As compared with *high speed homogenization*, the ultrasonication method was less effective

on cell walls disruption, but more effective on disintegrating the microalgal colonies into single individual cells [20], [37], [38], when an acoustic power level of 65 W and 130 W, was used for 25 min. Microalgae cell disruption by ultrasonic treatment was evaluated also on *Chlamydomonas reinhardtii* [39] and it was shown that 800 J/10 mL were needed to maximize the cell disruption, but is a risky procedure since free radicals can be released, affecting the quality of the sample.*Bead milling* is a mechanical blending unsing a physical grinding of the cell suspension with solid glass beads, the effeciency of disintegration increasing with bead loading [20]. A comparative study of different cell wall disrupting methods on *Chlorella* sp. showed that bead milling caused less wall breaking compared to grinding in liquid nitrogen [40]. *Microwave treatment* of cell suspensions at 2450 MHz determines a local heating of intracellular polar molecules (maily water) which reach the boiling point, resulting in its expansion within the cell, increase of internal pressure and damage of the cell wall/membrane releasing intracellular metabolites [36]. Studies on *Chlorella vulgaris* and *Scenedesmus* sp. cells showed that microwave treatment was optimum [41].

The *Pulsed electric field treatment* induces critical electrical potentials and disrupts the cell wall by electromechanical compression and electric field-induced tension (electroporation). The electric field strength and pulses, the size and number of the pores may vary and can be reversible or irreversible, not only destroying the cell wall, but also the intracellular molecules [36]. Using such treatments on *Auxenochlorella protothecoides*, the extraction could be considerably improved, as reported recently [42]. The three-phase partitioning is a rapid, simple and scalable separation technique for concentration, isolation and decontamination of proteins from crude samples [7]. A recent study [11] showed that the aqueous extraction of proteins from several microalgae followed the order: high-pressure cell disruption > chemical treatment > ultrasonication > manual grinding. The cell-wall of microalgae mostly fragile followed the order: *Haematococcus pluvialis* < *Nannochloropsis oculata* < *Chlorella vulgaris,* ≤ *Arthrospira platensis* [43].

The (bio)chemical methods (2) consist in cells lysis with chemicals or enzymes and osmotic shock. These methods are milder than mechanical processes, the cells being only perforated or permeabilized rather than being break up [36]. The *enzymatic degradation* of cell walls can be produced by cellulase, lipase, chitinase enzymes, combined for an increased efficacy. In spite of its higher costs, this method has some important advantages such as the selectivity of degradation, protecting the unstable biochemicals, preserving their functionality. It was demonstrated that chitinase, lysozyme, pectinase, sulfatase, β-glucuronidase, and laminarinase had the broadest effect across

the various *Chlorella* sp. strains and inhibited *Nannochloropsis* sp. and *Nannochloris* sp. strains [44], [45].

Cell disruption can be completed by several *chemical compounds* like antibiotics, chelating agents, chaotropes, detergents, solvents, hypochlorites, acids or alkali, but their selectivity is low, the efficiency being dependent on the cell wall composition [36].

New, emerging technologies are developing for microalgae cell disruption, e.g. explosive decompression with CO_2, propane or butane, laser treatment, microfluidization, pulsed electric discharge, high frequency focused ultrasonication, etc. [36]. Unfortunately, none of the methods presented above are considered ideal. To chose the most appropriate method for cell wall disruption, should be taken into account the characteristics of each species, the active compound needed to be extracted, costs, applicability for industrial processes, etc.

Extraction procedures. Generally, the bioactive compounds can be extracted from natural resources by *classical extraction techniques* based on different polar and unipolar organic solvents, associated or not with heat, other supplementary techniques used to enhance the extraction yield. The existing classical techniques are Soxhlet extraction, maceration and hydrodistillation. Soxhlet extraction is generally used for nonpolar, lipid derivatives and uses volatile, non polar solvents by solid-lichid extraction process into a Soxhlet extractor. Maceration is a cheaper method to get essential oils and bioactive compounds, by grinding and mixing the solid material with a solvent, followed by filtration and centrifugation of the extract. The hydrodistillation process, uses water and steam distillation or direct steam distillation which involves a hydrodiffusion of bioactive polar components [46]. The selection of the proper solvent for extraction needs to consider the polarity of solvents and of compounds to be extracted, their molecular affinity, mass transfer, possible use of co-solvents, environmental safety, human toxicity and financial feasibility [46].

The *modern extraction* and *isolation techniques* on different natural sources, including microalgae have been described [20]. To mention, Supercritical-fluid Extraction (SFE), Pressurized-Liquid Extraction (PLE) and microwave-assisted (MAE), Ultrasound-Assisted Extraction (UAE) or Solid-Phase Extraction (SPE) techniques, or their combination, were frequently used. In addition, the High-speed Counter-Current Chromatography (HCCC) provides also an effective liquid/liquid partition for metabolite isolation. Such techniques have been applied to the extraction of amino acids, fatty acids, natural pigments, saccharides, vitamins, toxins, and other metabolites from cyanobacteria, micro- or macro-algal species. The most commonly used SFE using CO_2 due to its favourable critical temperature and pressure (Tc=31.1°C

and Pc=73.9 bar), is ideal for the extraction of thermolabile compounds. In addition, the supercritical CO_2 has low viscosity, low surface tension, high diffusivity and good density and is also non-toxic, non-flammable, cheap, widely available, chemically inert under several conditions, and gaseous at normal pressure and temperature, eliminating the step of solvent evaporation after extraction. It gives a non-oxidizing atmosphere in extractions, thus preventing extracts from degradation [31]. A good example is the the use of this technique to extract carotenoids, clorophylls a, b and c from *Scenedesmus obliquus,* using different, optimal pressures and temperatures, depending on the active compound to be extracted [47]. MAE is an efficient method using microwave irradiation to accelerate the removal of a diversity of compounds from natural matrices, by concomitant heat and mass gradients [31]. Recent experimental results indicate that MAE increased extraction rate over 15 times for *Chlorella sorokiniana* and *Nannochloropsis salina* when compared with conventional solvent extraction [48]. UAE significantly reduces the extraction time and increases the extraction yields due to the production of cavitation bubbles in the solvent. This ability to cause cavitations depends on the characteristics of ultrasound wave, the solvent properties, and the ambient conditions [31]. Such methods were applied to extract lipids from *Nannochloropsis oculata*, at reduced extraction time and preservation of fatty acids quality [49]. PLE named also subcritical fluid extraction uses temperatures of 50–200 °C and pressures in the range of 35–200 bar, lower than the Tc and Pc of the solvents, which are kept in the liquid state and therefore enhances the solubility and mass transfer rate, reduces the viscosity and surface tension of the solvents. Water is the most widely used solvent but also propane and dimethyl ether were repored [14]. Such technique was applied for a successful extraction of polysacharides with antiviral activity from *Chlorella vulgaris* [50].

ANALYTICAL TECHNIQUES TO IDENTIFY AND QUANTIFY MICROALGAE METABOLITES

UV-VIS Spectrometry. The quantitative determination of chlorophylls *a, b* and carotenoids in a whole pigment extract of green microalgae by UV-VIS spectroscopy is dependent by the sample characteristics, solvent system, and spectrophotometer parameters. For example, increasing the polarity of the solvent, the red absorption maximum of chlorophyll *a* shifts from 660 to 665 nm, and the blue absorption maximum from 428 to 432 nm. The same also applies to chlorophyll *b*, which shifts from 642 to 652 nm and 452 to 469 nm. In order to perform spectroscopic measurements in the right maximum regions,

one should determine the maximum red spectral position of pure chlorophyll a and b solutions with one's own spectrophotometer and compare them with those from the literature. The absorption spectrum of an extract of a green tissue is generally containing mixtures of chlorophyll *a* and *b* and total carotenoids, being dominated by the absorption of chlorophyll *a* at A_{428} (blue) and A_{661} (red). Chlorophyll *b* and the carotenoids absorb broadly in the blue region (400 to 500 nm) [51].

Traditionally, the quantification of microalgae carbohydrates is made by phenol–sulfuric acid protocol, where sugars are hydrolyzed to furans and measured spectrophotometrically at 490 nm for hexoses and 480 nm for pentoses and uronic acids [6]. For mycosporine-like aminoacids the quantification need absorbtion values at 330 and 310 nm [13].

Thin Layer Chromatography (TLC) and High Performance-Thin Layer Chromatography (HP-TLC). TLC is the oldest and widespread analytical chromatographic technique for the screening of plant and microalgae extracts. The separation process involves a suitable adsorbent (stationary phase) and a solvent or solvent mixture (mobile phase). By TLC methods, a broad range of substances dissolved in all solvents even aggressive reagents can be tested [52]. Recently, HP-TLS is often used also for screening the pigments from microalgae.

High-Performance Liquid Chromatography (HPLC) is the emerging technique to be used in laboratories worldwide over the past decades, coupled with UV- or photodiode array (PDA) detection. It is one of the best suited techniques for an efficient separation of the crude extracts or fractions. The reversed-phase columns are the best choice for the analytical separation, even if new stationary phases have been exploited [45]. Chromatography offers an efficient way to identify the carbohydrates, fatty acids, mycosporine like amino acids, carotenoids and other active compounds from microalgae [6], [20], [53]. Our present experimental studies are related to the application of HPLC-ESI^+-MS carotenoid profiles of *Chlorella sorokiniana* and other microalgae, either in aqueous suspensions or powders obtained by freeze drying [54].

Liquid Chromatography coupled with Mass Spectrometry (LC-MS) combines the high separation power of high-performance liquid chromatography with the structural information of mass spectrometry. The sensitivity and specificity of LC-MS methods are drastically improved relatively to the traditional UV/PDA detection and allows the use of very fast chromatographic separations with high peak purity value. A key

development of this technique is the use of Electron Spray Ionization (ESO) or Atmospheric Pressure Chemical Ionization (APCI) that transfers the analyte molecules from solution to the gas phase, suitable for fragmentation in the mass spectrometer [45]. LC-ESI/APCI-MS has been used to identify carotenoid esters present in extracts of pigmented freshwater microalgae and for the identification and quantification of glycolipids from microalgae [47].

Matrix Assisted Laser Desorption Ionization time-of-flight mass spectrometry (MALDI-TOF-MS). MALDI-TOF MS is high performance technique ro screen the protein fingerprint and characterize the phenotype (genus, species), and in some cases, the strains also of microalgae, comparing the spectra of unknown microorganisms to reference spectra found in international databases [55].The possibility of using MALDI-TOF-MS for the rapid identification of pathogenic and non-pathogenic species of the genus *Prototheca* has been recently demonstrated [30]. This provides reproductible and unique spectra covering a wide m/z range (2000–20 000 Da) for each of the strains used in the present study. The reproducibility of the spectra was further confirmed by employing composite correlation index calculation and main spectra library (MSP) dendrogram creation, available with MALDI Biotyper software [56].

CONCLUSION

Microalgae species have a high potential to synthesise a wide range and number of specific, bioactive metabolites, by a versatile metabolism, adaptative to environmental conditions. Considering the economic and health-beneficial action of their primary and secondary metabolites, new procedures and biorefinery technologies were released the last years. Bioactive molecules (amino acids and proteins, unsaturated lipids and fatty acids, sterols, carbohydrates, pigments, vitamins, etc.) may be extracted specifically by new, less distructive physical or biochemical procedures and then analysed by advanced techniques like high-performance chromatography coupled with mass spectrometry or by direct MALDI-TOF –MS screening. This overview may offer new ideas for improving the recovery and characterization of the microalgae biomass, as well considering the limits and challenges of such technologies. Nevertheless, supplementary scientific and technological inputs are expected in the next years for increasing the sustainability of microalgae biorefinery approach applied in this important category of natural resources.

ACKNOWLEDGMENTS

This work was supported by a Research ERANET-LAC project SCREAM nr.26/2016, funded by the Romanian National Authority for Scientific Research and Innovation UEFISCDI, within PNCDI III program.

REFERENCES

1. E. Christaki, E. Bonos, I. Giannenas, P. C. Florou-Paneri, *Journal of the Science of Food and Agriculture*, **2013**, 93(1), 5.
2. M. Greque de Morais, B. da Silva Vaz, E. Greque de Morais, J.A. Vieira Costa, *BioMed Research International*, **2015**, ID 835761, 1.
3. A. Villarruel-Lopez, F. Ascencio, K.Nuno, *Polish Journal Of Food And Nutrition Sciences* , **2017**, 67, 251
4. K.H. Wiltshire, M. Boersma, A. Möller, H. Buhtz, *Aquatic Ecology*, **2000**, 34, 120.
5. S.M. Mostafa, *Plant Science*, **2012**, chapter 12.
6. K.H.M. Cardozo, T. Guaratini, M.P. Barros, V.R. Falcão, A.P. Tonon, N.P. Lopes, S. Campos, M.A. Torres, A.O. Souza, P. Colepicolo, E. Pinto, *Comparative Biochemistry and Physiology*, **2007**, C 146, 60.
7. E. Gunerken, E. D'Hondt, M.H.M. Eppink, L. Garcia-Gonzalez, K. Elst, R.H. Wijffels, *Biotechnology Advances*, **2015**, 33(2), 243.
8. A.G. Waghmare, M.K. Salve, J.G. LeBlanc, S.S. Arya, *Bioresources and Bioprocessing*, **2016**, 3, 16.
9. D.W. Templeton, M. Quinn, S. Van Wychen, D. Hyman, L.M.L. Laurens, *Journal of Chromatography* A, **2012**, 1270, 225.
10. Z. Cheng-Wu, O. Zmora, R. Kopel, A. Richmond, *Aquaculture*, **2001**, 195, 35.
11. Z. Cohen, M. Reungjitchachawali, W. Siangdung, M. Tanticharoen, *Journal of Applied Phycology*, **1993**, 24, 312.
12. C. Safi, A.V. Ursu, C. Laroche, B. Zebib, O. Merah, P.Y. Pontalier, C. Vaca-Garcia, *Algal Research***, 2014**, 3, 61.
13. A.Z. Mustopa, R. Isworo, M. Nurilmala, D. Susilaningsih, *Annales Bogorienses*, **2016**, 20(2), 47.
14. C. Schulze, M. Wetzel, J. Reinhardt, M. Schmidt, L. Felten, S. Mundt, *Journal of Applied Phycology*, **2016**, 28, 2719.
15. C.A. Llewellyn, R.L. Airs, *Marine Drugs*, **2010**, 8, 1273.
16. J.I. Carreto, M.O. Carignan, N.G Montoya, *Marine Biology*, **2005**, 146, 237.
17. Y. Li, F. Ghasemi Naghdi, S. Garg, T.C. Adarme-Vega, K.J. Thurecht, W.A. Ghafor, S. Tannock, P.M. Schenk, *Microbial Cell Factories*, **2014**, 13(1), 1.
18. S.S. Suh, J. Hwang, M. Park, H.H. Seo, H.S. Kim, J.H Lee, S.H. Moh, T.K. Lee, *Marine Drugs*, **2014**, 12(10), 5174.

19. M. Henriques, A. Silva, J. Rocha, Extraction and quantification of pigments from a marine microalga: a simple and reproducible method, Communicating Current Research and Educational Topics and Trends in Applied Microbiology, Formatex, Spain, Vol. 2, **2007**, 586.
20. A. Ilavarasi, D. Pandiaraj, D. Mubarakali, M.H. Ilyas , N. Thajuddin, *Pakistan Journal of Biological Sciences*, **2012**, 15, 883.
21. S.M. Abdo, E. Ahmed, S. Abo El-Enin, R.S. El Din, G. El Diwani, G. Ali, *Journal of Algal Biomass Utilization*, **2014**, 5(3), 23.
22. C. Hu, M. Li, J. Li, Q. Zhu, Z. Liu, *World Journal of Microbiology and Biotehnology*, **2008**, 24, 1209.
23. Y. Jiang, K.W. Fan, R.T.Y. Wong, F. Chen, *Journal of Agricultural and Food Chemistry*, **2004**, 52(5),1196.
24. J. Maligan, A. Saksony, V. Widayanti, *Conference Proceeding*, **2011**.
25. A.P. Carvalho, F.X. Malcata*, Marine Biotechnology*, **2005**, 7(4), 381.
26. N. Sato, M. Tsuzuki, A. Kawaguchi, *Biochimica et Biophysica Acta*, **2003**, 1633(1), 35.
27. E. Ryckebosch, K. Muylaert, I. Foubert, *Journal of the American Oil Chemists' Society*, **2012**, 89, 189.
28. E.C. Carballo-Cárdenas, P.M. Tuan, M. Janssen, R.H. Wijffels, *Biomolecular Engineering*, **2003**, 20(4-6), 139.
29. T. Řezanka, L. Nedbalová, L. Procházková, K. Sigler, *Phytochemistr*y, **2014**, 100, 34.
30. E. da Costa, J. Silva, S. Hoffman Mendonça, M.H. Abreu, M.R. Domingues, *Marine Drugs*, **2016**, 14(101), 1.
31. S. Ramaraj, J.S. Ki, A Review of the Biological Activities of Microalgal Carotenoids and Their Potential Use in Healthcare and Cosmetic Industries, *Marine Drugs,* **2018**, 16, article 26.
32. C. Grosso, P. Valentão, F. Ferreres, P. Andrade, *Marine Drugs*, **2015**, 13, 3184.
33. B. Tartarotti, R. Sommaruga, *Archiv für Hydrobiologie*, **2002**, 154(4), 691.
34. K. Skjånes, C. Rebours, P. Lindblad, *Critical Reviews in Biotechnology*, **2013**, 33(2), 195.
35. A. Jayshree, N. Thangaraju, *Journal of Algal Biomass Utilization*, **2014**, 5, 61
36. D. Mouna, H. Bilel, M.Barkallah, et al., *Bioresource Technology* , **2018,** 249, 510
37. E. Gunerken, E. D'Hondt, M.H.M. Eppink, L. Garcia-Gonzalez, K. Elst, R.H. Wijffels, *Biotechnology Advances*, **2015**, 33(2), 243.
38. C.W. Yong, L. H. Yong, *Applied Sciences-Basel,* **2018,** 8, article 26
39. M.Stramarkou, S.Papadaki, K. Kyriakopoulou et al, *J. Applied Phycology*, **2017,** 29, 2947.
40. J.A. Gerde, M. Montalbo-Lomboy, L. Yao, D. Grewell, T. Wang, *Bioresource Technology*, **2012**, 125, 175.
41. H. Zheng, J. Yin, Z. Gao, H. Huang, X. Ji, C. Dou, *Applied Biochemistry and Biotechnology*, **2011**, 164, 1215.
42. J.Y. Lee, C. Yoo, S.Y. Jun, C.Y. Ahn, H.M. Oh, *Bioresource Technology*, **2010**, 101(1), S75.

43. C. Eing, M. Goettel, R. Straessner, C. Gusbeth, W. Frey, *IEEE Transactions on Plasma Science*, **2013**, 41(10), 2901.
44. S. Papadaki, K. Kyriakopoulou, K. Magdalini, *IOSR Journal of Environmental Science*, Toxicology and Food Technology, **2017**, 10, 53.
45. H.G. Gerken, B. Donohoe, E.P. Knoshaug, *Planta*, **2013**, 237(1), 239.
46. J. Asma, R. Brandon, H. Soleiman et al., *Biomedical Journa*l, et al. **2017,** 40, 339.
47. J. Azmir, I.S.M. Zaidul, M.M. Rahman, K.M. Sharif, A. Mohamed, F. Sahena, M.H.A. Jahurul, K. Ghafoor, N.A.N. Norulaini, A.K.M. Omar, *Journal of Food Engineering*, **2013**, 117(4), 426.
48. A.C. Guedes, M.S. Giao, A.A. Matias, A.V.M. Nunes, M.E. Pintado, C.M.M. Duarte, F.X. Malcata, *Journal of Food Engineering*, **2013**, 116, 478.
49. J. Pan, T. Muppaneni, Y. Sun, H.K. Reddy, J. Fu, X. Lu, S. Deng, *Fuel*, **2016**, 178, 49.
50. F. Adam, M. Abert-Vian, G. Peltier, F. Chemat, *Bioresource Technology*, **2012**, 114(5), 457.
51. S. Santoyo, M. Plaza, L. Jaime, E. Ibanez, G. Reglero, F.J. Senorans, *Journal of Agricultural and Food Chemistry*, **2010**, 58, 8522.
52. D. Martin-Creuzburg, P. Merkel, *Journal Plankton Research*, **2016**, 38(4), 865.
53. H.K. Lichtenthaler, C. Buschmann, Chlorophylls and carotenoids: measurement and characterization by UV-VIS spectroscopy, Current Protocols in Food Analytical Chemistry, John Wiley & Sons, Inc.**, 2001**, UNIT F4.3.
54. A.Bertoli, B. Ruffoni, L. Pistelli, L. Pistelli, Analytical methods for the extraction and identification of secondary metabolite production in 'In Vitro' Plant Cell Cultures, Bio‑Farms for Nutraceuticals, Springer US, **2010**, Chapter 19.
55. C. Moraru, K. Skjanes, D. Patras, C. Socaciu, CJJ Spetz, Proc. 18th *Int. Symp. On Carotenoids, Basel, 9-14* July 2017 (poster presentation).
56. I. Lang, L. Hodac, T. Friedl, I. Feussner, *BMC Plant Biology*, **2011**, 11, 124.
57. D. Barbano, R. Diaz, L. Zhang, T. Sandrin, H. Gerken, T. Dempster, *PLOS One*, **2015**, 10(8).

STUDIA UBB CHEMIA, LXIII, 1, 2018 (p. 37-53)
(RECOMMENDED CITATION)
DOI:10.24193/subbchem.2018.1.03

THE ASSESSMENT OF FLUOROPHORES ADVANCED GLYCATION END PRODUCTS-TO-KYNURENINE RATIO IN HEALTHY AND DIABETIC RATS AND HUMANS

LOREDANA ELENA OLAR[a*], DANA MIHAELA CIOBANU[b], FLORICA MATEI[a], IONEL PAPUC[a]

ABSTRACT. In this study, we calculated the ratio of the serum contributions of two highly studied fluorophore products (advanced glycation end products - AGEs and kynurenine - KYN) in the area of nutrition and metabolic diseases including diabetes mellitus (DM), by using a non-invasive, economical and easy-to-perform method. Blood serum spectrofluorimetric analysis was performed both in the case of normoglycemic (n=10) and diabetic rats (n=10), and in the case of non-diabetic (n=14) and type 2 diabetes mellitus (T2DM) patients (n=52). Our results showed a significant increase in the contributions of the two products in diabetic patients and rats compared to the control group. The ratio of the two compounds was positively correlated with serum glucose levels in the case of rats, and with serum triglyceride values in the case of humans. Also, the presence of DM complications in human subjects and the subsequent calculation of ROC curves led to a predictive value of the investigated ratio (AGEs/KYN) for the presence of peripheral diabetic polyneuropathy (PNP). The obtained results suggest a high potential for the investigated ratio to be considered as a new biomarker for the presence of PNP.

Keywords: *Advanced glycation end products, Kynurenine, Blood serum, Diabetes Mellitus, Fluorescence Spectroscopy*.

INTRODUCTION

According to IDF statistics, the prevalence of diabetes mellitus (DM) has currently reached global epidemic levels. If in 2007, 39 million persons were diagnosed with diabetes, in 2010 this figure increased to 285 million,

[a] *University of Agricultural Sciences and Veterinary Medicine, Faculty of Veterinary Medicine, 3-5 Calea Manastur Street, 400372 Cluj-Napoca, Romania.*
[b] *"Iuliu Hatieganu" University of Medicine and Pharmacy, Faculty of Medicine, Department of Diabetes, Nutrition and Metabolic Disease, 2-4 Clinicilor Street, 400006 Cluj-Napoca, Romania.*
[*] *Corresponding author: loredana.olar@usamvcluj.ro*

and by 2040 it is estimated that 642 million persons will be affected by this disease [1, 2]. The situation is equally worrying for animals; thus, a 79.7% increase in the prevalence of canine diabetes cases was evidenced in 2015 compared to 2006 [3]. All these statistical data emphasize the need to introduce new biomarkers, as well as to identify new correlations between the existing biomarkers in order to gain a better understanding of the pathogenesis of diabetes mellitus in both animals and humans.

A useful aid in this respect is provided by the introduction of spectroscopy techniques in general and spectrofluorimetric in particular for the analysis of tissues and biological fluids from patients with a suspicion and diagnosis of diabetes mellitus. The main purpose of these techniques is to provide semi-quantitative information about the biodistribution of fluorophores in tissues and biological fluids, as well as to assess their biochemical composition [4]. Two classes of fluorophores investigated using these techniques and correlated with the study of diabetes and its complications are advanced glycation end products (AGEs) and kynurenine (KYN). Although AGEs and KYN have been studied separately in the context of DM, the relationship established between them, i.e. the ratio of the fluorophores has not been investigated. Furthermore, according to the current literature, there are no comparative data available regarding the simultaneous fluorescence investigation of AGEs and KYN and their ratio in the presence of DM and its complications.

AGEs or Maillard products are heterogeneous molecules produced through the non-enzymatic reaction of proteins with reducing sugars [5, 6, 7] (Figure 1). The multitude of physiological processes occurring in the body determines their continuous formation in cells and tissues. However, the AGE formation rate is increased in DM as a consequence of hyperglycemia [8, 6]. A great number of studies suggest the implication of AGEs in the pathogenesis of diabetes complications such as: retinopathy, neuropathy, chronic renal disease and cardiovascular disease [6, 8, 9]. The other investigated compound, KYN, is a fluorescent metabolite of tryptophan (TRP) and one of the parameters frequently associated with protein oxidative stress and other systemic inflammatory disorders. Thus, in inflammatory diseases such as diabetes, frequently associated with depression, there is an activation of the hepatic enzyme indoleamine 2,3-dioxygenase, responsible for metabolization of TRP to KYN, with the production of high KYN concentrations [10]. Previous studies have demonstrated the presence of a relationship between depression and one of the complications of diabetes – neuropathy, among patients with type 2 diabetes mellitus (T2DM) [11]. One of the objectives of this study was to check for the presence of a disturbance of TRP and implicitly KYN metabolism in the case of patients with T2DM diagnosed with this type of complication. We also aimed to simultaneously investigate AGEs and KYN by fluorescence

spectroscopy in order to assess their serum levels in healthy and diabetic rats, as well as in non-diabetic and T2DM human subjects. In addition, their simultaneous evaluation was performed in the context of DM complications in humans. According to the studied literature, these aspects have not been investigated before. In this context, we calculated the ratio between the contributions of the two classes of fluorophores to total serum fluorescence, with a view to considering this ratio as a new biomarker for the presence of some diabetes complications.

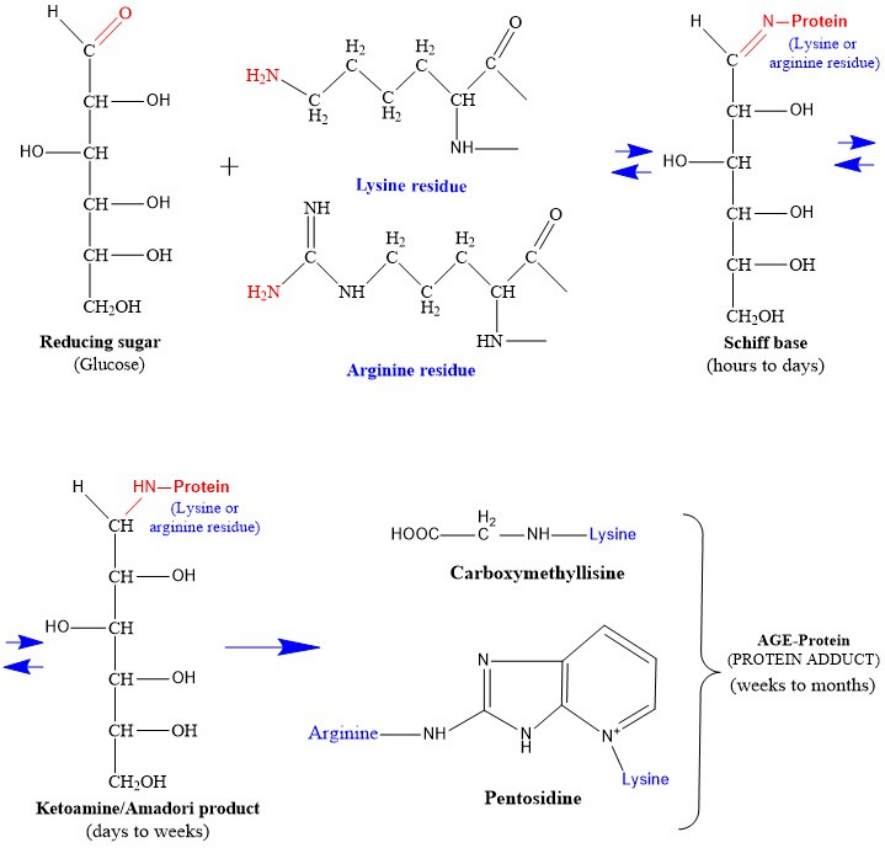

Figure 1. The schematic presentation of advanced glycation end products formation through Maillard reaction. Firstly, a reversible Schiff base is formed within hours through the reaction of reactive carbonyl groups of a reducing sugar with the free amino groups of proteins. Secondly, the Amadori product is formed by multiple chemical rearrangements over a period of days. Finally, through others multiple chemical rearrangements and over a period of weeks, advanced glycation end products such as: carboxymethyllisine and pentosidine are formed.

RESULTS AND DISCUSSION

The characteristics of non-diabetic rats and rats with streptozotocin-induced diabetes were described in the material and method section. Blood glucose levels were significantly higher in rats with streptozotocin-induced diabetes (20.43±6.12 mmol/l) compared to control rats (5.8±0.26 mmol/l). The characteristics of human subjects are shown in Table 1. Significant differences regarding age, duration of diabetes, body mass index, waist circumference, glycated hemoglobin and blood glucose levels were found between healthy and diabetic patients.

Table 1. Characterization of non-diabetic subjects and patients diagnosed with type 2 diabetes mellitus

Variables	Healthy subjects	Patients – type 2 diabetes mellitus
	n=14	n=52
Age (years, IQR)	52.00(40.50-59.00)	59(57-65)
Subjects – men (n, %)	8 (57.14%)	24(46.15%)
Smoking status (n, %)	5 (35.71%)	14 (26.92%)
Duration of diabetes (years)	0	10 (8)
Body mass index (kg/m^2)	25.86±4.54	30.49±4.83*
Waist circumference (cm)	94.21±13.30	108.25±11.20*
HbA1c (%)	<6.5	10.09±2.29*
Blood glucose (mmol/l, IQR)	5.44(4.78-5.78)	9.28(7.89-10.83)
Triglycerides (mmol/l, IQR)	1.12(0.68-1.44)	2.65(1.40-3.64)
Diabetic retinopathy (n, %)	0	20 (38.5%)
Diabetic neuropathy (n, %)	0	27 (51.92%)
Diabetic nephropathy (n, %)	0	20 (38.46%)
Cardiovascular disease (n, %)	0	26 (50 %)
Arterial hypertension (n, %)	0	34 (65.4 %)

Values are expressed as mean ± standard deviation, median and interquartile range or number and percentage, *p <0.05

The contributions of AGEs and KYN to total serum fluorescence were significantly greater in rats with streptozotocin-induced diabetes compared to the control group. Also, the ratio of contributions of the two classes of fluorophores (AGEs/KYN) to total serum fluorescence was significantly higher in rats with streptozotocin-induced diabetes compared to healthy rats (Table 2).

Table 2. Contributions of AGEs (advanced glycation end products), KYN (kynurenine) and the AGEs to KYN ratio in rats and humans

Parameter	Rats			Humans		
	Control	Diabetic	p value	Control	Diabetic	p value
AGEs	15.58±4.07	20.2±2.85	<0.013	16.42±1.27	18.87±3.48	<0.001
KYN	42.16±6.53	10.9±2.18	<0.001	18.41±2.09	21.40±4.42	0.001
AGEs-to-KYN ratio	0.38±0.10	1.89±0.40	<0.001	0.90±0.09	0.93±0.27	0.566

In patients with T2DM, significantly greater contributions of the fluorophores to total serum fluorescence were evidenced compared to the control group. The AGEs to KYN ratio was higher in diabetic patients compared to healthy subjects, but without statistical significance (Table 2).

The positive correlation of the ratio of fluorophores contributions to total serum fluorescence (AGEs/KYN) with serum glucose levels resulted in a Pearson's correlation coefficient value of 0.928 with CI=[0.743, 1.113], for a p value < 0.001. The significant correlation with the serum glucose level was maintained in the case of the two classes of fluorophores investigated separately; thus, for the contribution of AGEs to total serum fluorescence, the Pearson's correlation coefficient value was 0.463 with CI=[0.024, 0.902], with a p value = 0.040, and for the contribution of KYN to total serum fluorescence, the Pearson's correlation coefficient value was -0.867 with CI=[-1.114, -0.621], with a p value < 0.001.

Following evaluation of correlations between AGEs, KYN, their ratio (AGEs/KYN) and biochemical parameters frequently monitored in clinical practice, in the case of human subjects, a significant positive correlation of the ratio of the investigated fluorophores with serum triglyceride levels was established (r=0.43, [95% CI 0.18 to 0.63]; p<0.01). No other correlations were found between the ratio of the studied fluorophores compounds and the other investigated parameters and variables.

No other correlation was established between the contribution of AGEs to total serum fluorescence and the investigated biochemical parameters. Regarding the contribution of KYN to total serum fluorescence, a negative correlation with the triglyceride level was established, with a significantly negative Pearson's correlation coefficient of -0.41 with CI=[-0.63,-0.18] for p=0.01.

To evaluate the presence of possible correlations between the analyzed fluorophores and the development of diabetes complications, we initially considered the mean value of 20.77 as the threshold value for the contribution of KYN to total serum fluorescence; then, its contribution was converted to a dichotomous variable, with divided values above and below the threshold

value. Thus, a significant non-parametric Spearman correlation was obtained between the dichotomous KYN variable and polyneuropathy (PNP), with values of 0.34 at a p level of 0.01.

To investigate the possible correlations between the analyzed ratio (AGEs/KYN) and the presence of diabetes mellitus complications, the ratio (AGEs/KYN) was converted to a dichotomous variable, by using the 0.9233 value as the threshold value. The values obtained in the case of this ratio were above and below this threshold value. Thus, a weak association between the ratio of the fluorophores (AGEs/KYN) and PNP was evidenced, and an asymptomatic Pearson Chi Square test significance of 0.39 with p=0.05 and a contingency coefficient value of 0.246 was obtained (Table 3).

Table 3. Contingency table of the ratio (AGEs/KYN) between the contributions of advanced glycation end products (AGEs) and kynurenine (KYN) to total serum fluorescence and diabetic polyneuropathy (PNP)

			PNP		TOTAL
			ABSENT	PRESENT	
AGEs to KYN ratio	<0.9233	OBSERVED COUNT	19	20	39
		EXPECTED COUNT	23	16	39
	>0.9233	OBSERVED COUNT	20	7	27
		EXPECTED COUNT	16	11	27
TOTAL		TOTAL COUNT	39	27	66
		EXPECTED COUNT	39	27	66

Further, we performed the Mann-Whitney test; a significant difference was obtained between the presence and the absence of PNP regarding the analyzed ratio (AGEs/KYN), the asymptomatic significance value being 0.041.

Following the use of ROC curves, we obtained a mean predictive value for the presence of diabetic polyneuropathy (PNP) based on the assessment of the investigated ratio (AGEs/KYN) (AUC is 0.698±0.072, p=0.007) (Figure 2). Taken separately, the contributions of AGEs and KYN to total serum fluorescence were not predictive for the presence of PNP, which was evidenced by using the ROC curves. Thus, AUC for the evaluation of AGE contribution to total serum fluorescence was 0.519±0.074, with a p value = 0.789, without statistical significance. Also, AUC for the assessment of KYN contribution to total serum fluorescence was 0.255±0.066, with a p value = 0.001. The use of the ROC curve for the analysis of triglyceride levels resulted in an AUC value of 0.533±0.073, p=0.665.

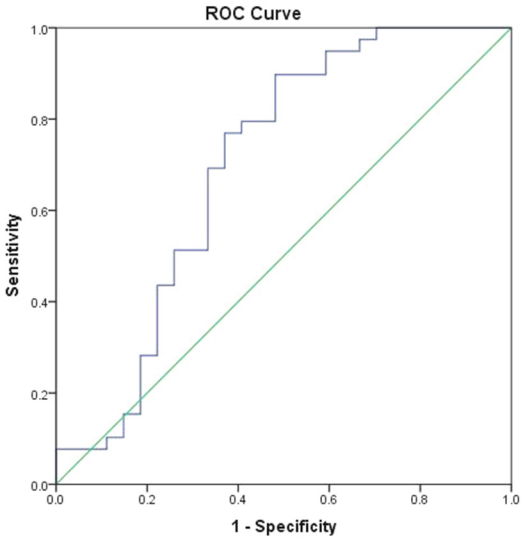

Figure 2. Use of ROC curve to assess the predictability of the AGEs to KYN ratio regarding the development of diabetic polyneuropathy (PNP).

The most important element evidenced by this spectrofluorimetric analysis is the finding that in the case of human subjects (T2DM), the ratio of contributions of the investigated fluorophores (AGEs/KYN) to the total serum fluorescence has a mean predictive value for one of the complications of diabetes, i.e. diabetic polyneuropathy, while the contributions of the products taken separately are not predictors. Thus, lower values of this ratio studied in the case of patients with polyneuropathy can be reported compared to subjects without this type of complication. According to the studied literature, such a predictive value of the ratio of contributions of the fluorophores, AGEs and KYN, for diabetic polyneuropathy, i.e. of the association of these two entities, has not been evidenced so far. This element is useful for investigations aimed at establishing a relationship between the metabolism of the two classes of fluorophores and the presence of diabetes complications, particularly polyneuropathy in diabetic patients. According to the studied literature, inflammatory diseases such as diabetes and implicitly, the development of its complications are determining factors that alter TRP and KYN metabolism and cause depression [12, 13]. These abnormalities in the metabolism of TRP and KYN are sufficiently strong conditions that can lead to an aggravation of diabetes complications and depression symptoms. Thus, according to the study of Bartoli et al. [11], conducted in patients diagnosed with type 2 diabetes mellitus, there is an increased association of neuropathy with the presence

of depression; these authors report that depression in these patients is the consequence of an altered adaptation and functional limitation related to neuropathy. Our study confirms these results, because the presence of neuropathy induces a disturbance of TRP metabolism and implicitly, KYN metabolism in our cases as well. Thus, among patients with T2DM, we evidenced a significant correlation between the contribution of KYN and the presence of polyneuropathy. What makes this study interesting is the fact that the ratio of the investigated fluorophores (AGEs/KYN) has a predictive value for the presence of polyneuropathy in T2DM patients, while in the case of KYN taken separately, such a predictive value for this complication of diabetes could not be established. Like in the case of KYN, recent studies describe the implication of AGEs in the pathogenesis of diabetes complications and implicitly, neuropathy [14, 15]. Peripheral nerves represent one of the favorite sites of AGEs both in the case of human subjects and experimental diabetes in animals [16]. The presence of carboxymethyllisine, one of the products belonging to this large class of AGEs, was described in vascular endothelial cells, pericytes, basement membrane, as well as in axons and Schwann cells belonging to peripheral nerve tissue [17]. Another action mechanism of AGEs which results in the development of neuropathy is through activation of AGE receptors (RAGEs) [18]; the interaction between AGEs and RAGEs leads to endoneural vascular dysfunction and implicitly, to the development of microangiopathies in peripheral nerves [19].

Another interesting observation of this study is the fact that in the case of human subjects, the ratio of contributions of the fluorophore compounds (AGEs/KYN) was significantly correlated with serum triglyceride levels, while no such correlation with the other investigated biochemical parameters could be evidenced. The separate investigation of the fluorophores allowed to obtain an inverse association with serum triglyceride levels only in the case of KYN, while for AGEs, such associations could not be established. In the case of the investigated rats, the studied ratio (AGEs/KYN) was significantly correlated with serum glucose levels, and the separate analysis of the compounds led in the case of each to a significant correlation with serum glucose values. A possible explanation attributed to the correlation between the investigated ratio and serum triglyceride levels in the case of human subjects could be represented by one of the reactions that induce AGE formation; thus, according to the study performed by Bucala et al. [20], the reaction between glucose and amino-containing phospholipids, as well as between glucose and apoproteins initiates AGE formation, finally resulting in the formation of lipid-linked AGEs (AGE-lipid) and apolipoprotein-linked AGEs (AGE-ApoB). Also, the study conducted by Chang et al. (2011) [21] established a positive correlation between AGE level and the patients' lipid profile, as

well as between AGE level and the patients' atherosclerotic characteristics, this type of correlation being much better than those established between the same fluorophore compounds and glucose or HbA1C levels. As regards the effect of KYN on lipid metabolism, this is a currently debated subject [22]. In our study, in the case of patients diagnosed with T2DM, an inverse association of KYN with serum triglyceride levels was obtained; so, it can be concluded that increased contributions of this TRP metabolite induce a decrease of serum triglyceride levels in the case of these patients. Although TRP degradation through the KYN pathway and the effects of the metabolites of this pathway on serum lipid levels were not closely analyzed in this study, the observation of our study is supported by other studies, which report the fact that administration of 3-hydroxyanthranilic acid, a KYN metabolite, causes a decrease in plasma triglycerides in the case of Ldlr (-/-) mice (mice deficient in the LDL receptor) predisposed to the development of atherosclerotic lesions [23]. This reduction in the surface of lipid lesions was explained by a low degree of lipid loading of macrophages, the 3-hydroxyanthranilic acid inhibiting the uptake of oxidized low-density lipoproteins (oxLDL) by macrophages [23].

Another surprise of this study was the correlation established only in the case of rats between both the studied ratio and the contribution of the fluorophores to total serum fluorescence and serum glucose levels. A possible explanation for this correlation only in the case of rats, unlike human subjects, might be the application of multiple treatments over time in the case of humans, with the aim to correct hyperglycemia, the mean duration of diabetes in their case being 10 years. In the case of rats, diabetes was induced and had a short duration, the rats being subjected to spectrofluorimetric analysis immediately after induction of diabetes. The literature provides additional explanations in favor of this aspect. Knowing the difference between early glycation end products and advanced glycation end products could be a useful element. The levels of early glycation end products are deeply influenced by blood glucose concentration. Thus, these levels increase following onset of hyperglycemia, and they normalize when glucose concentration is normalized by treatment [24]. Furthermore, it was observed that with time, in chronic diabetes, these products no longer accumulate in collagen or other stable tissue proteins [25]. In any case, there is the possibility that some of these early glycation end products in collagen or long-life proteins belonging to blood vessels may not dissociate. They are subjected to other chemical reactions resulting in the generation of advanced glycation end products, with the mention that these do not normalize with the correction of hyperglycemia [24].

Our results indicated significantly greater contributions of AGEs to total serum fluorescence both in rats with induced diabetes and patients with T2DM compared to non-diabetic rats and humans. In this case, our results are supported

by other studies which associate the intensification of protein glycation, the increase in AGE formation, respectively, with the development of diabetes mellitus and diabetes complications [9, 8, 6, 44]. Comazzi et al. [8] report an increase of AGEs in the plasma of dogs with well and less well controlled diabetes compared to healthy dogs. An increase of these products was also evidenced in human subjects diagnosed with T2DM, but not T1DM, compared to the control group [26]. However, in both studies mentioned above, AGE concentrations were expressed in AU, which made impossible the comparison or correlation with other species, and the assessment of correlations with diabetes mellitus complications. An element of novelty attributed to our study is the expression of AGE contributions to total serum fluorescence in percentage units, by using the integral of the surface of the band derived from Gaussian spectral deconvolution. This allowed us to compare AGE contributions to total serum fluorescence in the two investigated species, and to assess the degree of correlation with diabetes complications in human subjects.

Regarding the contributions of KYN to total serum fluorescence, the results of our study evidenced significantly greater contributions of this metabolite in patients with T2DM compared to non-diabetic patients, while in the case of rats, significantly greater contributions of this fluorophore to total serum fluorescence were found in the control group compared to the group with streptozotocin-induced diabetes. The results obtained in the case of this TRP metabolite are controversial. Thus, higher contributions of this metabolite in humans are easy to explain; similar results suggest an association of the TRP degradation pathway to KYN and particularly, of KYN with oxidative stress, inflammation and the prevalence of cardiovascular diseases in patients with end-stage renal disease mainly due to DM [27]. These changes, i.e. a significant increase in KYN levels accompanied by a concomitant decrease in TRP levels, were attributed to altered renal function [28], or to a reduced efficiency of dialysis therapy [29]. Also, a significant increase in KYN-modified serum proteins was evidenced in the case of patients diagnosed with T2DM compared to healthy subjects, the presence of cardiovascular disease determining a significant increase in these KYNs [30]. In the case of rats, the decrease of KYN in diabetic animals compared to non-diabetic animals might be explained by the presence of a more intense KYN metabolism in the first category of rats. Thus, in diabetic rats, KYN can be rapidly metabolized through various KYN degradation pathways, with the rapid production of other metabolites. The literature describes significantly increased KYN metabolites such as xanthurenic acid and kynurenic acid in diabetic patients compared to healthy subjects [31, 32, 33]. The mechanisms through which these compounds exert their diabetogenic effect are multiple and varied. One of these mechanisms consists of the fact that these two metabolites of KYN can inhibit proinsulin

synthesis in the pancreatic cells of rats [34]. The absence of much expected significant differences in KYN concentrations between depressive patients and control subjects was also obtained in the study carried out by Myint et al. (2007) [35]. An explanation of extensive TRP degradation in the absence of increased KYN concentrations could be the rapid metabolization of KYN in the case of depressive patients. KYN is further metabolized very rapidly either through the toxic quinolone pathway, generating intermediate products such as 3-hydroxykynurenine, 3-hydroxyanthranilate and finally, quinolonic acid, or through the KYN pathway, with the neuroprotective kynurenic acid as the final metabolite [36, 37].

CONCLUSIONS

In conclusion, it can be said that in human subjects with T2DM as well as in diabetic rats, there is a significant increase in the contributions of AGEs and KYN to total serum fluorescence compared to control groups. The calculation of the ratio of the fluorophore compounds evidenced a significant correlation of this ratio with serum triglyceride levels in humans and with serum glucose levels in rats. By far, the most important result of this study is the identification of this ratio - AGEs/KYN as a predictive factor for the development of PNP in the case of human subjects. Thus, a new potential biomarker for the presence of diabetic PNP is proposed.

EXPERIMENTAL SECTION

1. Biological Material – Rats

We used 10 Wistar rats with a weight between 250 and 300 g. The rats were kept in two stainless steel cages, each cage accommodated 5 rats, and each rat was well individualized. Throughout the study, the rats were maintained under standard environmental conditions: temperature 24±5°C, light/dark cycle (12h/12h), relative humidity 60±4%, free access to food and water during the entire period of investigation. The same rats were used in the first and the second part of the study, after induction of diabetes. All procedures used in this experiment were in accordance with Romanian laws regarding correct manipulation of laboratory animals, and the entire experimental procedure was approved by the Ethics Committee of the University of Agricultural Sciences and Veterinary Medicine in Cluj-Napoca, Romania.

1.1. Blood Collection and Biochemical Determinations

Blood samples (0.2 ml) from the orbital sinus of healthy rats and rats with streptozotocin-induced diabetes were collected in 0.5 ml Eppendorf tubes. Subsequently, the samples were subjected to centrifugation (1000 g for 10 min) in order to obtain blood serum. Glycemia was assessed immediately after sample collection using routine laboratory methods (Hitachi, Roche Diagnostics). Immediately after centrifugation of blood samples, 4 µL blood serum were used for spectrofluorimetric analysis.

1.2. Induction of Diabetes

For induction of diabetes in rats, 60 mg/kg streptozotocin (Sigma, Aldrich) were injected intraperitoneally. Streptozotocin induces diabetes in 1 to 4 days by destruction of insulin-producing pancreatic cells [38]. Hyperglycemia (>300 mg/dl) was detected within 3 days of streptozotocin administration. Rats with glucose values higher than 300 mg/dl were considered diabetic [39].

2. Biological Material – Human Subjects

2.1. Selection of Subjects

This observational study included 66 subjects. Thus, 52 T2DM patients who presented to the Center for Diabetes, Nutrition and Metabolic Diseases in Cluj-Napoca, Romania, from July 2013 to February 2014 were enrolled. The exclusion criteria for the patients included in the study were the following: unstable cardiovascular disease, kidney failure, liver failure, inflammatory diseases, malignant diseases or depressive disorders. The information regarding the patients' personal data was collected using a questionnaire (age, sex, smoking or non-smoking status). T2DM was diagnosed according to the criteria of the American Diabetes Association [40]. The presence of chronic diabetes complications (retinopathy, neuropathy, chronic renal disease, cardiovascular disease) was established by accessing the patients' medical files. The control group, including patients without diabetes or not meeting the above mentioned criteria (n=14), was selected from the Department of Internal Medicine, Medical Clinic I, Clinical Emergency Hospital Cluj-Napoca, Romania.

According to the World Medical Association's Declaration of Helsinki revised in Edinburgh, 2000, and institutional guidelines, the protocol used in this experiment was approved by the Ethics Committee of the "Iuliu Haţieganu" University of Medicine and Pharmacy in Cluj-Napoca, Romania. All participants were aware of the experimental nature of the study and gave their written consent before any study procedure.

2.2. Biochemical Determinations

The blood samples were collected in the morning, before medical examination, after a night of alimentary rest. Glycated hemoglobin, glycemia, cholesterol, triglycerides, HDL cholesterol, creatinine, transaminase were evaluated immediately, using commercially available methods (Hitachi, Roche Diagnostics). A blood sample was taken from each subject and was subsequently subjected to centrifugation, the serum obtained being stored at -80°C until spectrofluorimetric analysis.

3. Spectrofluorimetric Determination of AGEs and KYN

In order to compare and determine the contributions of AGEs and KYN to total serum fluorescence, the blood serum taken from 10 healthy rats and 14 non-diabetic human subjects, as well as from 10 rats with streptozotocin-induced diabetes and 52 patients with T2DM was assessed by spectrofluorimetry. To obtain a good emission spectrum using a minimal blood serum amount, all serum samples were diluted with physiological serum (NaCl 0.9%), in a ratio of 1:500 [41]. Fluorescence intensity was recorded at a maximum emission of ~ 435 nm for AGEs [42, 6] and ~ 485 nm for KYN [43], after an excitation at 370 nm (JASCO FP-8200 spectrofluorimeter). Wavelength accuracy was ±2 nm. The data obtained were processed using the Origin Pro 8.1 software. The relative contribution of AGEs and KYN to total serum fluorescence was established following calculation of the integral of bands derived from Gaussian spectral deconvolution (Figure 3). Thus, using the Gaussian deconvolution

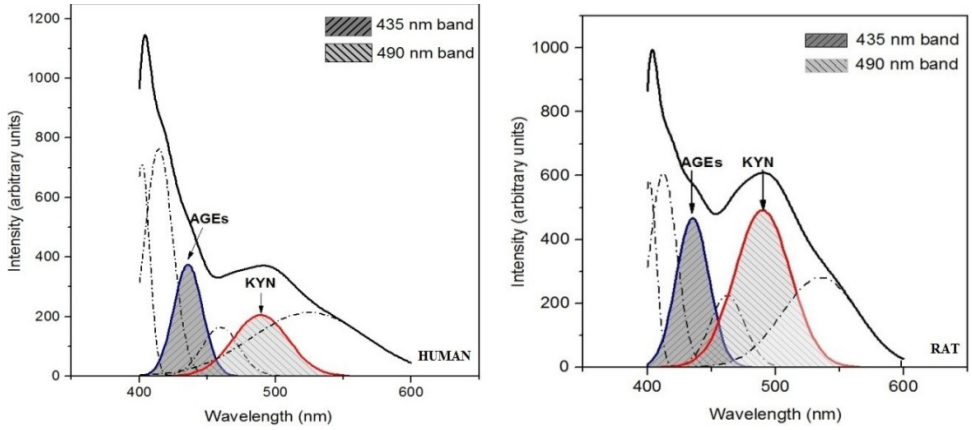

Figure 3. Deconvolution of the serum emission spectrum belonging to a patient with type 2 diabetes mellitus and a rat with streptozotocin-induced diabetes. Representation of Gaussian band components: advanced glycation end products (435 nm) and kynurenine (490 nm), along with the experimental spectrum obtained by spectrofluorimetric analysis.

algorithm as part of the peak analysis option, we carried out deconvolutions of the obtained spectra. Both in humans and rats, we used a combination of six Gaussian bands, whose peak position and width at maximum height were well established, while intensity was allowed to vary so as to match the experimental line shape of the spectra [42]. In the literature, there is currently no dependence function between the integral of the surface of bands derived from Gaussian spectral deconvolution and the total number of AGE and KYN molecules. Thus, for a better quantification of AGE and KYN contributions to total serum fluorescence, we chose to calculate the ratio between the two classes of compounds (AGEs/KYN).

4. Statistical Analysis

Statistical analysis was performed with the SPSS software, the version 22. The Kolmogorov-Smirnov test was used to check for the normality of variable distribution. The mean and standard deviation characterized continuous data with normal distribution. Non-parametric data were characterized by using the median and interquartile range. Dichotomous and categorical data were expressed in absolute and percentage values. The Mann-Whitney test was employed to compare the groups of variables whose data were not normally distributed. Pearson's correlation coefficient was used to assess correlations between parametric variables, and Spearman's correlation coefficient for non-parametric variables. The test used for associations was χ^2; the measure of associations was studied using the contingency coefficient. Also, Fisher's test was employed as an alternative to χ^2. According to the null hypothesis, there was no association between characteristics. The predictive value of the AGEs to KYN ratio regarding the presence of diabetic polyneuropathy (PNP) was studied via ROC (receiver operating characteristic) curves. All results were considered statistically significant at a p value < 0.05.

Limitations

As it can be seen, there are some interesting results in this study, but there are also some limitations. A first limitation would be diet and physical activity, which were not well monitored in this study. This might influence the results obtained; however, the presence of significant differences between diabetic and non-diabetic patients regarding the analyzed compounds excludes the major contribution of these two elements to the results obtained. Another aspect would be the cross-sectional nature of our study. A study designed and carried out over a longer time period could provide more specific causal relationships between AGEs, KYN and the other investigated variables. Finally,

inflammation might play an important role in identifying these relationships between the investigated fluorophores and endothelial dysfunctions present in the case of diabetic patients. We mention the fact that in this study, inflammation markers such as C-reactive protein, interleukin-6 or tumor necrosis factor were not measured. In the future, we propose to conduct further studies in this direction, for the identification of potential mechanisms.

Conflict of Interest: The authors declare that they have no conflict of interest.

Research involving human participants and/or animals

1) *Statement of human rights*

All procedures performed in studies involving human participants were in accordance with the ethical standards of the local Ethics Committee of the "Iuliu Haţieganu" University of Medicine and Pharmacy in Cluj-Napoca, Romania and with the 1964 Helsinki declaration and its later amendments or comparable ethical standards.

2) *Statement on the welfare of animals*

All procedures were in accordance with Romanian laws and approved by the local Ethical Committee of University of Agricultural Sciences and Veterinary Medicine in Cluj-Napoca, Romania.

Informed consent: Informed consent was obtained from all individual participants included in the study.

REFERENCES

1. International Diabetes Federation, Diabetes Atlas, 7th ed., **2015**, International Diabetes Federation, Brussels.
2. L.E. Egede, C. Ellis, *Diabetes Research Clinical Practice*, **2010**, *87*, 302.
3. S.D. Aja, The state of Pet Health **2016** Report, Benfield Pet Hospital's 2016; Section One: 12-14.
4. C.D. Geddes, J.R. Lakowicz, Reviews in Fluorescence, Springer US., **2006**;
5. I. Sadowska-Bartosz, S. Galiniak, G. Bartosz, *Molecules*, **2014**, *19*, 18828.
6. S.A. Bhat, A. Sohail, A.A. Siddiqui, B. Bano, *Journal of Fluorescence*, **2014**, *24*, 1107.
7. P. Gkogkolou, M. Böhm, *Dermatoendocrinological*, **2012**, *4*, 259.
8. S. Comazzi, W. Bertazzolo, U. Bonfanti, V.S.P. Spagnolo, *Research in Veterinary Science*, **2008**, *84*, 341.
9. A. Senfeld, Z. Pavlíček, *Journal of Fluorescence*, **1993**, *3*, 219.

10. A. Zinellu, S. Sotgia, A.A. Mangoni, M. Sanna, A.E. Satta, C. Carru, *Nutrition. Metabolism and Cardiovascular Diseases*, **2015**, *25*,153.
11. F. Bartoli, G. Carrà, C. Crocamo, D. Carretta, D. La Tegola, T. Tabacchi, P. Gamba, M. Clerici, *International Journal of Geriatric Psychiatry*, **2016**, *31*, 829.
12. R. Herrera, G. Manjarrez, J. Hernandez, *Nutrition Neuroscience*, **2005**, *8*, 57.
13. G.Z. Réus, K. Jansen, S. Titus, A.F. Carvalho, V. Gabbay, J. Quevedo, *Journal of Psychiatric Research*, **2015**, *68*, 316.
14. A. Negre-Salvayre, R. Salvayre, N. Augé, R. Pamplona, M. Portero-Otín, *Antioxidants and Redox Signaling*, **2009**, *11*, 3071.
15. V.P. Singh, A. Bali, N. Singh, J.A. Singh, *Korean Journal of Physiology and Pharmacology*, **2014**, *18*, 1.
16. R. Wada, Y. Nishizawa, N. Yagihashi, M. Takeuchi, Y. Ishikawa, K. Yasumura, M. Nakano, S. Yagihashi, *European Journal of Clinical Investigation*, **2001**, *31*, 513.
17. K Sugimoto, Y Nishizawa, S Horiuchi, S. Yagihashi, *Diabetologia*, **1997**, *40*, 1380.
18. J.W. Baynes, S.R. Thorpe, *Diabetes*, **1999**, *48*, 1.
19. R. Wada, S. Yagihashi, *Annals of the New York Academy of Sciences*, **2005**, *1043*, 598.
20. R. Bucala, Z. Makita, T. Koschinsky, A. Cerami, H. Vlassara, *Proceedings of the National Academy of Sciences of the United States of America*, **1993**, *90*, 6434.
21. J.B. Chang, N.F. Chu, J.T. Syu, A.T. Hsieh, Y.R. Hung, *Lipids Health Disease*, **2011**, *10*, 228.
22. K.A. Polyzos, D.F. Ketelhuth, *Hamostaseologie*, **2015**, *35*, 128.
23. L. Zhang, O. Ovchinnikova, A. Jönsson, A.M. Lundberg, M. Berg, G.K. Hansson, D.F. Ketelhuth, *European Heart Journal*, **2012**, *33*, 2025.
24. M. Brownlee, A. Cerami, H. Vlassara, *The New England Journal of Medicine*, **1988**, *318*, 1315.
25. V. Vishwanath, K.E. Frank, C.A. Elmets, P.J. Dauchot, V.M. Monnier, *Diabetes,* **1986**, *35*, 916.
26. M. Kalousová, J. Skrha, T. Zima, *Physiological Research*, **2002**, *51*, 597.
27. K. Pawlak, T. Domaniewski, M. Mysliwiec, D. Pawlak, *Atherosclerosis,* **2009**, *204*, 309.
28. D. Pawlak, A. Tankiewicz, T. Matys, W. Buczko, *Journal of Physiology and Pharmacology*, **2003**, *54*, 175.
29. D. Pawlak, K. Pawlak, J. Malyszko, M. Mysliwiec, W. Buczko, *International Urology and Nephrology*, **2001**, *33*, 399.
30. M.A. Ahmadou, S.M. Joha, *International Journal of Academic Scientific Research*, **2015**, *3*, 101.
31. M. Hattori, Y. Kotake, Y. Kotake, *Acta Vitaminologica et Enzymologica*, **1984**, *6*, 221.
32. A.D. Patterson, J.A. Bonzo, F. Li, K.W. Krausz, G.S. Eichler, S. Aslam, X. Tigno, J.N. Weinstein, B.C. Hansen, J.R. Idle, F.J. Gonzalez, *The Journal of Biological Chemistry*, **2011**, *286*, 19511.
33. G. Oxenkrug, *Molecular Neurobiology*, **2013**, *48*, 294.
34. Y. Noto, H. Okamoto, *Acta Diabetologica Latina*, **1978**, *15*, 273.

35. A.M. Myint, Y.K. Kim, R. Verkerk, S. Scharpé, H. Steinbusch, B. Leonard, *Journal of Affective Disorders*, **2007**, *98*, 143.
36. D.A. Bender, G.M. McCreanor, *Biochemical Society Transactions,* **1985**, *13*, 441.
37. A. Chiarugi, M. Calvani, E. Meli, E. Traggiai, F. Moroni, *Journal of Neuroimmunology*, **2001**, *120*, 190.
38. A. Akbarzadeh, D. Norouzian, M.R. Mehrabi, S. Jamshidi, A. Farhangi, A.A. Verdi, S.M.A. Mofidian, B.L. Rad, *Indian Journal of Clinical Biochemistry*, **2007**, *22*, 60;
39. Y.S. Kim, N.H. Kim, S.W. Lee, Y.M. Lee, D.S. Jang, J.S. Kim, *European Journal of Pharmacology*, **2007**, *569*, 171.
40. A.D. Association, Classification and diagnosis of diabetes, *Diabetes Care*, **2015**, *38*, S8.
41. G. Münch, R. Keis, A. Wessels, P. Riederer, U. Bahner, A. Heidland, T. Niwa, H.D. Lemke, D. Schinzel, *European Journal of Clinical Chemistry and Clinical Biochemistry*, **1997**, *35*, 669.
42. D.M. Ciobanu, L.E. Olar, R. Stefan, I.A. Veresiu, C.G. Bala, P.A. Mircea, G. Roman, *Journal of Diabetes and its Complications*, **2015**, *29*, 893.
43. W.G. Lesniak, A. Jyoti, M.K. Mishra, N. Louissaint, R. Romero, D.C. Chugani, S. Kannan, R.M. Kannan, *Analitical Biochemistry*, **2013**, *443*, 222.
44. L.E. Olar, R. Stefan, C. Berce, D. Ciobanu, I. Papuc, *Bulletin of University of Agricultural Sciences and Veterinary Medicine Cluj-Napoca. Veterinary Medicine*, **2015**, *72*, 106.

STUDIA UBB CHEMIA, LXIII, 1, 2018 (p. 55-62)
(RECOMMENDED CITATION)
DOI:10.24193/subbchem.2018.1.04

VARIABILITY IN BIOCHEMICAL COMPOSITION OF MILK AMONG THREE REPRESENTATIVE BREEDS OF DAIRY COWS FROM ROMANIA

RADU SILAGHI-DUMITRESCU[a*], NICOLETA TOMOIAGA[a], EUGEN JURCO[b]

ABSTRACT. Reported here is a comparative analysis of the milk from three representative breeds of dairy cows from Romania – Maramures Brown (Brună de Maramureş), Romanian Spotted (Bălțata Românească) and Black Spotted Romanian (Bălțata cu Negru Românească) - in terms of SDS-PAGE analysis of the protein distribution, total contents of protein, lipids, lactose, dry substance, somatic cell counts, pH and yield of milk. The Maramures Brown displays the highest percentage of proteins and of dry matter, the lowest yield of milk, the highest amounts of α-lactalbumin and β-lactoglobulin (tied with the Spotted Romanian for the latter) and the lowest serum albumin and immunoglobulin. The Black Spotted Romanian shows the highest yield of milk, the highest content of lactose, the lowest content in lipids and protein and dry matter, the highest content of casein and BSA, and the lowest content of α-lactalbumin and immunoglobulin. The Spotted Romanian shows the highest content of lipids, the highest SSC and the highest proportion of lactoferrin. Positive correlations with r values at 0.6-0.8 are found between the relative contents of various components - α vs. β casein, Ig vs. α casein, Ig vs. βLgb, lactoglobulin vs. lactalbumin, β casein and αLac, BSA vs. β casein and αLac, total protein content vs. dry residue, SSC vs. lactoferrin and β casein. A weak negative correlation is seen between the total lipid content and lactose (-0.6).

Keywords*: milk, SDS-PAGE, protein, casein, whey*

[a] *Babes-Bolyai University, Faculty of Chemistry and Chemical Engineering, RO-400028, Cluj-Napoca, Romania.*
[b] *University of Agricultural Sciences and Veterinary Medicine RO-400372, Cluj-Napoca, Romania.*
[*] *Corresponding author: rsilaghi@chem.ubbcluj.ro*

INTRODUCTION

Of obvious practical interest, chemical variability in milk is traditionally confined to standard compulsory analyses such as yield of milk, total protein content, lactose, pH and others – with occasional incursions into such details as the variability in protein distribution and/or variability within or among races.[1–14] In terms of the relative content of various proteins within the milk, the studies are typically confined to a small number of the major proteins (caseins, lactalbumin and lactoglobulin especially), either analyzed qualitatively with gel electrophoresis or, with even narrower focus on variations such as glycosylation and alleles, quantitatively with more advanced chromatographic techniques. Other studies, in terms of genetic variability or of technological parameters (mainly yield of milk) are also available.[1–4,6,8,15]

Of the proteins in whole milk, by far the most abundant ones are the caseins (α S1, α S2, β, k, all at cca 25-30 kDa and with α and β much more abundant than k), α-lactalbumin (αLac, 14 kDa), and β-lactoglobulin (βLgb, 18 kDa). All other proteins except casein are generally also referred to as whey proteins; these include α-lactalbumin and β-lactoglobulin as the dominant components, plus a number of others among which bovine serum albumin (BSA, ~68 kDa), lactoferrin (Lf, ~80 kDa depending on the degree of glycosylation) and immunoglobulin A (~70 kDa for the heavy chain, ~15 kDa for the light chain; other immunoglobulins are at 160-1000 kDa) are typically discussed – though often inconsistently assigned in SDS-PAGE analyses.[1,2,4,5,8,10–12,15–18]

A number of studies have been reported on the variability of a limited number of components within the milk of dairy cows from a small set of regions (e.g., Holland and European Northern regions, or Bulgaria).[2,4,8] To our knowledge there is not, at this time, a detailed study dedicated to the chemical composition (and variability thereof) in the milk of dairy cows endemic/specific to Romania. The three most common dairy cattle breeds in Romania are Maramures Brown (Bruna, the result of crossing between the Grey Romanian Cattle native breed with Schwyz), Romanian Spotted (Bălțata Românească, the result of crossing between the Grey Romanian Cattle native breed with Simmental bulls) and Black Spotted Romanian (Bălțata cu Negru Românească, evolved more recently from Dobrogean Red, Romanian Spotted and Brown).[9,13,18] Milk from these breeds is analyzed in the present study in terms of SDS-PAGE analysis of the protein distribution, total contents of protein, lipids, lactose, dry substance, somatic cell counts, pH and yield of milk. Also reported here is to our knowledge the first example of comparative quantitative SDS-PAGE analysis of milk samples from various breeds, as well as an analysis of the correlations between various parameters.

RESULTS ANS DISCUSSION

Samples from 15 animals (five each from the respective races - Maramures Brown B, Romanian Spotted RS and Black Spotted Romanian BSR), all housed under similar conditions at a farm representative for the northwestern part of Romania (Transylvania) - were analyzed for total contents of protein, lipids, lactose, dry substance, somatic cell counts, pH as standard parameters assayed in dairy farms. Table 1 shows the average values of these indicators for the three races. At the outset, one may note that the standard deviation values are generally larger than the differences in values among races. Nevertheless, one may note that on average the Brown shows the highest protein content (implicitly the highest content of dry substance) and the lowest content in lactose as well as the lowest yield of milk. The Romanian Spotted shows the highest content of lipids. The Black Spotted Romanian shows the highest content in lactose and the lowest content in lipids and protein alongside the highest yield of milk. The urea and SSC parameters are generally indicative the well-being of the animal (urea for nutrition, SSC for possible infection) - and fall within normal parameters in the present dataset.

Table 1. Average values (with standard deviations in parentheses) for total contents of lipids, protein, lactose, dry residue (excluding lipids) (all expressed in g/100 g), pH, urea (mg/mL), somatic cell count SCC (per mL, x1000) and yield of milk (L/session) for the three races (Brown B, Spotted Romanian SR, and Black Spotted Romanian BSR). The complete set of individual values is available as Supporting Information. The lowest and highest values for each parameter are highlighted in bold and grey, respectively.

Race	Lipids	Protein	Lactose	dry	pH	Urea	SSC	yield
B	4.02 (0.66)	**3.88 (0.27)**	4.63 (0.25)	**9.28 (0.30)**	6.62 (0.09)	4.90 (2.97)	71.5 (38.7)	6.7 (1.3)
BSR	3.80 (0.69)	3.52 (0.26)	**4.84 (0.10)**	9.16 (0.26)	6.58 (0.07)	3.04 (1.73)	77.6 (51.2)	**8.9 (1.0**)
SR	**4.14 (0.27)**	3.67 (0.35)	4.70 (0.11)	9.18 (0.33)	6.59 (0.08)	**6.98 (2.91)**	240.4 (264.9)	7.6 (1.0)

Figure 1 shows the results of SDS-PAGE measurements of the three types of milk. Using an automated analysis, 14 bands were identified across the 18 lanes of milk in Figure 1 – though not all bands display detectable values in all lanes. Table 2 shows the intensities of the bands, computed from two types of measurements – either from the gels of the three samples each representing mixtures of milk from five animals, or as average of the values measured form gels of each of the respective individuals, per race.

Based on previous data,[2–5,15,17] one may assign the two most abundant proteins (lanes 8 and 9 amounting to more than 50% of the protein) to α and β casein (calculated MW at 26 and 23 kDa, respectively) – with k-casein in lane 10 (calculated MW at 21 kDa). Regardless of the mode of measurements (whether directly on mixtures of milk from cows of the same breed, or by averaging the values measured individually for each cow of the same breed), Romanian Black Spotted appears to show more casein (especially α) than the other two races. Next, one may also assign bands 13 and 14 to lactoglobulin (βLgb, at an apparent MW of 15 kDa) and lactalbumin (αLac, 14 kDa), respectively. There is a clear trend B>BSR>RS for βLgb and B~SR>BSR for αLac. The remaining proteins are, as discussed above, inconsistently assigned in the literature. As shown in Table 2, we propose to assign lane 4 to BSA (typically the strongest band in the 50-130 kDa range in milk, computed here at 71 kDa), lane 3 to lactoferrin (Lf, 108 kDa) and lane 5 to the heavy chain of immunoglobulin A (Ig, 62 kDa). If so, then BSA appears more abundant in BSR than in the other two races (with RS then slightly higher than B), while RS shows distinctly more Lf than the other two races. The Ig values are very similar across the three races, with BSR showing slightly lower values than the other two.

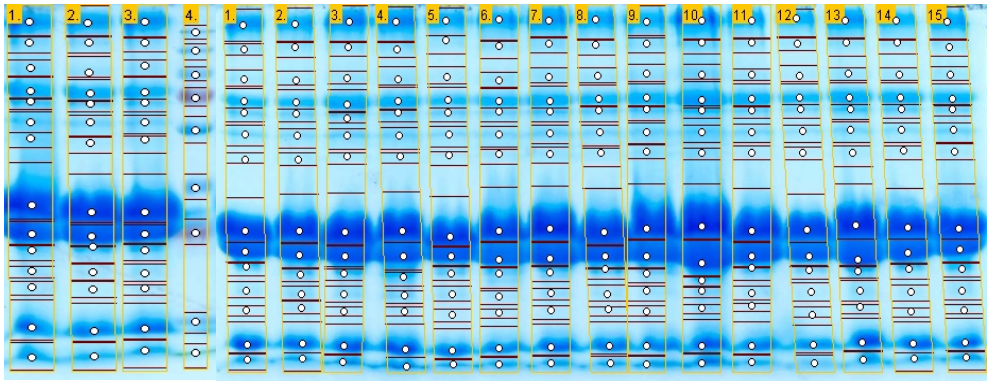

Figure 1. SDS-PAGE gels of milk. The left panel shows samples of equi-volumetric mixtures of the 5 samples of milk from Spotted Romanian (lane 1), Black Spotted Romanian (lane 2), and Brown (lane 3), alongside molecular weight markets (lane 4, with values in kDa in ascending order as follows: 10, 15, 25, 35, 55, 75, 100, 130, 250). The right panel shows individual samples from the 15 animals (B – 1-5, SR – 6-10, BSR – 11-15).

Table 2. Values for the intensities of the 14 protein bands (shown as percentages of the sum of intensities over each respective lane) in the SDS-PAGE of milk. In each cell, the averages of individual values for the animals of the same race and those measured for mixtures of milk from the five animals of the respective race cf Figure 1 are shown, in this order. Molecular weights (MW) were estimated based on the molecular weight markers indicated in Figure 1 using the fitting function $y = 13.095 * x^{(-1.173)}$. The complete set of individual values is available as Supporting Information.

Protein	**1**	**2**	**3**	**4**	**5**	**6**	**7**	**8**	**9**	**10**	**11**	**12**	**13**	**14**
MW (kDa)	*473*	*186*	*108*	*71*	*62*	*50*	*42*	*26*	*23*	*21*	*19*	*18*	*15*	*14*
	15	1.2	0.54	6.8	2.1	2.0	0.14	32	19	2.5	0.65	0.07	13	5.0
B	13	1.1	0.4	6.5	1.7	1.3	0.27	32	17	3.0	0.44	0.13	15	7.5
	12	0.8	0.44	7.6	2.0	1.4	0.16	35	21	2.5	0.36	0.01	12	4.6
BSR	11	1.4	0.5	7.3	1.4	1.6	0.14	33	19	3.3	0.17	0.05	14	6.9
	14	1.2	0.77	7.1	2.1	1.5	0.31	34	21	2.2	0.28	0.04	11	4.8
RS	15	1.5	0.8	6.6	1.4	1.3	0.33	31	18	1.9	0.15	0.10	13	7.7

Table 3 shows correlation coefficients across all the values measured in the present study. A general lack of correlation between the 14 proteins observed in the SDS-PAGE gels can be reconciled with the concept that there is indeed complex variability in terms of protein composition across the races. Some correlations were perhaps expected and are observed as such. For instance, bands 8 and 9 (α and β casein) show a positive correlation coefficient of ~0.8. For the two key components of whey, βLgb and αLac (lanes 13 and 14), the correlation coefficient is 0.7. There are also a 0.7 correlation coefficients between Ig and α casein and Ig and βLgb, respectively (plus a slightly weaker correlation, at 0.6, between β casein and αLac. BSA shows correlation with β casein (0.7) as well as with αLac (0.6). Also, expectedly, there is positive correlation (0.8) between the total protein content and the dry residue. A weak negative correlation is seen between the total lipid content and lactose (-0.6). The somatic cell count shows a 0.6 correlation coefficient with lactoferrin (to some extent expectedly given their function in defense/immunity) as well as with β casein. The amount of milk shows very little correlation with any of the parameters; the highest value, ~0.5, is seen with BSA.

CONCLUSIONS

The main three races of local dairy cows from a representative farm in northwestern Romania (Maramures Brown, Spotted Romanian and Black Spotted Romanian) were analyzed in terms of the yield and composition of the milk (SDS-PAGE analysis of the protein distribution, total contents of protein, lipids, lactose, dry substance, somatic cell counts, pH). The differences between the races are small but may be summarized as follows.

The Maramures Brown (Bruna) stands out with the highest percentage of proteins and of dry matter, but the lowest yield of milk. In terms of the percentages of proteins (as determined from SDS-PAGE analyses), this race also shows the highest amounts of α-lactalbumin and β-lactoglobulin (tied with the Spotted Romanian for the latter) but lowest serum albumin and immunoglobulin.

The Black Spotted Romanian (Bălțata cu Negru Românească) shows the highest yield of milk and the highest content of lactose, offset by the lowest content in lipids, protein and dry matter. In terms of relative contributions of the various proteins, BSR shows the highest content of casein and BSA – as opposed to the lowest content of α-lactalbumin and immunoglobulin.

The Spotted Romanian (Bălțata Românească) shows the highest content of lipids, the highest SSC and the highest proportion of lactoferrin.

Positive correlations with r values at 0.6-0.8 are found between the relative contents of various components - α vs. β casein, Ig vs. α casein, Ig vs. βLgb, lactoglobulin vs. lactalbumin, β casein and αLac, BSA vs. β casein and αLac, total protein content vs. dry residue, SSC vs. lactoferrin and β casein.

Table 3. Correlation coefficients (Pearson's r) among the Table 1 and Table 2 data measured for the 15 milk samples from the three races (see Supporting Information for individual values of each parameter). The r values at ~0.6 of higher are highlighted.

	Lip	Pro	Lac	dry	pH	Ure	SC	1	2	3	4	5	6	7	8	9	10	11	12	13	14	yield
Lip	1.00	0.28	**-0.58**	-0.08	-0.54	0.21	0.16	-0.04	0.25	0.35	-0.46	-0.39	-0.12	0.01	-0.32	-0.18	-0.23	0.00	0.16	-0.10	0.03	-0.27
Pro	0.28	1.00	-0.46	**0.78**	-0.10	0.01	-0.28	**0.66**	0.53	-0.12	0.04	0.13	**0.69**	0.40	-0.05	-0.36	0.34	0.50	0.11	0.38	0.22	-0.37
Lac	**-0.58**	-0.46	1.00	0.20	0.52	-0.49	-0.20	-0.31	-0.37	-0.20	0.03	0.00	-0.29	-0.06	0.04	-0.10	0.14	-0.28	-0.49	-0.45	-0.52	0.30
dry	-0.08	**0.78**	0.20	1.00	0.28	-0.40	-0.42	0.53	0.37	-0.21	0.07	0.14	0.55	0.42	-0.02	-0.45	0.49	0.34	-0.24	0.09	-0.10	-0.20
pH	-0.54	-0.10	0.52	0.28	1.00	-0.29	0.10	0.34	0.12	0.33	0.33	0.39	0.34	-0.18	-0.01	0.06	0.32	-0.08	-0.28	0.04	-0.02	-0.05
Ure	0.21	0.01	-0.49	-0.40	-0.29	1.00	0.39	0.27	0.14	0.19	-0.11	-0.07	0.11	0.14	-0.01	0.12	0.04	-0.15	0.46	-0.02	0.15	-0.32
SC	0.16	-0.28	-0.20	-0.42	0.10	0.39	1.00	0.15	0.20	**0.61**	0.39	0.21	-0.07	-0.01	0.15	**0.60**	-0.10	-0.54	0.15	0.04	0.51	0.16
1	-0.04	**0.66**	-0.31	0.53	0.34	0.27	0.15	1.00	**0.66**	0.22	0.40	0.50	**0.81**	0.38	0.26	0.10	0.54	0.21	-0.16	0.51	0.51	-0.31
2	0.25	0.53	-0.37	0.37	0.12	0.14	0.20	**0.66**	1.00	0.43	0.19	0.24	0.45	0.38	0.26	0.14	0.09	0.36	-0.13	0.22	0.49	-0.31
3	0.35	-0.12	-0.20	-0.21	0.33	0.19	**0.61**	0.22	0.43	1.00	0.22	0.10	0.11	-0.08	-0.04	0.35	-0.19	-0.38	-0.10	-0.08	0.31	-0.06
4	-0.46	0.04	0.03	0.07	0.33	-0.11	0.39	0.40	0.19	0.22	1.00	0.54	0.49	0.17	0.52	**0.66**	0.08	-0.31	-0.23	0.33	**0.61**	0.52
5	-0.39	0.13	0.00	0.14	0.39	-0.07	0.21	0.50	0.24	0.10	0.54	1.00	0.44	0.36	**0.68**	0.59	0.35	-0.06	-0.18	**0.73**	0.49	-0.24
6	-0.12	**0.69**	-0.29	0.55	0.34	0.11	-0.07	**0.81**	0.45	0.11	0.49	0.44	1.00	0.08	0.05	-0.04	0.42	0.31	-0.13	0.57	0.42	-0.25
7	0.01	0.40	-0.06	0.42	-0.18	0.14	-0.01	0.38	0.38	-0.08	0.17	0.36	0.08	1.00	**0.62**	0.29	0.36	-0.15	-0.10	0.04	0.11	-0.12
8	-0.32	-0.05	0.04	-0.02	-0.01	-0.01	0.15	0.26	0.26	-0.04	0.52	**0.68**	0.05	**0.62**	1.00	**0.77**	0.15	-0.18	-0.14	0.37	0.51	0.10
9	-0.18	-0.36	-0.10	-0.45	0.06	0.12	**0.60**	0.10	0.14	0.35	**0.66**	0.59	-0.04	0.29	**0.77**	1.00	-0.05	-0.51	-0.04	0.27	**0.62**	0.29
10	-0.23	0.34	0.14	0.49	0.32	0.04	-0.10	0.54	0.09	-0.19	0.08	0.35	0.42	0.36	0.15	-0.05	1.00	0.15	-0.19	0.31	0.13	-0.41
11	0.00	0.50	-0.28	0.34	-0.08	-0.15	-0.54	0.21	0.36	-0.38	-0.31	-0.06	0.31	-0.15	-0.18	-0.51	0.15	1.00	0.12	0.40	0.12	-0.47
12	0.16	0.11	-0.49	-0.24	-0.28	0.46	0.15	-0.16	-0.13	-0.10	-0.23	-0.18	-0.13	-0.10	-0.14	-0.04	-0.19	0.12	1.00	0.07	0.15	-0.21
13	-0.10	0.38	-0.45	0.09	0.04	-0.02	0.04	0.51	0.22	-0.08	0.33	**0.73**	0.57	0.04	0.37	0.27	0.31	0.40	0.07	1.00	**0.68**	-0.39
14	0.03	0.22	-0.52	-0.10	-0.02	0.15	0.51	0.51	0.49	0.31	**0.61**	0.49	0.42	0.11	0.51	**0.62**	0.13	0.12	0.15	**0.68**	1.00	0.01
yield	-0.27	-0.37	0.30	-0.20	-0.05	-0.32	0.16	-0.31	-0.31	-0.06	0.52	-0.24	-0.25	-0.12	0.10	0.29	-0.41	-0.47	-0.21	-0.39	0.01	1.00

The highest correlation of the yield of milk is with BSA. A weak negative correlation is seen between the total lipid content and lactose (-0.6). Beyond these, a number of other potential correlations with r values at +/- 0.4-0.5 may deserve further attention in future studies with larger sets of samples.

Further exploration of the correlations and trends reported in the present study may be warranted, partly considering the relatively large variations within the parameters collected and partly considering the prospective practical applications in terms of potential selection of breeds based on the desired composition of the milk. Such studies, including evaluation of the parameters over time/age/lactation cycle, dependence on nutrition, environmental parameters (including indoor as well as outdoor variables as well as geographical ones) and other factors are currently under way. Such studies are of particular interest given the current crisis of milk in Romania (in terms of yields, number of animals, adaptation of animals to local conditions).[14,19]

EXPERIMENTAL SECTION

Milk samples from five animals of each race were collected for analysis on the same, day, in November 2017 at the Experimental and Didactic Farm of the University of Agricultural Sciences and Veterinary Medicine at Cojocna, Cluj county, Romania. The animals were fed a uniform standard fodder (mixture of lucerne hey, maize silage and concentrates) under conditions previously described.[14]

For electrophoresis, the milk samples were centrifuged for 10 minutes at 5000 g in order to remove the lipids, after which 5 µL of milk were mixed with 35 µL of PBS buffer and 10 µL of 5x loading dyes followed by 10 minutes of 90 °C incubation. A volume of 20 µL of the obtained solution was loaded onto a 15% SDS-PAGE as previously described. After protein migration was complete, the gel was incubated in fixing buffer (45% methanol, 45% water, and 10% glacial acetic acid) for 10 minutes and then treated with staining solution (0.1% (w/v) Coomassie blue, and 10% (v/v) acetic acid, 20% (v/v) methanol overnight followed by distaining in 50% (v/v) methanol, 50% (v/v) water with 10% (v/v) acetic acid.[1,20] The SDS-PAGE gels were analyzed using the Gel Analyzer 2010a software (gelanalyzer.com).

The total contents of protein, lipids, lactose, dry substance, somatic cell counts and pH were determined by standard procedures as previously described.[6,9]

Supporting Information is available from the authors upon request (Table S1 - Individual values for total contents of components, Table S2 - Individual values of intensities/weights of the bands identified in the SDS-PAGE analyses, Figure S1 and Figure S2- Band profiles of the lanes in Figure 1).

ACKNOWLEDGEMENTS

Drs. Marioara Moldovan and Augustin C. Moț (BBU) are thanked for helpful discussions.

REFERENCES

1. D. Prodan, M. Filip, M. Moldovan, I. Perhaita, F. Scurtu, L. Silaghi-Dumitrescu, A. Dreanca, I. Marcus, *Journal of Environmental Protection and Ecology,* **2018**, in press.
2. A.K. Rosengaard, Aarhus University, **2016**.
3. F.F. Costa, M.A.V.P. Brito, M.A.M. Furtado, M.F. Martins, M.A.L. De Oliveira, P.M. Barra, L.A. de C. Garridoc, A.S. Dos Santos, *Analytical Methods,* **2014**, 1666.
4. L. Zagorchev, M. Dimitrova, M. Odjakova, D. Teofanova, P. Hristov, *Bulgarian Journal of Agricultural Sciences,* **2013**, *19*, 197.
5. S. Jovanovic, M. Barac, O. Macej, T. Vucic, C. Lacnjevac, *Sensors,* **2007**, *7*, 371.
6. V.A. Balteanu, *Bulletin UASVM Animal Science and Biotechnolologies,* **2011**, *68*, 71.
7. S.E. Georgescu, M.A. Manea, Z. Mihaela, M. Costache, *Romanian Biotechnological Letters,* **2009**, *14*, 4194.
8. R.A. Vătăsescu-Balcan, S.E. Georgescu, M.A. Manea, A. Dinischiotu, C.D. Tesio, M. Costache, *Zootehnie si Biotehnologie,* **2008**, *41*, 169.
9. G. Muresan, E. Jurco, S. Cărcu, C. Pop, *Sci. Pap. Ser. Manag. , Economic Engineering Agric Rural Development,* **2013**, *13*, 245.
10. F. Liu, M. Teodorowicz, M.A. van Boekel, H.J. Wichers, K.A. Hettinga, *Food and Function,* **2016**, *7*, 239
11. A. Nikkhah, *Journal of Nutrition and Food Science,* **2011**, *1*, 1000116.
12. E. Rojas, G. Torres, *Food Science and Technology,* **2013**, *33*, 14.
13. G. Onaciu, E.C. Jurco, L. Ognean, *Bulletin UASVM Animal Science and Biotechnology,* **2014**, *71*, 250.
14. E.C. Jurco, G. Onaciu, Z. Marchis, L. Ognean, *Bulletin UASVM Animal Science and Biotechnology,* **2016**, *73*, 243–244.
15. C.C. Chen, S.T. Chen, J.F. Hsieh, *Molecules,* **2015**, *20*, 7737–7749.
16. Neelima; R. Sharma, Y.S. Rajput, B. Mann, *Dairy Science Technology,* **2013**, *93*, 21.
17. W.L. Hurley, **2009**, Available at: http://ansci.illinois.edu/static/ansc438/Milkcompsynth/milksynth_proteinbiochem.html. (Accessed: 7th January 2018)
18. C. Velea, G. Marginean, G., *Tratat de cresterea bovinelor,* vol. 1, Editura Risoprint, **2012**.
19. A. Popescu, *Sci. Pap. Ser. Manag. Econ. Eng. Agric. Rural Dev.,* **2017**, *17*, 281.
20. M. Arkosi, F. Scurtu, A. Vulpoi, R. Silaghi-Dumitrescu, D.M. Kurtz Jr., *Artificial Cells Blood Substitutes Biotechnology,* **2017**, *45*, 218–223.

STUDIA UBB CHEMIA, LXIII, 1, 2018 (p. 63-72)
(RECOMMENDED CITATION)
DOI:10.24193/subbchem.2018.1.05

ESTER PLASTICIZERS BASED ON FATTY ACIDS FROM SOYBEAN OIL USED IN PELICULOGEN COMPOSITIONS

SORINA BORAN, SABINA NITU[a*]

ABSTRACT. In this paper is described the synthesis and characterization of esters based on soybean oil fatty acids and an assessment of their potential use as plasticizers in wood, concrete or metal paints. Esters of fatty acids were obtained in a chemical reactor with microwave heating, using soybean oil fatty acids and *n*-butanol or isopentanol in acidic conditions.

Keywords: *ester, vegetable oil, fatty acids esters, microwave reactor, peliculogen*

INTRODUCTION

Synthetic ester oils and vegetable oils are base oils in the production of adhesives with superior properties [1-5].

Processes for the synthesis of ester compounds in microwave heating reactors lead to the production of advanced purity products. Also, the use of this process has the advantage of shortening the reaction time, ultimately resulting in high reaction conversions [6-8].

Energy efficient processes and environmental friendly ones designed to replace the classical technologies are the aim of modern technologies. Reactions performed in bubble column reactors in polymerization [9-12] or in esterification processes may be considered to be environmentally protective ones and with a low energetic consumption [13]. As presented by Popa et al. [14-17] polymers synthesized in a bubble gas column reactor are ecological ones, because they do not contain residual monomer. An important technological issue is the intensification of heat transfer of all thermal processes, so the calculation of boiling heat transfer coefficients may be of high value [18-21].

[a] *Politehnica University Timișoara, Faculty of Industrial Chemistry and Environmental Engineering, Bv.V. Pârvan 6, 300223, Timișoara, România*
[*] *Corresponding author: sabina.nitu@upt.ro*

An important issue in present researches represents the negative effects of industrial activities on the environment. Some of the solutions described in literature are reducing wastes by recycling some of these materials [22-25], reusing wastes to obtain other useful products [26-27] or immobilizing other hazardous waste [28-29] and replacing of raw materials with new products.

RESULTS AND DISCUSSION

Physico-chemical properties of two types of ester products prepared by the esterification of soy bean fatty acids with *n*-butanol (P1**)** and respectively isopentanol (P2)**,** are shown in Table 1.

Table 1. Physico-chemical properties of the synthesized esters P1 și P2

Property	P1	P2
Density, ρ^{20} [kg m^{-3}]	880.5	1100.5
Refractive index, n_D^{20}	1.4545	1.4600
Viscosity, η^{20} [mPa s]	81.33	82.66
Saponification index, [mg KOH g^{-1}]	222	150
Acid number, [mg KOH g^{-1}]	< 1	< 1
Iodine index, [g I_2 100 g^{-1}]	110	111

Both products P1 and P2 have density, refractive index and viscosity values comparable to those of vegetable oils. In all cases, the acidity index is subunit. Iodine index values for the synthesized compounds are comparable to those of lower unsaturated oils.

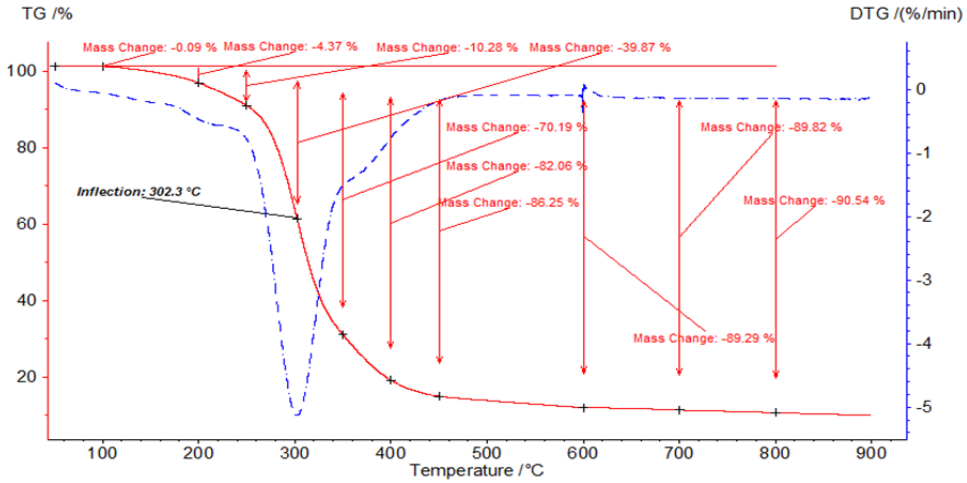

Figure 1. TG/DTG curves – P1 sample in nitrogen atmosphere

Figures 1 and 2 present the TG/DTG curves for the synthetized compounds P1 and P2 in nitrogen atmosphere.

It can be observed a good thermal behavior, where the weight loss is insignificant, up to about 200^{0}C. Above 250^{0}C, the mass loss rises as the temperature is higher. In both cases, both for compound P1 and for compound P2, total mass loss occurs above 500^{0}C.

In the case of P1 sample (figure 1) the TG curve shows a continuous mass loss process with a major loss at 302.3^{0}C, loss of 39.87% and a maximum of 90.54% at 800^{0}C.

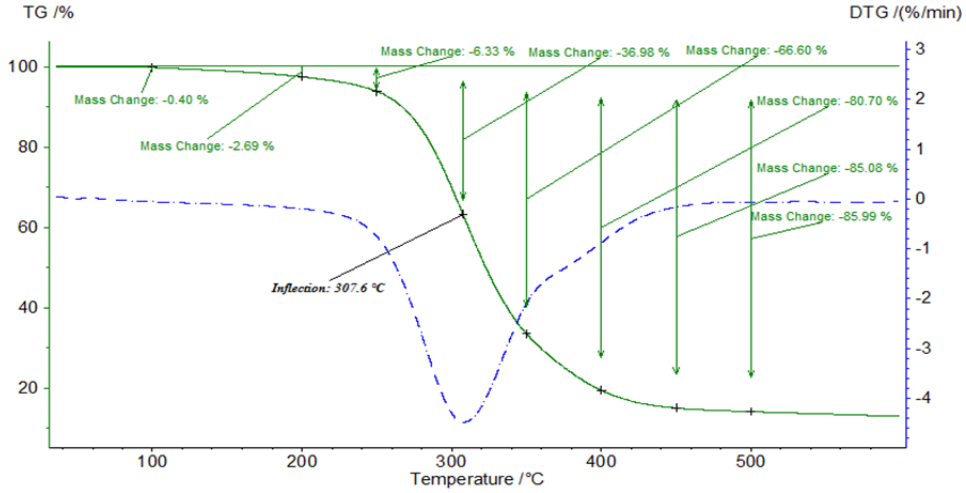

Figure2. TG/DTG curves - P2 sample in nitrogen atmosphere

Table 2. Characteristics for coatings type composites based on nitrocellulose based films obtained with the synthesized ester products P1, P2

Technical characteristics	**Sample**		
	1	**2**	**3**
For the liquid product			
Aspect	VOF	VOF	VOF
Content in nonvolatile subst., 2 h, 120^{0}C, %	38	42	42
Leakage time, cup DIN 4 mm, 20^{0}C, sec.	50	52	53
Density, 20^{0}C, gr/cc	1050	1051	1052
Fine friction, microns	15	15	15
Film			
Aspect	HF	HF	HF
Drying time, D type, at 20^{o}C, h	0.5	1	1
Erichsen elasticity, mm	7.2	7.6	7.8
Adherence, grid 2 mm, grip figure	2	2	2
Flexibility, mm	3	3	3
Thickness of the dry film, μm	20	20	20
Resistance to hit-directly, 0.5 kgf/cm^2	25	30	35
Persozhardness, sec	153	131	130
Degree of gloss angle 60^0, %	70	75	71

VOF– Viscous HomogeneFluid, HF –Homogene Film

Analogue to sample P1, the sample P2 (figure 2) on the TG curve also shows a continuous mass loss process with a major loss at 307.6^{0}C, of 36.98% and a maximum of 85.99% at 500^{0}C.

After characterization from the physico-chemical point of view of an organic substance, the synthesized esters were analyzed as plasticizers in nitrocellulose-based films and chlorinated rubber lacquer-based films compositions.

Table 2 presents the analytical values for coatings type composites based on nitrocellulose-based films obtained with the synthesized products.

The samples evaluated were based on nitrocellulose films, introducing the P1 and P2 synthesized products as follows:

- sample 1: contains only primary plasticizer (di-2-ethylhexyl phthalate) (1.87%), with no content of P1 or P2;
- sample 2: besides the primary plasticizer, contains 6.25% P1;
- sample 3: besides the primary plasticizer, contains 6.25% P2,
- P1 and P2 have the role of secondary plasticizers.

Nitrocellulose based films have the following composition: nitrocellulose (17%), resin CSM45 (13%), titanium (20%), di-2-ethylhexyl phthalate (1.87%), nitro diluent (48.13).

Interpretation of results:

For the liquid product: the appearance of the samples is of a viscous homogeneous fluids; the content of non-volatile substances is slightly increased at samples 2 and 3, respectively, against the control sample (sample 1); the leakage time is only slightly modified in the samples where the synthesized products were added, ranging from the standard range: 45-80 s; The density of samples with the addition of plasticizers (secondary) - P1 and P2 - does not change essentially; Addition of samples P1 and P2 does not affect friction.

For the film: appearance – homogeneous; the drying time by the introduction of any of the two synthesized plasticizers increases; the Erichsen elasticity increases at the introduction of P1 and P2 products, which, in its turn, brings an improvement over the standard sample (1); the adhesion, flexibility and thickness of the film does not change when adding the synthesized products; impact resistance is improved most in sample 3, with efficacy as plasticizers P2 > P1; in samples 2 and 3, their hardness is lower than the standard sample (1), which means that the two synthesized products act as secondary plasticizers; the degree of gloss increases by adding the two synthesized compounds.

Table 3 presents the analytical values for composites based on chlorinated rubber lacquer based films compositions obtained with the synthesized products.

Table3. Characteristics for composites based on chlorinated rubber lacquer based films compositions obtained with the synthesized products

Technical characteristics	Sample		
	4	5	6
Liquid			
Aspect	VOF	VOF	VOF
Content in nonvolatile subst., 2 h, 120^{0}C, [%]	45	49	49
Leakage time, cup DIN 4 mm, 20^{0}C, [s].	80	70	65
Density, 20^{0}C, [g/cm^3]	1106	1107	1108
Fine friction, [microns]	15	15	15
Film			
Aspect	HF	HF	HF
Drying time, D type, at 20^{o}C, [h]	1	2	2
Erichsen elasticity, [mm]	4.2	7.8	7.8
Adherence, grid 2 mm, grip figure	2	2	2
Flexibility, [mm]	5	3	3
Thickness of the dry film, [μm]	25	25	20
Resistance to hit-directly, 0.5 kgf/cm^2	10	35	35
Persozhardness, [s]	66	60	62
Degree of gloss angle 60^0, [%]	70	81	84

VOF – Viscous Homogene Fluid, HF – Homogene Film

The samples evaluated were based on nitrocellulose film, introducing the P1 and P2 synthesized products as follows:

- sample 4: represents the standard sample with no content of P1 or P2;
- sample 5: contains 6.25% P1;
- sample 6: contains 6.25% P2.
- P1 and P2 have the role of secondary plasticizers.

Chlorinated rubber lacquer-based films have the following composition: chlorinated rubber (35%), chlorinated paraffin (5%), diluent (60%).

Interpretation of results:

For the liquid product: No large changes are seen in the liquid product, except that leakage time decreases with the addition of compound P1, and by the addition of compound P2 it decreases more than in sample 4, and even 5; the rest of the technical characteristics remaining approximately constant.

For the film: the Erichsen elasticity is greatly improved when adding the two synthesized compounds (from 4.2 to 7.8 mm). Another characteristic that shows us the effectiveness of P1 and P2 as plasticizers is the resistance to impact which is much higher for samples 5 and 6 (35 cm).

Decreasing of hardness value (from 66 s for the standard to 60-62 s for the analyzed samples) as well as increasing the degree of gloss (81% with P1 and 84% with P2 respectively) proves the role of plasticizers of P1 and P2 products.

CONCLUSIONS

In the present paper, the main topics are the synthesis and characterization of esters based on soybean oil fatty acids and the assessment for their use as plasticizers in composites of nitrocellulose based films and chlorinated rubber lacquer based films compositions. Esters of fatty acids were obtained in a chemical reactor with microwave heating, using as an acidic component soybean oil fatty acids, and *n*-butanol and isopentanol as the hydroxyl component. The reactions occurred in the presence of the catalyst, *p*-toluenesulfonic acid (0.3% versus fatty acids in soybean oil), at reflux temperature.

The introduction of P1 and P2 compounds into nitrocellulose-based films compositions results in the improvement of the following features: Erichsen elasticity, impact resistance and gloss degree. The adhesion, flexibility and thickness of the film does not change when adding synthesized products. The drying time increases, and these mixtures can be used if a slower drying is desired. In terms of hardness, the synthesized compounds act as secondary plasticizers.

The introduction of P1 and P2 compounds into composites based on chlorinated lacquer based films compositions leads to an improvement in the following characteristics: Erichsen elasticity and impact resistance. No large changes are seen in the liquid product, except that leakage time decreases with the addition of compounds P1 and P2. The other technical characteristics remain approximately constant. Decreasing the value of hardness and increasing the degree of gloss again prove the role of plasticizers (especially secondary) of P1 and P2 products.

EXPERIMENTAL SECTION

Esters of fatty acids were obtained in a microwave reactor. The acidic component composed of the soybean oil fatty acids, combined with two different alcohols: *n*-butanol which gave esters mixture P1, and respectively isopentanol (3-methyl-1-butanol) which yielded esters mixture P2. The reactions were carried out in the presence of the catalyst, the *p*-toluenesulfonic acid, at the reflux temperature.

Synthetic variants thereof are shown in Table 4.

The physico-chemical properties of fatty acids from soybean oil: appearance: viscous liquid without mechanical impurities; color: yellow; molecular weight, g / mole: 280; density at 20^{o}C, g/cm^{3}: 0.89; melting point, ^{o}C: 14-16; acid number, mg KOH/ g: 193.4; refraction index, la 20^{o}C: 1.458. The alcohols used are from Fluka. The characteristics of the chemical

reactor with microwave heating are: model: MW-2000; microwave power: :0 ~ 1800 W; microwave frequency: 2450 + 50MHz.

Table 4. The synthesis variants of esters from soybean oil fatty acids

Raw materials	MU	Synthesis variant abbreviations	
		P1	P2
soybean oil fatty acids	mols	1	1
n-butanol	mols	1.3	-
isopentanol	mols	-	1.15
p-toluenesulphonic acid	%	0.3	0.3
Reaction conditions			
Time of reaction	min.	240	280
Temperature of reaction	^{0} C	118-160	118-180

The variation of the acid number of the reaction mass according to the reaction time was the tracking reaction parameter.

For esters mixture P1, synthesis parameters are drawn in Table 5.

Table 5. Reaction parameters for the esters P1

Time, min	Temperature, ^{o}C	Acid number [mg KOH/g]
0	13.3	148.8
15	108.8	48.86
30	116	17.93
60	117.8	10.27
90	117	10.1
120	120.4	9.54
180	127.5	7.92
240	139.9	6.48

For P2, synthesis parameters are presented in Table 6.

Table 6. Reaction parameters for the ester P2

Time, min	Temperature, ^{o}C	Acid number, mg KOH/g
0	14	147.54
30	103	72.65
60	107	58.76
90	117	38.85
120	118	26.96
150	129	20.04
180	140	16.34
225	140	8.62
280	176	3.34

Conversion of the reaction in both cases is shown in Figures 3 and 4.

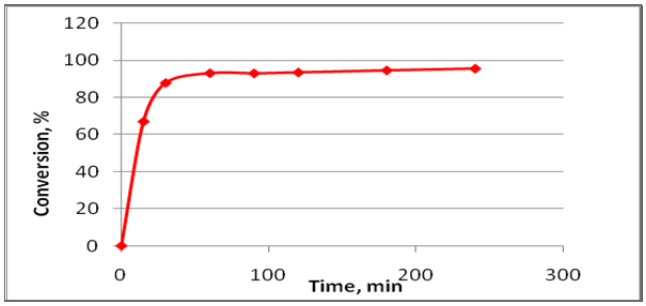

Figure 3. Conversion variation – P1 synthesis

From the chart depicted in Figure 3, there is a sharp increase in conversion in the first 30 minutes followed by a slow increase, so in the end a very good conversion of about 95.63% is obtained.

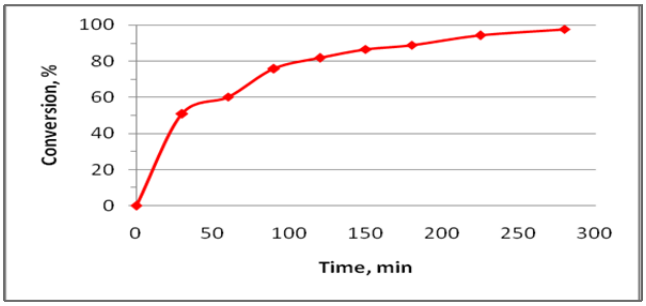

Figure 4. Conversion variation – P2 synthesis

In the case of synthesis P2, the variation of the conversion achieved by reaction time (Figure 4) is gradual and almost constant over time, reaching a 97.74% conversion.

Methods:

a) Structural characterization of P1 and P2 esters synthesized: the dynamic viscosity - the viscometer type RV-Rheotest (EBV Prüfgeräte-WerkMedingen / Dresden); refractive index - Abbe refractometer at 20^0C; density - the pycnometer at 20^0C; the acid number – according to SR ISO 3682; saponification index - ISO 3657: 2013 iodine index - according to SR EN ISO 3961: 2013A; thermogravimetric analysis (TG)/(DTG) and differential scanning calorimetry (DSC) were performed with NETZSCH STA apparatus STA449F1A 449F1-0220-M. A quantity of between 3 ÷ 7

mg sample was heated in a crucible of Al2O3, with the rate of 5^0C/min., under a nitrogen atmosphere in the temperature range of 25 ÷ 900^0C.

b) Evaluation of P1 and P2 synthesized esters as plasticizer for protective coatings: aspect – visual; the dynamic viscosity - the viscometer type RV-Rheotest (EBV Prüfgeräte-WerkMedingen / Dresden); content in nonvolatile subst. – SR EN ISO 3251:2008; drying time –SR EN ISO 9117-6:2012; Erichsen elasticity –SR EN ISO 1520:2007; adherence –SR ISO 2409:2013; flexibility –SR EN ISO 1519:1999; thickness of the dry film – SR ISO 2808:2007; resistance to hit-directly – SR EN ISO 6272-1:2012; Persozhardness – SR EN ISO 1522:2007; degree of gloss angle – SR EN ISO 2813:2003.

REFERENCES

1. M. Suzuki, Y. Taira, C. Kato, K. Shinkai, Y. Katoh, *Journal of Dentistry*, **2016**, doi: 10.1016/j.jdent.2015.11.005.
2. J. Li, J. Luo, X. Li, Z. Yi, Q. Gao, J. Li, *Industrial Crops and Products*, **2015**, 74, 613.
3. E. Lépine, B. Riedl, X.-M. Wang, A. Pizzi, L. Delmotte, J.-M. Hardy, M. J. R. Da Cruz, *InternationalJournalofAdhesion&Adhesives*, **2015**, 63, 74.
4. S. Boran, S. Nitu, *Revista de MaterialePlastice*, **2017**, 54, 2, 386.
5. W. Maassen, M.A.R. Meier, N. Willenbacher, *International Journal of Adhesion & Adhesives*, **2016**, 64, 65.
6. P.N. Dange, V.K. Rathod, *Resource-Efficient Technologies*, **2017**, 3, 1, 64.
7. T. Lieu, S. Yusup, M. Moniruzzaman, *Bioresource Technology*, **2016**, 211, 248.
8. S.P. Bowen, D.R. Kanis, C. McDaniel, R.C Richter, *Journal of Chemistry and Biochemistry*, **2014**, 2, 2, 1.
9. N.Plesu, G., Ilia, G. Bandur, S.Popa, *Journal of the Serbian Chemical Society*, **2005**, 70, 10, 1169.
10. N. Plesu, G., Ilia, S. Iliescu, A. Popa, G. Bandur, S.Popa, *MaterialePlastice*, **2004**, 41, 3, 143.
11. N. Plesu, G. Bandur, I. Manoviciu, S.Popa, D.Jurcau, *MaterialePlastice*, **2003**, 40, 1, 21.
12. N. Plesu, R. Rad, I. Manoviciu, G. Bandur, S.Popa, *Revista de Chimie*, **2003**, 54, 8, 685.
13. S. Popa, S.Boran, *Materialeplastice*, **2016**, 53, 3, 410.
14. S.Popa, C.Csunderlik, V.Jascanu, D.Jurcau, N.Plesu, *Materialeplastice*, **2004**, 41, 2, 62.
15. S. Popa, C.Csunderlik, V. Jascanu, D. Jurcau, N. Plesu, *Materialeplastice*, **2003**, 40, 4, 177.
16. S. Popa, V. Jascanu, D. Jurcau, N. Plesu, *Revista de chimie*, **2003**, 54, 7, 595.

17. S. Popa, C.Csunderlik, S. Florea, V. Jascanu, N. Plesu,*Revista de Chimie*, **2002**, 53, 4, 259.
18. D. Kohn, S. Popa, *Experimental Heat Transfer*, **1999**, 12, 3, 193.
19. S. Popa, S.Boran, *Thermal Science*, **2015**, DOI: 10.2298/TSCI150728203P
20. S. Popa, S. Boran, *Rev. Roum. Chim.*,**2016**, 61, 11-12, 851.
21. S. Popa, S. Boran, *Rev.Rou. Chim.*,**2015**, 60, 10, 991.
22. G. Mosoarca, P. Negrea, M. Motoc, M. Craciunescu, M. Anghel, D. David, *Revista de Chimie*, **2009**, 60, 6, 636.
23. G. Mosoarca, V. Pode, *Revista de Chimie*, **2009**, 60, 8, 836.
24. G. Mosoarca, P. Negrea, C. Vancea, M. Motoc, M. Anghel, D. David, *Revista de Chimie*, **2010**, 61,10, 983.
25. G. Mosoarca, A. Negrea,*Journal of Environmental Protection and Ecology*, **2012**, 13, 1, 198.
26. I. Lazau, C. Vancea, *Romanian Journal of Materials*, 2012, 42, 3, 270.
27. C. Vancea, I. Lazau, *Central European Journal of Chemistry*, **2014**, 12, 7, 804.
28. I. Lazau, C. Vancea, G. Mosoarca,*Romanian Journal of Materials*, **2013**, 43, 2, 210.
29. C. Vancea, G. Mosoarca,A. Negrea,A. Latia, R.M. Jurca, *Romanian Journal of Materials*, **2016**, 46, 3, 296.

STUDIA UBB CHEMIA, LXIII, 1, 2018 (p. 73-86)
(RECOMMENDED CITATION)
DOI:10.24193/subbchem.2018.1.06

NEW EXPERIMENTAL SULFOALUMINATE CLINKERS FROM NATURAL RAW MATERIAL MIXTURES

TIMEA HALMAGYI[a], EMILIA MOSONYI[b,*], JÓZSEF FAZAKAS[a]

ABSTRACT. The paper presents new different raw materials mixtures which should lead to the theoretical mineralogical compositions of sulfoaluminate belitic (SAB) clinkers. The mixtures, composed of limestone, gypsum, clay, diatomite, basaltic scoria, volcanic tuff and red mud (bauxite ore processing by-product), have been burned at 1220, 1240 and 1260 °C for one hour in an electrical laboratory furnace, then quenched in fresh air. The resulted clinker samples were studied in thin sections under a polarizing petrographic microscope for clinker structure, microtexture and mineralogical association. The mineralogical assemblage assessment by XRD analyses was completed. The sample XRD patterns (processed by Match software and pdf2 database) have been allowed a qualitative and a semiquantitative estimation (external standard method) of the main mineralogical compounds: C_2S (belite), C_4AF (brownmillerite), $C\overline{S}$ (anhydrite), $C_4A_3\overline{S}$ (sulfoaluminate), proper for sulfoaluminate belitic clinkers. The identified minor and secondary mineral phases were: alkali (Na, K, Na- K) sulfates, natroalunite ($NKA_6\ \overline{S}\ H$), limeite (C), periclase (M), gehlenite ($C_2(A_{1-x},M_x)$(AS)). The following abbreviations were used: C= CaO; S = SiO_2; A= Al_2O_3; F= Fe_2O_3; $\overline{S}$ = SO_3; H = H_2O; M= MgO; N(K)= $Na_2O(K_2O)$.

Keywords: *Sulfoaluminate belitic clinker, clinker chemistry, raw materials, transmission polarizing microscopy, XRD analyses*

INTRODUCTION

The modern civil engineering requirements impose the obtaining of a new sort of cement which has a good quality, is environmentally friendly and needs low energy consumption. For these reasons, the low energy

[a] *Babeş-Bolyai University, Faculty of Chemstry and Chemical Engineering, 11 Arany Janos str., RO-400028, Cluj-Napoca, Romania*
[b] *Babeş-Bolyai University, Faculty of Biology and Geology, 1 Kogalniceanu str., RO-400082, Cluj-Napoca, Romania*
[*] *Corresponding author: emilia.mosonyi@ubbcluj.ro*

cement manufacturing is attractive from economic and ecological points of view. These cements could be used where there are needs of high early strength or expansion compensation, but increased durability.

The low energy clinkers/cements comprise those materials which belong to the $CaO - SiO_2 – Al_2O_3 - Fe_2O_3 – CaSO_4$ system and they are mainly sulfoaluminate belite and sulfoferroaluminate belite cements [1] They may be manufactured both from natural raw materials and raw materials mixed with industrial by-products or industrial waste, by firing at lower temperature than Portland cement clinker.

In the $CaO - Al_2O_3 – SiO_2 – CaSO_4$ system there are two ternary compounds: the calcium sulfoaluminate ($C_4A_3\overline{S}$) and calcium sulfosilicate ("sulfo- spurrite" $C_5S_2\overline{S}$), the later hydraulically inactive [2].

Data about chemical composition, manufacturing and features of sulfoaluminate belitic (SAB) cement may be found in cement related literature [3, 4, 5, 6, 7]. A large variety of cements based on $C_4A_3\overline{S}$ were experimented on in China and used mainly for concrete preparation. These were standardized and named as "Third Cement Series" [8].

The "Third Series" of cements were developed in China, those sulfoferritic since 1972 and those sulfoferroaluminate types since 1983, using Fe-rich raw materials. These cements have special features such as: quick setting time, good impermeability, rapid strength development even at low temperature [9, 10].Their main mineral phases are: belite (C_2S), $C_4A_3\overline{S}$ and tetracalcium ferroaluminate (C_4AF), in different ratios. Such clinker composition comprises: 53% $C_4A_3\overline{S}$, 18% C_2S, 12% C and 15% C_4AF (2% residue) [4].The main mineral phases of SAB cements are: β-C_2S (25-65 %), $C_4A_3\overline{S}$ (10-20 %), C_4AF (15-40 %) and sometimes, $C\overline{S}$ (10-20 %), depending on the SO_3-content of raw mixture [11, 12]. Different mineral proportions of such clinkers results cements with different hydraulic properties. The tetracalcium ferroaluminate (C_4AF), formed at lower temperatures (1200 $^{\circ}$C), due to its solid phase reactions is much more reactive than the similar mineral from the Portland cement clinker, which is generated from a melt by late crystallization [13].

The calcium sulfoaluminate, $C_4A_3\overline{S}$, known also as „Klein compound" [14,15, 16, 17, 18,19, 20], has a similar structure to the natural mineral haüyn or to another mineral, sodalite and can already be sinterized at about 1300 $^{\circ}$C beside belite (β-C_2S) and ferrite (C_4AF) [21]. The $C_4A_3\overline{S}$ forms at about 1250 $^{\circ}$C and is stable up to the 1350 $^{\circ}$C [9]. High sulfoaluminate contents imply a high early strength of cement binder, chemical corrosion resistance and controlled expansion. [8, 22]. Using gypsum as a mineralizer for the stabilization of the β-C_2S polymorph in the $CaO- Al_2O_3- SiO_2$ system the low temperature clinker resulted, in which the main mineral components were β-C_2S and $C_4A_3\overline{S}$ [23].

Obviously, the burning temperature of SAB clinkers is between 1200-1350°C, depending on the raw mixture composition and minor element impurities, such as: phosphates, sulfates, borates and different oxides. The firing temperature of such clinkers may be low, of about 1200- 1250 °C, when waste materials (blast furnace slag, phosphogypsum, pyrite ash) containing many minor elements are used for clinker recipes. The oxide-type impurities work as mineralizers [6, 9] in the sintering process. The energy saving clinkers' manufacturing takes place at temperatures of about 200-300°C lower than those Portland cement needs [21, 24]. The energy-saving advantage is accompanied by an ecological one, due to the lowering of CO_2 (greenhouse) gas emissions and reusing of industrial waste materials, which partly can replace the natural raw materials or may be used as cement mineral additions.

During sulfoaluminate cements manufacturing were established a diminishing with 43% the CO_2 emissions [4], or with 20- 30% [25] respectively. In the same processes a diminishing with 14% the specific heat consumption and with about 25% of the total energy consumption [12] was observed, when compared to the Portland cement technology. Finally a lowering with 40% of the clinker milling energy (due to more brittle mineral contents) was found, using as reference the same technology data.

The SAB clinkers are environmentally friendly, because their manufacturing needs industrial waste materials, the storage of which may imply environment pollution risks. In the world clinkers sinterized from mixtures containing materials such as: red muds as by-products of bauxite ore preparation [9, 22, 26, 27], fly ash [9, 28, 29, 30], steelmaking slags [22], dust from filters, fluidized bed combustion ash [30], blast furnace ash [31] were investigated.

The hydraulic properties of sulfoferrite cements with increased content of C_4AF are highly influenced by the applied thermal treatment, mainly by the quenching rate [11, 24].

The sulfoaluminate belite and sulfoferroaluminate belite cements may have different applications due to the changing quality and dosage of additions, such as: blast furnace slag, power-station ash [31, 32]. The SAB cements, obtained at low temperatures, are good sulfate- and moderate chloride- resisting binders [33].

The SAB cements are also attractive for their physico - mechanical properties, presenting good early strength.

In the last decades the Lafarge' researchers have also been experimenting with a new class of lower-carbon clinkers, or 'Aether' clinkers [34, 35, 36, 37], based either on sulfoaluminate clinker (SAC) containing 55-75% ye'elimite ($C_4A_3\overline{S}$), 15-30% belite (C_2S) and 3-6% ferrite ($C_2(A,F)$) or on ferroaluminate clinker (FAC) containing 45-65% ye'elimite, 15-35% belite and 10-25% ferrite. [38]

Industrial scale experimental clinkers of such compositions require significantly less calcium carbonate in the kiln feed, and in situ measurements evidenced CO_2 savings between 25-30% [39, 40]. Hydraulic properties of Aether clinkers are based on $C_4A_3\overline{S}$, which ensures the reactivity of the binder and the early strength up to seven days before the C_2S and the C_4AF phases take over. The hydration of the latter two phases ensures the final strength of this binder type [41].

The aim of our studies was to continue previous work [42] with testing low energy cement recipes series, comprising natural raw materials and red mud (bauxite ore preparation by-product) from Romania. In these experimental works we used as starting point theoretical mineral compositions of such clinker types, published in the cement literature [1, 4, 6].

The raw mixture series (samples 1, 4, 5, 6, 7, 9, 10, 12), even if of non- reagent- grade kiln feeding compounds, were fired between 1220-1240°C, then, resulted clinkers were checked for mineral compositions and compared with theoretical low energy clinker compositions.

RESULTS AND DISCUSSION

The experimental clinker samples were investigated in thin sections by petrographic microscopy, in plane polarized (1N) and cross polarized light (N+). The samples microscopically comprise 2 main components: particles (clusters, nests) of different sizes (200- 250 μm), and an interstitial partially crystalline component. The particles are composed by lime silicate crystals and the interstitial of light greenish up to green-olive color, contains isotropic sulfoaluminates, dark brownish laths of zoned brownmillerite, isolated or twinned laths of anhydrite, limeite (C), periclase (M).

Frequently, the lime silicate nests and clusters, present complex inner structures with all three belite morphology. (Detailed characterization of observed belites and clinker fabric from these experimental series (clinker samples 2A, 3, 8A, 11A, 11B) were presented in a previous article [42].) There are also pores with circular or elliptical contours, their walls being covered by alkali sulfates and/or anhydrite (see center of Figures 1a, 1b.).

A few studied clinker thin section images may be observed in Figures 1a, b - 4a, b.

For all sample thin section microscopic images were taken on same image both in plane polarized light (a) and cross polarized light (b). Few interpretations of microstructures were made after Campbell book. The red colored scale bar from all microscopic images is 50μm.

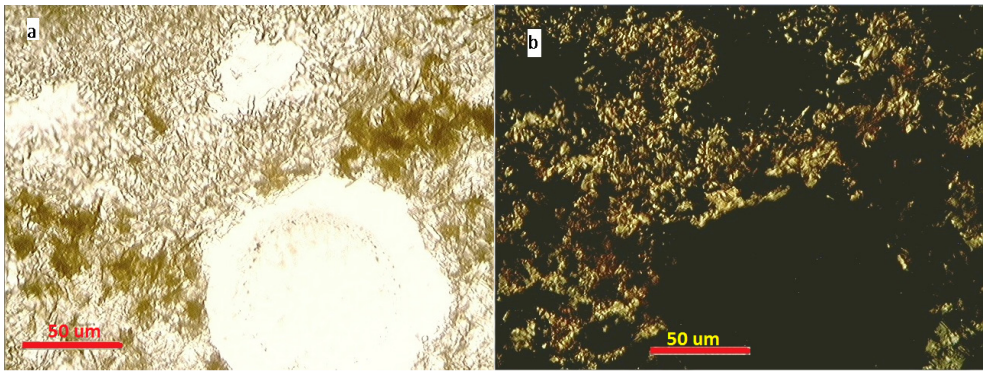

Figure 1. Microscopic image of Sample 7A, fired at 1240°C, raw mix containing 4.69% basaltic scoria. a. (1N); b. Same as a., but N+ .

In Sample 7A (with raw mixture containing basaltic scoria) with Microscopic images from Figures 1a, there is a greenish- olive interstitial phase as droplets (containing brownish laths and rosettes of brownmillerite needles, greenish sulfoaluminate and twinned laths of colorless anhydrite) between greyish-yellow colored clusters of belite I (presenting two twinning directions in bottom left corner and high relief, and belite developed mainly around pores). There are also: pores (P) coated in inner part by a ring of alkali sulfates (with low relief). Figure 1b is the same as Figure 1a**,** but observed in cross polarized light. There are belitic nests and clusters (presenting yellowish birefringence) sometimes with inner zonal arrangements of belite types [43] like belite I (two directions of twin lamellae) and belite II (one direction of twin lamellae). The interstitials are: brownmillerite with high birefringence (reddish brown), isotropic sulfoaluminate and anhydrite laths beside very low quantity of amorphous phase.

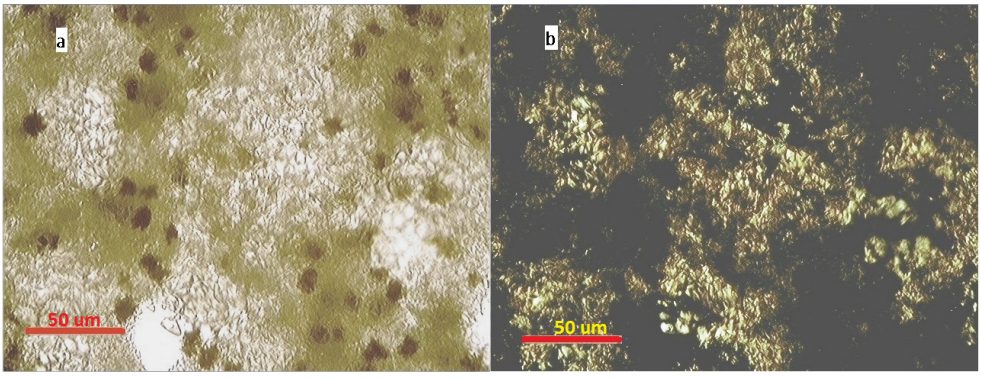

Figure 2. Microscopic images of Sample 6 A, fired at 1240°C, raw mix recipe containing 7.84% diatomite: a (1N); b. Same as a, but N+,

In Figures 2a and 2b there are belitic nests and clusters (ex. image centre). In figure 2a, around light colored nests there is a cryptocrystalline groundmass, comprising dark brown ferrite rosettes and greenish sulfoaluminate crystals beside rare laths of colorless anhydrite. In cross polarized light (N+) the sulfoaluminate is isotropic, having an anhydrite corona (light colored, anomalous birefringence, top left corner of b. image). Around pores (P) were also developed ring structures of belite I or belite II.

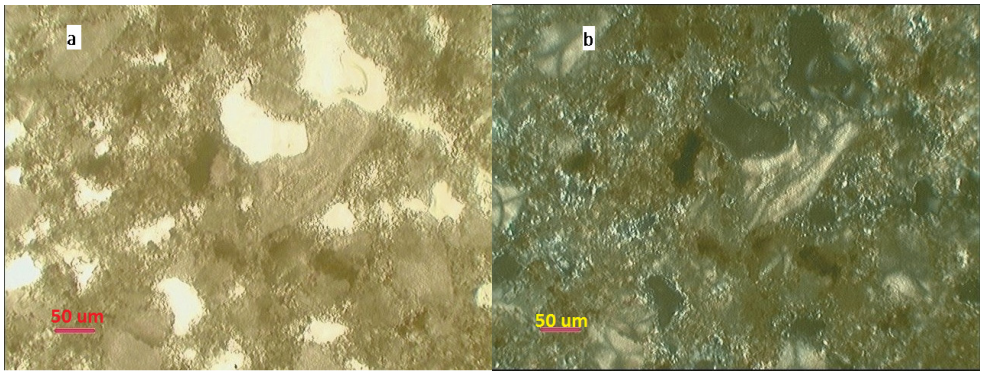

Figure 3. a(1N), b(N+): Microscopic image of Sample 1 (fired at 1220°C, raw dosages containing 7.09% clay):

In thin section of Sample 1 (Figure 3) there are many spherolites of belite III (with ondulatory extinction, ex in the center of b., due to the intergrowth of very fine dendritic crystals), presenting zonal microstructure in a.: with darker core zone containing little iron-bearing exsolutions spots and a rim zone corroded by the interstitial brown-greenish colored brownmillerite (which is also zoned compositionally). The matrix corrosion may be interpret as reducing burning conditions.

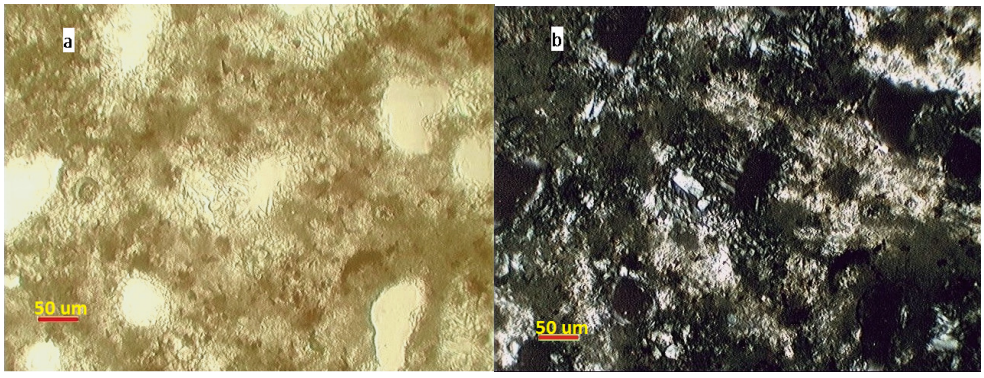

Figure 4. a(1N), b(N+). Microscopic image of Sample 12 (burned at 1220°C, raw mixture containing 2.74% diatomite).

Figure 4 is the thin section image of Sample 12 and presents in a, brownish grey colored slightly differentiated interstitial (brown ferrite and greyish sulfoaluminate, which in figure b is almost isotropic) many pores with yellowish- amber colored belite I nest and clusters in a. (belite yellowish- grey color could mean low hydraulic properties). Some belite I nests have in the central part prismatic comb-like arranged relic alite of 30- 40um size with grey birefringence and polysynthetic twins (center of image, around pore, in b) . Sometimes the belitic nests possess prolongations into the matrix ("ragged belite") or present splintery fractures (in the top center of image), specific for the γ-belite with low hydraulic properties. The ragged belite may be interpreted as slow cooling rate conditions during clinker formation.

The complex inner arrangement of belite types from nests and clusters, chemical zonality of belite, ferrite phases (optically observed as zonal distribution of its colors) and coarse grain size of minerals are all due to a slow diffusion rate during sintering and quenching processes.

Few crystalline phases could not identify under the optical microscope, but were evidenced by XRD analyses, such as alkali (Na, K, Na- K) sulfates, natroalunite ($NKA_6\,\overline{S}\,H$), limeite (C), periclase (M), gehlenite ($C_2(A_{1-x},M_x)(AS)$).

The sulfoaluminate, identified in all clinker samples, crystallizes in the cubic system, has high relief, similar to the other lime silicates. It however differs from the other colorless lime sulfoaluminates, described in the cement literature [23, 43, 44, 45, 46], because it presents greenish-yellow up to olive pleochroic colors (probably due to Fe^{2+} content, which ions isomorphically replace the Ca^{2+} or Fe^{3+} ions which replace Al^{3+} in the mineral molecule). The correct chemical characterization of this mineral should be done also by SEM-EDX. In this solid solution situation, the correct mineral formula should be written $C_4A_{3-x}F_x\overline{S}$ [47]. The sulfoaluminate presents isolated crystals (sized of around 10- 20μm) or grouped as spots between the glass droplets and brownish ferrite prisms or rosettes.

The XRD patterns of clinkers were interpreted by Match 2.0 software (RIR method, of Chung [48], using I/Ic ratio suggested by Wolff and Viser [49]), which permitted a semiquantitative estimation (±5% error) of main and minor crystalline phases, (without amorphous phase) such as those from SAB clinkers. These compositions were comprised in Figure 5 beside the tentative (theoretical) mineral compositions.

In Figure 5 those experimental compositions which are the closest to the theoretical ones are clinker 4A (fired at 1240°C, feeding material containing 2.4% diatomite), 6A (burned at 1240°C, raw mix containing 7.8% diatomite), 7A (burned at 1240°C, containing 4.7% basaltic scoria) and 12 (fired at 1220 °C, raw mix containing 2.7% diatomite). By using around 23-55% gypsum in raw mix for all burned samples, a higher anhydrite content

resulted when compared to theoretical one (more with 2-3%), the latter possessing good hydraulic properties.

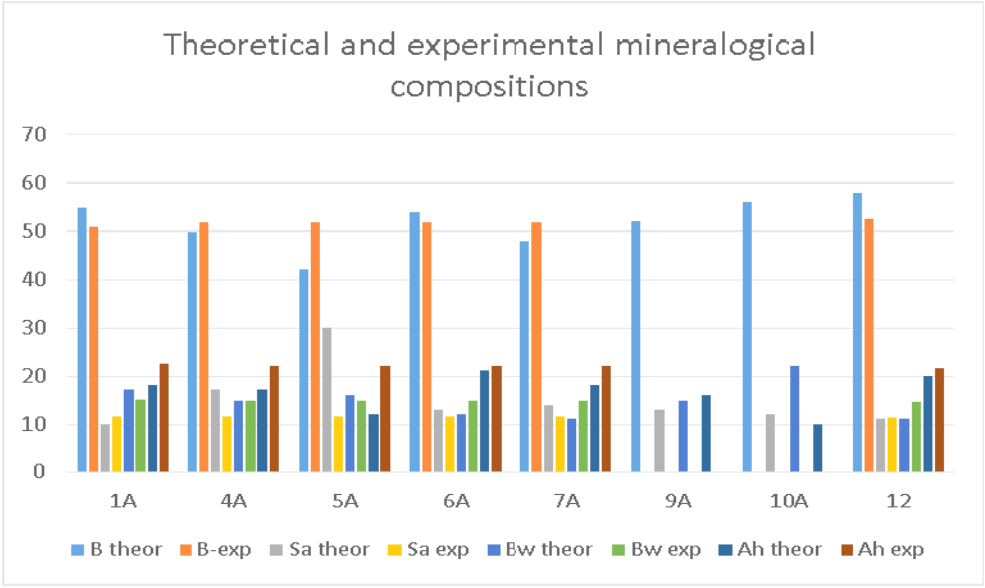

Figure 5. Comparison experimentally tested (XRD) mineralogical compositions with theoretical ones. Sample marked as "A" means clinkering temperature 1240°C and name without "A" - clinkering at 1220°C. Samples 9A and 10A were not analyzed by XRD, but with optical microscopy. (B- belite, Sa- sulfoaluminate, Ah- anhydrite, Bw- brownmillerite)

The belite contents of experimental clinkers are around 50%, but in samples 1A and 12 it appears that the trial compositions were poorer than in theoretical ones. The most belite-rich clinker samples were 4A and 7A, when compared to theoretical compositions, probably explained by optimal Fe_2O_3 (5-7%) and other different mineralizers' (TiO_2, MgO, alkali oxides) bringing material in the raw mix such as volcanic rocks, clay or diatomite. The red mud brings into the raw mix composition of sample 5 a relative high MgO and Na_2O content beside optimal Fe_2O_3 percent for monoclinic β-belite stabilization, but this latter clinker sample however contain lower percent (around 10%) sulfoaluminate than in theoretical composition.

The anhydrite contents present higher values than theoretical compositions.

By firing the presented raw material mixtures clinkers (sample 1A-1240°C, 4A-1240°C, 5A-1240°C, 6A-1240°C, 7A-1240°C, 12- 1220°C) having a main mineral phase specific to the SAB type resulted. The XRD powder pattern of investigated clinker samples were grouped in the Figure 6.

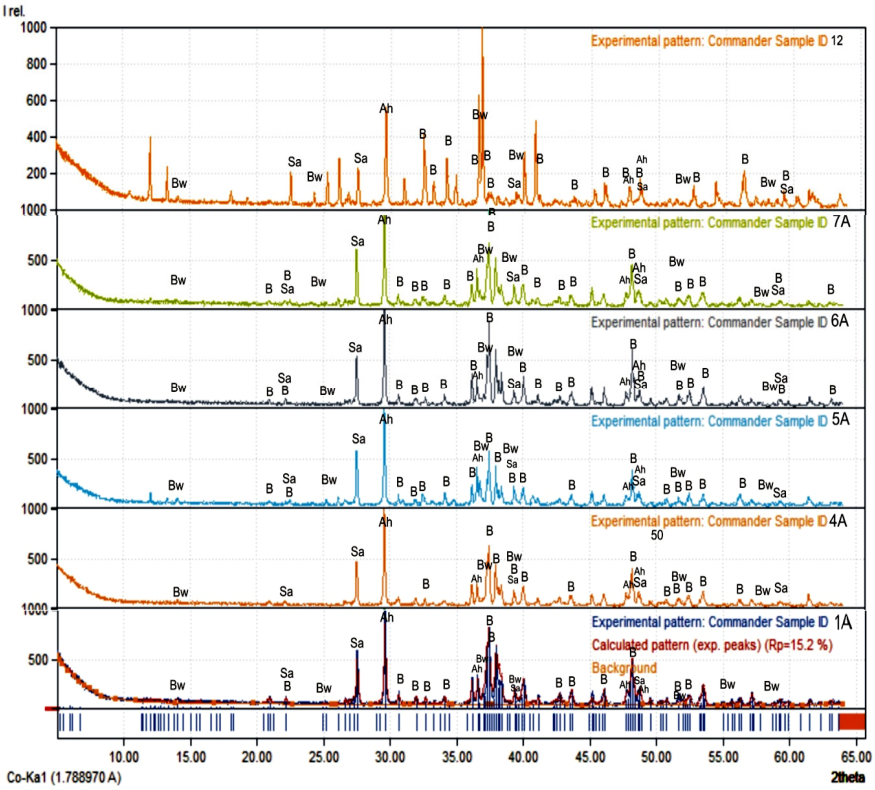

Figure 6. The XRD powder patterns of clinker samples. The mineral abbreviations same as in Figure 5.

Other minor mineral components, unmarked in figure 6 were, in sample 1A: periclase (M), limeite (C), $K_2\overline{S}$, C_3S; in sample 4A: C, M, $N_2\overline{S}$, $K_3N\overline{S}_2$, gehlenite ($C_2(A_{1-x},M_x)(AS)$); in sample 5A: C, $K_3N\overline{S}_2$; in sample 6A: C, M, $K_2\overline{S}$, gehlenite; in sample 7A: $N_2\overline{S}$, gehlenite and in sample 12: M, C, natroalunite ($NKA_6\,\overline{S}\,H$), gehlenite.

Missing desirable phases from present trial clinkers probably were compensated by other Mg- mineral formation for example such as diopside (CMS_2), which can react with $CaCO_3$ and a solid solution between gehlenite-åkermanite ($C_2A(AS)_2$ - C_2MS_2) results beside CO_2 [50]. Gehlenite, a mineral with non-hydraulic features, was outlined in our experimental clinkers.[c]

[c] Koch and Sztrokay authors in the same "Systematic mineralogy" book also wrote, that the higher Fe and alkali content may promote in the mentioned chemical reaction a melilite group ($(C,N,K)_2(M,F^{2+},F^{3+},A)(S, A)_2$,) mineral with lower melting point, down to 1100- 1200°C).

CONCLUSIONS

Based on the microscopic investigations and XRD analyses on the experimental clinker samples, it can be concluded that: for all raw material mixtures, heated at temperatures between 1220-1240 $^{\circ}$C, clinkers containing C_2S, $C_4A_3\overline{S}$, C_4AF, $C\overline{S}$ resulted. The microscopic observations on clinker microstructure and mineral grain -size drove to conclusion that clinkers were quenched slowly, affecting the binder quality of cement pastes.

The sulfoaluminate, ensuring the early strength of cement binder, represents a lower percent than in theoretical compositions, but belite contents, imprinting final strength of such binders quantitatively are very close to the theoretical ones. Unfortunately, the stabilised belite polymorphs are not always those with the highest hydraulic properties (ex. sample 12). The ferrite phase, which also should contribute to the final strength of binders, has a lower content than in the theoretical composition. It could also be compensated by minor quantities of aluminosilicates.

Differences between theoretical and experimental mineralogical compositions of clinkers, taking into consideration our observations may be due to: non-reagent grade (main cause), heterogeneous chemical composition of raw meal materials, their impurities quantities which could catalyse or block the same hydraulic mineral formation, heating and slow cooling rate, reducing or oxidizing sintering conditions.

In the current stage of our researches, using the presented raw material mixtures permitted to obtain clinkers with mineralogical compositions, specific for the low energy type belitic clinkers: C_2S= 45-50%, $C_4A_3\overline{S}$ =10-12%, C_4AF=15-25 %, $C\overline{S}$ =20-22%.

Checking the binder quality, physico- mechanical features of cement pastes or using some additives for improving the cement pastes workability and final strength will be initiated in the next research stage.

EXPERIMENTAL SECTION

The natural raw materials, used for experimental clinkers, were: Vârghiș limestones, Nucșoara gypsum, Bodoc clays (in samples 1), basaltic scoria from Racoșul de Jos (in sample 7), Filia diatomite (in samples 4, 5, 6, 12) all from Carpathian orocline, mixed with red muds (industrial by-product) from Oradea (in sample 5, 9, 10). The selected raw materials were studied chemically by SEM-EDX (limestone, red mud, diatomite and basaltic scoria) and by wet chemical methods (gypsum and clay) and their compositions were outlined in a previous paper [42]. The mentioned raw materials were used for 12 different clinker recipes. Four recipes (raw material mix samples 2,

3, 8, 11) were checked by firing and their experimental data were published in a previous paper [42]. The other recipes (raw material mix samples 1, 4, 5, 6, 7, 9, 10, 12) were also experimented on and their data represents the topic of the present paper.

The estimation of desirable clinker chemical compositions are based on few SAB cement theoretical mineralogical compositions, counted by reverse Bogue methods [9, 32]. Such compositions were evidenced in Figure 7 and 8.

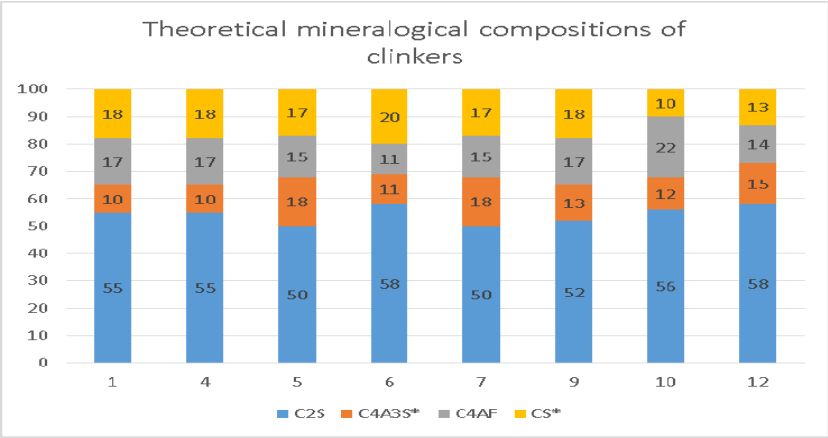

Figure 7. Theoretical mineralogical compositions of few SAB clinkers.

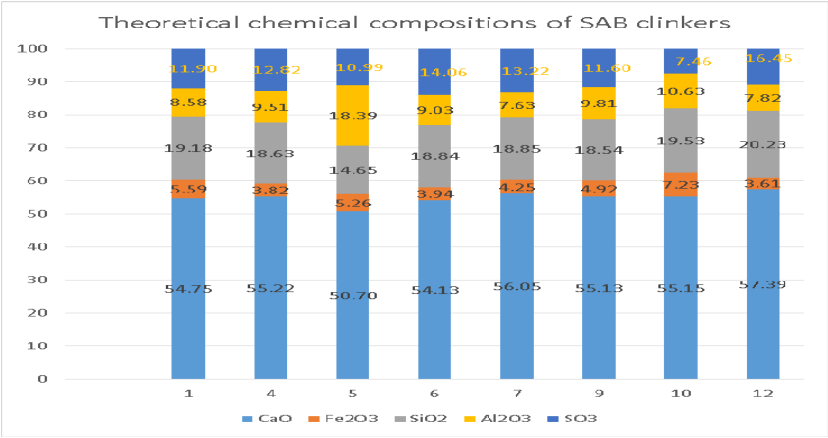

Figure 8. Theoretical chemical compositions of SAB clinkers, based on reverse Bogue counting.

In Figure 9 the used recipes for the feeding material mixtures, submitted for present experiments (recipes of sample 1, 4, 5, 6, 7, 9, 10, 12) are outlined.

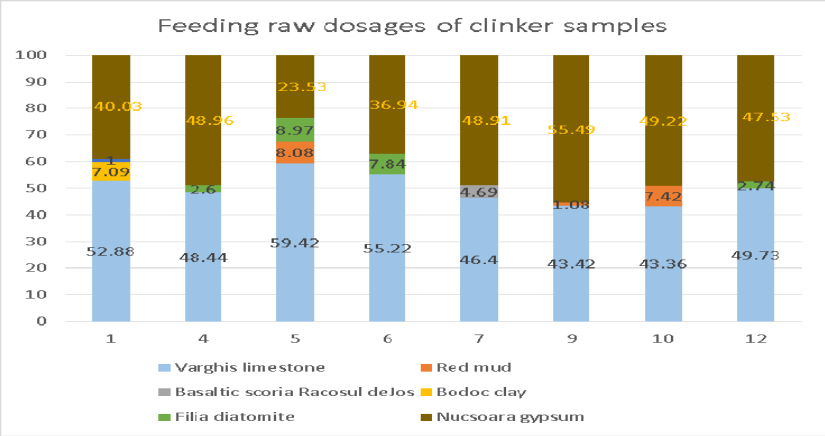

Figure 9. Dosages of raw material mixtures, counted by reverse Bogue method from a theoretical mineralogical composition of SAB clinkers.

The feeding materials were dried in a furnace, grinded in a mill with porcelain balls for two hours then homogenised for one hour. From the milled and homogenised raw mixtures (+ gypsum) cubic briquettes of 25 x 25 x 25mm sizes were shaped, then heated for one hour at peak temperatures (dwell) 1220 °C and 1240 °C (the later temperature marked as „A" in clinker sample name from figures 5, 6) in a laboratory electrical- kiln. The cooling times were 12 hours, using fresh air.

The resulted clinkers were investigated in thin sections (prepared in a laboratory of the Geological Department of Biology and Geology Faculty from Babeș- Bolyai University) under Jenapol optical microscope, in polarised light, by transmission which helped us to assess phase composition and clinker fabric, in order to estimate or improve clinker quality, burning conditions or cooling rate. Microscopic images of thin section images in plane polarized and cross polarized light were taken. The clinkers' mineral phases were also revealed/completed qualitatively and semiquantitatively by XRD method. The XRD powder analyses were performed at the Geology Department of Babeş- Bolyai University, Cluj-Napoca, by a Brüker D8 Advance diffractometer with Bragg-Brentano geometry, CoKα1 with λ = 1.78897, Fe filter and an one-dimensional detector, using corundum (NIST SRM1976a) as internal standard. The data were collected on a 2θ = 5- 64° interval at a 0.02°, with the measuring step of 0.2 seconds. The assessment of the mineral phases was performed with Match 2.0 software and pdf2 database.

ACKNOWLEDGMENTS

The authors deeply acknowledge the work of Dr. Ferenc Forray in XRD testing.

REFERENCES

1. Y. Wang, M. Su, J. Den, D. Li, *Journal of The Chinese Ceramic Society* **1982**, *04*.
2. J. Beretka, M Marroccoli, N. Sherman, G.L. Valenti, *Cement and Concrete Researches* **1996,** *26* (11), 1673.
3. K. Quillin, *Cement and Concrete Researches* **2001,** *31* (9), 1341.
4. A. Alaoui, A. Feraille, A. Steckmeyer, R. Le Roy, *12th International Congress on the Chemistry of Cement* **2007**.
5. E. Dan, "The low energy cements durability, manufactured with addition of industrial waste materials". Phd thesis, Polytechnic University from Bucharest **2004**.
6. C. D. Lawrence, H. J. Sharp, M. Muntean, *The 2nd International Symposium of Construction Industry Building Materials and Urban Development*, Hanoi **1995**, *1*.
7. D.C. Lawrence, "Nowel low energy cements based on belite", Brasov, Romania **1996**.
8. L. Zhang, M. Su, Y. Wang, *Advances in Cement Researches* **1999**,*1*:15.
9. I. Soner, "Utilization of Fluidized Bed Combustion Ashes as Raw Material in the Production of a Special Cement", Middle EastTechnical University, Haziran. Turkey **2009**.
10. Y. X. Yongmo, G. Chunlei, *Advances in Material Researches* **2012**; *368–373*, 478.
11. I. Teoreanu, M. Muntean, *Cement and Concret Researches* **1983**, *13*, 711.
12. K.P.Mehta, *World Cement Technology* **1980,** *11* (4), 166.
13. K. P. Mehta, *World Cement Technology* **1978**, *144* (60),11.
14. P. C. Hewlett "Lea's chemistry of cement and concrete". Elsevier Butterworth-Heinmann **2004**. 1057 p.
15. J. H. Sharp, C. D. Lawrencef, R. Yang, *Advanced in Cement Researches* **1999,** *11*(1), 3.
16. A. Telesca, M. Marroccoli, M.L. Pace, M.Tomasulo, G.L.Valenti, PJM.Monteiro, *Cement and Concrete Composites* **2014,** *53*, 224.
17. M. C. G. Juenger, F. Winnefeld, J. L. Provis, J. H. Ideker, *Cement and Concret Researches* **2011,** *41* (12), 1232.
18. A. Klein, *Google Patents* **1966**.
19. I. Odler, "Improving Energy Efficiency In Portland Clinker Manufacturing", SN Ghosh, Ed. New Delhi, ABI books **1991,** 174.
20. I. Odler, "Special Inorganic Cements". First. Taylor and Francis, Ed., London and New York, CRC Press **2000**.
21. I. Janotka, Ľ. Krajči, *Ceramics − Silikaty* **2002,** *46* (3), 110.
22. D. Adolfsson, N. Menad, E. Viggh, B. Björkman, *Advances in Cement Researches* **2007,** *19* (4), 147.
23. I. Janotka, L.Krajči, S.C.Mojumdar, *Ceramics - Silikáty* **2007,** *51* (2), 74.
24. D.C. Popescu. M. Muntean, H.J. Sharp, *Cement and Concrete Composites* **2003**, *25* (7), 689.

25. A. Alaoui, A. Feraille, A. Steckmeyer, R Le Roy, *12th International Congress on the Chemistry of Cement.* **2007***, 1.*
26. G.L. Valenti. M. Marroccoli. F. Montagnaro. M. Nobili, A. Telesca, *Proceedings of the 12th International Congress on the Chemistry of Cement*. Montreal, Canada **2007**, 1.
27. F.P. Glasser, L. Zhang, *Cement and Concret Researches* **2001,** , *31* (12), 1881.
28. S. Sahu, J. Majling, *Cement and Concret Researches* **1994**, *24* (6), 1065.
29. P. Arjunan. R.M. Silsbee, M.D. Roy, *Cement and Concret Researches* **1999**, *29*, 1305.
30. R.B. Jewell, R.F. Rathbone, T.L. Robl, *World of Coal Ash Conference*, Covington, KY **2007**, *May(7–10)*, 18.
31. I. Odler, "Special inorganic cements- Modern Concrete Technology" 8. First, Francis and Taylor, editor, London and New York, E & FN Spon, **2000**, 395 p.
32. I.A. Chen, "Synthesis of Portland Cement and Calcium Sulfoaluminate-Belite Cement for Sustainable Development and Performance". Phd thesis, Texas at Austin **2009**.
33. E. Dan, I. Janotka, *Ceramics - Silikaty* **2003**, *47* (4), 141.
34. A. Gies, D. Knofel and M. Bujan, *Cement and Concret Researches*. **1986**, *16* (c), 411.
35. A. K. Chatterjee, *Proceedings of 11th International Congress on the Chemistry of Cement,* Durban, South Africa **2003**, 31.
36. T. Staněk, P. Sulovský, *Cement and Concret Researches* **2015**, *68*, 203.
37. Tongbo Sui, Lei Fan, Zhaijun Wen, Jing Wang, *Journal of Civil Engineer Architure* **2015**, *9* (4), 384.
38. E.M. Gartner, D.E. Macphee, *Cement and Concret Researches* **2011,** *41* (7), 736.
39. E. M. Gartner, *Cement and Concret Researches* **2004**, *34*(9), 1489.
40. E. M. Gartner, C. Comparet, B. Albert, A.M. Dunster, *International Cement Rev*. **2014**, *1067*, 107.
41. B. Lothenbach, B. Albert, V. Morin, E.M. Gartner, *14th International Congress on Chemistry and Cement* **2015**, (October).
42. E. Mosonyi, M. Spataru, T. Halmagyi, *Studia UBB Chemia* **2016**, *LXI/* 4, 163.
43. H. Insley, *Journal of Research of the National Bureau of Standards* **1936**, *17* (3), 353.
44. Y. Ono, *Proceedings of the Third Annual International Conference On Cement Microscopy*, Houston, Texas, USA, International Cement Microscopy Association **1981**, 198.
45. B.Tavasci, *Cement* **1978**, *3,* 363.
46. D. H. Campbell, "Microscopical Examination and Interpretation of Portland Cement and Clinker". Second, Natalie C. Holz AEPCA, editor, Portland Cement Association, Skokie, IL, USA, Portland Cement Association **1999**, 201 p
47. F. Bullerjahn, *International Congress on the Chemistry of Cement* **2015**, (October).
48. F. H. Chung, *Journal of Applied Crystallography* **1974**, *7* (6), 519.
49. P. M. de Wolff, J. Visser,. *Powder Diffraction* **1988**, *3*, 202.
50. S. Koch, K. I. Sztrókay, "Ásványtan II", Athenaeum Nyomda Nemzeti Tankönyvkiadó, M. Glasner, Ed., Budapest, **1968**, 675.

STUDIA UBB CHEMIA, LXIII, 1, 2018 (p. 87-98)
(RECOMMENDED CITATION)
DOI:10.24193/subbchem.2018.1.07

ACCUMULATION OF HEAVY METALS IN *PLANTAGO MAJOR* GROWN IN URBAN AND POST-INDUSTRIAL AREAS

LEVENTE LEVEI[a,b], ENIKO KOVACS[a], MARIA-ALEXANDRA HOAGHIA[a], ALEXANDRU OZUNU[b,*]

ABSTRACT. The enrichment and accumulation of heavy metals (Cu, Pb, Zn, Cd, Cr, Ni) in *Plantago major* leafs was comparatively studied in an urban (Cluj-Napoca) and a post-industrial area (Baia-Mare) from Romania. These two sites were selected for study as in Cluj-Napoca the dominant metal pollution sources are related to traffic, urban runoff, residential heating and municipal landfill, while in Baia-Mare the main pollution sources are the former ore processing activities and the remaining metal rich mining wastes. The average concentrations of Zn and Pb were higher in the soils collected from the post-industrial area, while the Cr and Ni in those from the urban area. The Cu, Cd, Cr and Ni in plantain leafs were comparable in both areas, while Pb and Zn were higher in the post-industrial area. Based on the enrichment factor and the metal accumulation index, plantain was found to be tolerant to high metal contents and moderate accumulator of Cu and Zn.

Keywords: *Plantago major, heavy metal, soil, enrichment factor.*

INTRODUCTION

As a result of emissions from mining, industry, combustion of fossil fuels, road traffic and other human activities high loads of heavy metals (HMs) are released into the environment, affecting living organisms and the quality of soil, water and air. They can be naturally found in soils, but barely at harmful levels [1, 2]. Although the definition of HMs is still under debate [3-5], we use this term to refer to Cu, Pb, Zn, Cd, Cr and Ni. These metals are generally associated with environmental pollution and have adverse effects on plants in high amounts of bioavailable forms.

[a] *INCDO-INOE 2000 Research Institute for Analytical Instrumentation, 67 Donath str., RO-400293, Cluj-Napoca, Romania.*
[b] *Babeş-Bolyai University, Faculty of Environmental Sciences and Engineering, 30 Fantanele str., RO-400294, Cluj-Napoca, Romania.*
[*] *Corresponding author: alexandru.ozunu@ubbcluj.ro*

Over the years, mining activities altered the landscape and highly affected the environment due to the extensive quantity of waste materials. Soil is not only a pollution receptor, but also a potential secondary source of contamination for the ecosystem [6]. This occurs through the accumulation and diffusion of HMs or other contaminants during their bio-chemical and physical interactions with the soil [7]. High levels of HMs in urban areas are brought about by traffic, which is becoming an increasing issue globally. Urban agglomerations are both sources and receptors for pollutants. Emissions from traffic are comprised of gaseous pollutants that also accumulate in the air and after deposition affect roadside soils and plants [8].

HMs negatively affect plants physiology especially by reducing their growth and interfering with the photosynthesis processes [9]. There are several plant species that developed various mechanisms (exclusion, accumulation, tolerance, translocation) to cope with high contents of HMs. The ability of plants to accumulate HMs can be used to monitor soil pollution [10]. The herbaceous plants potential to be used as bioindicators or biomonitors was identified and evaluated by many studies [10, 11]. Among the most used species are dandelion (*Taraxacum officinale*), nettle (*Urtica dioica*) and plantain (*Plantago major*) [10, 12]. Among the herbaceous plants, *Plantago major* (plantain) is one of the most efficient bioindicators of HMs (Cu, Zn, Mn, Pb, Cr, Pd) pollution. It absorbs and accumulates metals, has tolerance for high metal levels, metal concentration in plant tissues correlates well with the soil and air pollution levels and it is easily identifiable and quite common in various ecoregions [13-15].

In this study, the accumulation of HMs (Cu, Pb, Zn, Cd, Cr, Ni) in plantain leafs collected from an urban (Cluj-Napoca) and a post-industrial (Baia-Mare) area was assessed by using the enrichment factor (EF) and the metal accumulation index (MAI).

RESULTS AND DISCUSSION

The limit of detection (LOD), limit of quantification (LOQ) and expanded uncertainty (U) of the HMs determination method in soil and leafs are summarized in Table 1.

Table 1. Analytical method performance data

HMs	Limit of detection (mg/kg)		Limit of quantification (mg/kg)		Uncertainty (%)	
	Soil	Leafs	Soil	Leafs	Soil	Leafs
Cu	0.10	0.02	0.30	0.06	10.2	10.6
Pb	0.05	0.01	0.15	0.03	8.9	9.2
Zn	0.06	0.01	0.18	0.03	9.2	9.6
Cd	0.03	0.006	0.09	0.018	10.4	10.6
Cr	0.05	0.01	0.15	0.03	9.0	10.2
Ni	0.05	0.01	0.15	0.03	8.6	9.8

Table 2. Recovery, certified and measured concentrations for CRMs

HMs	Certified (mg/kg)	Measured (mg/kg)	Recovery (%)
ERM-CC141 Loam soil CRM			
Cu	12.4±0.9	12.0±1.2	97
Pb	32.2±1.4	31.6±2.8	98
Zn	50±4	52±4.8	104
Cd	0.25±0.04	0.23±0.02	92
Cr	31±4	32±2.9	103
Ni	21.9±1.6	22.2±1.9	101
IAEA-359 Cabbage			
Cu	5.67±0.18	5.35±0.57	94
Pb	-	-	-
Zn	38.6±0.7	37.9±3.6	98
Cd	0.12±0.005*	0.11±0.01	92
Cr	1.3±0.06*	1.3±0.13	100
Ni	1.05±0.05*	1.00±0.10	95

*Indicative values

Table 3. Heavy metal contents in soil (mg/kg)

Sample	Cu	Pb	Zn	Cd	Cr	Ni
Urban area (Cluj-Napoca)						
S1	54.0	76.6	151	3.00	37.6	38.8
S2	30.2	23.3	83.9	3.30	71.1	75.9
S3	30.4	44.3	117	2.30	36.1	41.8
S4	25.1	33.1	95.4	3.30	46.3	55.6
S5	71.0	54.0	145	2.70	42.9	34.4
S6	35.1	87.2	156	3.90	41.8	38.3
Minimum	**25.1**	**23.3**	**83.9**	**2.30**	**36.1**	**34.4**
Maximum	**71.0**	**87.2**	**156**	**3.90**	**71.1**	**75.9**
Average	**41.0**	**53.1**	**125**	**3.08**	**46.0**	**47.5**
St. Dev.	**17.8**	**24.8**	**30.6**	**0.55**	**12.9**	**15.7**
Post-industrial area (Baia-Mare)						
S7	22.5	31.2	70.0	0.30	41.2	44.4
S8	62.8	170	180	6.10	7.2	18.0
S9	35.0	38.4	89.2	1.00	31.6	52.2
S10	232	207	583	5.60	18.0	17.5
S11	27.2	277	321	2.70	1.80	22.5
S12	50.4	158	271	4.90	32.4	26.0
Minimum	**22.5**	**31.2**	**70.0**	**0.30**	**1.80**	**17.5**
Maximum	**232**	**277**	**583**	**6.10**	**41.2**	**52.2**
Average	**71.7**	**147**	**252**	**3.43**	**22.0**	**30.1**
St. Dev.	**80.0**	**96.3**	**189**	**2.46**	**15.6**	**14.6**

The certified and measured results of certified reference materials (CRMs) together with the recovery degree are presented in Table 2. In accordance with Table 2, the results are in good agreement with the reference

values of CRMs. The recovery degrees for the determination of metals in CRMs were in the range of 92-104 % for soil and 92-100 % for leafs. The HMs content in soil and plantain leafs collected from the urban and post-industrial areas is presented in Table 3 and Table 4.

The HMs concentration varies widely in the post-industrial soils, while in urban soils it is more homogenous. In the urban area, the alert values for sensitive soil use given by the Romanian legislation [16] are exceeded in 3 samples for Pb (50 mg/kg), 1 sample for Ni (75 mg/kg) and in 4 samples for Cd (1 mg/kg). Hovewer, in none of the samples the corresponding intervention level is exceeded. In the post-industrial area, the alert values for sensitive use are exceeded in 1 sample for Cd and 3 samples for Zn (300 mg/kg), while the intervention levels are exceeded in 4 samples for Pb (100 mg/kg), 1 sample for Cu (200 mg/kg) and 2 samples for Cd (5 mg/kg). In both areas the most abundant HMs are Zn and Pb, but their average concentrations are two, respectively three times higher in the post-industrial area than in the urban area. The average content of Cd is comparable in the two areas, while the average Cr and Ni contents were higher in the urban area. The differences between the HMs concentrations in the two studied areas could be explained by the overlapping of industrial and urban pollution sources in the post-industrial Baia-Mare city, and the presence of urban pollution sources in Cluj-Napoca city. The average metal contents in soil decreases in the order Zn>Pb>Ni>Cr>Cu>Cd in the soil of urban area, while in those of post-industrial area the decrease order is Zn>Pb>Cu>Ni>Cr>Cd, suggesting different metal pollution sources in the two studied areas. The average Cu, Pb, Zn and Cd contents in the post-industrial area are significantly lower than those reported by Levei *et al.* [17] for the same area in 2007, suggesting that environmental protection measures along natural attenuation and closing of the most pollutant industrial activities were effective in pollution reduction. Moreover, the pollution sources changes from the industrial (smelting) to urban areas (fuel and oil additives, tires, brake liners, urban surfaces corrosion or erosion). The found average HMs contents in the soils of post-industrial area are comparable for Cd, higher for Cu and Pb and lower for Zn than those reported by Nadgorska-Socha *et al.* [12] in soils from Dabrowa Gornicza city, Poland, where ironworks and waste processing plants function. The average concentrations of Zn are comparable, Cd and Ni higher and Cu and Pb lower in soils from Cluj-Napoca city, than those reported by Horvath *et al.* [18] in urban soils from Sopron city, Hungary.

Similarly to soil, the HMs concentration has a broader range in plantain leafs from the post-industrial area, than in those from the urban area. The average concentrations of Pb and Zn are much higher in the plantain leafs from post-industrial area, while the average concentrations of Cu, Cd, Cr

and Ni are comparable in the two areas, indicating that plantain has a metal excluding mechanism that allows the tolerance of high contents of Cu, Cd, Cr and Ni.

The contents of Cu, Pb, Zn found in plantain leafs from Cluj-Napoca were much lower than those found in Rome, Italy [10], while in leafs from Baia-Mare are considerably lower than those found in Kosovska Mitrovica city, Serbia, where a Pb and Zn smelter is operational [14]. Compared to HMs in *Plantago lanceolata* grown in soils from mining and smelting sites in the southern part of Poland [19], the contents of Cd, Pb and Zn in the *Plantago major* leafs determined in our study in the post-industrial area were much lower, while those of Cu were higher.

Table 4. Heavy metal contents in plantain leafs (mg/kg)

Sample	Cu	Pb	Zn	Cd	Cr	Ni
Urban area (Cluj-Napoca)						
P1	5.36	0.38	25.6	0.10	1.27	2.27
P2	7.21	0.10	17.9	0.21	3.35	3.35
P3	6.96	1.37	25.2	0.10	1.68	2.66
P4	9.51	0.39	40.7	0.14	0.82	3.93
P5	6.41	0.32	28.7	0.22	1.04	2.64
P6	7.46	0.37	20.9	0.07	1.02	2.47
Minimum	**5.36**	**0.10**	**17.9**	**0.07**	**0.82**	**2.27**
Maximum	**9.51**	**1.37**	**40.7**	**0.22**	**3.35**	**3.93**
Average	**7.15**	**0.49**	**26.5**	**0.14**	**1.53**	**2.88**
St. Dev.	**1.38**	**0.45**	**7.93**	**0.06**	**0.94**	**0.63**
Ij	**5.20**	**1.10**	**3.34**	**2.25**	**1.63**	**4.60**
Post-industrial area (Baia-Mare)						
P7	6.61	0.54	32.6	0.06	0.42	2.51
P8	7.51	2.54	49.4	0.31	0.82	2.47
P9	5.91	0.97	26.0	0.11	1.07	1.86
P10	16.0	2.50	162	1.50	2.76	4.95
P11	11.1	3.07	52.9	0.11	0.33	1.10
P12	10.7	4.79	120	0.83	2.12	3.14
Minimum	**5.91**	**0.54**	**26.0**	**0.06**	**0.33**	**1.10**
Maximum	**16.0**	**4.79**	**162**	**1.50**	**2.76**	**4.95**
Average	**9.61**	**2.40**	**73.8**	**0.49**	**1.25**	**2.67**
St. Dev.	**3.78**	**1.53**	**54.6**	**0.57**	**0.98**	**1.31**
Ij	**2.55**	**1.57**	**1.35**	**0.85**	**1.28**	**2.04**

The decreasing trend of the average HMs content is similar in the plantain leafs from post-industrial (Zn>Cu>Ni>Pb>Cr>Cd), and urban (Zn>Cu> Ni>Cr>Pb>Cd) areas, except for Pb and Cr. However, the decreasing trend is very different from that found in soil, suggesting that HMs concentration in plantain and soil does not vary proportionally, probably due to the different

uptake mechanisms of individual HMs. A similar HMs order was found by Galal and Shehata [9] in plantain shoots grown in traffic polluted soils from the vicinity of Zagazig–Banha highway in Egypt. Except 1 sample for Zn, the HMs concentration in plantain leafs did not exceed the excessive or toxic concentrations: 20-100 mg/kg Cu, 30-300 mg/kg Pb, 100-400 Zn, 10-100 Ni, 5-30 Cd and Cr [20].

To evaluate the plantain ability to take up HMs from soil, the enrichment factor (EF) was calculated according to equation 1. The EFs>1 indicate the plantain capacity to uptake HMs from soils and transfer them to leafs, EFs values near 1 suggest that the HMs content in plantain is not influenced by the HMs content in soil, while EFs<1 indicate that plantain exclude the HMs from uptake [9].

$$EF_j = \frac{C_{p,j}}{C_s,j} \quad \text{Eq. 1}$$

where, EF_j is the enrichment factor of a specific HM, $C_{p,j}$ is the HM concentration in plantain leafs, expressed in mg/kg and $C_{s,j}$ is the HM concentration in soil, expressed in mg/kg.

The EFs (Table 5) are below 0.5 in both sites and for all investigated HMs, the highest EF is found for Zn in the post-industrial site, probably as a consequence of the low HMs bioavailability or the development of exclusion mechanism in plantains grown on polluted substrate.

Table 5. Heavy metal enrichment factor in plantain leafs

EF	Cu	Pb	Zn	Cd	Cr	Ni
Urban area (Cluj-Napoca)						
EF1	0.099	0.005	0.170	0.033	0.034	0.059
EF2	0.239	0.004	0.213	0.064	0.047	0.044
EF3	0.229	0.031	0.215	0.043	0.047	0.064
EF4	0.379	0.012	0.427	0.042	0.018	0.071
EF5	0.090	0.006	0.198	0.081	0.024	0.077
EF6	0.213	0.004	0.134	0.018	0.024	0.064
Minimum	**0.090**	**0.004**	**0.134**	**0.018**	**0.018**	**0.044**
Maximum	**0.379**	**0.031**	**0.427**	**0.081**	**0.047**	**0.077**
Average	**0.208**	**0.010**	**0.226**	**0.047**	**0.032**	**0.063**
St. Dev.	**0.106**	**0.010**	**0.103**	**0.022**	**0.012**	**0.011**
Post-industrial area (Baia-Mare)						
EF7	0.294	0.017	0.466	0.200	0.010	0.057
EF8	0.120	0.015	0.274	0.051	0.114	0.137
EF9	0.169	0.025	0.291	0.110	0.034	0.036
EF10	0.069	0.012	0.278	0.268	0.153	0.283
EF11	0.408	0.011	0.165	0.041	0.183	0.049
EF12	0.212	0.030	0.443	0.169	0.065	0.121
Minimum	**0.069**	**0.011**	**0.165**	**0.041**	**0.010**	**0.036**
Maximum	**0.408**	**0.030**	**0.466**	**0.268**	**0.183**	**0.283**
Average	**0.212**	**0.018**	**0.320**	**0.140**	**0.093**	**0.114**
St. Dev.	**0.123**	**0.008**	**0.114**	**0.089**	**0.068**	**0.092**

According to the EFs, the plantain's uptake capability is in the order Zn>Cu>Ni>Cd>Cr>Pb in urban area and Zn>Cu> Cd>Ni>Cr>Pb in post-industrial area. The similar trend confirms once again the exclusion capability of plantain that enables its tolerance to high levels of HMs allowing the colonization of highly contaminated soils. The EFs in the present study were lower compared to those reported in the Zagazig–Banha heavy-traffic highway, Egypt, comparable with those in *Plantago lanceolata* from a smelting area in Poland [9, 19]. Compared to EFs reported in *Urtica dioica* from Baia-Mare area our results are lower for Cd, Cr, Ni, higher for Cu and comparable for Pb and Zn [21]. Although plantain was reported as a good Pb and Zn accumulator [14], the study confirms the accumulation capacity for Zn, but in case of Pb such capacity was not observed. A possible explanation could be either the low Pb bioavailability in soil or the fast adaptive tolerance of plantain to polymetallic pollution [22].

The range and average of EFs for the investigated elements in the two sites are presented in Figure 1.

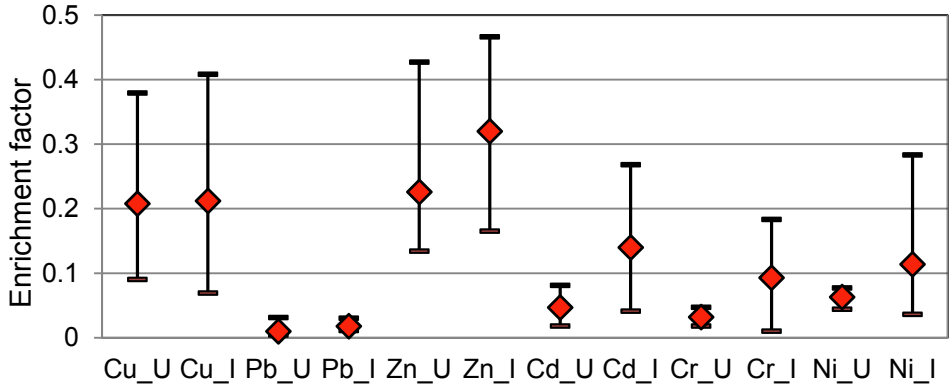

Figure 1. Range (min-max) and average EFs in urban (U) and post-industrial (I) areas

Although, generally low EFs were determined in the two sites, differences in terms of range and average can be noticed both among HMs and among sites. Thus, the EFs for Cu, Pb and Zn have similar ranges in the two areas, a high variability being observed for Cu and Zn. On the other hand, in the case of Cd, Cr and Ni, the ranges are wider in the post-industrial area than in the urban area. The average EFs in the two areas are comparable in case of Cu and Pb and higher in the industrial area for Zn, Cd, Cr, Ni. Based on the enrichment factor, plantain was found to be tolerant to high Cu, Pb, Zn, Cd, Cr and Ni contents.

To assess the HMs accumulation capability of plantain, metal accumulation index (MAI) was calculated according to Equation 2. Plants with high MAI are suitable to be used as barriers between contaminated and vulnerable areas, such as parks and residential areas [12, 23].

$$MAI = \frac{1}{N}\sum_{j=1}^{N} I_j \qquad \text{Eq. 2}$$

where N is the number of metals determined (6) and I_j is the ratio of average concentration for each HMs in plantain leafs and its standard deviation.

The MAI for urban area is 3.02, while for the post-industrial area is 1.61, suggesting a moderate to good capability of plantain to accumulate metals from the surrounding environment. The contribution of each HM to MAI (Figure 2) revealed that in urban area the main accumulated elements are Cu, Ni and Zn, while in the post-industrial area Cu, Ni and Pb.

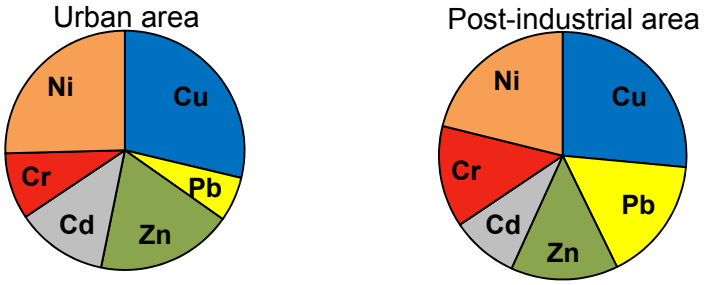

Figure 2. Heavy metal contribution to metal accumulation index (MAI)

The obtained MAI values were comparable with those of dandelion (*Taraxacum officinale*) grown in an area with intense traffic in Cuneo, Italy [23], but much lower than those of *Plantago lanceolata* grown in a smelting area from Poland [12].

CONCLUSIONS

This study was conducted to screen the *Plantago major* potential for heavy metal accumulation in soils from urban and post-industrial areas. The results of the study revealed significant differences between the contents of the analysed heavy metals in the soil and plantain leafs, of both urban and post-industrial areas. In both sites, Zn and Pb were the most abundant in soil, although the average concentrations of Zn and Pb were higher in the post-industrial area, while Cr and Ni in the urban area. The Cu, Cd, Cr and Ni in plantain leafs are comparable in the two areas, while

Pb and Zn were higher in the post-industrial area. The soil-plantain enrichment factors below 0.5 in both sites and for all investigated metals indicated that *Plantago major* has developed an adaptive tolerance to heavy metal contaminated substrates. The metal accumulation index confirmed that plantain has a moderate to good capability to accumulate Cu and Zn from the surrounding environment.

EXPERIMENTAL SECTION

Study species and areas

Plantago major (plantain) is a member of the *Plantaginaceae* family, frequently found near roads, pastures, cultivated fields and landfills [9, 24]. It is a widely spread perennial herbaceous plant that thrives even in compacted soils with low water and nutrient contents. The oval-shaped, parallel-veined leafs with acute apex and smooth margin form a rosette. The flowers are small, greenish-brown with purple stamens, produced in a dense spike on top of a stem. The plant has medicinal applications since ancient times for wound healing, gastrointestinal disorders and respiratory infections [24]. Although an edible herb, rich in biological active compounds as flavonoids, vitamins (A, B, C, K) and micronutrients (Cr, Fe, Mg, Mn, P, K, Se, Si), it is considered more a weed than a foodstuff [9, 24].

Situated in the North-Western part of Romania, Cluj-Napoca is the fourth largest city, with about 350000 inhabitants. The main metal pollution sources are related to traffic, urban runoff, residential heating and municipal landfill [25, 26]. As a consequence of economic changes from heavy industry to services, the main industrial polluting sources have been removed progressively during the past decades. Situated in the North of Romania, Baia-Mare city has about 150000 inhabitants and was considered a pollution hotspot due to its long history of mining and ore processing activities [17]. The main pollution source is represented by the former metallurgical industry that produced base-metal (Pb, Cu, Zn) concentrates, Au and Ag from nonferrous sulfidic ores [27, 28]. In the last two decades both the extractive and metallurgical industry gradually declined. Currently all industrial activities are under conservation of decommissioned.

Sampling, sample preparation and analysis

Plantago major (P) and the adjacent soil (S) were collected at the end of their vegetative period (October 2016) in Cluj-Napoca urban (1-6) and Baia-Mare post-industrial (7-12) areas in the North-West Romania. Leafs were collected using a Teflon coated knife. Leafs affected by chlorosis or necrosis were discarded. Plant leafs were thoroughly washed with tap water, rinsed three

times with distilled water and freeze-dried using a FreeZone 2.5 freeze-drying system (Labconco) at -40°C and -25 psi for 2 days. The dried samples were ground into a powder using GM200 Grindomix Knife Mill (Retsch). Soil samples were collected from root depth (0-10 cm) using a stainless steel scoop, air dried, ground to a fine powder and sieved through a 250 µm sieve.

For sample preparation and analysis, certified standard solutions, high purity reagents (Merck) and ultrapure water (Direct-Q3 UV Millipore) were used. All glassware was cleaned with 5% HNO_3 prior to use. An amount of 1 g soil was exposed to acid digestion with 28 ml *aqua regia* (21 ml of 37% HCl and 7 ml of 65% HNO_3) for 16 h at room temperature to produce slow oxidation of the organic matter, and then the temperature of the reaction mixture was raised to reflux conditions and maintained for 2 h. After cooling to room temperature, the slurry was filtered and diluted to 100 ml with distilled water. An amount of 1 g plantain powder was digested with 5 ml of 65% HNO_3 and 2 ml of 30% H_2O_2 in a closed polytetrafluoroethylene vessel microwave digestion system (Berghof MWS-3+, Eningen, Germany) [29, 30]. The digested samples were filtered and diluted to 20 ml with ultrapure water. The contents of Cu, Pb, Zn, Cd, Cr and Ni in the digested samples were determined by inductively coupled plasma mass spectrometry (Elan DRC II, Sciex, Perkin Elmer). The HMs concentration in both soil and leaf samples were measured in duplicate and the results were reported as average.

Method performance and quality control

The method performance was studied by determining the LOD, LOQ and U. The LOD of each element was calculated as the HMs concentration that corresponds to 3 times the standard deviation of ten independent measurements of the blank, divided by the slope of the calibration curve. The LOQ was calculated as 3 times the LOD [31, 32]. The U was estimated by a bottom-up approach, systematically evaluating all the uncertainty sources from calibration certificates and from statistical analysis of repeated measurements. The combined standard uncertainty was obtained by combining the uncertainties, according to the law of propagation of uncertainties. The final result was reported as expanded uncertainty, calculated by multiplying the standard uncertainty with the coverage factor (k=2), corresponding to a 95% confidence level [33]. The accuracy of measurements was assessed by determination of the studied elements in ERM-CC141 Loam Soil and IAEA-359 Cabbage CRMs.

ACKNOWLEDGMENTS

This work was supported by a grant of the Romanian National Authority for Scientific Research and Innovation, CCCDI – UEFISCDI, project number 91BM/2017 (IMPAACT).

REFERENCES

1. N. Massa, F. Andreucci, M. Poli, M. Aceto, M. Barbato, G. Berta, *Ecotoxicology and Environmental Safety*, **2010**, *73*, 1988.
2. S.M. Serbula, D.D.J. Milljkovic, R.M. Kovacevic, A.A. Ilic, *Ecotoxicology and Environmental Safety*, **2012**, *76*, 209.
3. H. Ali, E. Khan, *Toxicological & Environmental Chemistry*, **2018**, DOI: 10.1080/ 02772248.2017.1413652.
4. O. Pourret, J.C. Bollinger, *Science of the Total Environment*, **2018**, *610–611*, 419.
5. K.J. Appenroth, *Acta Physiologiae Plantarum*, **2010**, *32*, 615.
6. A. Gholizadeh, L. Boruvka, M.M. Seberioon, J. Kozak, R. Vasat, K. Nemecek, *Soil and Water Research*, **2015**, *10*, 218.
7. F.J. Zao, *European Journal of Soil Science,* **2010***, 61*,155.
8. G. Lough, J.J. Schauer, J.S. Park, M.M. Shafer, J.T. Deminter, J. Weinstein, *Environmental Science & Technology*, **2005**, *39*, 826.
9. T.M. Galal, H.S. Shehata, *Ecological Indicators*, **2015**, *48*, 244.
10. D. Malizia, A. Giuliano, G. Ortaggi, A. Masotti, *Chemistry Central Journal*, **2012**, *6*, S6.
11. M. K. Kurteva, *Phytologia Balcanica*, **2009**, *15*, 261.
12. A. Nadgorska-Socha, M. Kandziora-Ciupa, M. Trzesicki, G. Barczyk, *Chemosphere*, **2017**, *183*, 471.
13. A.A. Akram, A.A. Al-Homaidan, *Australian Journal of Basic and Applied Sciences*, **2007**, *1*, 467.
14. R. Filipovic-Trajkovic, Z.S. Ilic, L. Sunic, S. Andjelkovic, *Journal of Food, Agriculture & Environment*, **2012**, *10*, 959.
15. R. Djingova, I. Kuleff, *Chemistry and Ecology*, **1999**, *16*, 239.
16. Ministerial Order 956, *Official Journal of Romania*, **1997**, 303bis
17. E. Levei, T. Frentiu, M. Ponta, M. Senila, M. Miclean, C. Roman, E. Cordos, *International Journal of Environmental Analytical Chemistry*, **2009**, *89*, 635.
18. A. Horvath, P. Szucs, A. Bidlo, *Journal of Soils and Sediments*, **2015**, *15*, 1825.
19. A. Nadgorska-Socha, B. Ptasinski, A. Kita, *Ecotoxicology*, **2013**, *22*, 1422.
20. Kabata-Pendias, A., "Trace Elements in Soils and Plants" Fourth ed. CRC Press, Boca Raton, FL. **2010**, chapter 5.
21. C. Mihali, G. Oprea, A. Michnea, S.G. Jelea, M. Jelea, C. Man, M. Senila, L. Grigor, *Carpathian Journal of Earth and Environmental Sciences*, **2013**, *8*, 143.

22. E. Remon, J.L. Bouchardon, O. Faure, *Chemosphere*, **2007**, *69*, 41–47.
23. A. Giacomino, M. Malandrino, M.L. Colombo, S. Miaglia, P. Maimone, S. Blancato, E. Conca, O. Abollino, *Journal of Chemistry*, **2016**, *2016*, 9842987.
24. J. Vandana, A.K. Gupta, A. Mukerjee, *International Journal of Chemical and Physical Sciences*, **2017**, *6*, 26.
25. C. Florean, H. Szilagyi, A. Hegy, *Present Environment and Sustainable Development*, **2016**, *10*, 207.
26. N. Bican-Brisan, T. Enache, C. Rosu, *Studia UBB Chemia*, **2013**, *63*, 253.
27. C. Roba, C. Rosu, I. Pistea, A. Ozunu, C. Baciu, *Environmental Science and Pollution Research*, **2016**, *23*, 6062.
28. M. Senila, E.A. Levei, L.R. Senila, G.M. Oprea, C.M. Roman, *Journal of Environmental Science and Health, Part A: Toxic/Hazardous Substances and Environmental Engineering*, **2012**, *47*, 614.
29. E. A. Levei, M. Miclean, M. Senila, *Studia UBB Chemia*, **2012**, *62*, 103.
30. O. Cadar, M. Miclean, S. Cadar, C. Tanaselia, L. Senila, M. Senila *Environmental Engineering and Management Journal*, **2015**, *14*, 2523.
31. C. Voica, A. Dehelean, A. Ioardache, I. Geana, *Romanian Reports in Physics*, **2012**, *64*, 221.
32. T. Frentiu, M. Ponta, R. Hategan, *Chemistry Central Journal*, **2013**, *7*, 43.
33. M. Senila, A. Drolc, A. Pintar, L. Senila, E. Levei, *Journal of Analytical Science and Technology,* **2014**, *5*, 37.

STUDIA UBB CHEMIA, LXIII, 1, 2018 (p. 99-108)
(RECOMMENDED CITATION)
DOI:10.24193/subbchem.2018.1.08

STUDY ON THE PHYSICOCHEMICAL AND CHEMICAL PARAMETERS OF DRINKING AND SURFACE WATERS FROM MINE AREA AT VILLAGE BOV, BALKAN MOUNTAIN, BULGARIA

METODI MLADENOV[a,*], IRINA KARADJOVA[b], GALIA GENTSCHEVA[c,d], ALBENA PREDOEVA[e]

ABSTRACT. Water quality is influenced by natural local climate, geology and anthropogenic effects. In the present study, surface waters in hydrographic area, situated in mining region, in the vicinity of abandon copper mine, are characterized and their quality assessed from the view point of the requirements of European Water Frame Directive and Drinking Water Directive. Three sampling campaigns starting at 2012 from 16 sampling sites, in different seasons were performed in order to evaluate both natural, seasonal variations connected with water regimes and anthropogenic pressures. Chemical elements (Al, As, Ba, Cd, Cr, Co, Cu, Fe, Hg, Mn, Ni, Pb, Se, U, V, Zn and lanthanides) and physicochemical parameters (pH, conductivity, hardness, chemical oxygen demand (COD_{KMnO4}); biological oxygen demand (BOD_5); dissolved oxygen; dissolved solids; suspended matter; dry residue; chlorides; sulphates; nitrates; phosphates) were measured for characterization and evaluation of different water sources in the region. Conclusions for the further use of waters from this region as tap waters were presented and validated through the determination of much more chemical elements than these required from national legislation.

Keywords: *surface water, drinking water, chemical element, physicochemical parameter, ICP-MS.*

[a] *University of Chemical Technology and Metallurgy, Department of Engineering Ecology, 8 St. Kliment Ohridski blvd., Sofia, Bulgaria.*
[b] *University of Sofia, Faculty of Chemistry and Pharmacy, 1 James Bourchier blvd., Sofia, Bulgaria.*
[c] *Medical University–Pleven, Department of Chemistry and Biochemistry, 1, Sv. Kliment Ohridski Str., Pleven, Bulgaria.*
[d] *Institute of General and Inorganic Chemistry, Bulgarian Academy of Sciences, Akad. G. Bonchev Str, Bl. 11, Sofia, Bulgaria.*
[e] *Research Institute of Forensic Science and Criminology, 1 Aleksander Malinov blvd., Sofia, Bulgaria.*
[*] *Corresponding author: mladenov@uctm.edu*

INTRODUCTION

European Water Frame Directive [1] requires classification of surface waters in member states, based on the assessment of their ecological and chemical status. On the other side in some cases same surface waters are used as only source of drinking water for the people living in the same area and in this case quality standards of Drinking Water Directive should be taken into account [2].

In this study results from three monitoring campaigns of surface waters near the village Bov, are presented. Also, very often themselves sources used for drinking water, are reservoirs (or other type of intake) and control their maintenance is lowered. Main problem is the classification of the tested waters. In such places often, a surface water source is also used as drinking and precisely where the difficulty comes in the classification of water sources and conducting a further monitoring. In such cases, the question is which rules and regulations to implement: surface water [8] - With a view to environmental monitoring or drinking water [9, 10] – in order to ensure safety for the population?

Many similar studies [11-16] in which the element concentration, mainly of heavy metals are examined, it have, but the authors cannot find studies in which the hydrological regime to be taken into account.

As a result characterization of surface and drinking water sources in the area of Bov as well as dynamics of the changes in their composition in an extended period of time, and depending on the hydrological regime in the area will be presented.

RESULTS AND DISCUSSION

Physicochemical parameters

However, results obtained for surface waters do not confirm good ecological status especially for sampling points situated downstream after cities and parameters such as – biological oxygen demand and dissolved oxygen. It is worth mention that relatively different values were accepted as permissible limits for physicochemical parameters for drinking waters which were derived on the basis of human health safety and for surface waters derived on the basis of health and biodiversity of aquatic organism [8]. That is why different classification of waters might be obtained taking into account their different use and application.

Results for physicochemical parameters for all studied samples, for all sampling campaigns are below the permissible limits (pH=6,5-9,5; conductivity – 2.10^{-3} μS/cm; hardness – 12 mgeq.dm^{-3}; P-total – 0.5 mg.dm^{-3}; N-NO_3 – 30 mg.dm^{-3}; COD_{KMnO4} – 5.0 mg.dm^{-3}; SO_4^{2-} – 250 mg.dm^{-3}) accepted as national standards for drinking waters

As an example, the pH values obtained for drinking waters during the three sampling campaigns are given in Table 1. Statistically insignificant differences between results undoubtedly show no any influence of hydrological regime. Almost identical results were obtained for all other studied physicochemical parameters [10]. However, results obtained for surface waters do not confirm good ecological status especially for sampling points situated downstream after cities and parameterc such as – biological oxygen demand and dissolved oxygen. It is worth mention that relatively different values were accepted as permissible limits for physicochemical parameters for drinking waters which were derived on the basis of human health safety and for surface waters derived on the basis of health and biodiversity of aquatic organism [8]. That is why different classification of waters might be obtained taking into account their different use and application.

Table 1. pH values obtained for drinking waters.

pH		Sample number											Permissible range
		5	6	7	8	9	10	11	12	14	15	16	
Sampling campaign (SC)	**A**	8.15	7.83	8.07	7.85	7.94	7.96	8.11	7.98	7.07	7.52	7.58	6.5-9.5
	B	8.04	7.72	7.91	7.78	7.92	7.78	7.93	8.01	7.08	7.49	7.58	
	C	8.10	7.04	7.22	7.14	6.99	7.20	7.53	7.32	7.06	7.48	7.56	

Chemical elements content

Results obtained for elements (Al, As, Ba, Cd, Cr, Co, Cu, Fe, Mn, Ni, Pb, Se, U, V, Zn) content in all studied sampling sites (without local springs) are depicted in Table 2. The concentrations measured for Hg are close to their natural levels and much below the permissible limits for surface and drinking waters and are not included in Table 2. The same is valid for lanthanides; these elements were included in the present study because elevated concentrations might be expected near the abandon copper mine. However determined concentrations are very close to natural background levels in surface and spring waters.

Surface waters

Results obtained for priority pollutants (Cd, Hg, Ni and Pb) and specific pollutants (Al, As, Cr, Cu, Fe, Mn, U and Zn, accepted at national level) for surface waters were compared with accepted environmental quality

standards at European level for priority pollutants and with accepted environmental quality standards at national levels for specific pollutants [8]. As can be seen both chemical and ecological status of surface water at sampling point 13 is bad taking into account elevated concentrations measured for priority pollutants Cd and Pb and specific pollutants Cu and Zn. The influence of hydrological regime is evident as far as elements concentrations are statistically significantly lower for sampling campaign B in comparison with campaigns A and C. However due to the natural dilution, concentrations measured at sampling points 3 and 4 are remarkably lower and good chemical and ecological status could be assigned for river Treskavets at all.

Drinking waters

As already mention the drinking water standard might be different from those for surface waters, taking into account the way of their derivation and the purpose of their application. Sampling site 13 is water catchment in mining gallery and might be accepted as a surface water (spring of river Trescavets) and in the same time as a source of drinking water. National legislation for quality control of drinking waters requires compliance with accepted permissible limits for As, Cd, Cu, Ni, Pb, Cr, Se, Ba, V, Fe, Mn, Zn, Co.

The main water supply for drinking and household needs of the population in the region is fed from the spring of river Treskavets (sampling site 13) and controlled by sampling sites 10 and 11. As can be seen from the analytical results the concentration of Pb at the beginning is 70 μg L^{-1}, which is much above the statutory drinking water limit under regulation 12 – 10 μg L^{-1} [9]. The concentration of Pb in points 10 and 11 is three times lower, but still remain above the statutory limit. The values for all other chemical elements showed no deviation from the permissible limits. In early 2013 (B) source 13 is replaced by source 5. The results obtained during the second sampling showed values for all elements which meet the regulatory requirements in all points. Unexpectedly, relatively high concentrations over the statutory limits were found for Mn at point 13 during the last sampling. Evidently the spring at point 13 is a source of high elements concentrations and when switching it with a source 5 in the second sampling campaign, significantly lower values were observed for most of the elements. It is worth mention however that concentrations at sampling points 10 and 11 are still higher than these in initial point 5, which most probably is a sign that some elements accumulated in the pipeline network and still impact final concentrations.

Table 2. Element concentrations at every sampling point of the studied area (mean value, three parallel determinations)

Element	SC	***1***	***2***	***3***	***4***	***5***	***13***	***10***	***11***	***9***	***16***
Al, μg L^{-1}	**A**	6.8	6.1	6.6	6.4	8	2.13	5.5	5.3	8.4	9.0
	B	0.08	<0.05	<0.05	<0.05	<0.05	2.57	<0.05	<0.05	<0.05	<0.05
	C	0.05	<0.05	<0.05	0.19	<0.05	2.30	0.12	0.12	<0.05	<0.05
As, μg L^{-1}	**A**	1.58	1.86	0.89	1.21	0.12	1.78	1.3	1.4	0.95	0.9
	B	3.8	2.97	0.91	1.27	0.09	1.81	0.28	0.18	1.03	1.02
	C	6.36	3.32	0.77	1.53	0.13	1.94	0.97	0.99	1.51	1.47
Ba, μg L^{-1}	**A**	25	65	100	95	16	106	63	62	56	56
	B	32	102	101	99	15	112	15	17	56	52
	C	43	144	129	115	18	120	69	67	66	67
Cd, μg L^{-1}	**A**	<0.03	<0.03	0.03	<0.03	<0.03	1.97	1.11	1.08	<0.03	<0.03
	B	<0.03	<0.03	<0.03	0.03	<0.03	1.97	0.14	0.06	<0.03	<0.03
	C	<0.03	<0.03	<0.03	0.04	<0.03	2.24	1.17	1.13	<0.03	<0.03
Co, μg L^{-1}	**A**	0.25	0.26	0.19	0.21	0.22	20.3	10.98	11.08	0.23	0.25
	B	0.43	0.44	0.33	0.36	0.34	21.1	0.53	0.44	0.37	0.39
	C	0.41	0.41	0.39	0.42	0.25	24.4	12.01	12.07	0.44	0.48
Cr, μg L^{-1}	**A**	0.09	0.1	0.1	0.09	0.27	0.05	0.14	0.13	0.08	0.09
	B	0.07	0.07	0.06	0.06	0.09	0.03	0.1	0.1	0.1	0.1
	C	0.08	0.09	0.1	0.1	0.15	0.04	0.07	0.07	0.12	0.11
Cu, μg L^{-1}	**A**	0.7	1.22	1.46	1.87	1.05	272	79	89	0.48	0.67
	B	0.09	<0.03	0.04	0.83	<0.03	224	25.38	11.58	<0.03	<0.03
	C	1.98	1.86	2.26	3.94	0.67	349	201.9	204.7	2.41	2.52
Fe, μg L^{-1}	**A**	2.22	1.85	1.85	0.37	0.37	0.9	4.44	2.22	1.48	1.86
	B	2.21	2.11	1.71	1.65	2.1	0.8	2.33	2.31	2.53	1.65
	C	2.27	2.28	2.03	2.03	0.9	0.81	1.53	1.45	2.2	2.27
Mn, μg L^{-1}	**A**	2.16	2.6	1.25	2.14	0.25	52	13.05	13.6	0.04	0.08
	B	3.71	7.12	1.7	2.31	0.19	45	0.53	0.39	0.07	0.1
	C	6.52	2.64	1.8	4.65	0.20	56	23.18	24.67	0.16	0.2
Ni, μg L^{-1}	**A**	3.35	3.2	2.93	2.69	3.52	13.6	7.22	7.11	3.92	1.65
	B	1.36	1.41	0.95	1.04	1.18	10.1	1.5	1.37	1.37	1.52
	C	2.03	1.95	1.52	1.7	3.35	12.1	7.03	6.75	1.64	1.76
Pb, μg L^{-1}	**A**	0.04	0.05	0.42	0.48	0.07	66	26.95	29.91	0.17	0.17
	B	0.15	0.1	0.42	0.42	0.47	68	10.38	7.1	0.1	0.09
	C	0.65	0.54	0.73	0.74	<0.03	63	28.1	30.6	1.03	0.66
Se, μg L^{-1}	**A**	0.03	0.03	<0.02	0.03	0.02	0.06	<0.02	<0.02	<0.02	<0.02
	B	<0.02	<0.02	<0.02	<0.02	<0.02	0.12	0.09	0.12	0.24	0.20
	C	0.2	0.4	0.31	0.41	<0.02	0.41	0.48	0.38	0.65	0.67
V, μg L^{-1}	**A**	0.17	0.22	0.07	0.12	0.05	0.06	<0.03	<0.03	0.05	0.06
	B	0.34	0.37	0.13	0.18	0.11	0.07	0.08	0.09	0.13	0.13
	C	0.53	0.27	0.09	0.19	0.04	0.06	0.06	0.06	0.11	0.1
Zn, μg L^{-1}	**A**	7.28	6.79	7.02	8.49	10.31	124	132.5	60.33	5.65	8.9
	B	<0.05	<0.05	<0.05	<0.05	2	115	78.3	<0.05	<0.05	6.3
	C	1.58	0.97	2.11	5.34	12.09	136	101.8	67.72	3.04	28.62
RSD*,%		2-5	2-8	3-7	3-8	4-8	2-5	1-6	2-7	2-8	2-9

*RSD values range for all determinations of the element

Trace element content and physicochemical parameters of independent sources 5 and 13 (in the case when not in use to [10] power drinking water supply) and sources 6, 7, 8, 12, 14 and 15 have to meet the requirements set out in the ordinance. All tested independent sources meet the statutory values, except for the source 14. This source is located near the mine shaft used for ore extraction and Pb concentrations measured are almost 9 times higher than permissible limit of 10 μg L^{-1}.

In order to obtain more complete characterization of waters in this region several elements not mention in regulatory documents but existing and determined in copper ore were measured: Mo, Sr, Th, Tl, Se, Y, Be and lanthanides. The values for the elements Tl, Y and Be were below 0.5 μg L^{-1} for all studied sampling sites and close to their background levels. Only for element Sr were found relatively high concentrations from 90 to 340 μg L^{-1}, which however is close to the natural levels of this element in surface waters in the region. The content of lanthanides all are below <0.03 μg L^{-1}, except Eu, for which 0.03 μg L^{-1} were found in sample 3 in a first campaign (A). The probable explanation for the absence of these elements in waters in the region is that most likely they exist in the rocks and ores as slightly soluble or insoluble compounds.

CONCLUSIONS

All of the values for physicochemical parameters are below the permissible limits accepted as a national standard for drinking waters.

Results of chemical analysis show dependence between the hydrological regime and element concentration – the concentrations are statistically significantly lower for sampling campaign B in comparison with campaigns A and C.

Results obtained for priority pollutants (Cd, Hg, Ni and Pb) and specific pollutants (Al, As, Cr, Cu, Fe, Mn, U and Zn) for surface waters sources are good. Exception is sampling point 13, when it have elevated concentrations measured for priority pollutants Cd and Pb and specific pollutants Cu and Zn.

It was obtained, that values for all other chemical elements in drinking waters showed no deviation from the permissible limits, except the element Pb.

All tested independent sources meet the statutory values, except for the source 14, when the Pb concentrations measured are almost 9 times higher than permissible limit of 10 μg L^{-1}.

EXPERIMENTAL SECTION

Materials and methods

Characteristics of sampling sites

The sampling points were carefully chosen to represent the influence of various factors such as, industrial activities in the past, and other anthropogenic pressures on the quality of surface and drinking waters. The sampling points are presented in Fig. 1. 1 and 2 sampling points sequentially situated on river Bovska; 13 – spring of river Treskavets, used for drinking water; 3- sampling point on river Treskavets; 4 – sampling point on river Treskavets after the merger of river Bovska; 5, 6, 7, 8, 12, 14 and 15 – sampling points representing local springs, used for drinking water, but not included in village water supplies; 9 and 16 sampling points from drinking water supply 2; 10 and 11 sampling points from drinking water supply 1.

Three sampling campaign (SC) were performed in different seasons: summer 2012 (A) – relatively high waters (high rains one month before sampling), spring 2013 (B) – high waters (high rains in the period); autumn 2013 (C) – dry period (no any rains one months before sampling). In order to remove direct influence of rain water the sampling is performed in a period without rain at least 24 h before sampling.

The water supply 1 is feeded from the spring at sampling point 13 for the sampling campaigns A and C and from the spring at sampling point 5 for campaign B. The water supply 2 is feeded from spring at sampling point 6 for all sampling campaigns performed.

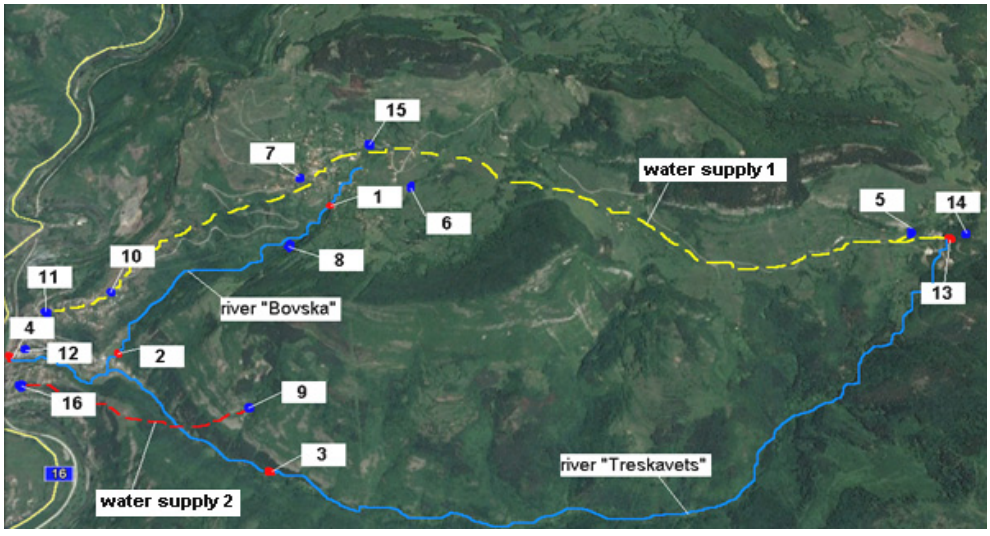

Figure 1. Region map with sampling points.

Sample collection and handling

For the determination of physicochemical parameters water samples were collected by grabsampling in polyethylene plastic bottles of 1.5 L, previously rinsed with 4 % nitric acid and then with MilliQ water. For the determination of trace metals, clean procedures were strictly followed through all experiments. Water samples of 100 ml were collected by grabsampling, immediately were filtered through 0.45 μm – cellulose membrane filters (Millipore) and acidified with 0.5 mL concentrated HNO_3 (Baker, Suprapur) until pH 2. All samples were kept at 4 ºC in a dark place before laboratory analysis.

Apparatus

Inductively coupled plasma-mass spectrometry measurements were carried out on mass spectrometer “X SERIES 2” – Thermo Scientific. Conductivity measurements and pH determinations were performed with combined pH meter “PCE-PHD1” – PCE instruments.

Reagents

High-purity reagents (Merck and Fluka Analytical), HNO_3 (65 % suprapur, Merck, Darmstadt, Germany) and Milli-Q water (0,01 $\mu S.cm^{-1}$) were used for all experiments. Quality control material for surface waters SPS-SW1 Surface Level 1 (Spectrapure Standards AS, Oslo, Norway) was used as additional calibrant. Certified Reference Material SLRS-5 (River Water Reference Material for Trace metals), National Research Council Canada was used for quality control of analytical results.

Analytical procedures

Physicochemical parameters: pH, conductivity, hardness, chemical oxygen demand (COD_{KMnO4}); biological oxygen demand (BOD_5); dissolved oxygen; dissolved solids; suspended matter; dry residue; chlorides; sulphates; nitrates and phosphates were determined according to the standard analytical procedures, accepted in national standards [17-29].

Concentrations of chemical elements (Al, As, Ba, Cd, Cr, Co, Cu, Fe, Hg, Mn, Ni, Se, U, V and Zn as well as lantanides were determined by inductively coupled plasma-mass spectrometry under optimal instrumental parameters.

REFERENCES

1. Directive 2000/60/EC of the European Parliament and of the Council, Framework for Community action in the field of water policy, 23 october 2000.
2. Directive 98/83/EC of 3 November 1998 on the quality of water intended for human consumption.
3. Zl. Zlatev, Precursory Paper of EIA (Environment Impact Assessment). Technical-economic Investigation about Improvement of Environment Safety for "Eliseina" Copper Works in Republic of Bulgaria. Baugrund Institute – KNIRIM – Ltd, Sofia, **1996**, chapter 3.
4. St. Stoyanov, Heavy Metals in the Environment and the Foodstuffs. Poisonous Influence on the Human. Clinical Pattern. Medical Treatment and Prophylaxis. PSSA, Sofia, **1999**, chapter 4 (in Bulgarian).
5. I. Gruev, D. Petkova, V. Valkov, Environment Impact Assessment Report of "Eliseina" JSC (Object in Exploitation). Scientific Research Center at UCTM-Sofia, **1999** (in Bulgarian).
6. I. Gruev, Assessment of the Impact of Old Contaminations at the "Eliseina" JSC. Scientific Research Center at UCTM-Sofia, **1999**, chapter 2.
7. I. Stoyanov, Assessment of the Impact of Old Contaminations at the "Eliseina" JSC – Stage 3. Geoecoconsult, Sofia, 2002.
8. SGRB (State Gazette of Republic of Bulgaria) Regulation №H-4/14.09.2012 for characterization of surface waters. State Gazette 22/05.03.2013 (in Bulgarian).
9. SGRB (State Gazette of Republic of Bulgaria), Regulation №12/18.02.2002 for quantities requirements for surfaces waters used for drinking purposes. State Gazette 63/28.06.2002 (in Bulgarian).
10. SGRB (State Gazette of Republic of Bulgaria), Regulation №9/16.03.2001 for quality of drinking waters. State Gazette 30/28.03.2001 (in Bulgarian).
11. X. Hao, D. Wang, P. Wang, Y. Wang, D. Zhou, *Environmental monitoring and assessment*, **2016**, *188*, 24.
12. T. Sevidik, E. Altundal, F. Kucuk, *Ekoloji*, **2015**, *24*(97), 14.
13. T. Stafilov, T.B. Balabanova, B.R. Sajn, D. Rokavec, Variability Assessment for Lithogenic and Anthropogenic Distribution of Trace and Macroelements in Water, Sediment and Soil Samples. Case Study: Bregalnica River Basin, Republic of Macedonia, Nova Science Publishers, Inc. In: Advances in Environmrntal Research, **2015**, Volume 43, Chapter 6, Editor: Justin A. Daniels.
14. O. Arkoc, *Journal of Environmental Protection and Ecology*, **2011**, 12(4), 1644.
15. M. Rasheed, P. Rao, B. Radha, M. Lakshmi, A. Dayal, *Journal of Environmental Protection and Ecology*, **2011,** *12*(2), 425.
16. A. Giouri, M. Vavelidisa, V. Melfosa, C. Christophoridis, *Journal of Environmental Protection and Ecology*, **2010**, *11*(2), 424.
17. BNS 17.1.4.27:1980 Environmental protection. Hydrosphere. Indicators for water quality. Method for pH measurement (in Bulgarian).
18. BNS EN 27888:2000 Water quality – Determination of electrical conductivity.

19. BNS 3775:1987 Drinking water. Method for determination of total hardness (in Bulgarian).
20. BNS 17.1.4.24:1980 Environmental protection. Hydrosphere. Indicators for water quality. Method for determination of chlorides (in Bulgarian).
21. BNS EN ISO 6878:2005 Water quality – Determination of phosphorus – Ammonium molybdate spectrometric method.
22. BNS 17.1.4.12:1979 Environmental protection. Hydrosphere. Indicators for water quality. Method for determination of nitrates (in Bulgarian).
23. BNS ISO 7150-1:2002 Water quality – Determination of ammonium – part 1. Manual spectrometric method (in Bulgarian).
24. BNS 17.1.4.02:1977 Environmental protection. Hydrosphere. Indicators for water quality. Method for determination of oxidizability (in Bulgarian).
25. BNS EN 1899-2:2004 Water quality – Determination of biochemical oxygen demand after after n days (BODn) – Part 2: Method for undiluted samples (ISO 5815:1989, modified).
26. BNS 17.1.4.16:1979 Environmental protection. Hydrosphere. Indicators for water quality. Method for determination of chemical oxygen demand (in Bulgarian).
27. BNS 17.1.4.03:1977 Environmental protection. Hydrosphere. Indicators for water quality. Method for determination of sulphates (in Bulgarian).
28. BNS 17.1.4.08:1978 Environmental protection. Hydrosphere. Indicators for water quality. Method for determination of dissolved oxygen content (in Bulgarian).
29. BNS 17.1.4.04:1980 Environmental protection. Hydrosphere. Indicators for water quality. Method for determination of dry residue, suspended matter and dissolved solids (in Bulgarian).

STUDIA UBB CHEMIA, LXIII, 1, 2018 (p. 109-123)
(RECOMMENDED CITATION)
DOI:10.24193/subbchem.2018.1.09

A 250-YEAR ISOTOPIC PROXY RAINFALL RECORD FROM SOUTHERN BOTSWANA

STEPHAN WOODBORNE[a,b*], GRANT HALL[b], CONNOR W. JONES[c], NEIL J. LOADER[c], ADRIAN PATRUT[d], ROXANA T. PATRUT[d], IAIN ROBERTSON[c], STEPHAN R. WINKLER[a], CHRISTIAAN W. WINTERBACH[e]

ABSTRACT. Climate records along aridity gradients where manifestations of climate change are most profound are important for testing climate models. The *Kalahari Transect* spans such a gradient, but instrumental records of climate parameters are limited in the sparsely populated region. We analysed the $\delta^{13}C$ and $\delta^{18}O$ record from a *Vachellia erioloba* (E.Mey) tree from the southern Kalahari Desert in Botswana to explore its potential as a climate proxy archive. Radiocarbon dates show that the record spans the period 1758-2013 CE. Both the $\delta^{13}C$ and $\delta^{18}O$ records correlate with local rainfall. The isotope proxies show a weak positive correlation with sea-surface temperature reconstruction from the southwestern Indian Ocean, and a stronger correlation with the El Niño Southern Oscillation index. This appears to contradict previous evidence that higher sea-surface temperatures are associated with reduced summer rainfall over the southern African interior. Instead of eastward shifts in the temperate tropical trough synoptic system during elevated southwestern Indian Ocean temperature anomalies, the evidence supports a westwards shift. The result demonstrates the potential of *Vachellia erioloba* as a climate proxy archive that may yield past climate variability from the arid regions of southern Africa.

Keywords: *ENSO, drought, Southern Africa, AMS radiocarbon dating, Vachellia erioloba, oxygen isotopes, carbon isotopes.*

[a] *iThemba LABS, Private Bag 11, WITS 2050, South Africa.*
[b] *Mammal Research Institute, University of Pretoria, Private Bag X20, Hatfield 0028, South Africa.*
[c] *Swansea University, Department of Geography, Swansea SA2 8PP, UK.*
[d] *Babeş-Bolyai University, Faculty of Chemistry and Chemical Engineering, 11 Arany Janos, RO-400028, Cluj-Napoca, Romania.*
[e] *Tau Consultants (Pty) Ltd, P/Bag 83, Maun, Botswana.*
[*] *Corresponding author: swoodborne@tlabs.ac.za*

INTRODUCTION

The majority of the inhabitants of southern Africa are dependent on non-commercial rain-fed agricultural subsistence strategies [1]. A persistent threat to this economy is rainfall variability, and although the region experiences substantial droughts, the instrumental rainfall records that might elucidate the underlying forcing are generally of short duration. Attempts to understand wet/dry cycles in Botswana, for example, have relied on records as short as 30- [2] to 50- [3,4] years. Despite the poor instrumental records there is strong evidence for the role of the El Niño Southern Oscillation (ENSO) in mediating droughts [5], but the relationship is not linear. While most El Niño events are associated with droughts, some are associated with wetter conditions [6-8]. The ENSO phenomenon operates at an inter-annual time scale, but there is also evidence for large-scale synoptic changes that drive rainfall variability at near-decadal time scales. Since most of the moisture advected over the southern African continent comes from the southwestern Indian Ocean [9] the most likely large scale forcing is in response to sea-surface temperature changes (SWIO SST) in that region [5,10,11].

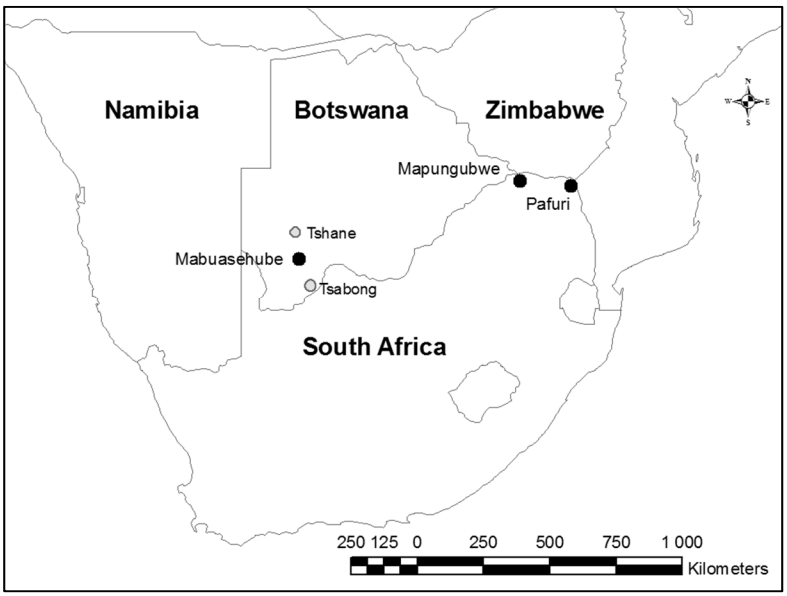

Figure 1. Map of the study region showing the location of tree sampling sites (black symbols) and towns (grey symbols) mentioned in the text.

The short- and long-term forcing mechanisms for rainfall over southern Africa may operate to reinforce or annul one another, and the net effect is that wet/dry cycles are not random, but instead seem to oscillate at a 16-20 year periodicity [12]. If an underlying driver of rainfall variability changes over longer periods (multi-decadal to centennial time scales) then the ability to discern the effect is severely limited owing to the short duration of the instrumental data. Not only is this relevant for understanding the return time of droughts, but it is very relevant to understand the mechanisms underlying projected future climate changes. Climate change forecasts suggest that parts of the study area will be among the fastest warming areas on Earth, and the same regions will also experience significant reductions in rainfall [13,14]. The vulnerability of communities and even the National GDP of countries to drought in southern Africa are likely to be exacerbated into the future. Testing the skill of climate forecasts is necessary, but the poor instrumental record is a strong constraint.

Southern Africa is characterized by strong climatic gradients between hot, dry deserts and more mesic regions. The ecological gradients have been studied in the context of ecosystem services along the *Kalahari Transect* [15], but they also offer sensitive indicators of climate change and climate forcing. Verification of forcing mechanisms requires longer time series for rainfall, which in the absence of good instrumental records, is often derived from tree ring analyses. Classic applications of ring width chronologies in southern Africa are rare [16-21] because few tree species have been shown to grow annual rings that record climate variability. Recent studies have made use of the correlation between leaf-level transpiration regulation and stable carbon isotope ratios ($\delta^{13}C$) in wood [11, 22-24] to generate proxy rainfall records. Most of this research focused on tree species that do not occur in the xeric regions. In this study we attempt to generate a climate record from a *Vachellia erioloba* tree from southern Botswana (**Figure 1**) using stable isotope proxies and a radiocarbon based age model. *Vachellia erioloba* is a cornerstone species in the arid regions and preliminary studies suggest that its sensitivity to environmental forcing (rainfall) and longevity [25], and its low sensitivity to intrinsic water-use efficiency changes with elevated CO_2 [26] make it a potentially valuable archive of climate variability.

RESULTS AND DISCUSSION

The age model suggests that the Mabuasehube *Vachellia erioloba* specimen died in approximately 2013 CE (**Figure 2**), - 2 years prior to sampling, which accords with its physical appearance. It started growing in approximately

1758 CE and so the radial section records the growth over the last 255 years. The implication of the age model is that sampling density is sub-annual (average 1.43 samples per year) post 1947 CE, and near biennial (average 0.52 samples per year) prior to 1947 CE.

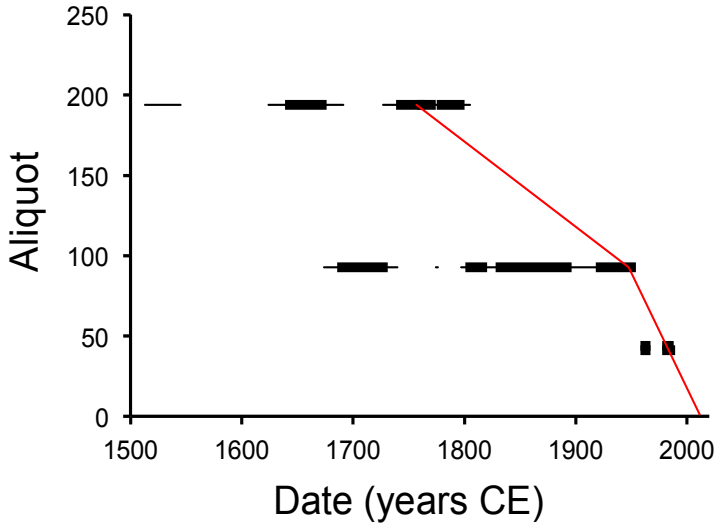

Figure 2. Age model for the Mabuasehube *Vachellia erioloba*. The 1-sigma calibrated intercept ranges for the four radiocarbon dates in Table 1 are represented by bold horizontal black lines while 2-sigma ranges are represented by thin horizontal black lines. The age model (red line) is a linear relationship between aliquot number (commencing with 0=bark) and calendar age with a gradient change at aliquot 93. The age model intercepts all the radiocarbon ages in the 1-sigma range.

The $\delta^{13}C$ and $\delta^{18}O$ isotopic time series are presented in **Figure 3**. In this representation the $\delta^{13}C$ y-axis is inverted because less negative/more positive values are associated with dry conditions, and more negative/less positive values with wetter conditions. An inverted $\delta^{13}C$ y-axis may intuitively be interpreted as a proxy rainfall scale. Since $\delta^{13}C$ and $\delta^{18}O$ co-vary ($r=0.424$, $p<0.001$, $n=142$), the y-axis for $\delta^{18}O$ is also inverted to accentuate this pattern. Both records show a high frequency component with inter-annual variability, but they also show near-decadal scale variability.

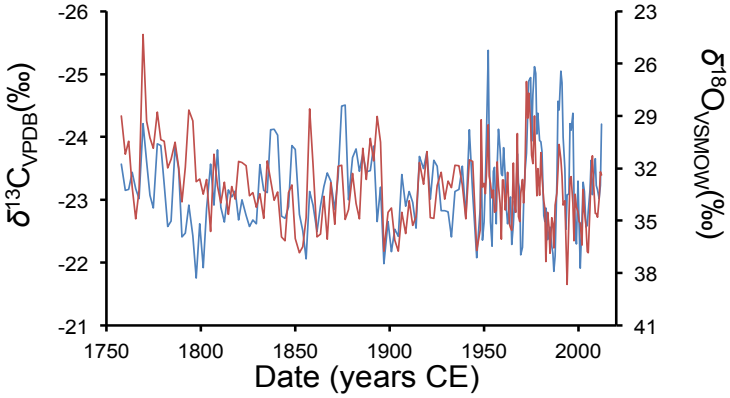

Figure 3. $\delta^{13}C$ (red, left y-axis) and $\delta^{18}O$ (blue, right y-axis) from the Mabuasehube *Vachellia erioloba.* The $\delta^{13}C$ y-axis is inverted to intuitively represent a rainfall proxy scale with high rainfall at the top of the graph and low rainfall at the bottom (see **Figure 4**). The $\delta^{18}O$ y-axis is also inverted to highlight the co-variance with $\delta^{13}C$.

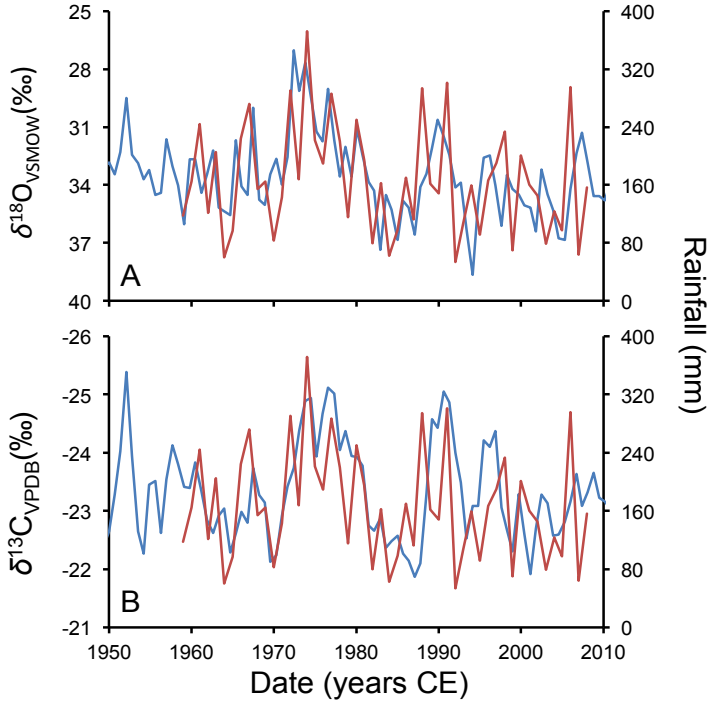

Figure 4. A: The measured $\delta^{18}O$ values, and B: $\delta^{13}C$ values (both blue, left y-axes) show a strong covariance with rainfall (red, right y-axes) from the stations at Tshane and Tsabong [3] (r=-0.778 for $\delta^{18}O$ and r= -0.668 for $\delta^{13}C$). Note that the isotope y-axes are inverted.

Wood $\delta^{18}O$ values typically respond to variations in the isotopic value of source water, or to leaf-level evaporation [27]. In southern Africa the amount effect has been shown to be relatively weak [28] (although this study was done in the winter rainfall area which is distinct from the summer rainfall system at Mabuasehube), while leaf-level evaporation mediated by temperature is dominant [29]. In the summer rainfall area low rainfall and high temperatures coincide and these effects reinforce one another in respect of $\delta^{18}O$ values. The area of the Kalahari Desert from which this tree was sampled is sparsely populated and local rainfall records are rare. We made use of published rainfall records from Tshane, located 115 km north of the sampling site, and Tsabong, located 115 km south of the site [3]. The rainfall from these two sites was averaged to account for the localized variability in convective rainfall in southern Africa [11]. Despite potential problems with the age model based on the assumption of linear radial growth rates the result shows a significant correlation between rainfall and $\delta^{18}O$ values (**Figure 4A**) ($r=-0.778$, $p<0.001$, $n=48$). Irrespective of the role of leaf-level evaporation, and source water effects, this indicates that wood $\delta^{18}O$ values are controlled by rainfall.

The relationship between $\delta^{13}C$ values in wood, and environmental drivers may be affected by a number of variables [27]. In open savanna environments with high ambient growing season temperatures it is anticipated that the dominant factor with be edaphic water availability. In order to verify this the $\delta^{13}C$ record is compared with local rainfall (**Figure 4B**). In the Mabuasehube *Vachellia erioloba* record rainfall is significantly correlated with the $\delta^{13}C$ record ($r=-0.668$, $p<0.0001$, $n=48$), and it suggests that the water-use physiology of *Vachellia erioloba* responds to rainfall, and is reflected in the wood $\delta^{13}C$ values.

The significant empirical correlations between the $\delta^{13}C$ and $\delta^{18}O$ isotopic time series from the Mabuasehube *Vachellia erioloba* specimen and instrumental rainfall records accords with theoretical expectations of stomatal water regulation on $\delta^{13}C$ and source water effects on $\delta^{18}O$. Both isotopic time series proxy rainfall, but the correlation between the $\delta^{13}C$ and $\delta^{18}O$ is not perfect. This is likely the effect of leaf-level evaporation that will affect the $\delta^{18}O$ record, but not the $\delta^{13}C$ record. We conclude that the 255-year rainfall proxy record from the Mabuasehube *Vachellia erioloba* specimen has the potential to provide a basis for assessing long-term climate forcing that cannot be assessed using the short duration instrumental record for the region.

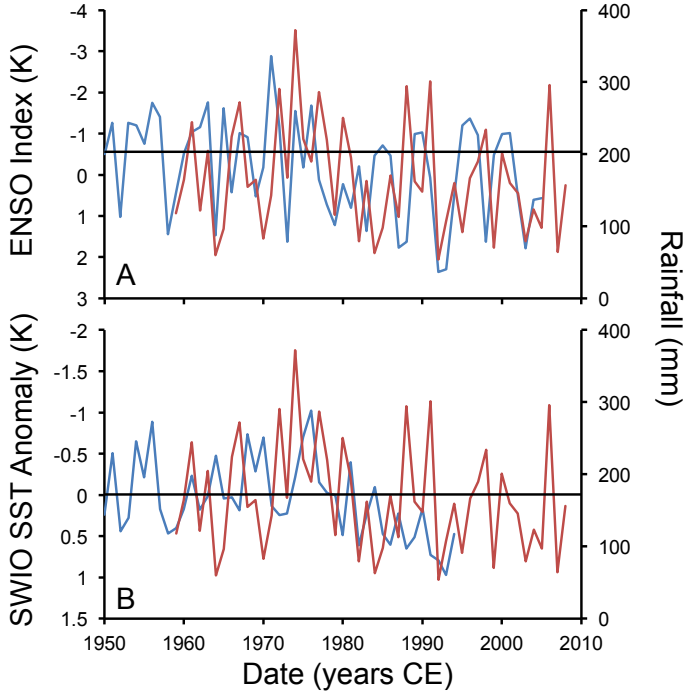

Figure 5. A: Comparison between the instrumental rainfall record (red, right axis) and the ENSO index of Li et al. [30] (blue, left axis). B: instrumental rainfall (red, right axis) and SWIO SST [31] (blue, left axis). Note inverted y-axes in order for the indices to be associate with high rainfall at the top of each plot.

The forcing of rainfall in southern Botswana is reflected in the covariance between the instrumental rainfall records with the indices for ENSO [30] and SWIO SST [31]. While the effect of ENSO (**Figure 5A**) appears to show some intuitive correspondence with rainfall, with positive ENSO index values (that reflect El Niño events) associated with drought conditions, the correlation is not significant ($r=-0.191$, $p=0.120$, $n=47$). Similarly, the correspondence between SWIO SST and the instrumental rainfall record (**Figure 5B**) indicates that warm SST anomalies are associated with drought conditions, but again the correlation is not significant ($r=-0.067$, $p=0.698$, $n=36$). This reaffirms that there is a strong interactive relationship between ENSO and SWIO SST in forcing rainfall in southern Botswana, and that these forces occasionally reinforce one another, and on other occasions act against one another. The instrumental record is not of sufficient duration to be able to determine the interactive modulation of these drivers.

When the covariance between the isotopic proxies and the indices for ENSO and SWIO SST are considered, the dataset provides insight in to the long-term rainfall forcing. As was noted for the instrumental data, there is a strong indication that El Niño is associated with drought and La Niña with wet conditions in both the $\delta^{18}O$ (**Figure 6A**) and the $\delta^{13}C$ records (**Figure 6C**).

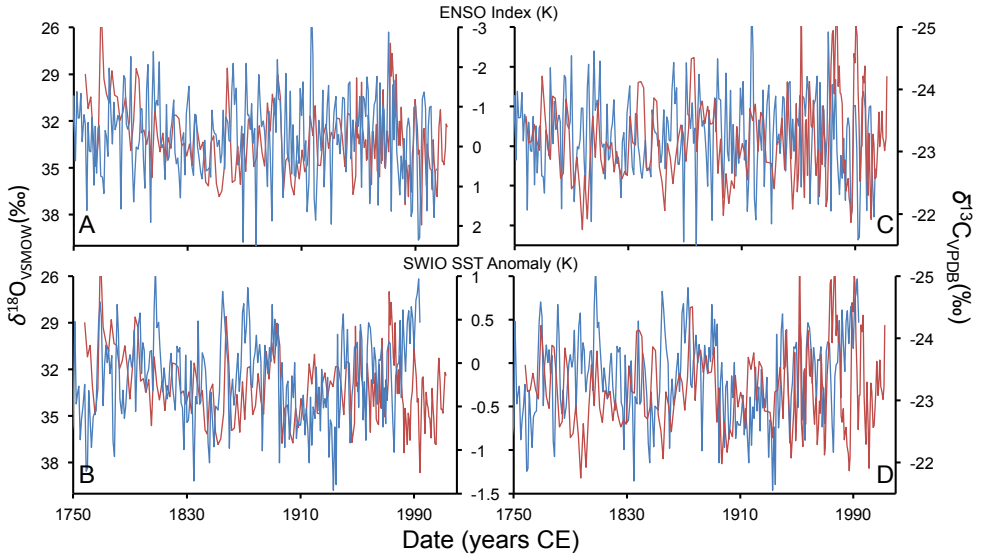

Figure 6. Comparison between isotope records from the Mabuasehube *Vachellia erioloba* and reconstructions of forcing parameters. A: comparison between the $\delta^{18}O$ record and the ENSO index of Li et al. [30]. B: comparison between the $\delta^{18}O$ record and the SWIO SST anomaly record of Zinke et al. [31]. C & D: similar comparisons to A & B using the $\delta^{13}C$ record. Isotopic records are depicted in red, and the ENSO and SWIO SST indices are depicted in blue. Note some y-axes are inverted to depict high rainfall at the top of each plot and low rainfall at the bottom.

In the case of $\delta^{18}O$ the correlation with ENSO is significant (r=0.387, p=0.007, n=56), but the correlation is insignificant when using the $\delta^{13}C$ record (r=-0.012, p=0.931, n=56). The correlation between the $\delta^{18}O$ record and SWIO SST is marginally significant (r=0.355, p=0.027, n=45), but with the $\delta^{13}C$ record is insignificant (r=-0.020, p=0.899, n=45) (**Figure 6B** and **Figure 6D**).

The effect that SWIO SST has on rainfall appears to have changed from a positive correlation in which increased SST leads to increased rainfall (**Figure 5B**), to a negative correlation in which the opposite is true (**Figure 6B** and **Figure 6D**). The transition seems to take place in about 1980 CE. In an

analysis of instrumental rainfall records across Botswana, Mphale et al. [3] also noted a breakdown in the relationship between SST and rainfall and between ENSO and rainfall. These authors identified the date threshold for this change as 1982 CE, and attributed it to an eastward shift of the main rainfall bearing synoptic system that led to a significant reduction in rainfall at this time. Woodborne et al. [11] also mooted an east/west shift in the synoptic system to explain isotopic proxy rainfall records from baobabs in the Mapungubwe and Pafuri areas of South Africa (**Figure 1**). The proposed mechanism suggested that warmer SST drives eastward displacement of the temperate tropical troughs that are responsible for most of the Austral summer rainfall in the region [32]. The mechanism predicts that Botswana should become drier when SST increases. The evidence from the Mabuasehube *Vachellia erioloba* specimen appears to run counter to this as prior to 1980 CE increased SST is associated with higher rainfall (**Figure 6B** and **Figure 6D**).

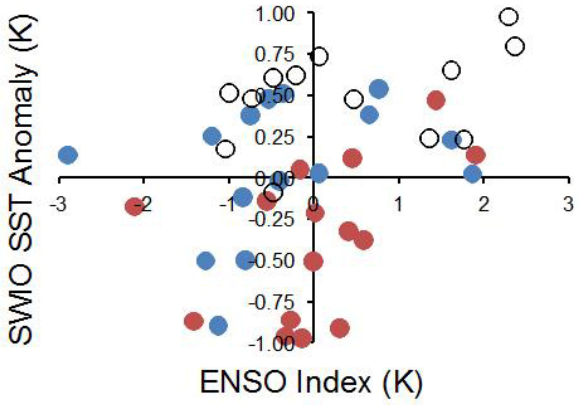

Figure 7. Rainfall forcing of wet and dry years. The 15 wettest years (blue symbols) pre-1980 CE are associated with positive SWIO SST anomalies [31] or negative ENSO indices [30] (La Niña conditions). The 15 driest years pre-1980 CE (red symbols) are associated with negative SWIO SST anomalies or positive ENSO indices (El Niño conditions). The post-1980 CE period (open symbols) is dominated by strong El Niño conditions with weak interleaved La Niña conditions, and an unprecedented warming of the SWIO SST. Both wet and dry conditions prevailed but the period is generally drier and ENSO is the dominant forcing (**Figure 5A**).

The evidence presents a conundrum in which the role of ENSO appears to be relatively coherent with El Niño associated with drought and La Niña with wet conditions, but the modulating effect of SWIO SST changes through time. To unravel the knot, it is necessary to have long-term data.

We divided the record in to pre- and post-1982 CE, and then ranked the pre-1982 CE record from wettest to driest years using the $\delta^{18}O$ record, which is the most consistent indicator of rainfall in the foregoing analysis. We analysed the ENSO and SWIO SST conditions that prevailed during the 15 wettest and 15 driest years pre-1980 CE and compared them with the conditions that have prevailed post-1980 CE (**Figure 7**).

Pre-1980 CE the wet conditions (blue symbols in **Figure 7**) were associated with either negative ENSO index values (La Niña conditions), or with positive SWIO SST anomalies. It is important to note that El Niño events are included in the portfolio of wet years. Conversely positive SWIO SST anomalies alone do not determine wet conditions. Pre-1980 CE the dry conditions (red symbols in **Figure 7**) are dominated by positive ENSO index values (El Niño conditions) or negative SWIO SST anomalies. Again La Niña conditions are among the droughts, but these were associated with negative SWIO SST anomalies. The evidence suggests that both ENSO and SWIO SST played an important role in modulating rainfall, and when ENSO and SWIO SST anomalies have the opposite signs they reinforce one another to produce definitive drought (+ ENSO, - SWIO SST) or definitive wet (- ENSO, + SWIO SST) conditions. The highest uncertainty is when both ENSO and SWIO SST indices have the same sign. Under these conditions ENSO and SWIO SST act against one another, and there is no pattern to indicate whether the wet or the dry forcing will dominate.

The post-1980 CE period represents the most persistent dry conditions across Botswana since 1950 CE [3]. This is also patent in the isotope proxy records for the last 255 years (**Figure 3**, **Figure 6**). The post-1980 CE period is characterized by an unprecedented positive shift in the SWIO SST, which shows only positive indices for this period (**Figure 7**). It also has a high frequency of intense El Niño interspersed with weak La Niña conditions. In the pre-1980 CE period positive SWIO SST anomalies appear to have facilitated wet conditions, but in the post-1980 CE period the ENSO signal is the dominant force (**Figure 5A**) resulting in drier conditions because of the frequency and intensity of El Niño events.

CONCLUSIONS

Mphale et al. [3] suggested that rainfall has decreased over Botswana over the last 50 years; but the 250-year record from the Mabuasehube *Vachellia erioloba* specimen shows no significant trend over the longer period. Instead our analysis suggests that a post-1980 CE decline in average rainfall is the result of interactive ENSO and SWIO SST forcing of rainfall. The frequency and intensity of El Niño events has been the dominant effect since 1980 CE.

The analysis also shows that east/west shifts of the temperate tropical trough synoptic systems that have been invoked to explain wet/dry cycles at Pafuri and Mapungubwe [11] are not supported by the Botswana evidence. The temperate tropical trough system is responsible for the majority of the summer rainfall over southern Africa, and a coherent response across the entire region would be expected. Dry conditions at Mapungubwe and Pafuri during periods of elevated SWIO SST were attributed to an eastward shift of the temperate tropical trough system, and should have led to hyper-arid conditions in Botswana. Instead the Mabuasehube *Vachellia erioloba* record indicates wetter conditions with elevated SWIO SST. The evidence suggests an alternative possibility: that the temperate tropical trough system shifts westward during positive SWIO SST anomalies. This scenario would still lead to drier conditions at Mapungubwe and Pafuri, but wetter conditions in Botswana.

This study demonstrates that the $\delta^{13}C$ and $\delta^{18}O$ values in the wood of *Vachellia erioloba* yield records of rainfall variability. Since this species achieves great age, and is widely distributed in the xeric regions of the Kalahari and Namib Deserts, it holds the potential to elucidate past climate where instrumental records are rare. Additional specimens from across the arid Kalahari Desert, including the possibly of sampling longer-lived specimens, will clarify the patterns that have been tentatively identified in this study.

EXPERIMENTAL SECTION

Sample collection. Permission to sample trees in Botswana was obtained from the Ministry of Environment, Wildlife and Tourism under permits reference EWT8/36/4CCVIII (18) and (28). A *Vachellia erioloba* specimen was identified in the Mabuasehube Game Reserve in southern Botswana (25°05'52.36"S, 21°59'47.80"E) (**Figure 1**). The tree was selected because it had recently died (indicated by bark loss and absence of leaves, while still retaining some of the fine branch structures). It was located in an area with a sandy substrate with no evidence of drainage lines so that edaphic moisture is regulated by rainfall. In 2015 a disk was removed from the stem using a chainsaw and imported in to South Africa under a permit P0073346 issued by the South Africa Department of Agriculture, Forestry and Fisheries.

Sample preparation. A radial section of approximately 1 cm width, which included all the growth rings pith to bark, was removed from the disk. In order to curate a witness section, the sample radius was mounted between pinewood backing blocks using water-soluble glue, and then split to produce mirror image sections. These sections were archived until required for this analysis. For the analysis the glue was removed from the analysis section

by soaking it in hot water for two hours. As the wood was extremely hard, *ca.* 1 mm slivers were cut using a chisel and a modified wood plane. A total of 196 aliquots were removed along the 243 mm radius.

Isotopic analysis. Lignin was oxidised with acidified sodium chlorite and the hemicelluloses were subsequently hydrolysed with sodium hydroxide to yield α-cellulose [33, 34] that was homogenized using a Hielscher ultrasonic probe [35]. The samples were freeze-dried in a Thermo Savant ModulyoD freeze drier at -45°C for at least 48h. Aliquots of 0.30–0.35 mg of α-cellulose were weighed into silver capsules and pyrolyzed over glassy carbon at a temperature of 1,090°C in a PDZ Europa ANCA GSL elemental analyser interfaced to a PDZ Europa 20–20 stable isotope ratio mass spectrometer. Isotope ratios are expressed as per mille deviations using the standard delta notation relative to VPDB (carbon) and VSMOW (oxygen) standards. Analytical precision was typically ±0.1‰ for carbon and ±0.3‰ for oxygen.

Data corrections. The $\delta^{13}C$ record was corrected for changes in the $\delta^{13}C$ of atmospheric CO_2 using the southern Hemisphere record of [36] with online updates of the dataset (http://cdiac.ornl.gov/ftp/db1014/isotope.cgo). The correction of the $\delta^{13}C$ record to account for increased atmospheric CO_2 concentration was done using the approach of Woodborne et al. [11, 23].

Dating and calibration. Dating samples were taken from the residual material from the isotopic analysis and since these were processed to the level of α-cellulose no additional pretreatment was required. Three samples were selected, with two chosen to fall within the bomb carbon period. Samples were measured by Accelerator Mass Spectrometry at iThemba LABS [37]. Calibration was done using the SHcal13 and SHZ1_2 datasets on the online version of CALIBomb (http://calib.org/CALIBomb/) (**Table 1**).

Table 1. Radiocarbon dating results from the Mabuasehube *Vachellia erioloba.*

Sample	Laboratory number	$\delta^{13}C$	pMC	pMC error	Age	Age error	Calibration range (year CE)
41	IT-C-1069	-23.0	123.14	0.53			1962-1963, 1982-1985
44	IT-C-1097	-23.1	124.33	0.47			1962-1963, 1982-1984
93	IT-C-1070	-23.8	97.29	0.39	221	32	1960-1727, 1805-1816, 1832-1892, 1922-1950
192-4 (193)	IT-C-1071	-23.3	96.80	0.42	261	35	1643-1672, 1743-1760, 1762-1770, 1779-1796

Age model construction. An age model was constructed using a linear fit between age and sample number. Samples 41 and 44 (samples numbers increased from the bark towards the centre of the tree) both contained bomb carbon with sample 44 having a higher percent modern carbon value indicating that the descending section of the bomb calibration curve applied. This leaves little latitude for the age assignment, and the linear age model was extrapolated to intercept the 1-sigma calibration range of the third date (sample 92). This linear extrapolation implies that that the termination of growth took place in 2013, which is consistent with the death of the tree within a year or two of the sampling in 2015.

The radiocarbon date on the inner ring (sample 193) indicates that the growth rate of the Mabuasehube *Vachellia erioloba* was not constant through time and the linear age model spanning samples 0-93 does not intersect with the 1-sigma age range for sample 193. A separate linear extrapolation of age was used for samples 93-194 using the most probable calibrated age for sample 193. The age model patently includes inaccuracies because of the assumption of linear growth, and assuming a single inflection point for the change in growth rate. Year-to-year variation in environmental conditions will lead to faster and slower growth, which manifests as errors in the age model. As a result it is acknowledged that the age model approximates average growth and cannot be used to assign the year of growth for individual samples.

Statistical analysis. The statistical comparison of the time series was done using the KNMI Climate Explorer online tools (http://climexp.knmi.nl/userseries.cgi) accessed 30 December 2017. Rainfall derived from convective systems is spatially variable: the comparison between the two instrumental records used in this study, from Tshane and Tsabong, does not yield a perfect correlation ($r=0.639$, $p<0.001$, $n=50$). The statistical comparison between rainfall proxies and instrumental records need to account for this. In addition the approach used to construct the age model does not have sufficient precision to assign an isotope measurement to a growth year with high levels of confidence. The local variability in rainfall and the lack of precision in the age model prevent the use of the isotope records in assessing annual scale variability, and a 3-year running average for all parameters is used in the assessment of slightly longer-term forcing effects.

ACKNOWLEDGMENTS

This project was funded by The National Research Foundation (NRF) of South Africa under the Research Grant for Unrated Researchers number CSUR13092647960. AMS radiocarbon analyses were supported by the Romanian Ministry of Research and Innovation CNCS-UEFISCDI under grant PN-III-P4-ID-PCE-2016-0776, Nr. 90/2017.

REFERENCES

1. J. Rockstrom, *Physics and Chemistry of the Earth, Part B: Hydrology, Oceans and Atmosphere,* **2000**, *25*, 275.
2. J. A. Adedoyin, *Meteorology Atmospheric Physics,* **2000**, *75*, 135.
3. K. M. Mphale, S. K. Dash, A. Adedoyin, S. K. Panda, *Theoretical and applied climatology*, **2014**, *116*(1-2), 75.
4. M. Hoerling, J. Hurrell, J. Eischeid, A. Phillips, *Journal of Climate*, **2006**, *19*(16), 3989.
5. S. E. Nicholson, D. Leposo, J. Grist, *Journal of Climate*, **2001**, *14*, 323.
6. D. J. Nash, G. H. Endfield, *Climatic Change*, **2008**, *86*(3-4), 257.
7. R. Neukon, D. J. Nash, G. H. Enfield, S. W. Grab, C. A. Grove, C. Kelso, C. H. Vogel, J. Zinke, *Climate Dynamics*, **2013**, DOI 10.1007/s00382-013-1886-6
8. Y. Richard, S. Trzaska, P. Roucou, M. Rouault, *Climate Dynamics*, **2000**, *16*(12), 883.
9. L. Gimeno, A. Drumond, R. Nieto, R. M. Trigo, A. Stohl, *Geophysical Research Letters*, **2010**, *37*(13).
10. N. Fauchereau, B. Pohl, C. J. C. Reason, M. Rouault, Y. Richard, *Climate Dynamics*, **2009**, *33*(4), 575.
11. S. Woodborne, P. Gandiwa, G. Hall, A. Patrut, J. Finch, *PloS one*, **2016**, *11*(7), p.e0159361.
12. P.D. Tyson, G. R. J. Cooper, T. S. McCarthy, *International Journal of Climatology,* **2002**, *22*(9), 1105.
13. F. A. Engelbrecht, W. A. Landman, C. J. Engelbrecht, S. Landman, M. M. Bopape, B. Roux, J. L. McGregor, M. Thatcher, M., *Water SA*, **2011**, *37*(5), 647.
14. F. Engelbrecht, J. Adegoke, M. J. Bopape, M. Naidoo, R. Garland, M. Thatcher, J. McGregor, J. Katzfey, M. Werner, C. Ichoku, C. Gatebe, *Environmental Research Letters*, **2015**,*10*(8), p.085004.
15. H. H. Shugart, S. A. Macko, P. Lesolle, T. A. Szuba, M. M. Mukelabai, P. Dowty, R. J. Swap, *Global Change Biology*, **2004**, *10*(3), 273.
16. D. W. Stahle, P. T. Mushove, M. K. Cleaveland, F. Roig, G. A. Haynes, *Forest Ecology and Management*, **1999**, *124*(2), 217.
17. M.D. Therrell, D. W. Stahle, L. P. Ries, H. H. Shugart, *Climate Dynamics*, **2006**, *26*(7-8), 677.
18. M. Hall, *Annals of the Natal Museum*, **1976**, *22*(3), 693.
19. J. C. Vogel, A. Fuls, E. Visser, *South African Journal of Science*, **2001**, *97*(3-4), 164.
20. J. F.Thackeray, S. Potze, *Annals of the Transvaal Museum,* **2000**, *37*, 131.
21. P. D. Dunwiddie, V. C. LaMarche, *Nature*, **1980**, *286*(5775), 796.
22. G. Hall, S. Woodborne, M. Pienaar, *The Holocene*, **2009**, *19*(2), 251.
23. S. Woodborne, G. Hall, I. Robertson, A. Patrut, M. Rouault, N. J. Loader, M. Hofmeyr, *PLoS One*, **2015**, *10*(5), p.e0124202.

24. E. Norström, K. Holmgren, C. M. Morth, *South African Journal of Science*, **2005**, *101*(3-4), 162.
25. S. Woodborne, S., 2004. *CSIR Environmentek,* **2004**. Available from author.
26. T. H. Wils, I. Robertson, S. Woodborne, G. Hall, M. Koprowski, Z. Eshetu, *Journal of Quaternary Science*, **2016**, *31*(4), 386.
27. D. McCarroll, N. J. Loader, *Quaternary Science Reviews*, **2004**, *23*(7), 771.
28. C. Harris, C. Burgers, J. Miller, F. Rawoot, *South African Journal of Geology*, **2010**, *113*(1), 33.
29. O. W. Cape, *South African Journal of Science*, **1997**, *93*.
30. J. Li, S. P. Xie, E. R. Cook, G. Huang, R. D'arrigo, F. Liu, J. Ma, X. T. Zheng, *Nature Climate Change*, **2011**, *1*(2), 114.
31. J. Zinke, B. R. Loveday, C. J. C. Reason, W. C. Dullo, D. Kroon, *Scientific reports*, **2014**, *4*, 4393.
32. M. S. J. Harrison, *International Journal of Climatology*, **1984**, *4*(5), 547.
33. N. J. Loader, I. Robertson, A. C. Barker, V. R. Switsur, J. S. Waterhouse, *Chemical Geology*, **1997**, *136*(3-4), 313.
34. K. T. Rinne, T. Boettger, N. J. Loader, I. Robertson, V. R. Switsur, J. S. Waterhouse, *Chemical Geology*, **2005**, *222*(1), 75.
35. W. Laumer, L. Andreu, G. Helle, G. H. Schleser, T. Wieloch, H. Wissel, *Rapid Communications in Mass Spectrometry,* **2009**, *23*, 1934.
36. R. J. Francey, C. E. Allison, D. M. Etheridge, C. M. Trudinger, I. G. Enting, M. Leuenberger, R. L. Langenfelds, E. Michel, L. P. Steele, *Tellus B*, **1999**, *51*(2), 170.
37. V. L. Mbele, S. M. Mullins, S. R. Winkler, S. Woodborne, *Physics Proceedia*, **2017**, *90*, 10.

STUDIA UBB CHEMIA, LXIII, 1, 2018 (p. 125-136)
(RECOMMENDED CITATION)
DOI:10.24193/subbchem.2018.1.10

ASSESSMENT OF GROUNDWATER QUALITY AND ASSOCIATED HEALTH RISKS IN RURAL AREAS OF SINDH (PAKISTAN)

MUHAMMAD SARFRAZ[a,*], NARGIS SULTANA[b], MUHAMMAD ILYAS TARIQ[b]

ABSTRACT. Groundwater quality has considerable impact on public health, especially in areas where majority of the people rely on groundwater for drinking purpose. In this scenario, investigation of 175 groundwater samples collected from district Jacobabad and Kashmor, Sindh Pakistan was carried out for physicochemical parameters (color, odor, taste, pH, EC, turbidity, alkalinity, hardness, Cl, SO_4^{-2}, NO_3^- and TDS), major cations (Na^+, K^+, Ca^{+2} and Mg^{+2}), trace elements (F, As, Fe and Zn) and microbiological organisms (*total coliform* and *faecal coliform*). Analysis results showed high level of microbial contamination as 66 and 62% sampling sites were laden with *total coliform* and *faecal coliform* organisms respectively. On the other hand, chemicals constituents like hardness, Ca, Mg, Na, K, SO_4, Cl, and TDS in 54, 72, 21, 47, 25, 73 and 49% water samples respectively were higher than GVs. Other than this, trace elements like F, Zn, As and Fe were also found in high concentration in 11, 04, 22 and 53% water samples respectively. Health risk assessment due to Fe, As and Zn revealed that arsenic HRI>1 in 22 and 13% water samples for children and adults respectively and overall CDIs and HRI were found in the order of As>Zn>Fe whereas, pollution index (Pi) for Fe was significant among all trace elements investigated.

Keywords: *Contamination; pollution index; risk assessment; trace metals; groundwater.*

INTRODUCTION

Quality of groundwater, the major source of drinking water and household use [1] is deteriorated by a number of things including materials on seepage routes, general human activities, sewerage or disposal system

[a] *Pakistan Council of Research in Water Resources (PCRWR), MoST, Pakistan.*
[b] *Department of Chemistry, University of Sargodha, 40100, Pakistan.*
** Corresponding author e-mail: sarfrazzed@gmail.com*

and dissolved solids and minerals. Flooding, one of the major natural disasters causes contamination of water by mixing different kinds of contaminants like industrial, human and animal wastes into the water body through unprotected bore holes and surface water sources. Waterborne diseases are the major threat to the healthy lives of the people. Literature shows that waterborne disease as a result of *faecal* pollution of drinking water wiped out entire population of cities [2]. It is estimated that nearly 80% of total diseases like diarrhea, dysentery, hepatitis, tooth decay and anemia in children are due to consumption of poor quality water [3]. In Pakistan over 40% of urban deaths are linked to waterborne diseases originated due to consumption of contaminated water [4]. A number of studies have been documented on severe contamination of drinking water sources with hazardous pathogenic bacteria like *Shigella sp*., *V. cholerae*, *P. aeruginosa*, *Salmonella*, and *S. aureus* in different areas of Pakistan caused by recent floods, which have resulted diseases like diarrhea, cholera, typhoid fever, food poisoning, dysentery, gastroenteritis, and other serious infections [5-8].

Minerals and micronutrients are considered to be an essential part of drinking water but their excess beyond certain limit causes serious health implications. Calcium is considered to be an important component of basic structure of bone, soft tissues and teeth but its excess intake can interact with iron, magnesium, zinc, and phosphorus within the intestine and reduces their absorption. Higher concentrations of sulphate along with sodium and magnesium impair water taste and have laxative effect. Similarly, high concentration of sodium aid in increasing consumer's blood pressure. It has been reported that all hand pumps and 73% well water are not potable due to excess of nitrate, magnesium and sulphate in district Bannu (KPK), Pakistan [9].

Trace elements like fluoride, iron, zinc and arsenic can cause complex health hazards if ingested in excess for prolonged time, therefore, it is necessary to estimate potential health risk associated with these elements. Different studies conducted to evaluate heavy metal concentration and health risk assessment showed that overall all of these metals in excess concentration are toxic [4], [10]. Due to ingestion of As rich water, it is estimated that about 200 million people globally are at the health risk of As poisoning [11]. A number of other investigations have also been carried out to evaluate physicochemical and microbiological quality of drinking water and possible health risks [8], [12-15]. Similarly, high concentration of different minerals and trace metals have also been highlighted in a recent study conducted in district, Rajanpur, Pakistan [16]. Physicochemical and microbiological investigation of drinking water quality and possible health risks assessment have been carried out through a number of other studies

which revealed that most of water samples have chemical and/or microbiological contamination and are unsuitable for human consumption as found in Pakistan [13-14], [17], Cambodia [18], Ghana [19], Bangladesh [20], Romania [21], and many other Asian and European countries along with USA [22, 23].

In order to explore post flood groundwater profile, we have designed present research study to evaluate physicochemical and microbiological status and health risk associated with consumption of available potable groundwater in flood affected rural areas of district Jacobabad and Kashmor, Sindh, Pakistan.

RESULT AND DISCUSSION

Water samples collected under present investigated were evaluated for physico-chemical parameters (color, odor, pH, turbidity, conductivity, alkalinity, Cl^-, SO_4^{-2}, NO_3^- and TDS), major cations (Na^+, K^+, Ca^{+2}, Mg^{+2}), trace elements (Fe, F, As and Zn) and microbiological constituents (*total coliform* and *faecal coliform*) and finally analysis results were compared with guidelines values (GVs). Range and mean values of major water quality indicators are shown in **Table 1** whereas detail regarding sampling locations and variation of major water quality parameters as supplementary information can be available from the authors upon request.

Physico-chemical parameters

Evaluation of physical and aesthetic indicators like taste, odour, colour and turbidity showed that most of the water samples were in agreement with GVs with the exception of a few having saline taste. Analysis data indicated that pH ranged from 6.60-8.26 which was in accordance with WHO GVs of 6.5-8.5 [2]. Conductivity is an indicator of ions concentration and their mobility, therefore, an increase in ion concentration increases EC of water [18]. In present investigation EC varied from 550µS/cm to 28040µS/cm which indicates high level of dissolved ionic concentration. Generally, conductivity of water samples collected from district Jacobabad was higher than Kashmor and highest value of 28040µS/cm was recorded for sample collected from village Rehmatullah Khoso. Alkalinity is also an important constituent of water but its concentration beyond certain limit is associated with problems like hardness, gas trouble, kidney stone, severe irritation of eyes, skin, and mucous membrane and damage of metallic pipes [24]. Analysis data showed that in presented study alkalinity ranged from 120-513 mg/L.

Table 1: Range and mean value of physico-chemical parameters

Parameter	Range	Mean	Parameter	Range	Mean
EC (µS/cm)	550-28040	3953	Na (mg/L)	34-2900	456
pH	6.60-8.26	7.4	K (mg/L)	2-130	12.2
Turbidity (NTU)	0.4-8.9	1.7	Ca (mg/L)	20-1280	218
Hardness (mg/L)	110-8550	1047	Mg (mg/L)	9.7-1446	122
Alkalinity (mg/L)	120-513	257	F (mg/L)	0.40-1.80	1.05
SO_4 (mg/L)	32-3680	745	Fe (mg/L)	0.05-2.0	0.42
NO_3 (mg/L)	0.01-12.6	1.38	Zn (mg/L)	0.50-4.50	1.06
TDS (mg/L)	315-14876	2414	As (µg/L)	0.0-15.35	5.05

Literature showed that elevated concentration of chloride may create problems in throat and digestive system along with imparting saline taste and corrosion problems [25]. Presented data showed that Cl ranged from 23-8575 mg/l and overall 49% water samples have high concentration of Cl than GVs. Higher Cl content was reported in water samples collected from villages Allah Dito, Lal Bux and Rehmatullah Khoso. The major portion of total hardness is caused by calcium and magnesium ions and its high level may instigate heart diseases in residents [26]. Hardness varied from 110-8550 mg/l and 54% water samples have higher level than WHO GVs. Similarly, it has been reported that people ingesting high SO4 through drinking water may face diarrhea [27]. In present study SO_4 ranged from 32-3680 mg/l and overall 73% water samples possessed high SO4 contents than WHO GVs. Seawater intrusion is considered to be responsible for pollution of groundwater systems with high Cl and hardness in Shah Bundar area [28]. Water samples collected from the house of Sohbat Khan, village Rehmatullah Khoso and Ramzan, Village Jabar and Rasoolabad has highest value of hardness and SO_4 respectively. Nitrate for only 02 water samples in presented data have high content than GVs. Literature shows that groundwater in Pakistan have very less concentration of nitrate, however, higher level may be reported due to different agriculture and non-agriculture sources [19]. High TDS is associated with taste, hardness, corrosion properties and tendency to incrustation. Presence of high concentration of Na, K, Ca, Cl, SO_4 and many more minerals contribute towards high level of TDS that may cause gastrointestinal exasperation [29]. In the presented study, TDS varied from 315 to 14877 mg/L and total of 115 (66%) water samples have TDS value higher than WHO permissible limit (**Fig. 1).**

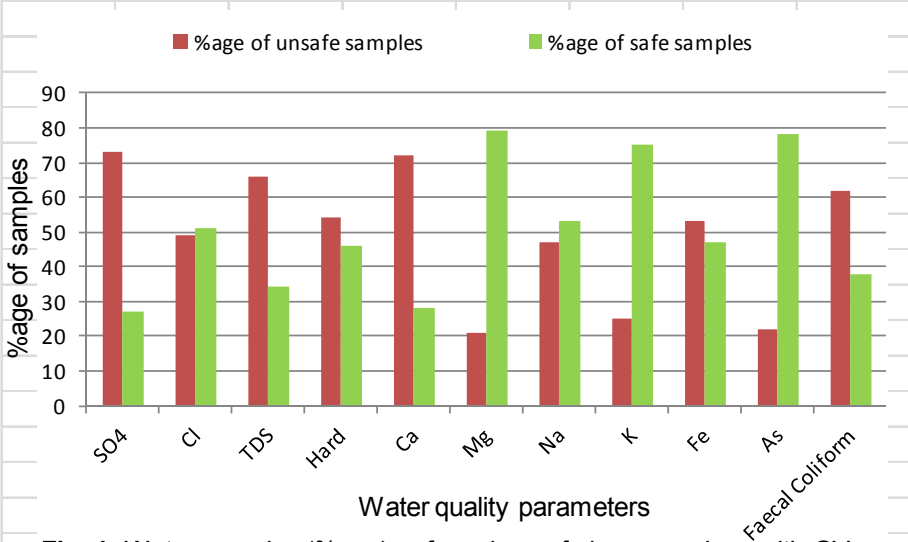

Fig. 1: Water samples (%age) safe and unsafe in comparison with GVs

Major cations

Although, metals like Na, K, Ca and Mg are responsible for carrying out very important physiological functions in human body but an unsuitable intake and consumption of these minerals may lead towards health implications. Literature shows that short term exposure to high concentration of Ca does not create any health implications, but long time intake may lead towards hypercalcemia, urinary tract calculi and calcification in kidneys and in arterial walls besides suppression of bone re-modeling [7]. High level of Na is associated with an increase in blood pressure in children, male and female of all ages [30]. Potassium is an important micronutrient for living organisms but, excess amount in drinking water may lead towards nervous and digestive disorder [31]. It has been reported that hard water due to the association of Mg with SO_4 ion may possess laxative properties and cause gastrointestinal disorders [15]. Presented data indicated that 72, 21, 47 and 25% water samples have high concentration of Ca, Mg, Na and K respectively (**Fig.1**).

Trace elements

Present study indicated that 04, 11, 23 and 53% water samples carry high content of Zn, F, As and Fe respectively (**Fig. 1**). Literature

presents that tooth decay and skeletal and non-skeletal fluorosis is associated with higher concentration of F in drinking water [32]. Intake of high contents of iron via food or drink may result toxic effects in human body. The formation of hydroxyl radicals and deposition of iron (due to these Fe^{+2} ions) in a typical kidney cell may harm kidney cells. The excess amount of iron may accelerate the formation of free radicals resulting in instigation of mutagenicity, nephrotoxicity and renal carcinoma [33]. Researcher documented that exposure to high level of As may cause hepatic, neurological, diabetic, hematological, cardiovascular, respiratory and reproductive effects in consumers. Carcinogenic symptoms including liver, skin, bladder, lung and kidney cancers are associated with exposure to high level of As [11]. In addition, consumption of arsenic contaminated water can also causes several noncancerous diseases such as liver disorders, hypertension, peripheral vascular diseases, diabetes mellitus and other respiratory and neurological issues [20].

Health risk assessment

Chronic daily intake (CDI) and health risk index (HRI) measurement for both children and adults were carried out to estimate health risk associated with ingestion of heavy metal as shown in **Table 2**. Calculated CDI values for Fe, As and Zn ranged from 0.002-0.061, 0.000-0.469 and 0.015-0.138 μg•kg-1•day-1 and0.001-0.056, 0.000-0.426 and 0.014-0.125μg•kg-1•day-1 for children and adults respectively. Calculated mean CDIs were found in the order of As>Zn>Fe.

HRI assessment showed that As HRI value is higher than other metals and overall 22 and 13% water samples have HRI>1 for children and adults respectively indicating future consumer's health risk associated with consumption of polluted water for drinking purpose. HRI for Fe, As and Zn ranged from 2.18E-06 to 8.74E-05, 0.000-1.565 and 5.10E-05 to 4.59E-04 for children and 1.98E-06 to 7.94E-05, 0.000-1.421 and 4.63E-05 to 4.17E-04 for adults respectively which indicate that HRI<1 for Fe and Zn. HRI calculations showed that heavy metals in ground water of district Rajanpur were found in order of As>Zn>Fe. Literature shows high to very high carcinogenic and non-carcinogenic health risk for both children and adults associated with elevated As concentration in drinking water and its correlation with Fe and other heavy metals [34].

Table 2: Calculated range and mean values of CDI and HRI of trace metals

		CDI		HRI	
		Children	Adults	Children	Adults
Fe	Range	0.002-0.061	0.001-0.056	2.18E-06 to 8.74E-05	1.98E-06 to 7.94E-05
	Mean	0.013	0.012	1.82E-05	1.65E-05
As	Range	0.000-0.469	0.000-0.426	0.000-1.565	0.000-1.421
	Mean	0.156	0.141	0.519	0.471
Zn	Range	0.015-0.138	0.014-0.125	5.10E-05 to 4.59E-04	4.63E-05 to 4.17E-04
	Mean	0.032	0.029	1.08E-04	9.78E-05

Pollution index (Pi)

The Pi data showed that Fe have shown significant pollution amongst all the studied trace elements (**Table 3**).

Table 3: Pi data of trace elements in water samples

Trace metals	Pollution index (Pi)
Fe	1.4
Zn	0.4
F	0.7
As	0.5

Microbiological monitoring

Present study revealed that 66 and 62% water samples are contaminated with *total coliform* and *faecal coliform* organism respectively as shown in Fig.1.Contamination of groundwater sources was evident from high level of open air defecation and practice of tethering animals close to human dwellings. Rain and flood water carry these human and animal's faecal wastes, which may carry pathogens and contaminates the water sources in the region and direct consumption from these sources may cause infectious diseases [28].

CONCLUSION

Physicochemical and microbiological assessment of groundwater being used for drinking purpose by residents of district Jacobabad and Kashmor revealed that there was high level of microbial contamination as 66% sites were found contaminated with *total coliforms* and another 62 %

were overloaded with *faecal coliform* bacteria. The study also highlighted that a large number of sampling sites were polluted with other chemicals, minerals and trace metals like Ca, SO_4, Na, K, Fe, As and TDS. Health risk assessment showed that HRI >1for As in 22 and 13% water samples for children and adults respectively. Net result of present study is that most of the waterborne diseases prevailing in the region are due to consumption of substandard water after flood. A concrete policy should be devised to treat the ground water and address post-flood environmental effects on life and human health so that safety from hazardous effects associated with bacterial contamination and elevated concentration of toxic components may be ensured.

EXPERIMENTAL

Sampling location

Jacobabad and kashmor are two adjacent districts of Sind, Pakistan located at 28. 25 00°N & 68.8333°E and 28.4333°N & 69.5833°E respectively. A total of 175 water samples were collected from flood effected locations of both districts comprising 13 union councils and 47 villages as shown by highlighted areas on the map.

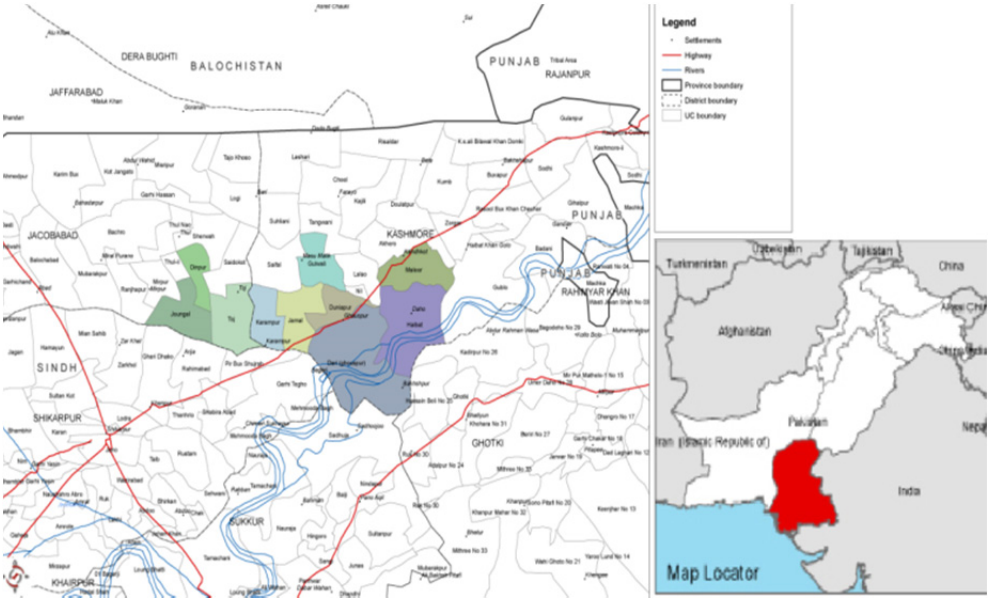

Fig. 2: Map of study area in district Jacobabad and Kashmor, Sindh

Water sample collection

From each sampling site, three water samples were collected in clean poly propylene bottles (600ml) for physico-chemical, trace elements and aesthetic parameters evaluation. Water sample for microbiological analysis were collected in sterilized bottles (250ml), stored in ice box and shifted to water quality laboratory for immediate analysis.

Reagent and instrumentation

All chemicals and calibration reagent used for the study were of analytical grade and calibration of all instruments was done prior to use. Instruments employed for evaluation of chemical parameters includes Louibond PCH63739 Germany turbidity meter, Jenway 350 EU pH meter,, HANNA HI 99300 Italy EC meter,Flame Photometer Italy, Optizen 2120 UV Plus Spectrophotometer, Mecasy Co. Ltd. Korea, HACH DR 2800 and Analytik Jena, AAS were used for analysis of chemical constituents and trace metals. Ca, Mg and hardness were estimated by complexometric titration method using EDTA whereas Cl was analyzed by following argentometric titration methodology. TDS was calculated by addition of cations and anions and *total coliform* and *faecal coliform* organisms were tested by membrane filtration technique.

Analytical investigation

Field testing instruments were employed for testing of aesthetic and physical parameters like color, taste, turbidity and pH at sampling site and analysis data was recorded. Chemical analysis of other water quality parameters including electrical conductivity (EC), hardness, calcium (Ca^{+2}), sodium (Na^{+}), magnesium (Mg^{+2}), potassium (K^{+}), nitrate (NO_3^{-}), sulphate (SO_4^{-2}), fluoride (F^{-}), alkalinity, chloride (Cl^{-}), iron (Fe), zinc (Zn), arsenic (As) and TDS was carried out at PCRWR water quality laboratory applying APHA standard methods after proper calibration and standardization of instruments [35].

Microbiological analysis

Analysis of *total coliform* and *faecal coliform* organisms was done by following membrane filtration technique [36]. Water sample (100ml) was filtered through sterile filter paper (0.45µ) using filtration assembly and placed on m-Endo and m-FC agar plates for analysis of *total coliform* and

faecal coliform respectively. Typical *coliform* colonies have pink to dark red colour with metallic sheen and *faecal coliform* colonies have blue colour which was counted after incubation of 24hrs at 35^0C and 45^0C respectively.

Health risk assessment

Health hazard associated with ingestion of heavy metals through drinking water was studied by calculating chronic daily intake (CDI) and health risk index (HRI) for both adults and children by using equation 1&2 respectively [37,38];

$$CDI = \frac{Mc \times Lw}{Wb} \qquad (1)$$

$$HRI = \frac{CDI}{RfD} \times 0.001 \qquad (2)$$

where Mc (ppb) is the heavy metal concentration whereas Lw (L/day) denotes daily water intake that is assumed as 1L/day for child and 2 L/day for adult and Wb (kg) is body weight of consumer that is considered as 32.7 kg and 72 kg for child and adult respectively [39]. RfD is the reference dose for oral toxicity which is 0.0003, 0.7 and 0.3 mg.kg-1•day-1 for As, Fe and Zn respectively, HRI is measured health risk index and 0.001 is the conversion factor used to downscale the reference dose (RfD) from mg to µg. Water samples having HRI<1 will be safe for consumption.

Pollution index (Pi)

Pollution index (Pi) is an important indicator for estimating relative pollution due to individual water samples and is calculated by following equation;

Pollution index (Pi)=Concentration/Standard

Significant degree of pollution is indicated by water samples having Pi >1 [40-41].

ACKNOWLEDGEMENT

The authors of this paper acknowledge the efforts of Pakistan Council for Research in Water Resources (PCRWR) staff for cooperation in water sample analysis.

CONFLICT OF INTEREST

The authors declare no conflict of interest.

REFERENCES

1. M. A. Malik, E. M. Azam, A. Saboor, "Water Quality Status of Upper KPK and Northern Areas of Pakistan", Water Resources Research Center, Peshawar, Ministry of Science and Technology, Peshawar, Report No.: 142, **2010**.
2. W. H. Organization, "Trace Elements in Human Nutrition And Health", **1996**.
3. M. Memon, M. S. Soomro, M. S. Akhtar, K. S. Memon, *Environmental Monitoring and Assessment,* **2011**, *177*, 39.
4. A. Adepoju-Bello, O. Alabi, *The Nigerian Journal of Pharmacy,* **2005,** *37*, 41.
5. A. Farooqi, H. Masuda, N. Firdous, *Environmental Pollution,* **2007**, *145*, 839.
6. J. Aziz, *Eastern Mediterranean Health Journal,* **2005,** *11***,** 1087.
7. A. Azizullah, M. N. K. Khattak, P. Richter, D.P. Häder, *Environment International,* **2011,** *37*, 479.
8. T. U. Saeed, H. Attaullah, *British Journal of Environment & Climate Change,* **2014,** *4*, 133.
9. S. A. Baig, X. Xu, M. N. Navedullah, Z. U. Khan, *Journal of Applied Sciences in Environmental Sanitation,* **2012,** *7*, 49.
10. S. Venkatramanan, S. Chung, T. Kim, M. Prasanna, S. Hamm, *Water Quality, Exposure and Health,* **2015,** *7*, 219.
11. M. M. Rahman, J. C. Ng, R. Naidu, *Environmental Geochemistry and Health,* **2009,** *31*, 189.
12. G. Akhter, Z. Ahmad, J. Iqbal, N. Shaheen, M. H. Shah, *Journal of Chemical Society of Pakistan,* **2010,** *32*, 306.
13. A. Alamgir, M. A. Khan, J. Schilling, S. S. Shaukat, S. Shahab, *Environmental Monitoring and Assessment,* **2016,** *188*, 1.
14. F. Perveen, U. Asghar, T. H. Usmani, *Journal of Chemical Society of Pakistan,* **2007,** *29*, 458.
15. T. Brock, K. Brock, "Basic Microbiology With Apllication 2nd", Prentice Hall. Inc. New Jersey, **1978**.
16. M. Sarfraz, N. Sultana, M. Jamil, R. Ashraf. *Journal of Environmental Analytical Chemistry,* **2016***,3*, 2.
17. R. F. Spalding, M. E. Exner, *Journal of Environmental Quality,* **1993,** *22*, 392.
18. C. Laluraj, G. Gopinath, *Environmental Monitoring and Assessment,* **2006,** *117*, 45.
19. F. T. Wakida, D. N. Lerner, *Water Research,* **2005,** *39*, 3.
20. W. H. Organization, 'World health statistics", World Health Organization, Geneva, **2010**.
21. S. Butaciu, M Senila, C. Sarbu, M Ponta, C. Tanaselia, O. Cadar, M. Roman, E Radu, M. Sima, T Frentiu, *Chemosphere*, **2017**, *172*, 127.

22. C. K. Jain, R. D. Singh, *J. Environmental Management,* **2012**, *107*, 1.
23. D. Mohan, C. U. Pittman Jr., *Journal of Hazardous Materials,* **2007**, *142*, 1.
24. S. Alam, *Journal of Chemical Society of Pakistan,* **2008,** 30, 521.
25. S. T. Hakim, F. Afaque, S. Javed, S. U. Kazmi, S. G. Nadeem, *Open Journal of Medical Microbiology,* **2014,** *4(2)*, 106.
26. Z. Jamshidzadeh and S. Mirbagheri, *Desalination,* **2011,** *270*, 23.
27. O. N. Nze, I. B. Ikechukwu, *International Journal of Water Resources and Environmental Engineering,* **2013,** *5*, 194.
28. S. A. Bablani, S. A. Soomro, "Evaluation of seawater intrusions in left bank sediments of coastal district Thatta, Sindh, Pakistan", 1st SWIM-SWICA Joint Saltwater Intrusion Conference. **2006**, 24-29.
29. N. J. Ashbolt, *Toxicology,* **2004,** *198*, 229.
30. R. W. Tuthill, E. J. Calabrese, *Archives of Environmental Health: An International Journal,* **1979,** *34*, 197.
31. D. Tiwari, *Indian Journal of Environmental Health,* **2001,** *43*, 176.
32. A. A. Khan, H. Whelton, D. O'Mullane, *International Dental Journal,* **2002***, 52*, 291.
33. I. A. Al-Saleh, *Science of Total Environment,* **1996,** *181*, 215.
34. D. Van Halem, S. Olivero, W. de Vet, J. Verberk, G. Amy, J. van Dijk, *Water Research,* **2010,** *44*, 5761.
35. APHA, "Standard methods for the examination of water and wastewater"*.* **2005,** *21*, 258.
36. P. dll Version, "Method 1603: Escherichia coli (E. coli) in Water by Membrane Filtration using Modified membrane-Thermotolerant Escherichia coli Agar (Modified mTEC)", **2003**.
37. M. Shah, J. Ara, S. Muhammad, S. Khan, S. Tariq, *Journal of Geochemical Exploration,* **2012***,118*, 60.
38. S. Muhammad, M. T. Shah, S. Khan, *Food and Chemical Toxicology,* **2010,** *48*, 2855.
39. F. A. Jan, M. Ishaq, S. Khan, I. Ihsanullah, I. Ahmad, M. Shakirullah, *Journal of Hazardous Materials,* **2010,** *179*, 612.
40. O. Akpoveta, B. Okoh, S. Osakwe, *Current Research in Chemistry,* **2011,** *3*, 62.
41. U. Umeobika, V. Ajiwe, M. Iloamaeke, C. Alisa, *International Journal of Science Innovations and Discoveries,* **2013,** *3*, 56.

STUDIA UBB CHEMIA, LXIII, 1, 2018 (p. 137-155)
(RECOMMENDED CITATION)
DOI:10.24193/subbchem.2018.1.11

ELEMENTAL CONTENT AND LEAD-STRONTIUM ISOTOPE CHARACTERIZATION OF WINE

FLORIN DUMITRU BORA[a], ALINA DONICI[a], ANAMARIA CĂLUGĂR[b], PETER SOMSAI[c], DOINA CLAPA[c], EMESE GAL[d], CLAUDIU IOAN BUNEA[b], ADELINA DUMITRAȘ[b,*]

ABSTRACT. The ICP-MS technique was used to determine elemental composition (Pb, Sr, Cd, Ni, Co, Cu, Ni, Hg, As, Cr) of wines (Muscat Ottonel, Fetească Albă, Fetească Regală, Fetească Neagră, Merlot and Cabernet Sauvignon) produced during three consecutive years (2014-2016) in Dealu Bujorului Vineyard. The determination of $^{206}Pb/^{207}Pb$, $^{208}Pb/^{206}Pb$, $^{206}Pb/^{207}Pb$ and $^{87}Sr/^{86}Sr$ isotopes from wines was performed for establishing reliable markers for wine geographical origin. For all tested wine samples, the toxic metals contents were found in quantities below the limits imposed by legislation. The highest concentration of heavy metals (Cd and Pb) was found in red wine Cabernet Sauvignon [Cd (0.14±0.01 µg/L) (2013)], followed by the same variety of wine from 2012 [Cd (0.14±0.03 µg/L)], in case of Pb the highest concentration was recorded by Merlot [Pb (54.33±1.00 µg/L) (2011)] followed by the same variety of wine but from 2012 [Cd (51.20±1.19 µg/L). Concerning the concentration of the elements in the white wine, it can be noticed that they recorded close concentration as red wine, Muscat Ottonel [Cd (0.12±0.01 µg/L) (2011)], Feteasca Alba [Cd (0.12±0.01 µg/L) (2012)], in case of Pb from white wines the highest concentration was recorded by Feteasca Alba [Pb (52.07±0.50 µg/L) (2012)], Feteasca Regala [Cd (52.29±1.00 µg/L) (2012)]. The highest mean of $^{87}Sr/^{86}Sr$ isotopic ratio was obtained at Feteasca Neagra variety [0.726±0.004 (0.575%, 2014)] and Muscat Ottonel variety [0.723±0.003 (0.416 % 2016)]. A possible explanation for the higher mean of $^{87}Sr/^{86}Sr$ isotopic ration for wine can be

[a] *Research Station for Viticulture and Enology Targu Bujor, 65 G-ral Eremia Grigorescu Street, RO-805200, Galați, Romania.*
[b] *University of Agricultural Sciences and Veterinary Medicine, Department of Horticulture and Landscaping, 3-5 Mănăştur Street, RO-400372 Cluj-Napoca, Romania.*
[c] *University of Agricultural Sciences and Veterinary Medicine, Station of Horticulture Research, Cluj-Napoca, 5 Horticultorilor Street, RO-400457, Cluj-Napoca, Romania.*
[d] *Babeş-Bolyai University, Faculty of Chemistry and Chemical Engineering, 11 Arany Janos Street, RO-400028, Cluj-Napoca, Romania.*
[*] *Corresponding author: dumitrasadelina@gmail.com*

the mineral consistency of the vineyard soil and its different eco-climatic conditions. $^{206}Pb/^{207}Pb$ isotopic ratios in the analyzed wine samples indicated traces of pollution originated in automobile emissions. ($^{206}Pb/^{207}Pb$=1.1000-1.1400). The lowest mean $^{208}Pb/^{206}Pb$ and $^{206}Pb/^{204}Pb$ isotopic ratios was obtained at Muscat Ottonel variety [2.141±0.007 (0.346% 2015) and 17.469±0.016 (0.094 % 2014)]. The results confirm that the elemental profile and $^{207}Pb/^{206}Pb$, $^{208}Pb/^{206}Pb$, $^{204}Pb/^{206}Pb$, $^{87}Sr/^{86}Sr$ isotope ratio can be used to track the geographical origin of wine, discriminate between wine production regions, and can be used to characterize wine *terroirs* for forensic purpose.

Keywords: *geographical origin, elemental content, $^{207}Pb/^{206}Pb$, $^{208}Pb/^{206}Pb$, $^{204}Pb/^{206}Pb$, $^{87}Sr/^{86}Sr$ isotope ratio.*

INTRODUCTION

Wine quality testing is made by using the state of the art of analytical techniques, because of the European community demand to establish an integrated approach on beverage control. The main purpose is a high level of wines safety within the European Union through so called *soil-to-grape-to-wine-to-glass* measuring and monitoring, ensuring the effective functioning of the European market [1].

Quality of wine is not only a gift of nature, but also the result of a wide range of technological intervention throughout the entire production process [2]. Current oenological research defines wine quality in relation to its chemical composition, pharmacological properties and health safety [3]. It is very important to monitor food products and beverage, including wines, for heavy metal contamination and assess the source of food contamination. Must and wine has a primary content of elemental composition due to natural transfer soil-root-grape-wine [4, 5] and a secondary content due to natural [6, 7] and artificial contamination [8, 9]. The natural content of elemental composition of wine and of other beverage is affected and overlapped by the artificial contamination [10].

Quantification of several elements in wines can validate the original authentication [8, 9, 11, 12], the potential toxicity and role in human diet [6, 13, 14], the effect on wine stability and organoleptic characteristics [15, 16, 17].

Wine is a source for essential elements which might improve human health, but it may also expose the consumer to undesirable levels and types of heavy metals when it is consumed regularly and in large amount over a long period of time [6]. The concern in human exposure to the metal

content of various beverages received a raising attention, since the consumption of wines in large volumes, significantly contribute to the daily dietary trace element intake by humans and so far there have not been a precise characterization of the impact of a number and the amounts of metals found in different drinks (alcoholic and non-alcoholic) on human health [13, 18]. In the production of wines, the quality control checks have to be brought to ensure that the consumer is protected and possible sources of contaminations are traced. The origin of Cu in wines is due to copper-based sprays used in vineyards, whereas the As, Cd, and Pb contents reflect the differences in grape variety, environmental factors and the wine-processing methods [11]. The Pb, Hg and Cd are undoubtedly considered toxic and should be monitored all the time, but also Cu, Ni, Cr, V, Zn, Ag, and Al, which in high concentrations may impart a certain toxicity [6, 13, 18]. The determination of Cd, Pb, Cu and Zn in wines is of great interest from oenological and toxicological points of view and correct knowledge of these parameters is required by the law. The *Organisation International de la Vigne et du Vin* (OIV) established Maximum Acceptable Limits (M.A.L.) for only a few elements in wine (Pb, Cd, Cu, Na, Zn, Ag, As, F, Br, F, and B [1]. The determination of toxic, such as Cd, As and Pb and essential trace elements, like Cu, in wines is an important and challenging analytical task, which requires multi-element methods of good selectivity, sensitivity and robustness [11, 19, 20].

Heavy metals are defined as those with a higher density than 5 mg/l, but the collective term now includes As, Cd, Cr, Cu, Fe, Pb, Mn, Hg, Mo, Ni, V and Zn [6, 21]. Elements like K, Ca, Mg, Fe, Cu, Zn and Cr are expected to be found in wines due to their high intercellular content and physiological roles and processes in plant, in wine yeasts and humans [6].

The content of elements such as Cu, Fe, Mn, and Zn were found in higher amounts in red grapes than white grapes and in lower amounts in wines than grapes [22]. Some elements may be lost through winemaking process, but the exposure to precipitants (bentonites) and containers may contribute to the quantity of some metals in wines [23].

Studies of isotopic ratios of heavy metals such Pb and Sr provide additional information on the geographical origin of wines, due to fact that plants inherit the isotopic signature of both elements from the geological and pedological environment [24].

Lead isotopic analysis of wines from France (Bordeaux) showed that the lead content in wines changed over time and reflected the dominant source of atmospheric lead pollution in southern of France [25]. Other researchers have found that lead isotopic compositions in wine may not always reflect those of leaded petrol, but reflect the isotopic signature of

local, dominant metallurgical industries [26, 27]. These studies confirm atmospheric deposition as being the dominant contributor to the lead total concentration and isotopic composition from wines. Some studies have shown that contamination from tin-lead foil capsules in the presence of corrosion and cork disintegration can dominate the source of lead from wines [28]. Other researchers have attributed the lead in wine to machinery or additives used during the winemaking process where environmental contamination in this case is low [29].

Isotopic ratios of heavy elements of geological interest, such as $^{87}Sr/^{86}Sr$, $^{207}Pb/^{206}Pb$, $^{208}Pb/^{206}Pb$ and $^{204}Pb/^{206}Pb$ have raised an interest in tracking regional provenance of wine [30, 31]. The winemaking process of red and white wines does not affect the $^{87}Sr/^{86}Sr$ ratio of wine, so this allows to link the Sr-isotopes of wine to those of the vineyard substratum [32, 33].

Inductively coupled plasma mass spectrometry (ICP-MS) is a multi-element technique frequently used for the elemental analysis of different wines (young and aged, red, rose and white, table and fortified, dry and sweet wines) in (semi)quantitative mode providing high selectivity, sensitivity and lower detection limits than other multi-element techniques [34, 35]. Also, ICP-MS was used for lead and strontium isotopic composition determination in several types of wines [36].

The purpose of this study is to determine the elemental composition (Cd, Pb, U, Hg, As, Sr, Co, Cu, Ni and Cr) of white wines (Muscat Ottonel, Fetească albă, Fetească regală) and red wines (Fetească neagră, Merlot, Cabernet Sauvignon) from Dealu Bujorului Vineyard, using the ICP-MS technique (method approved by *L'Organisation International du Vie et Vin*). The results of this study may highlight the elemental composition of wine samples, assess the ability to discriminate wines by geographical origin and also complete the data regarding strontium ($^{87}Sr/^{86}Sr$) and lead ($^{206}Pb/^{204}Pb$, $^{207}Pb/^{204}Pb$, $^{208}Pb/^{204}Pb$) isotope ratios in wines from Dealu Bujorului Vineyard (Galati county, Romania).

RESULTS AND DISCUSSION

Wine Mineral Content

Table 1 summarizes the total content of Cd, Pb, U, Hg, As, Sr, Co, Cu, Ni and Cr in wine samples. In general, these elements are present in wine due to their extraction from grapes during the maceration period [37]. In grapes, these elements may occur by bioaccumulation in the vine plant from the soil, or they could originate from the pesticide agents used in plant

protection. During the maceration, extracted elements are absorbed at the cell membrane of yeast, and afterward, their declines as a result of precipitation together with the yeast cell or precipitation in complexation reactions. The contact of wine with equipment, the addition of fining agents, or the changing of filters, during post fermentation processes could increase the content of elements [37].

The mean contents of Cd, Pb and U were 0.10±0.01 µg/L, 41.51±1.05 µg/L and 0.26±0.03 µg/L, in case of Pb and U the highest concentrations were recorded in Feteasca regala [52.29±1.00 µg/L Pb (2014); 51.39±1.81 µg/L Pb (2015) and 0.38±0.03 µg/L U (2014); 0.40±0.01 µg/L U (2015)] while Cd was recorded the highest concentrations in Cabernet Sauvignon [0.14±0.01 µg/L Cd (2016); 0.14±0.03 µg/L Cd (2015) 0.13±0.02 µg/L Cd (2014)], Merlot [0.13±0.02 µg/L Cd (2014)] Feteasca Neagra [0.13±0.01 µg/L Cd (2014)]. The highest concentrations of heavy metals Cd and Pb were found in the red wine Cabernet Sauvignon [Cd (0.14±0.01 µg/L produced in 2013)], followed by the same variety of wine but produced in 2012 [Cd (0.14±0.03 µg/L)]; in the case of Pb the highest concentration was recorded in Merlot [Pb (54.33±1.00 µg/L) (2011)] followed by the same variety of wine but from 2012 [Pb (51.20±1.19 µg/L). Concerning the concentration of the elements in the white wine, it can be noticed that the recorded values are close to the red wine, *e.g*. Muscat Ottonel [Cd (0.12±0.01 µg/L) (2011)], Feteasca Alba [Cd (0.12±0.01 µg/L) (2012)]; in the case of Pb from white wines the highest concentration was recorded in Feteasca Alba [Pb (52.07±0.50 µg/L) (2012)], Feteasca Regala [Pb (52.29±1.00 µg/L) (2012)]. These results appear compatible with some other studies [37] reporting 0.25 µg/L (Cd), 46.00 µg/L (Pb), 0.11 µg/L (U), [8] 0.14 µg/L (Cd), 47.80 µg/L (Pb), but in some other reported results [38], the concentration of Cd appeared significantly higher (10.60 µg/L), while the reported values for Pb concentration appeared significantly lower (15.70 µg/L).

The concentration of Hg has recorded values between [0.58±0.04 µg/L Muscat Ottonel (2014); 0.51±0.04 µg/L Feteasca Neagra (2014)] and [0.24±0.04 µg/L Feteasca Neagra (2016); 0.19±0.02 µg/L Feteasca Neagra (2015)] with an average values of 0.28±0.03 µg/L. In this case, Fetească regală (<0.13 µg/L) and Merlot (<0.13 µg/L) have registered the values below the detection limit. Although the highest concentration was recorded in white wines, the average data shows that the red wines have the highest values 0.22 µg/L, compared to white wines 0.18 µg/L (Table 1). The results agree with those made in Romania [20] for Sauvignon Blanc 0.56 µg/L, Feteasca Alba 0.22 µg/L and Riesling 0.16 µg/L.

As and Sr content in wine ranged from [16.74±4.30 µg/L As; 6.20±0.23 µg/L As] and [277.49±3.64 µg/L Sr; 114.08±6.44 µg/L Sr] with an average values of 10.81±0.61 µg/L As and 205.29±5.63 µg/L Sr. In both

cases the maximum concentration were recorded in red wines Cabernet Sauvignon [16.74±4.30 µg/L As (2016); 14.41±2.75 µg/L As (2015)] and Feteasca Neagra [277.49±3.64 µg/L Sr (2016); 263.81±2.28 µg/L Sr (2015)] while the lowest concentrations were recorded in white wines Feteasca Alba [6.42±0.87 µg/L As (2015); 6.20±0.23 µg/L As (2014)] and Muscat Ottonel [149.12±5.50 µg/L Sr (2014); 114.08±6.44 µg/L Sr (2015)]. The average data shows that the red wines have the highest values [13.22 µg/L As and 228.44 µg/L Sr] compared to white wines values [9.25 µg/L As and 171.95 µg/L Sr] (Table 1). The results are comparable with those obtained in Serbia [8] 16.1 µg/L (As) for red wines and 9.46 (As) µg/L for white wines, in Macedonia [38] 11.7 µg/L (As), in Romania [20] 21.12 µg/L (As) and 154.90 µg/L (Sr), and higher compared to the results obtained in Italy [39] 2.91 µg/L for As, but for Sr the results obtained are significantly lower compared to the results obtained in Italy [39] 1340 µg/L (Sr).

Concentration of Co has recorded values between [6.74±0.48 µg/L Fetească regală (2015); 6.28±0.28 µg/L Feteasca Alba (2014)] and [3.55±0.39 µg/L Muscat Ottonel (2015); 3.71±0.21 µg/L Feteasca Neagra (2014)] with an average value of 4.54±0.21 µg/L. The average data shows that the red wines have the highest values [6.75 µg/L Co] compared to white wines values [2.97 µg/L Co] (Table 1). The results agree with other studies made in Macedonia [37, 38] 3.9 µg/L and 13.90 µg/L for Co, and in Serbia [8] 3.89 µg/L (Co) for red wines and 3.96 (Co) µg/L for white wines.

The mean contents of Ni and Cr were 573.11±2.85 µg/L Ni and 660.94±2.72 µg/L Cr, in case of Ni the highest concentrations were recorded in Feteasca Neagra [747.37±3.35 µg/L Ni (2014)] while Cr was recorded the highest concentrations in Muscat Ottonel [923.62±2.05 µg/L Cr (2014)]. In Fetească regală was recorded the lowest concentration of Ni [239.81±1.34 µg/L Ni (2016)] while in Feteasca Neagra was recorded the lowest concentration of Cr [323.92±4.09 µg/L Cr (2015)]. The results agree with those reported in Turkey [40] 520 µg/L Ni, in Romania [41] 147.73 µg/L Cr and significantly higher than the ones obtained in Serbia [8] 5.49 µg/L (Cr) red wines and 6.56 (Cr) µg/L white wines, in Italy [39] 54.57 µg/L (Ni) and 19.68 µg/L (Cr), in Macedonia [38] 32.10 µg/L (Cr) and 10.20 µg/L (Cr). The results indicated that Romanian wines are moderately rich in Cr (Table 1).

The concentration for Cu ranged from 0.48±0.03 mg/L to 0.91±0.05 mg/L, with average values of 0.72±0.04 mg/L, the latter value approaching the law limit (1 mg/L). The six samples [Fetească regală 0.85±0.07 mg/L (2014), Feteasca Regala 0.82±0.06 mg/L (2016), Feteasca Neagra 0.80±0.01 mg/L (2016), Cabernet Sauvignon 0.79±0.41 mg/L (2014), Feteasca Alba 0.77±0.08 mg/L (2015) and Feteasca Neagra 0.71±0.03 mg/L (2014)] showed relatively high concentration of Cu. Wide rages for Cu

concentration in wines have been previously found and reported by other researchers in Brazil [42] 0.056-0.764 mg/L Cu, in Hungary [43] 0.031-0.313 mg/L Cu, in Italy [44] 0.50-1.00 mg/L Cu and in Greece [45] 0.076-0.114 mg/L Cu (Table 1).

Examining the factors which influenced the content of metals in wines, it can be seen that the content in Cd, Pb, U, Hg, Sr, Co, Ni and Cr was significantly influenced by the Variety, Years and Variety x Years factors, while As and Cu content was significantly influenced only by the Variety factors.

Relating the obtained results [Cd average 0.10±0.01 µg/L (0.1mg/kg M.L.A. = Maximum Limit Allowed) Pb average 41.51±1.05 µg/L (0.15 mg/kg M.A.L); As average 10.81±0.61 µg/L (0.2 mg/kg M.A.L); Cu average 0.72±0.04 mg/L (1 mg/kg M.A.L) to national and international legislation we may say that the wines from Dealu Bujorului vineyard fall within the limits set by legislation (Table 1).

$^{206}Pb/^{207}Pb$, $^{208}Pb/^{206}Pb$, $^{206}Pb/^{204}Pb$, $^{87}Sr/^{86}Sr$, isotope ratio from wine samples

In Central Europe, the lead isotopic ratio, as signatures of pollution sources, ranges from relatively high $^{206}Pb/^{207}Pb$ ratios (natural Pb, coals, fly ashes, $^{206}Pb/^{207}Pb$=1.1700-1.2200) to low $^{206}Pb/^{207}Pb$ values (gasoline, petrol combustion, $^{206}Pb/^{207}Pb$ = 1.0600-1.1400) [20, 27].

The Pb isotopes ratio for the selected wines (Table 2) varies in range between 1.13896-1.12545 ($^{206}Pb/^{207}Pb$), 2.13857-2.12126 ($^{208}Pb/^{206}Pb$) and 17.30857-17.44944 ($^{206}Pb/^{204}Pb$) with average 1.13269 ($^{206}Pb/^{207}Pb$), 2.12824 ($^{208}Pb/^{206}Pb$) and 17.42213. Regarding $^{206}Pb/^{207}Pb$ isotope ratios based on analyses it can be concluded that the wine obtained from wine varieties grown in the Dealu Bujorului vineyards show traces of pollution originating from automobile emissions ($^{206}Pb/^{207}Pb$=1.1000-1.1400). The obtained isotope ratio values are comparable with other Romanian wines [20] (1.1100 to 1.2000) and Brazilian wines [36] (1.1440 to 1.1820).

The highest values of $^{208}Pb/^{206}Pb$ and $^{206}Pb/^{204}Pb$ were recorded for wines obtained from Muscat Ottonel variety from 2012 (2.13857±0.00699 [0.32697] $^{208}Pb/^{206}Pb$) and Muscat Ottonel variety from 2011 (17.44513±0.03613 [0.14977] $^{208}Pb/^{206}Pb$). While Feteasca Regala from 2012 (2.12126±0.00106 [0.05014] $^{208}Pb/^{206}Pb$), Feteasca Alba from 2013 (17.30857±0.00560 [0.03235] $^{206}Pb/^{204}Pb$), and also Cabernet Sauvignon from 2012 (1.12545±0.00200 [0.17771] $^{206}Pb/^{207}Pb$), recorded the lowest isotope ration.

The results are comparable with Brazilian wines [36] (2.0700 to 2.1570 for $^{208}Pb/^{206}Pb$ and 16.6670 to 17.9960 for $^{204}Pb/^{206}Pb$) and also with Italian wines [46] (2.0990 to 2.1030 for $^{208}Pb/^{206}Pb$ and 17.544 to 18.3210 for $^{204}Pb/^{206}Pb$).

Table 1. Variation of the metal content of white and red wines from Dealu Bujorului Vineyard (µg/L)

Area	*Variety*	*Year*	Cd M.L.A. **0.01 mg/L**	Pb M.L.A. **0.15 mg/L**	U M.L.A. **-**	Hg M.L.A. **-**	As M.L.A. **0.2 mg/L**	Sr M.L.A. **-**	Co M.L.A. **-**	Cu** M.L.A. **1 mg/L**	Ni M.L.A. **-**	Cr M.L.A. **-**
Dealu Bujorului Vineyard	Muscat Ottonel	2011	0.12±0.01^{abc} α	42.35±1.00^{d} α	0.15±0.02^{d} α	0.58±0.04^{a} α	8.20±0.62^{fg} β	149.12±5.50^{j} β	3.73±0.17^{ij} β	0.68±0.05^{ef} α	517.12±4.21^{k} α	851.09±1.36^{c} γ
		2012	LOQ^{g} β	47.78±6.67^{bc} α	LOQ^{f} β	0.40±0.01^{c} β	8.31±0.37^{fg} β	114.08±6.44^{l} γ	3.55±0.39^{j} β	0.49±0.03^{i} β	498.01±2.33^{k} β	923.62±2.05^{a} α
		2013	LOQ^{g} β	27.22±2.55^{gh} β	LOQ^{f} β	0.14±0.02^{g} γ	10.41±0.88^{def} α	161.45±1.91^{i} α	4.73±0.47^{defg} α	0.70±0.04^{de} α	460.89±2.14^{k} β	872.86±4.02^{b} β
	Feteasca Alba	2011	0.11±0.01^{cd} α	35.69±1.12^{e} β	0.28±0.03^{b} α	LOQ^{f} α	6.20±0.23^{g} β	186.11±7.36 g α	6.28±0.28^{ab} α	0.61±0.03^{fgh} β	650.72±0.93^{b} α	867.66±3.50^{b} α
		2012	0.12±0.01^{bcd} α	52.07±0.50^{ab} α	LOQ^{f} β	LOQ^{f} α	6.42±0.87^{g} β	173.38±3.01 h β	5.09±0.09^{cdef} β	0.77±0.08^{bcd} α	535.26±1.21^{gh} β	734.62±6.94^{f} γ
		2013	0.12±0.02 bcd α	29.23±3.02^{fg} γ	LOQ^{f} β	LOQ^{f} α	7.99±0.56^{fg} α	164.41±2.74 i β	4.56±0.38^{efgh} β	0.49±0.02^{i} γ	358.36±6.26^{m} γ	818.49±5.66^{d} β
	Feteasca Regala	2011	LOQ^{g} β	52.29±1.00^{a} β	0.38±0.03^{a} α	0.15±0.02^{fg} β	13.18±0.51^{b} α	187.22±6.69 g β	5.22±0.09^{cd} β	0.85±0.07^{ab} α	520.15±3.35^{i} β	761.45±5.53^{e} β
		2012	0.08±0.01^{f} α	51.39±1.81^{ab} α	0.40±0.01^{a} α	0.19±0.02^{ef} α	12.95±0.61^{bc} α	202.54±6.74 ef α	6.74±0.48^{a} α	0.91±0.05^{a} α	603.50±5.38^{d} α	821.61±2.00^{d} α
		2013	0.09±0.03^{f} α	24.26±0.53^{hij} α	0.21±0.01^{c} β	0.19±0.01^{efg} α	9.62±0.54^{ef} β	200.89±1.07 f α	5.15±0.21^{cde} β	0.82±0.06^{b} α	239.81±1.34^{n} γ	819.25±4.03^{d} α
	Feteasca Neagra	2011	0.13±0.01^{ab} α	23.01±1.54^{ij} β	0.16±0.02^{d} α	0.51±0.04^{b} α	10.17±0.76^{def} β	254.72±4.59 c γ	3.71±0.21^{ij} β	0.71±0.03^{cde} β	747.37±3.35^{a} α	355.90±1.74^{n} β
		2012	0.12±0.01^{bcd} αβ	20.28±1.09^{j} β	0.13±0.02^{d} β	0.19±0.02^{ef} β	11.98±1.28^{cdec} β	263.81±2.28 b β	4.48±0.23^{fgh} α	0.60±0.05^{gh} γ	592.65±6.08^{de} β	323.92±4.09^{o} γ
		2013	0.10±0.01^{e} β	32.79±1.46^{ef} α	LOQ^{f} γ	0.24±0.04^{d} β	12.39±1.03^{bcd} α	277.49±3.64 a α	4.61±0.50^{defge} α	0.80±0.01^{b} α	566.51±4.60^{f} γ	408.55±4.45^{m} α
	Merlot	2011	0.13±0.02^{ab} α	54.33±1.00^{a} α	0.27±0.04^{b} α	0.21±0.02^{de} α	13.46±0.76^{b} α	200.87±2.91 f β	4.25±0.36^{ghi} γ	0.69±0.04^{de} α	523.52±0.97^{ij} γ	478.45±2.86^{k} β
		2012	0.11±0.02^{cd} β	51.20±1.19^{ab} β	0.13±0.02^{d} β	LOQ^{f} γ	13.83±0.68^{b} α	185.92±2.63 g β	5.35±0.26^{c} β	0.68±0.03^{def} α	543.26±4.28^{g} β	429.95±1.18^{l} γ
		2013	LOQ^{g} γ	47.45±1.12^{d} γ	0.16±0.05^{d} β	0.16±0.04^{fg} β	12.29±1.00^{bcd} α	212.78±3.14 d α	6.02±0.34^{b} α	0.61±0.02^{fgh} β	636.69±5.08^{c} α	520.36±1.50^{i} α
	Cabernet Sauvigno n	2011	0.13±0.02^{ab} α	41.61±0.65^{d} β	0.30±0.05^{b} α	0.24±0.06^{d} α	13.67±1.41^{b} α	253.68±6.69 c α	4.04±0.13^{hij} β	0.79±0.04^{bc} α	479.78±4.28^{k} γ	651.07±1.34^{g} α
		2012	0.14±0.03^{abc} α	26.12±4.45^{ghij} γ	0.27±0.01^{b} α	0.22±0.03^{de} α	14.41±2.75^{ab} α	209.37±3.46^{de} β	5.08±0.50^{cdef} α	0.56±0.05^{hi} β	532.26±4.28^{hi} β	635.97±5.55^{h} β
		2013	0.14±0.01^{a} α	50.01±1.35^{ab} α	0.16±0.05^{d} β	0.23±0.03^{de} α	16.74±4.30^{a} α	189.03±1.97 g γ	5.07±0.17^{cdef} α	0.64±0.08^{efgh} β	587.39±5.37^{e} α	530.39±1.51^{i} γ
Average			**0.10±0.01**	**41.51±1.05**	**0.26±0.03**	**0.28±0.03**	**10.81±0.61**	**205.29±5.63**	**4.54±0.21**	**0.72±0.04**	**573.11±2.85**	**660.94±2.72**
Sig.			***	***	***	***	***	***	***	***	***	***
Variety	Sig.		***	***	***	***	***	***	***	***	***	***
Year	Sig.		***	***	***	***	ns	***	***	**	***	***
Variety x Year	Sig.		***	***	***	***	**	***	***	***	***	***
[1]				23.08±11.96	0.86±0.55			358.94±178.97	2.08±1.19	154.39±73.45**	18.39±1.19	146.18±70.96
[2]			0.41		0.55		7.10		4.65		24.90	
[3]			0.22	35.90		0.56	5.24	355.80	2.50			
[4]				235.90				1600.68	42.06	2594.79**	322.73	1725.80

Average value ± standard deviation (n = 3). Romans letters represent the significance of the variety difference ($p \leq 0.05$). Greeks letters represent the significance of the same variety cultivated in other year's difference ($p \leq 0.05$). The difference between any two values, followed by at least one common letter, is insignificant. M.L.A. - maximum limit allowed (OIV, 2005); LOQ - lower than the limit of quantification; Cu* = (mg/L); Cu** = (µg/L).

The abundance of the lead isotopes ^{204}Pb (non-radiogenic), ^{206}Pb, ^{207}Pb and ^{208}Pb (radiogenic) originated from the genesis of the substrate varies with geological ages. The original composition of the rock upon its formation and consequently, with geographical areas [47], this property is useful in order to identify of the source of lead in a subjected wine sample provided that the measurements of the isotope ratio is precise and accurate.

Concerning $^{87}Sr/^{86}Sr$ isotope ratio, the values are between the ranges from 0.72599±0.00645 [0.89970] to 0.71288±0.00048 [0.03012] with an average value of 0.72158±0.00042 [0.05763]. The highest values were registered to wine obtained from Fetească regala variety from 2011 (0.72599±0.00422 [0.58123]), the lowest value of $^{87}Sr/^{86}Sr$ isotope ratio was recorded to wine obtained from 2012 Feteasca Alba variety (0.71288±0.00098 [0.13715]).

The values of $^{87}Sr/^{86}Sr$ isotope ratio obtained are comparable with those obtain for other Romanian wines [48] (0.71015 to 0.72311) and [20] (0.7600 to 0.9300).

Combining multielement analysis and $^{206}Pb/^{207}Pb$, $^{208}Pb/^{206}Pb$, $^{206}Pb/^{204}Pb$, $^{87}Sr/^{86}Sr$, isotope ratio from wine samples for discrimination analysis

Multivariate chemometric method was used as a supervised learning technique for the differentiation of wines intro groups on the basis of grape variety and year of production and finding markers which showed a significant discrimination value (variables with Wilk's lambda near zero, *p* value <0.05 and higher *F* coefficients). Stepwise linear discriminant analysis (LDA) was used to identify significant tracers for classification to the geographical discrimination of the wines samples. Stepwise Discriminant Analysis (LDA) was used to designate suitable variables for classification of the samples, eliminating the variables that do not contribute to discrimination of the wine. In order to validate the proposed statistic model, based on variables which showed higher significance in first LDA assessment, we performed a second Liniar Discriminant Analysis (LDA) for the test set consisting of wines used to build statistical model (training set) together with data from other wine samples that are not included in the first LDA (control-set). Cross-validation was applied to determine the optimal number of variables required to obtain robust models.

In this study, the content of certain wines showed high concentration of metals, but not exceeding the maximum recommended by International Organisation of Vine and Wine [49]; this accumulation is mostly due to agricultural practices, fertilizers and technological winemaking processes.

Table 2. The $^{206}Pb/^{207}Pb$, $^{208}Pb/^{206}Pb$, $^{206}Pb/^{204}Pb$, $^{87}Sr/^{86}Sr$, isotope ratios obtained from wine samples from Dealu Bujorului Vineyard

Area	Variety	Year	$^{206}Pb/^{207}Pb$	SD	RSD (%)	$^{208}Pb/^{206}Pb$	SD	RSD (%)	$^{206}Pb/^{204}Pb$	SD	RSD (%)	$^{87}Sr/^{86}Sr$	SD	RSD (%)	Pb (µg/L)	Sr (µg/L)
Dealu Bujorului Vineyard	Muscat Ottonel	2011	1.13434^{abc} α	0.00277	0.24458	2.12495^{bcdef} β	0.00303	0.14269	17.44513 a α	0.03613	0.14977	0.71573^{cd} α	0.00573	0.80077	42.35±1.00^{ij} α	149.12±5.50^{i} β
		2012	1.13399^{abc} α	0.00168	0.14780	2.13857^{a} α	0.00699	0.32697	17.44443 a α	0.01981	0.11356	0.71539^{cd} α	0.00293	0.40990	47.78±6.67^{hc} α	114.08±6.44^{kl} γ
		2013	1.13205^{abcd} α	0.00512	0.45259	2.13259^{abc} αβ	0.00261	0.12254	17.43786 a α	0.03579	0.20525	0.72303^{ab} α	0.00302	0.41721	27.22±2.55^{gh} β	161.45±1.91^{f} α
	Feteasca Alba	2011	1.13456^{abc} α	0.00169	0.14872	2.12488^{cdef} α	0.00369	0.25334	17.42660 a α	0.03495	0.20089	0.72164^{abc} α	0.00022	0.03012	35.69±1.12^{ef} β	186.11±7.36^{gl} α
		2012	1.13363^{abc} α	0.00257	0.22633	2.12296^{ef} α	0.00039	0.01828	17.43213 a α	0.02427	0.13922	0.71288^{de} β	0.00098	0.13715	52.07±0.50^{ab} α	173.38±3.01^{h} β
		2013	1.13106^{bcd} α	0.00437	0.38601	2.12382^{def} α	0.00194	0.02748	17.30857 a β	0.00560	0.03235	0.72144^{abc} α	0.00020	0.02721	29.23±3.02^{fg} γ	164.41±2.74^{f} β
	Feteasca Regala	2011	1.13668^{ab} α	0.00102	0.08932	2.12323^{ef} α	0.00102	0.04781	17.42030 a α	0.09744	0.55933	0.72177^{abc} α	0.00078	0.10768	52.29±1.00^{a} β	187.22±6.69^{g} β
		2012	1.13896^{a} α	0.00642	0.56401	2.12126^{f} α	0.00106	0.05014	17.42944 a α	0.01932	0.11083	0.71823^{bcd} α	0.00569	0.79181	51.39±1.81^{ab} α	202.54±6.74^{ef} α
		2013	1.13205^{abcd} α	0.00567	0.50055	2.12315^{ef} α	0.00208	0.09793	17.44241 a α	0.01725	0.09890	0.72227^{abc} α	0.00098	0.13632	24.26±0.53^{hi} α	200.89±1.07^{d} α
	Feteasca Neagra	2011	1.13455^{abc} α	0.00185	0.16319	2.12903^{bcdef} α	0.00560	0.26302	17.42310 a α	0.01000	0.05737	0.72599^{a} α	0.00422	0.58123	23.01±1.54^{ij} β	254.72±4.59^{c} γ
		2012	1.13530^{ab} α	0.00073	0.06401	2.13308^{abc} α	0.00131	0.06148	17.42643 a α	0.00601	0.03450	0.71196^{e} α	0.00556	0.76679	20.28±1.09^{j} β	263.81±2.28^{b} β
		2013	1.13165^{abc} α	0.00299	0.26337	2.12933^{bcdef} α	0.00677	0.31794	17.42155 a α	0.00024	0.00135	0.72235^{abc} α	0.00651	0.90124	32.79±1.46^{gh} α	277.49±3.64^{b} α
	Merlot	2011	1.12605^{d} α	0.00018	0.01589	2.12223^{f} α	0.00591	0.27694	17.42563 a α	0.00566	0.03248	0.71965^{abc} α	0.00330	0.45850	54.33±1.00^{a} α	200.87±2.91^{d} β
		2012	1.12769^{cd} α	0.00713	0.63229	2.12843^{bcdef} α	0.00716	0.33637	17.42148 a α	0.00023	0.00129	0.72370^{ab} α	0.00320	0.44197	51.20±1.19^{ab} β	185.92±2.63^{g} β
		2013	1.13106^{bcd} α	0.00468	0.41419	2.12758^{bcde} α	0.00480	0.22537	17.41635 a α	0.00501	0.02878	0.71737^{bcd} α	0.00645	0.89970	47.45±1.12^{bc} γ	212.78±3.14^{d} α
	Cabernet Sauvignon	2011	1.13502^{abc} α	0.00046	0.04057	2.13344^{ab} α	0.00196	0.09199	17.42410 a β	0.00234	0.01341	0.72346^{ab} α	0.00214	0.29596	41.61±0.65^{cd} β	253.68±6.69^{c} α
		2012	1.12545^{d} β	0.00200	0.17771	2.13034^{bcde} α	0.00625	0.29339	17.41532 a β	0.00639	0.03669	0.72262^{abc} α	0.00185	0.25567	26.12±4.45^{gh} γ	209.37±3.46^{de} β
		2013	1.13115^{bcd} αβ	0.00514	0.45450	2.12990^{bcde} α	0.00473	0.22186	17.44944 a α	0.01690	0.09685	0.72158^{abc} α	0.00042	0.05763	50.01±1.35^{ab} α	189.03±1.97^{fg} γ
Average			**1.13269**	**0.00314**	**0.27968**	**2.12824**	**0.00374**	**0.17555**	**17.42213**	**0.01794**	**0.10294**	**0.72158**	**0.00042**	**0.05763**	**41.51±1.05**	**205.29±5.63**
Minimum Values			1.12545	0.00713	0.01589	2.12126	0.00039	0.01828	17.30857	0.00023	0.00129	0.71288	0.00022	0.03012	20.28±1.09	114.08±6.44
Maximum Values			1.13896	0.00018	0.63229	2.13857	0.00716	0.33637	17.44944	0.09744	0.20525	0.72599	0.00645	0.89970	54.33±1.00	277.49±3.64
F			2.663			3.484			3.594			2.517			78.680	265.319
Sig.			**			***			**			*			p ≤ 0.000	p ≤ 0.000
Variety			ns			ns			ns			ns			***	***
Year			ns			ns			ns			ns			***	***
Variety x Year			ns			ns			ns			ns			***	***
[5]												0.711235	0.00004			
[6]			1.14400		1.40000	2.15700		1.00000							76.00±13.00	
[7]			1.14000	0.10000	8.70000	2.10000	0.15000	7.10000				0.76000	0.01000	1.30000	35.90	171.40
[8]			1.74000	0.00300		2.09200	0.00700								11.11±5.28	
[9]												0.71000				
[10]			1.14200	0.00200	0.14000	2.12500	0.00300	0.16000	17.60000	0.30000	1.70000				42.90±0.05	
[11]												0.71021				
[12]			1.16620	0.00040	0.03000	2.09230	0.00060	0.03000	18.40000	0.10000	0.70000					
[13]b			1.10380	0.01750	1.58860	2.13420	0.01100	0.51660				0.89570	0.01930	2.15870	46.59±0.57	418.87±18.03
[14]			1.13500	0.00100	0.01830	2.10540	0.00390	0.18430	16.66630	0.03070	0.16450	0.71510	0.00160	021870	55.44±1.01	202.07±8.15
[15]												0.71000				
[16]												0.71300				
[17]			1.15400	0.07700											21.74	
[18]												0.71015			52.00	905.00

Average value ± standard deviation (n = 3). Romans letters represent the significance of the variety difference ($p \leq 0.05$).Greeks letters represent the significance of the same variety cultivated in other year's difference ($p \leq 0.05$). The difference between any two values, followed by at least one common letter, is = insignificant.

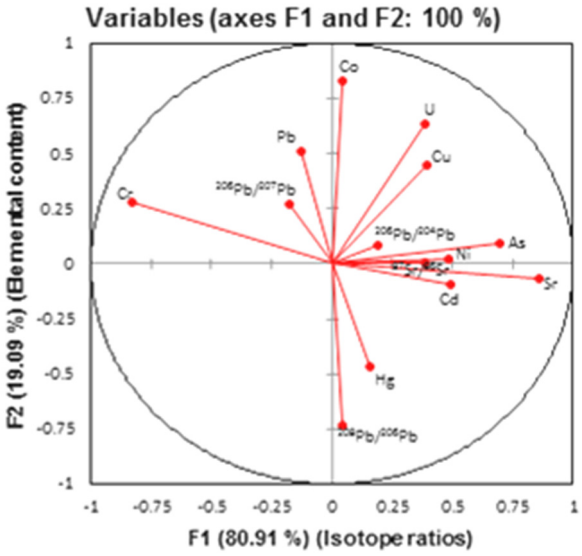

Figure 1. Correlation between analyzed parameters and the factors in discriminant analysis the origin of the wine

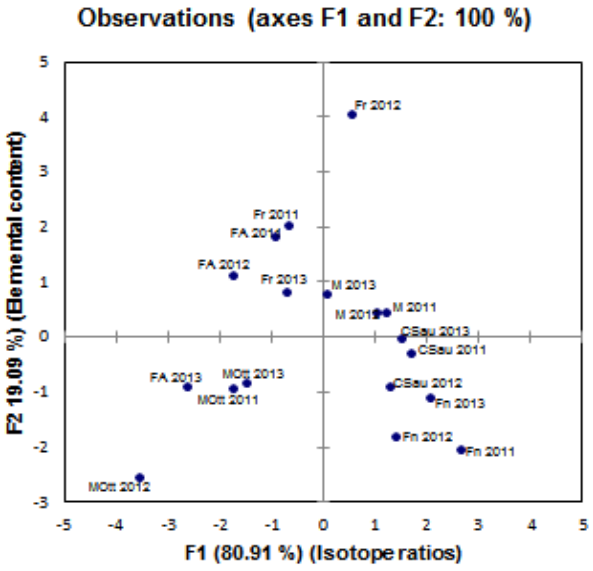

Figure 2. Differentiation of wines based on element contents and $^{206}Pb/^{207}Pb$, $^{208}Pb/^{206}Pb$, $^{206}Pb/^{204}Pb$, $^{87}Sr/^{86}Sr$ isotope ratios

Elements like Pb, Cu, Ni, Cd and Hg showed a high discriminatory power for geographic origin of Romanian, but additional new elements (Co, U, As, Sr, Cr) and $^{207}Pb/^{206}Pb$, $^{208}Pb/^{206}Pb$, $^{204}Pb/^{206}Pb$, $^{87}Sr/^{86}Sr$ isotope ratio have been investigated in order to identify new tracers for geographical traceability of Romanian wines [41].

Based on the elemental contents and $^{207}Pb/^{206}Pb$, $^{208}Pb/^{206}Pb$, $^{204}Pb/^{206}Pb$, $^{87}Sr/^{86}Sr$ isotopes ratio, the cross-validation technique provided a 100 % percentage of predicted membership according to the origin of the wine (F1 = 80.91 % and F2 = 19.09 %). The linear correlation revealed acceptable scores for the two defined discriminant factors (F1 and F2) (Figure 1). A significant differentiation of wines according to the year of wine production was carried out for wines samples, which demonstrates the importance of elemental profile for the geographical traceability of wines (Figure 2).

CONCLUSIONS

In this work the elemental composition and $^{207}Pb/^{206}Pb$, $^{208}Pb/^{206}Pb$, $^{204}Pb/^{206}Pb$, $^{87}Sr/^{86}Sr$ isotope ratio of white wines (Muscat Ottonel, Feteasca Alba, Feteasca Regala) and red wines (Feteasca Neagra, Merlot, Cabernet Sauvignon) was studied in order to highlight the elemental composition of wine samples.

Concentration of Cd, Pb, As and Cu heavy metals in analysed wine samples were under Maximum Limit Allowed (M.L.A.), respectively as published by the Organization of Vine and Wine. The content of potentially toxic elements such as Cd, Pb, U, Hg, As, Cu, Ni and Cr are lower than the recommended values found in literature, highlighting the safety and quality of the analyzed Romanian wines.

Our results confirm that the $^{207}Pb/^{206}Pb$, $^{208}Pb/^{206}Pb$, $^{204}Pb/^{206}Pb$ and $^{87}Sr/^{86}Sr$ isotope ratio can be used to track the origin of wine, to discriminate between the wine produced in different years and can be used to characterize wine terroirs for forensic purpose. Based on the elemental profile and $^{207}Pb/^{206}Pb$, $^{208}Pb/^{206}Pb$, $^{204}Pb/^{206}Pb$, $^{87}Sr/^{86}Sr$ isotope ratio, a relevant discrimination of wines according to the production year was performed. The variation of $^{207}Pb/^{206}Pb$, $^{208}Pb/^{206}Pb$, $^{204}Pb/^{206}Pb$, $^{87}Sr/^{86}Sr$ isotope ratio represents a strong geological marker for wines geographical traceability. The proposed methodology allowed successful classification of wines according to the region of provenance and also the production year.

EXPERIMENTAL SECTION

Study area

A total of 54 wine samples were analysed (3 white wines and 3 red wines). Samples originated from Dealu Bujorului vineyard (45°52′10″ N, 27°55′8″E). The Dealu Bujorului region is characterized by an alternate landscape, from flat to hilly areas, with altitude between 100 and 225 m and the predominant soil is levigated chernozem having a clayey sand texture with pH between values 7.4 and 8.1. Although they have moisture deficit, natural conditions (ecoclimatic and ecopedological) offer viable ecosystem for the development of vineyard. The vineyard is crossed by the parallel 46° latitude north, intersected by the 28° longitude meridian. Dealu Bujorului vineyard belongs to Galați country. The specificity of the transition area is highlighted by the predominance of deposits of clays and sands. Versants were made from clay deposits and sandy sands.

Sample collection and microvinification process

The samples used in this experiment were obtained from the wines produced from Muscat Ottonel, Feteasca Alba, Feteasca Regala, Feteasca neagra, Merlot and Cabernet Sauvignon under the conditions of 2011, 2012 and 2013. The wine samples resulted from micro-wine production. Micro-wine production was done according to the methodology describe by Bora et al. [12]. All wines were providing by the wineries as finished wines in 750 mL bottles with cork stoppers and were stored at 3-4°C before analysis. All vines were planted since 1979, and the vine plantation was organized with 2.2 x 1 m distance between rows and plants. Vines were pruned according to the Guyot system and were grown on speliers.

Reagents and solutions

Ten elements (Cd, Pb, U, Hg, As, Sr, Co, Cu, Ni and Cr) were determined in order to assess their ability to discriminate wines by geographical origin. The analysis was made using multielement analysis and ICP-MS technique, after an appropriate dilution, using external standard calibration method. The calibration was performed using XXICertiPUR multielement standard, and from individual standard solution

of Cr and Hg. The working standards and the control sample were prepared daily from the intermediate standards that were prepared from the stock solution. The intermediate solutions stored in polyethylene bottles and glassware was cleaned by soaking in 10% v/v HNO_3 for 24 hours and rinsing at least ten rimes with ultrapure water (18.2 MΩ cm^{-1} ultrapure water-Types 1). The accuracy of the methods was evaluated by replicate analyses of fortified samples (10 µL-10 mL concentrations) and the obtained values ranged between 0.8-13.1 percent, depending on the element. The global recovery for each element was estimated and the obtained values were between 84.6-100.9% [48].

For quality control purpose, blanks and triplicates samples (n = 3) were analyzed during the procedure. The variation coefficient was under 5% and detection limits (ppb) were determined by the calibration curve method. Limit of detection (LoD) and Limit of quantification (LoQ) limits were calculated according to the next mathematical formulas: LoD = 3SD/s and LoQ = 10 SD/s (SD = estimation of the standard deviation of the regression line; s = slope of the calibration curve) (Table 3).

Table 3. Instrumental conditions for the determination of each element (ICP-MS technique)

Element	Correlation coefficient	LoD* (µg/L)	LoQ*** (µg/L)	BEC** (µg/L)
Cd	0.9999	0.0202	0.0673	0.027
U	0.9999	0.0253	0.0842	0.005
As	0.9999	0.2335	0.7776	0.538
Co	0.9999	0.0365	0.1215	0.152
Ni	0.9999	0.0591	0.1968	0.091
Pb	0.9999	0.0003	0.0010	0.002
Hg	0.9999	0.0417	0.1379	0.128
Sr	0.9999	0.1434	0.4775	0.955
Cu	0.9999	0.0402	0.1339	0.237
Cr	0.9999	1.6630	5.5378	0.636

*Detection limit; **Background equivalent concentration; ***Quantification limit.

For calibration and to verify the achieved accuracy and precision, ten NIST-SRM 987 and NIST-SRM 982 analysis results were pooled together with the calculated relative standard deviation presented in Table 4. Based on the obtained results, it was verified that, applying quadrupole ICP-MS, relative standard deviation and reproducibility of approximately 0.5% for $^{87}Sr/^{86}Sr$, $^{206}Pb/^{207}Pb$ and $^{208}Pb/^{206}Pb$ are feasible. The results were in agreement with those reported by [48, 50].

Table 4. Lead isotopic ration and Lead isotopic ration determination precision and accuracy based on the NIST SRM 982 (Lead) NIST SRM 987 (Strontium) (n=10)

Replicate	$^{207}Pb/^{206}Pb$ (a)	RSD (%)	$^{208}Pb/^{206}Pb$ (b)	RSD (%)	$^{204}Pb/^{206}Pb$ (c)	RSD (%)	$^{87}Sr/^{86}Sr$ (d)	RSD (%)
1	0.46483	0.51	0.99891	0.67	0.00271	0.32	0.70493	0.31
2	0.47891	0.48	0.99452	0.61	0.00272	0.41	0.72046	0.45
3	0.46978	0.32	0.99794	0.55	0.00275	0.28	0.70325	0.63
4	0.47123	0.64	0.99688	0.64	0.00273	0.51	0.70634	0.48
5	0.46987	0.56	0.99726	0.48	0.00246	0.14	0.71478	0.36
6	0.46154	0.37	0.99647	0.56	0.00258	0.39	0.71245	0.59
7	0.47362	0.70	0.99969	0.34	0.00279	0.47	0.70987	0.46
8	0.45641	0.43	0.99744	0.58	0.00278	0.51	0.72326	0.42
9	0.41562	0.36	0.99576	0.59	0.00273	0.49	0.70845	0.68
10	0.45612	0.45	0.99874	0.61	0.00278	0.36	0.10789	0.47
Average	0.46179	0.48	0.99736	0.56	0.00270	0.41	0.71117	0.49

[a]Certified value=$^{207}Pb/^{206}Pb$ (0.46707±0.00020); [b]Certified value=$^{208}Pb/^{206}Pb$ (1.00016±0.00036); [c]Certified value=$^{204}Pb/^{206}Pb$ (0.027219±0.00027); [d]Certified value=$^{87}Sr/^{86}Sr$ (0.71034±0.00026); RSD (%) = relative standard deviation.

Sample preparation for determination of heavy metals and isotopic ration from wine using ICP-MS.

For the determination of elements from wine samples were used an amount of 0.5 mL wine and adjust 8 mL (7 mL HNO_3 65%+1 mL H_2O_2) were placed in a clean Teflon digestion vessel, after 15-30 minutes the mineralization was performed using a microwave system Milestone START D Microwave Digestion System set in three steps: step I (time 10 min., temperature 200ºC), step II (time 15 min., temperature 200ºC) and step III (time 40 min., ventilation - temperature 32ºC). After mineralization, samples were filtered through a 0.45 mm filter and brought to a volume of 50 mL. The Pb and Sr isotope ration in the analysed wine samples ($^{206}Pb/^{207}Pb$, $^{208}Pb/^{206}Pb$, $^{206}Pb/^{204}Pb$, $^{87}Sr/^{86}Sr$,) were determined according to the methodology indicated by Mihaljevič *et al*. [51]; Geana et al. [21]; Bora *et al.* [24].

In order to confirm the best-chosen conditions for wine digestion standard additions for checking accuracy of the microwave digestion and recoveries were calculated (Table 5). The digestion seemed visually completed in all of the combinations, but the spiked recoveries showed significant differences for total elements content (*p* - Value = *0.005*).

Table 5. Standard additions for checking accuracy of the microwave digestion ICP-MS method (n = 3)

Element	Certified Concentration (mg/L)	Measured Concentration (mg/L)
Cd	6.568±0.073	6.473±0.106
U	9.994±0.016	9.981±0.012
As	56.85±0.37	53.09±0.31
Co	27.06±0.28	24.13±0.06
Ni	62.41±0.69	61.32±0.21
Pb	19.63±0.21	19.13±0.09
Hg	0.1016±0.0017	0.1102±0.0012
Sr	314.00±19.00	314.09±09.06
Cu	21.44±0.70	21.25±0.21
Cr	18.32±0.10	19.18±0.21

Instrumentation

The determination of metals was performed on mass spectrometer with inductively coupled plasma, (ICP-MS) iCAP Q Thermo scientific model, based polyatomic species before they reach the quadrupole mass spectrometer, using a PFA micro flow concentric nebulizer. The argon used was of 99.99% purity (Messer, Austria). The instrument was daily optimized to give maximum sensitivity for M^+ ions and the double ionization and oxides monitored by the means of the rations between Ba^{2+}/Ba^+ and Ce^{2+}/CeO^+, respectively, these always being less than 2%. The experimental conditions were: argon flow on nebulizer (0.82 L/min.), auxiliary gas flow 0.80 L/min., argon flow in plasma 15 L/min., lens voltage 7.30 V; RF power in plasma 1100 W, spray chamber temperature (2.50±1.00^{o}C). Accuracy was calculated for the elements taken into consideration (0.5-5.0%).

Statistical analysis

The statistical interpretation of the results was performed using the Duncan test, SPSS Version 24 (SPSS Inc., Chicago, IL., USA). The statistical processing of the results was primarily performed in order to calculate the following statistical parameters: average and standard deviation. This data was interpreted with the analysis of variance (ANOVA) and the average separation was performed with the DUNCAN test at $p \leq 0.05$. Multivariate chemometric method was used as a supervised learning technique for the differentiation of wines intro groups on the basis of grape variety and year of production and finding markers which showed a

significant discrimination value (variables with Wilk's lambda near zero, *p* value <0.05 and higher *F* coefficients). Stepwise linear discriminant analysis (LDA) was used to identify significant tracers for classification to the geographical discrimination of the wines samples. Stepwise Discriminant Analysis (LDA) was used to designate suitable variables for classification of the samples, eliminating the variables that do not contribute to discrimination of the wine. In order to validate the proposed statistic model, based on variables which showed higher significance in first LDA assessment, we performed a second Linear Discriminant Analysis (LDA) for the test set consisting of wines used to build statistical model (training set) together with data from other wine samples that are not included in the first LDA (control-set). Cross-validation was applied to determine the optimal number of variables required to obtain robust models. Linear discriminant analysis (LDA) was performed using Microsoft Excel 2016 and XLSTAT Addinsoft version 15.5.03.3707.

ACKNOWLEDGMENTS

This paper was published under the frame of the Romanian Ministry of Agriculture and Rural Development, project ADER no. 14.2.2. "Quantitative studies on assessment and monitoring contaminants, on the chain of viticulture and winemaking to minimize the amount of pesticides and heavy metals as principal pollutants".

REFERENCES

1. OIV, *International Code of Oenological Practices, Annex: Maximum Acceptable Limits*, **2015,** Issue 2015/01. Paris, France.
2. F. Stoica, *Carpathian Journal of Food Science and Technology*, **2015,** *7(4)*, 139-144.
3. G.L. La Torre, R. Rando, M. Saitta, M. Alfa, R. Malsano, G. Dugo, *Italian Journal of Food Science*, **2010**,*1*(22), 28-40.
4. Y. Vystavna, L. Zaichenko, L. Klimenko, R. Ratsep, *Journal of Science Food and Agriculture*, **2017,** *97*, 4520–4525.
5. J. Halili, K. Bislimi, I. Mazreku, A. Behluli, F. Osmani, A. Maloku, F. Halili, *13th SGEM GeoConference on Ecology, Economics, Education and Legislation, Conference Proceedings*, **2013**, *1*, 531– 538.

6. M.D. Blackhurst, A.D. Marais, *Journal of Endocrinology, Metabolism and Diabetes of South Africa*, **2009**, *44*(2), 77-79.
7. I.M. Alkis, S. Oz, A. Akatol, N. Yilmaz, R. E. Anli, O. Akatol, *Journal of Food Compostion and Analysis*, **2014**, *33*, 105-110.
8. S. Đurđic, M. Pantelic, J. Trifkovic, V. Vukojevic, M. Natic, ˇZ. Tesica, J. Mutic, *RSC Advances*, **2017,** *7*, 2151-2162.
9. I. Geană, A. Iordache, R. Ionete, A. Marinescu, A. Ranca, M. Culea, *Food Chemistry*, **2013**, *138*, 1125-1134.
10. M. A. I. Chukwujindu, A. L. Ojelum, F. I. Bassey, *Food Science and Nutrition*, **2014**, *2(6):* 724–733.
11. K. Pyrzynska, *Critical Reviews in Analytical Chemistry,* **2004***, 34,* 69-83.
12. F. D. Bora, A. Donici, C. Voica, T. Rusu, L. Mihaly-Cozmuța, A. Mihaly-Cozmuța, C. Cimpoiu, D. E. Mihăiescu*, Advances in Agriculture and Botanics - International Journal of the Bioflux Society,* **2016***, 8(3),* 129-142.
13. K. M. Towle, L. C. Garnick, A. D. Monnot, *International Journal of Food Contamination,* **2017***, 4*:7.
14. P. Hajeb, J. J. Sloth, S. Shakibazadeh, N. A. Mahyudin, L. Afsah-Hejri, *Comprehensive Reviews in Food Science and Food Safety*, **2014**, *13,* 457-472.
15. J. Cacho, J. E. Castells, A. Esteban, B. Laguna, N. Sagrista, *American Journal of Enology and Viticulture,* **1995**, *46*, 381-384.
16. K. A. Riganakos, P.G. Veltsistas, *Food Chemistry*, **2003**, *82*, 637-643.
17. P. Bentez, R. Castro, J.A. S. Pazo, C.G. Barroso, *Food Research International,* **2002**, *35*, 785-791.
18. A.D. Monnot, B.E. Tvermoes, R. Gerads, H. Gürleyük, D. Paustenbach, *Food Chemistry,* **2016**, *211*, 107-113.
19. S. Ražić, A. Onjia, *American Journal of Enology and Viticulture*, **2010**, *61*(4), 506-511.
20. V. Avram, C. Voica, A. Hosu, C. Cimpoiu, C. Măruțoiu, *Revue Roumaine de Chimie*, **2014**, *59*(11-12), 1009-1019.
21. L. Järup, *British Medical Bulletin*, **2003**, *68* (1), 167-182.
22. V. Orescanin, A. Katunar, A. Kutle, V. Valkovic, *Journal of Trace and Microprobe Tehniques Trace Bioelements*, **2003**, *21*(1), 171–180.
23. S. Catarino, M. Madeira, F. Monteiro, F. Rocha, A. S. Curvelo-Garcia, R. Bruno De Sousa, *Journal of Agricultural and Food Chemistry*, **2008**, *56*, 158-165.
24. F. D. Bora, A. Donici, T. Rusu, A. Bunea, D. Popescu, C. I. Bunea, *Notulae Botanicae Horti Agrobotanicae,* **2018**, *46(1)*, 223-239.
25. B. Médina, S. Augagneur, M. Barbaste, F.E. Grousset, P.I. Buat-Ménard, *Food Additives and Contaminants*, **2000**, *17(6),* 435-445.
26. R. Larcher, G. Nicolini, P. Pangrazzi, *Journal of Agricultural and Food Chemistry*, **2003**, *51(20)*, 5956-5961.
27. M. Mihaljevic, V. Ettler, O. Sebek, L. Strnad, V. Chrastny, *Journal of Geochemistry Exploration*, **2006**, *88*, 130-133.
28. B.L. Gulson, T.H. Lee, K.J. Mizon, M.J. Korsch, H.R. Eschnauer, *American Journal of Enology and Viticulture*, **1992**, *43*, 180-190.

29. C.M.R. Almeida, M.T.S.D. Vasconcelors, *Journal of Agricultural and Food Chemistry*, **2003**, *51*, 4788-4798.
30. C.M.R. Almeida, M.T.S.D. Vasconcelors, *Food Chemistry*, **2004**, *85*, 7-12.
31. F.D. Bora, A. Donici, A. Călugăr, I.V. Petrescu Mag, E. Gál, C.I. Bunea, *Studia UBB Chemia*, **2017**, LXII, 4, Tom II, 317-332.
32. S. Marchionni, A. Buccianti, A. Bollati, E. Braschi, F. Cifelli, P. Molin, M, Paratto, M. Mattei, S. Tommasini, S. Conticelli, *Food Chemistry*, **2016**, *190*, 777-785.
33. I. Tescione, S. Marchionni, M. Mattei, F. Tassi, C. Romano, S. Conticelli, *Procedia Earth Planetary Science*, **2015**, *13*, 169-172.
34. E. Tatár, V. G. Mihucz, I. Virág, L. Rácz, G. Záray, *Microchemistry Journal*, **2007**, *85*, 132-135.
35. A. Deheleanu, C. Voica, *Romanian Journal of Physics*, **2012**, *57(7-8),* 1194-1203.
36. C. M. S. Almeida, A. C. Almeida, M. L. D. P. Godoy, T. D. Saint'Pierre, J. M. Godoy, *Journal of Brazilian Chemistry Society*, **2016**, *27(6)*, 1026-1031.
37. V. Ivanova-Petropulos, H. Wiltsche, T. Stafilov, M. Stefova, H. Motter, E. Lankmayr, *Macedonian Journal of Chemistry and Chemistry Engineering*, **2013**, *32(2),* 265-281.
38. V. Ivanova-Petropulos, B. Balavanova, S. Mitrev, D. Nedelkovski, V. Dimovska, R. Gulaboski, *Food Analytical Methods,* **2016**, *9(1)*, 48-60.
39. F. Galgano, F. Favati, M. Caruso, T. Scarpa, A. Palma, *Food Science and Technology,* **2008**, *41*, 1808-1815.
40. D. Karataș, F. Aydin, I. Aydin, H. Karataș, *Czech Journal of Food Science*, **2015**, *33(3)*, 228-236.
41. E. I. Geana, A. Marinescu, A. M. Iordache, C. Sandru, R. E. Ionete, C. Bala, *Food Analytical Methods*, **2014**, *48(2)*, 2064-2074.
42. D. Schiavo, I.Y. Neira, I.A. Nóbrega, *Talanta*, **2008**, *76*, 1113-1118.
43. Z. Ajtony, N. Szoboszlai, E.K. Suskó, P. Mezei, K. György, L. Bencs, *Talanta*, **2008**, *76*, 627-634.
44. G. Dugo, L. La Pera, T.M Pellicanó, G. Di Bella, M. D'Imperio, *Food Chemistry*, **2005**, *91*, 355-363.
45. S. Galani-Nikolakaki, N. Kallithrakas-Kontos, A.A. Katsanos, *Science of the Total Environment*, **2002**, *285*, 155-163.
46. M. Barbaste, L. Halicz, A. Galy, B. Medina, H. Emteborg, F. C. Adams, R. Lobinski, *Talanta*, **2001**, *54,* 307-317.
47. B.L. Gulson, T.H. Lee, K.J. Mizon, M.J. Korsch, H.R. Eschnauer, *American Journal of Enology and Viticulture*, **1992**, *43*, 180-190.
48. E.I. Geană, C. Sandru, V. Stanciu, R.E. Ionete, *Food Analytical Methods*, **2017**, *10(1)*, 63-73.
49. OIV. Maximum acceptable limits of various substances contained in wine. In: OIV Editor. *Compendium of international methods of analysis of wine and must analysis*. Place: Paris (Pa); **2016**.
50. M. Barbaste, K. Robinson, S. Guilfoyle, B. Medina, R. Lobinsky, *Journal of Analytical Atomic Spectrometry*, **2002**, *17*, 135-137.

STUDIA UBB CHEMIA, LXIII, 1, 2018 (p. 157-175)
(RECOMMENDED CITATION)
DOI:10.24193/subbchem.2018.1.12

RAPID ULTRASOUND ASSISTED REDUCTION OF AZO DYES FOR SCREENING BANNED AROMATIC AMINES

RAJKUMAR DEWANI[a,b,*], FARMAN AHMED[a], MUNAWWER RASHEED[b,c], MUHAMMAD KASHIF PERVEZ[a], MUHAMMAD FAROOQ WAHAB[d], TAHIRA AYAZ[a]

ABSTRACT. The screening of harmful colorants in consumer products is a global concern. Majority of textile and leather exports undergo extensive quality testing, consuming a lot of time and energy. Consequently, improvements in the rate of reduction of standard method for harmful azo dyes, EN 14362-1:2012 (Annex. F), by combining conventional heating with ultrasonication have been explored to adopt a greener approach. Basic dye behavior was investigated by UV-visible spectroscopy, so that more efficient reduction methods could be designed for high-tech instruments of analysis like HPLC with diode array detection (DAD) and GC with mass spectrophotometer (GC-MS). Four dyes were selected, namely Acid red 1 (AR-1), Direct blue 15 (DB-15), Direct red 28 (DR-28), and Direct red 7 (DR-7) containing one harmful aromatic amine in their structures which make them critical for analyses. Basic observation that absorbance of dyes (having azo chromospheres in their structure) decreases with their reduction to amines was exploited using UV-visible spectroscopic analysis with preselected absorption bands in the visible region from 400 to 700 nm. The dyes were subjected to two types of ultrasound assisted reduction (UAR) methods; less vigorous (experimental method 1) and more vigorous (experimental method 2). All dyes achieved reductions through ultrasonic assistance, higher than the reference method within ten min of time at or before 70 °C except DR-28, according to experimental method 1. According to experimental method 2, DB-15 and DR-7 achieved reductions equivalent to the reference method in 15 min of UAR at 70 °C whereas AR-1 and DR-28 achieved in 20 min of UAR. Finally, DR-28 was further subjected to experimental method 3, which was simply EN 14362-1:2012 (F) method for

[a] *Leather Research Center, PCSIR, D/102, South Avenue, S.I.T.E, Karachi, Pakistan*
[b] *Dept. of Chemistry, University of Karachi, University Road, Karachi-75270, Pakistan*
[c] *Centre of Excellence in Marine Biology, University of Karachi, University Road, Karachi-75270, Pakistan*
[d] *Dept. of Chemistry & Biochemistry, University of Texas at Arlington, TX, USA*
[*] *Corresponding author: rajdewaan@gmail.com*

colorants, with UAR. At this stage, standard techniques of analysis exploiting HPLC-DAD and GC-MS were used. According to experimental method 3, even 15 min of UAR caused a greater reduction of DR-28 dye as compared to the standard method (BS EN 14362-1, F). Ultrasonication at 70°C reduced the total dye reduction time by 42% and energy consumption by 85%.

Keywords: *Azo dyes, Green chemistry, Ultrasound assisted reduction (UAR), Banned aromatic amines*

INTRODUCTION

Colors enhance the beauty and diversity in our lives. The major part of colorants (dyes and pigments) in human use is synthetic, having several chromophores and auxochromes in their structures. Majority of chromophores are azo. Unfortunately, sometimes there are serious issues associated with dyes having azo bonds in their structures. In some cases, the azo chromophore may undergo reductive cleavage, releasing mutagenic or carcinogenic aromatic amines into the environment. These aromatic amines create acute and chronic diseases in humans [1, 2], other terrestrial [3-7] and aquatic living organisms [8, 9]. Azo bond stability and the type of aromatic amines present in a dye play a decisive part in the acceptance of a dyed product. There are 22 aromatic amines (24 in case of leather) banned by the EU, USA, and many other countries [10]. Standard test methods are available to check the release of harmful aromatic amines from colorants [11], dyed leather [12] and textile products [13]. Standard test methods are based on three sequential steps; (i) controlled reduction, (ii) solid phase extraction, and finally (iii) identification and determination. The reduction step consumes around 1 h and is critical for the test.

A number of methods were used for the reduction of azo dyes using; 25% sodium dithionite [14], sodium dithionite in boiling water [15], in water, methanol mixture, 25% [16], and 40% [17] tin chloride solutions. Similarly, extraction of aromatic amines has been reported through liquid-liquid extraction with 1,1,1-trichloroethane [16], with chloroform [15, 18], ethyl acetate [14, 17], and diethyl-ether [19]. The extracted aromatic amines were analyzed through TLC and IR spectroscopy [15, 16], HPLC with UV detection [19], with DAD [20], HPLC-MS [14, 17] and GC-MS [17, 18]. Most common techniques reported for aromatic amines are GC-MS and HPLC-DAD, but some studies prefer the later over the former [21].

In recent years reactions and processes are being transformed on the principles of green chemistry to be safe for the environment. Among other techniques used in green chemistry, microwave heating and ultrasonication find vast applications for improving the efficiency of different reactions and extractions [22-26]. Ultrasonication causes cavitations in the liquid medium due to acoustic energy, forming bubbles that implode to dissipate the energy by raising local temperatures and pressures [27]. Two types of ultrasound frequencies are generally utilized for chemical reactions, power ultrasound (20 to 100 kHz) and sonochemical ultrasound (300 to 1000 kHz).

Several studies on degradation of dyes have been reported through ultrasonication alone [23-25]. Ultrasonic degradation of basic azo and anthraquinone dyes at 300 kHz were reported in exhausted dye baths at acidic and near acidic pH [23]. Similarly, four textile dyes were degraded in water by 520 kHz of ultrasonic energy [24]. Likewise, two mono azo dyes, acid orange 7 and acid orange 8 were sonochemically degraded from their tautomeric forms in solution at 300 kHz [28]. Ultrasonic energy has been coupled with biodegradation [29-33], catalytic degradation [34], and with other processes [35-39] for dye cleavage.

It has been established that the degradation of dyes is influenced by their azo chromophores. Hydroxyl radicals generated in the ultrasonication of water in the sonochemical range attack the azo bonds preferably, resulting in color disappearance [24]. Ultrasonication favors dye degradation by protonating the molecule more effectively at acidic media (pH = 6.0), making it slightly hydrophobic and more prone to the negatively charged cavity bubbles created and destroyed during ultrasonication [40].

The current study presents the reductive degradation of an acid and three direct dyes containing mono and bisazo chromophores, respectively, exploiting UV-Visible spectroscopy.

Four dyes (Figure 1), AR-1, DB-15, DR-28, and DR-7 were chosen due to the presence of at least one harmful amine in their structure, their water solubility, vast applications on leather and textile, and availability in local market. Several methods incorporating mild to vigorous reduction techniques have been reported for the analyses of azo dyes individually as well as in dyed matrices [41]. Internationally recognized standard method for the analyses of certain aromatic amines derived from azo colorants is BS EN 14362-1 (annex. F) [11].

The reduction procedure in the standard method utilizes sodium dithionite at 70 ºC for 30 min in a pre-heated citrate buffer adjusted to pH 6.0. In this study, the standard method of analyzing harmful aromatic amines in azo colorants has been modified by the incorporation of heated ultrasonication as an alternative greener approach for dye reduction.

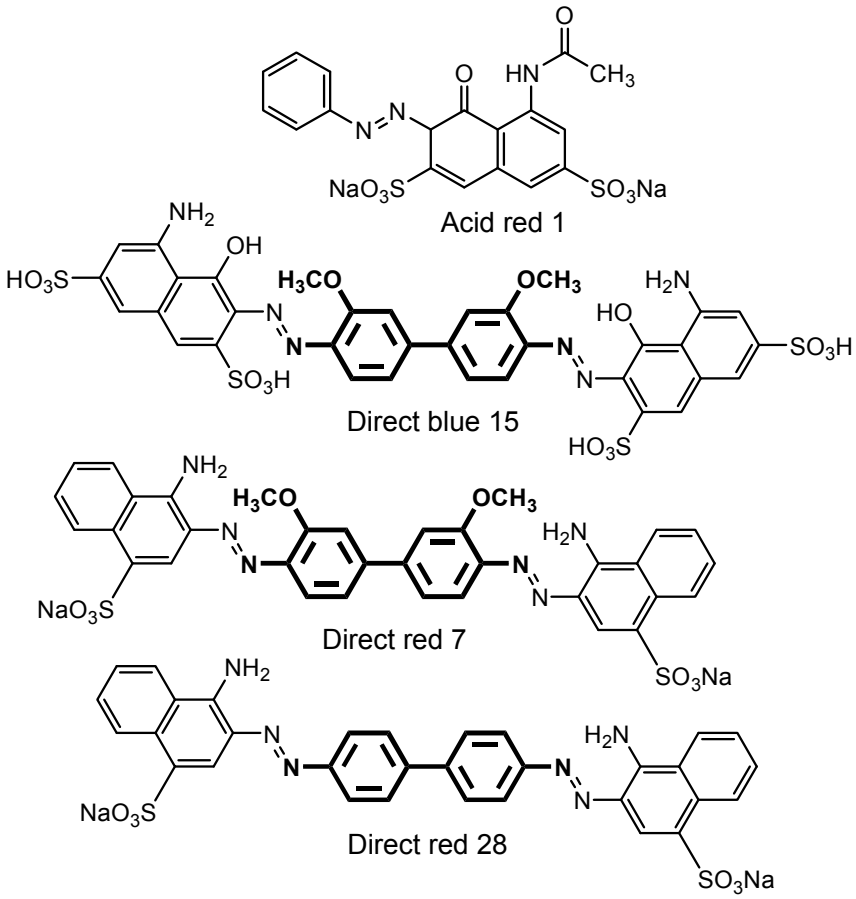

Figure 1. Dye structures with banned aromatic amine component in bold

RESULTS AND DISCUSSION

The change in UV and visible absorptions in different azo (direct and acid) dyes upon reduction by sodium dithionite, helped to monitor (a) the effects of changing temperature on UAR and (b) effects of changing UAR time at fixed temperature.

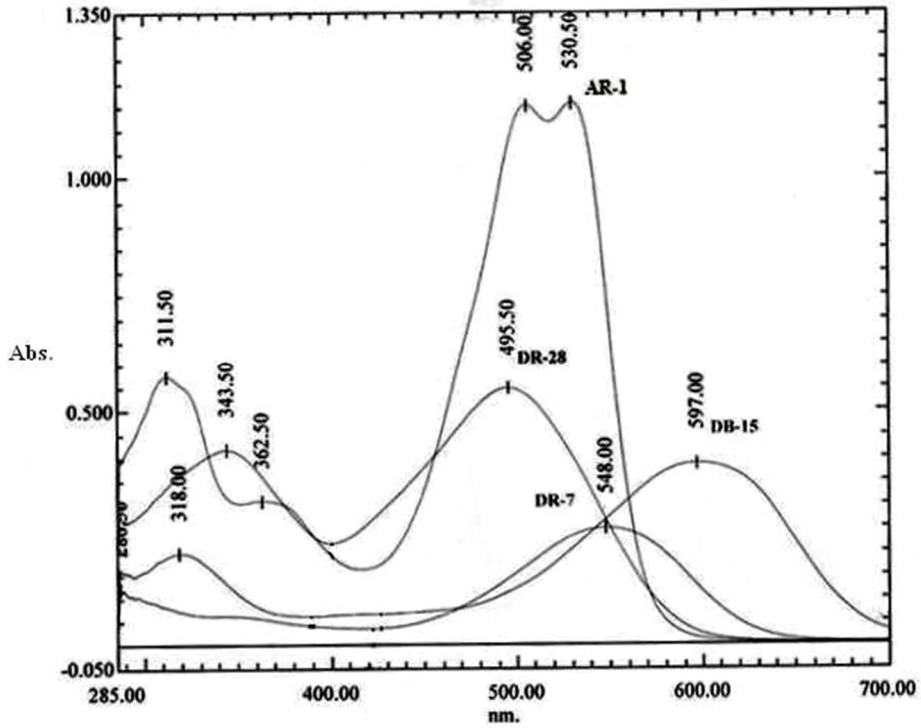

Figure 2. UV-Visible scans of Direct red 28, Acid red 1, Direct red 7 and Direct blue 15 dyes (with peaks marked)

UV-visible scans of the dyes; DB-15, AR-1, DR-7, and DR-28 were recorded in water (Figure 2).

The frequency range from 300 to 1000 kHz, recommended for chemical modifications, is referred to as sonochemical effects ultrasound whereas frequency range from 20 to 100 kHz, mostly used for cleaning and degassing purposes, is called power ultrasound [40]. Power ultrasound is employed in the reduction as a supportive aid to sodium dithionite [37, 40]. Sonochemical effects ultrasound could cause some additional reactions [42]. The study is focused on the cleavage of the azo bond using power ultrasound (40 kHz).

Selected wavelengths for each dye are presented in Table 1. In case of DR-28 dye, absorbance changes were prominent, hence only one wavelength was used in experimental method 1.

Table 1. Selected wavelengths for dyes analyses and associated information

Dyes	C. I. number	Mol. wt. (g/mol)	Wavelengths 'λ' used (nm)	
			Experimental method 1	Experimental method 2
AR-1	118050	509.42	506, 530	506, 530
DB-15	24400	992.80	580, 608	580, 594,608
DR-7	24100	756.72	547, 570	544, 547
DR-28	22120	696.66	505	488, 505

The reduction reactions have been carried out at low dye concentrations to enable direct absorbance measurements. UV-visible scans of buffer and dithionite solutions were also recorded to check for possible interferences (if any) and they showed maximum absorbance in the far and middle UV regions (200 - 330 nm). Absorbance in the visible region was negligible. The upper limit on dye concentration was set roughly to 19 times less than that in the reference methods. Concentration of sodium dithionite is 5 times less than in the reference method for three reasons; (a) it is taken in excess (b) it does not absorb significantly in the visible region and (c) the reduction mechanism is likely to be altered when the concentration of sodium dithionite is reduced below a critical level. Sodium dithionite generates sulfur dioxide radical anions according to the following reaction [43]:

$$S_2O_4^{2-} \rightleftarrows 2SO_2^{\cdot -}$$

Both these species are responsible for the reducing property, but dithionite is comparatively a weaker reducing agent.

It is ascertained that the concentration of sulphur dioxide radical anion is inversely proportional to dithionite concentration and vice versa [44]. The concentration of all components of the reaction mixtures were adjusted appropriately in each experimental method and the reactions were conducted using these concentrations (Table 2). Concentrations of dyes, however, were different for the two experimental methods. In experimental method 1, each dye was reduced at 40, 50, 60, and 70 °C respectively, for 10 min with ultrasound assistance. The degree of reduction was monitored by the change in absorbance. The standard method reduction was similar to experimental method 3 but without ultrasound exposure, having reduction duration of 30 min. The idea behind the research design was to find out greener reaction conditions that could make the test method environmental friendly [45].

Table 2. Comparison of reduction methods used for dye analysis

Experimental parameter	Reference method	Experimental method 1	Experimental method 2	Experimental method 3
Dye concentration range (mg/100ml)	Same as expe rimental method 1 and 2	2.2 – 4.2	3.2 – 7.8	588 – 1000 (approx.)
Dyes analyzed	DR-7, AR-1, DB-15 and DR-28	DR-7, AR-1, DB-15 and DR-28	DR-7, AR-1, DB-15 and DR-28	DR-28
Buffer strength (M)	0.03	0.03	0.03	0.06
Preheat time (min)	30	-	20	20
Preheat temperature (°C)	70	-	70	70
Dithionite strength (g/3ml)	0.12	0.12	0.12	0.60
Reduction time (min)	30	10	10 or 15	15 or 20
Reduction temperature (°C)	70	50, 60, 70	70	70
Reaction vessel	Glass RB	Glass RB	PTFE	PTFE
Ultrasound exposure	-	40 KHz	40 KHz	40 KHz

Effect of temperature on the reduction of dyes applying fixed Ultrasonication (Experimental method 1)

The results of experimental method 1 are presented in Figure 3. Comparing the trend in case of AR-1 absorbance decreases initially from 30 to 60 °C.

After ~ 60 °C the absorbance starts increasing in the visible region with the formation of pale yellow colored intermediates, disodium 5-(acetylamino)-3-amino-4-hydroxy-3,4-dihydronaphthalene-2,7-disulfonate and aniline. Both aromatic amines were generated because of cleavage of the azo bond present in AR-1. The yellow color was predominant when the dye was reduced completely with acidic tin chloride solution [14, 17]. The reduction profile of DB-15 is an almost linear decrease in absorbance with respect to increasing temperature at both 580 and 608 nm. The reduction of DR-7, under the reaction conditions of experimental method 1 showed no noticeable change. A marked degradation was observed when DR-28 was subjected to UAR. A general decrease in absorbance at 505 nm can be noticed.

Figure 4 gives a comparative account of percent dye reduction of reference method and experimental method 1, at selected wavelengths.

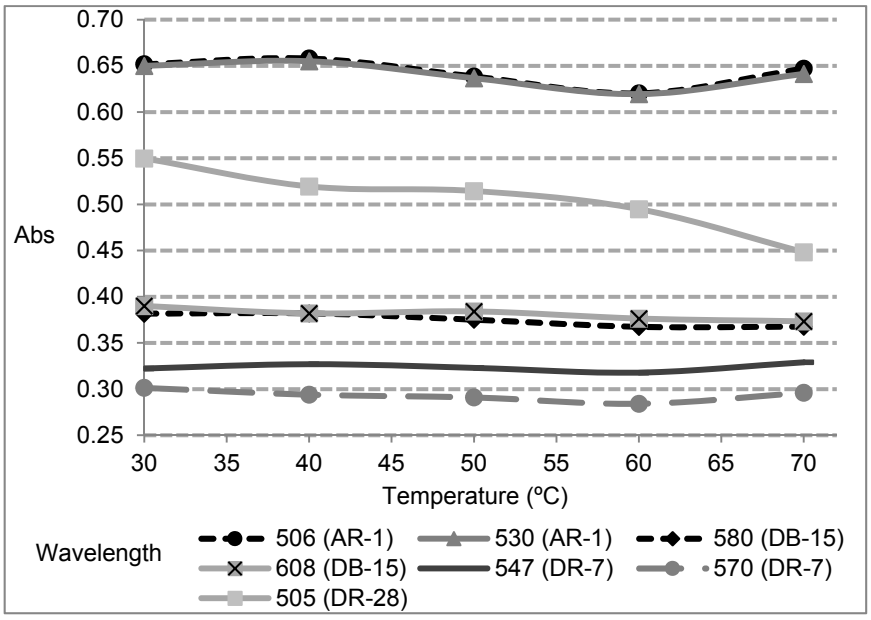

Figure 3. Effect of reaction temperatures on UAR of dyes (Experimental method 1)

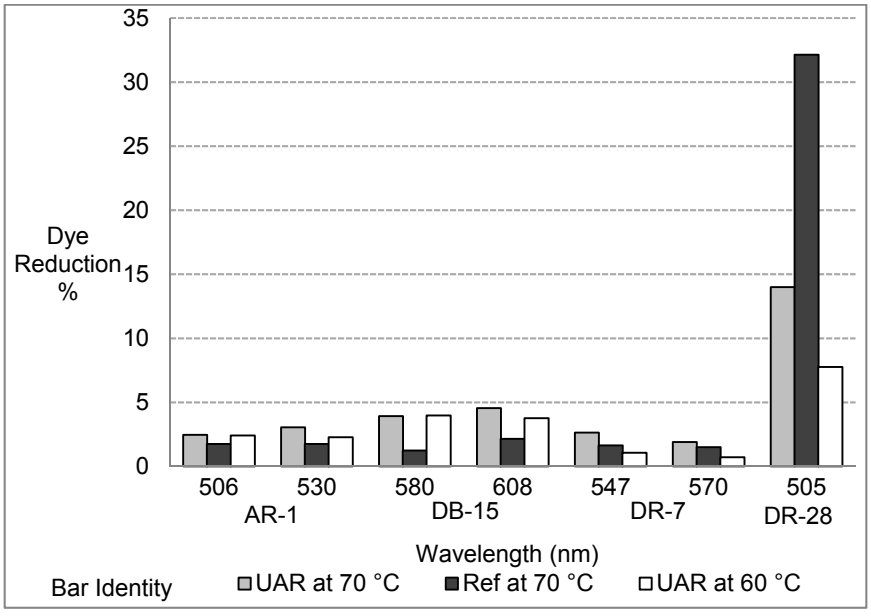

Figure 4. Comparative absorbance difference at selected wavelengths after dyes reduction at 70 °C between experimental method 1 and reference method

In AR-1, at 506 nm the UAR at 70 and 60 °C resulted in a slightly greater reduction as compared to the reference method. Similarly, at 530 nm, the reduction results at both 70 and 60 °C are better than the reference method but the former are slightly better than the later. Similarly, in case of DB-15 the results from ten min of UAR in the visible region (580 and 608 nm) at 60 and 70 °C are better than those obtained by reference method carried out for half an hour at 70 °C. Again, the UAR at 70 °C is greater than 60 °C at 608 nm. DR-7 is the most stable among the selected dyes and is hardly affected in the given experimental conditions as reflected in the Figure 3. However, the results at 547 and 570 nm suggest that the order of dye reduction is UAR at 70 °C > reference method > UAR at 60 °C. On the other hand, DR-28 disintegrates to the greatest extent among the selected dyes. However, it is also evident from Figure 4 that 10 min of ultrasound assisted heating at 70 °C and below is not enough to cause a reduction equivalent to the reference reduction method. To conclude, the exposure of ultrasound waves for 10 min at 70 °C caused enhanced reductive degradation in all the four dyes with results parallel to the reference method (30 min) except DR-28.

Effect of exposure of ultrasonication on the reduction of dyes at fixed temperature (Experimental method 2)

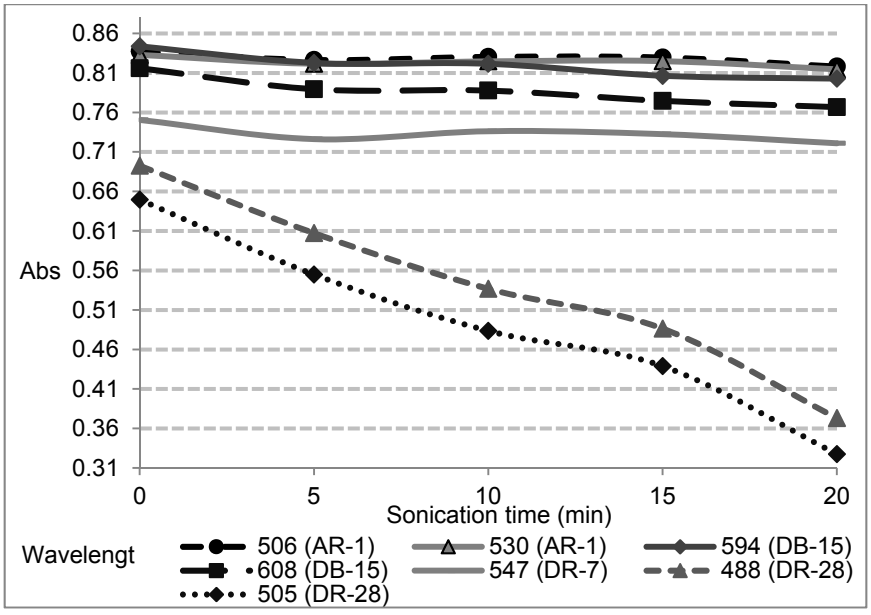

Figure 5. Effect of UAR time on dye degradation (Experimental method 2)

Considering the results of experimental method 1, the parameters were modified and experimental method 2 was carried out at 70 °C, exposing the samples with ultrasound for different durations. Reaction temperature was maintained at 70 °C in analogy to the standard method [11]. Dye concentrations were increased, and the wavelengths were slightly modified to optimize the monitoring of absorbance change (Table 2). Figure 5 gives the reduction profile of the four dyes at conditions stated in experimental method 2.

Figure 6 depicts the potential of UAR, presenting the results of experimental method 2 at 15 and 20 min in comparison to reference method.

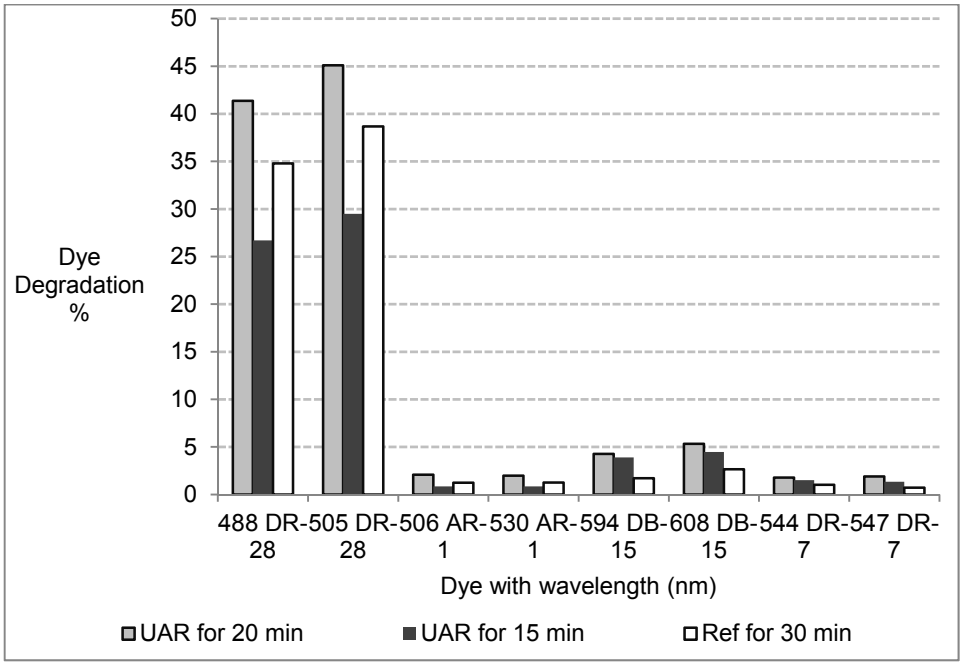

Figure 6. Comparative absorbance difference at selected wavelengths after dyes reduction at 70 °C between experimental method 2 and reference method

The findings of experimental method 2 were comparable to experimental method 1 for AR-1. Absorbance in the visible region shows slow and gradual reduction till 20 min of UAR. Considering the results of AR-1 at 506 and 530 nm (Figure 6), 20 min of UAR is better than reference reduction whereas 15 min is not comparable to the reference method.

The results of DB-15 (Figure 5 and 6) are also interesting with the key wavelengths (580, 594 and 608 nm) in the visible region, favoring the UAR method. The trend of dye cleavage is in the order UAR at 20 min > UAR at 15 min > reference method.

Results of DR-7 (Figure 5) are also in agreement with other dyes with slow and gradual degradation till 20 min of UAR. The effectiveness of UAR at 544 and 547 nm is in the same order as in the case of DB-15, however with comparatively lower dye degradation (Figure 6). DR-7 is the most stable dye among the dyes studied, showing only 1.57% average degradation by reference method.

The most prominent absorbance changes were observed in the case of DR-28 (Figure 5) showing 36.7% degradation by the reference method. Results of DR-28 obtained from experimental method 1 and 2 are in good agreement. In experimental method 1, 10 min of UAR was not enough to cause a reduction equivalent to the reference method even at 70°C. But, in method 2, it took almost 20 min of UAR for the dye to achieve a higher level of reduction than the reference method (Figure 6). The dye is reduced to a significant level and the change in absorbance is gradual and almost linear at 488 and 505 nm. On comparing the results of DR-28 (Figure 6) in UAR with reference method, it is quite evident that the ultrasound energy has caused the reaction to complete in lesser time. This could be attributed to the cumulative amount of energy transmitted through ultrasound and conventional heating which is probably higher than the conventional heating alone.

Effect of ultrasound on reduction through modified standard method (experimental method 3)

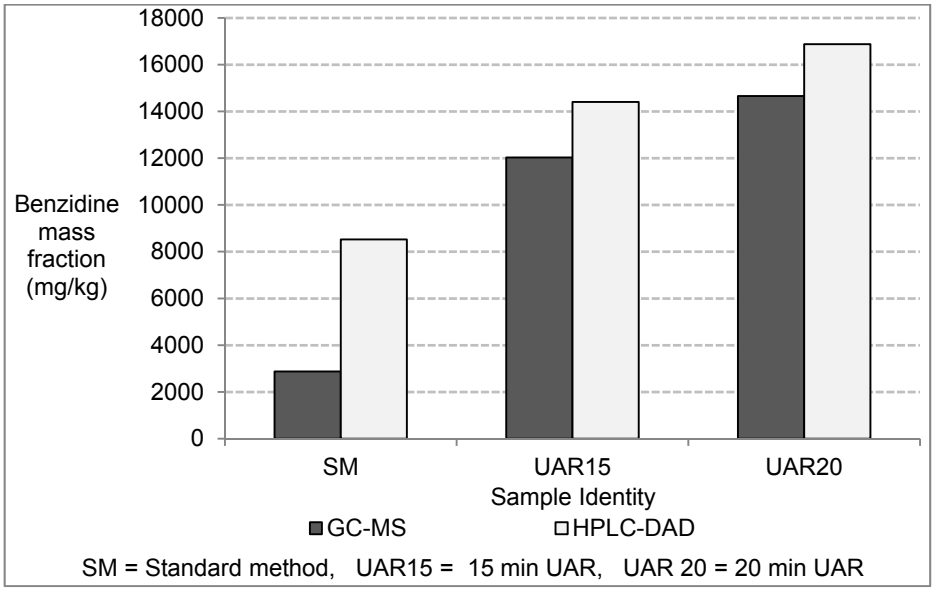

Figure 7. Comparative benzidine profile of standard method reduction and UAR for DR-28 dye

Results of experimental method 1 and 2 obtained through UV-visible spectroscopy proved very helpful in designing experimental method 3 and were also confirmed by experimental method 3. For this purpose, DR-28 dye was selected as it showed highest degradation among the selected dyes. The mass fraction (mg/kg) of benzidine (biphenyl-4,4'-diamine) directly indicates the reduction of DR-28 dye in Figure 7.

Results from GC-MS and HPLC-DAD are in good agreement however results obtained from HPLC in general are slightly higher. But the general trend through both the techniques is same. Previous results obtained from UV-visible spectroscopy were further confirmed by GC-MS and HPLC-DAD showing that 15 min of UAR through experimental method 3 caused greater degradation of DR-28 as compared to the standard test method for azo colorants [11]. The degradation after 20 min of UAR was even higher. Chromatograms obtained from GC-MS and HPLC-DAD are shown in Figure 8.

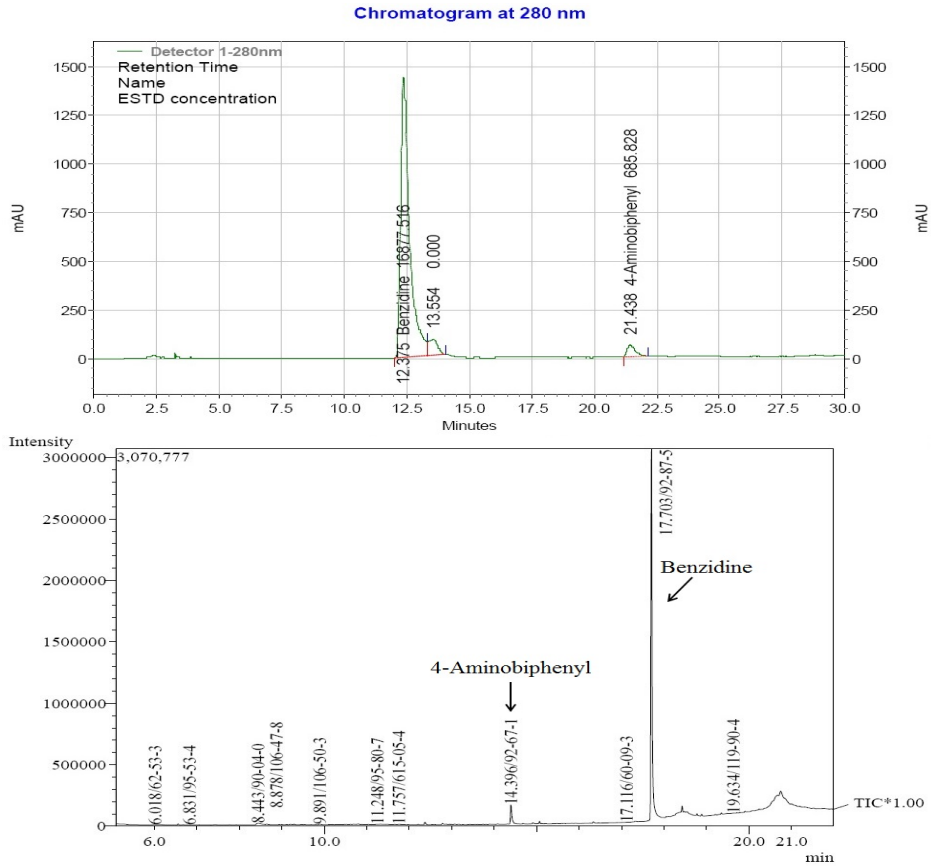

Figure 8. Chromatograms of DR-28 dye subjected to UAR for 20 min, Above: HPLC-DAD (at 280 nm), Below: GC-MS

The effect of ultrasound is profound at 70 °C causing a reduction in reaction time of approximately 42%. There are several factors that contribute to the reduction of dyes. It has been established that an overall low molecular weight, sterically less hindered diazo bonds and structural simplicity promote dye decolonization. However, the trend of ease of reduction is not exclusively based on these factors. Other factors such as high pKa values, less number of SO_3^- groups, and preference of hydrazone epimer over the azo epimer (dye) also make the dye susceptible towards ultrasound degradation [40, 46-48]. It should also be mentioned here that UAR methods are more suitable for solvent soluble azo dyes and are likely to yield shorter reduction times because water soluble dyes containing highly polar groups are less likely to get into the gas liquid interface produced during sonication and therefore are not directly exposed to the high temperature and pressure conditions [40, 49]. Longer durations of UAR were not trialed because these would not support the hypothesis of time effectiveness as compared to standard method.

It is usually easy to reduce a dye powder as compared to a dye present in a matrix (leather, textile etc.). The main reason could be the interaction of the reducing agent with the matrix components. Besides, the reducing agent would have to penetrate the sample matrix to reach the active sites (azo chromophores) present on the dye molecule. However, ultrasonication would enhance the penetration of the reducing agent into the matrix. It is quite evident that the dyes which are reduced to a significant level by the reference method are also responding well to UAR. Therefore, it may be inferred that the percent reduction, using modified method may be useful in predicting the fate of a dyed product in terms of acceptance or rejection for export.

CONCLUSIONS

Ultrasound is a greener and environmental friendly technique. Ultrasound assisted reduction has the potential to reduce studied dyes in shorter time. All dyes showed good response to UAR, proportional to reaction temperature as analyzed by UV-visible spectroscopy. The results of experimental method 1 showed that AR-1 and DB-15 achieved reductions through UAR, higher than the reference method within ten min of time at 60 °C whereas DR-7 achieved at 70 °C. However, degradation of DR-28 in ten min of UAR was not comparable to the reference method, even at 70 °C. According to experimental method 2, DB-15 and DR-7 achieved reductions equivalent to the reference method in 15 min of UAR at 70 °C whereas AR-1 and DR-28 achieved in 20 min of UAR.

According to the results of experimental method 3 obtained through GC-MS and HPLC-DAD for DR-28 dye, even 15 min of UAR caused a greater reduction as compared to the standard method (BS EN 14362-1, F) for colorants. Results of 20 min of UAR are even better in terms of dye degradation. The results from GC-MS and HPLC-DAD are comparatively more reliable as compared to the results of UV-visible spectroscopy. Energy saving in UAR would be ~ 85% as compared to standard method of reduction for colorants. Similarly, the time saving in case of UAR would be around 42% i.e. 25 min per analysis. Results suggest that these figures could be improved further if similar data is collected for more azo dyes.

The screening of azo dyes for their ability to release potentially harmful aromatic amines is routinely carried out in labs around the world for existing and new dyes. The proposed greener approach for standard method of reduction will allow the test to be carried out in comparatively shorter time, with parallel saving of energy.

EXPERIMENTAL SECTION

Reagent grade sodium dithionite (>87%), extra pure tin (II) chloride dihydrate and silica gel 60 (70-230 mesh ASTM) were obtained from Merck (Germany). Tertiary butyl methyl ether solvent (reagent grade) was acquired from Fisher scientific, UK. Four dyes; AR-1, DR-15, DR-28 and DR-7 were obtained from local market in Karachi, Pakistan. Citric acid powder (general purpose reagent grade) and hydrochloric acid (AR grade, 37%) were purchased from BDH Ltd. (England) whereas sodium hydroxide (AR grade) was procured from Riedel-deHaën (Germany).

Stock solutions using 0.106, 0.115, 0.109, and 0.140 g of DR-28, AR-1, DB-15, and DR-7, respectively, were prepared in 500 ml of distilled water. The UV-Visible scans for DB-15, AR-1, DR-7, and DR-28 dyes were recorded with dilutions of 2.3, 4.3, 2.3, and 3.7, mg/100ml, respectively. Citrate buffer (pH = 6.0) was prepared using citric acid and sodium hydroxide solution [50].

Reference method

The reaction mixtures were prepared by pipetting appropriate volumes (to get the dye concentrations stated in Table 2) from the stock solutions into the reaction vessel. Total volumes were made upto17 ml by adding 0.03 M citrate buffer as solvent with the help of graduated pipettes. The reaction was initiated in a 50 ml round bottomed flask (Pyrex) by the addition of 3 ml of

freshly prepared dithionite solution containing 0.12 g of sodium dithionite. Reduction step was kept mild, analogous to the standard method for colorants (BS EN 14362-1:2012, F). Reference reactions were performed in a thermostatic water bath (Memmert, Germany) at 70 °C, for 30 min and then cooled down immediately to ~10 °C in ice cooled water bath. The absorbance measurements were taken on a Nicolet Evolution 100, double beam spectrophotometer from Thermo Electron Corporation (USA) using standard quartz cuvettes.

Reference method modified with ultrasound assisted reduction at different temperatures (Experimental method 1)

The dye concentrations used for reduction in experimental method 1 are 2.3, 2.2, 2.8 and 4.2 mg/100ml for AR-1, DB-15, DR-7 and DR-28 respectively. For other experimental conditions refer to Table 2. Ultrasound assisted reductions were carried out in a 135 W, temperature controlled, Ultrasonic bath, Labsonic, LBS2-4,5, Italy, equipped with digital timer, having internal dimensions of 300x150x100 mm (4.5 L capacity), with an operational frequency of 40 kHz and temperature range of 20 to 80 °C.

The sample vessel was adjusted in the center of the sonicator at the same depth and water level in all the experiments to minimize exposure variations. The reactions were carried out at different temperatures for 10 min.

Reference method modified with ultrasound assisted reduction at fixed temperature (Experimental method 2)

The dye concentrations used for reduction in experimental method 2 are 3.2, 5.5, 7.8 and 5.1 mg/100ml for AR-1, DB-15, DR-7 and DR-28 respectively. For other experimental conditions refer to Table 2. These experiments were conducted in recommended polytetrafluoroethylene (PTFE) vessels for 5, 10, and 15 min. Reaction mixtures were maintained at 70 ± 1 °C by placing these in preheated water bath at 77 °C for 20 min prior to sodium dithionite addition. The temperature-time correlations were obtained from a separate set of experiments presented in Figure 9.

The concentrations of dyes were then raised to get maximum sensitivity as shown in Table 2. Reference reactions were repeated and validated in these PTFE vessels. To confirm the findings of experimental method 1 and 2, DR-28 was tested with standard test method EN 14362-1:2012 [11] and experimental method 3.

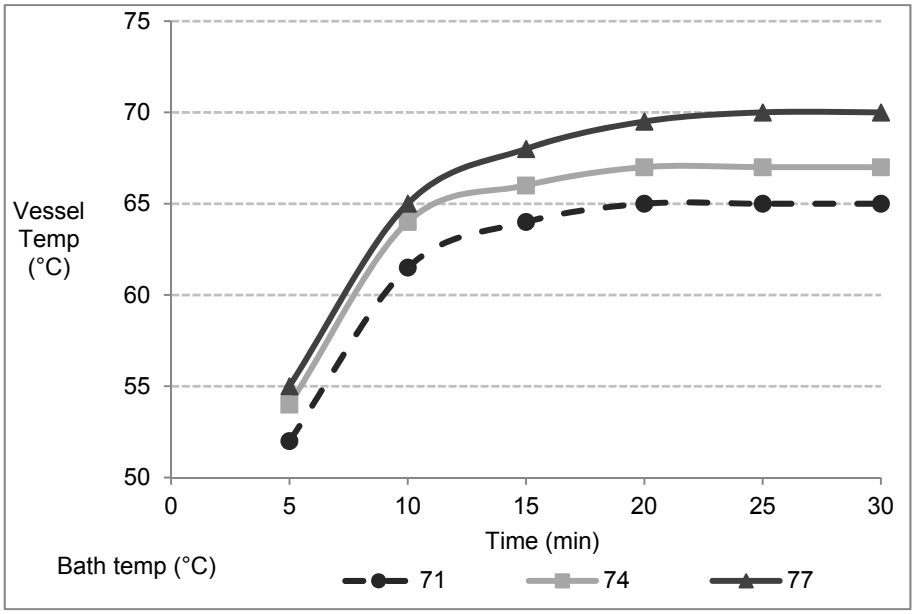

Figure 9. Relation between water bath and Teflon vessel content temperatures

Standard method BS EN 14362-1:2012 (annex F)

Direct red 28 dye was analyzed by standard method for determination of certain aromatic amines in colorants, BS EN 14362-1:2012 (F), [11]. The final extract solutions were subjected to instrumental analysis by GC-MS and reconfirmed using HPLC-DAD.

Gas chromatographic analyses were carried out on GC-2010 from Shimadzu, Japan equipped with AOC-20i+s auto sampler/injector assembly linked with a computer through GC-MS Real time analysis software. The instrument was coupled with a mass spectrometer detector, QP2010. GC column, DB-35MS (25.0 m x 0.20 mm, 0.33 μm df) specific for aromatic amines was used. The 26 aromatic amine standards were obtained from Dr. Ehrenstorfer Quality (EQ) GmbH, Germany. Separate stock solutions containing 2000 ppm of each amine were prepared, followed by working solution mixtures of all standards having 200 ppm of each amine. 1, 5, 15 and 30 ppm dilutions were prepared for calibration of GC-MS method.

All standards and samples were injected in 'Split' mode with a split ratio of 1:10. The temperature program was set as follows; initial temperature 60 °C was held for 1 min, ramped at 14 °C/min to 320 °C and finally hold for

5 min. Total run time was ~25 min. Acquisition was carried out in SIM mode for better detection limit. Target ion *m/z* was 184 for benzidine, with first and second qualifier ions at *m/z* 185 and 156 respectively for confirmation.

A HPLC system (LabAlliance, 2500 Plus, USA) with quaternary pumps and diode array detector (LabAlliance, UV6000LP, USA) assisted by a computer through EZchrome Elite software was used. HPLC column was reverse phase Spherisorb®, 5.0 µm, ODS1 from Waters, having dimensions 4.0x250 mm. A linear gradient method for leather was optimized for eight aromatic amines. A 10 µL sample loop was used. Three chromatograms were recorded at 240, 280 and 305 nm. Column oven temperature was set at 40 °C. Eluent 1 was modified to 30% acetonitrile in methanol and eluent 2 was phosphate buffer (pH 6.9). The gradient started with 25% eluent 1, increasing linearly to 80% within 30 min. The total solvent flow rate was adjusted to 0.65 ml/min. A three-point calibration was carried out with standard amine mixture containing 2, 20 and 40 ppm of eight selected amines. λ_{max} used for the confirmation of benzidine was 278 nm.

Standard method (EN 14362-1) modified with ultrasound assisted reduction (Experimental method 3)

The standard method for determination of certain aromatic amines in colorants, EN 14362-1:2012 (F), [11] was repeated for DR-28, modified by replacing standard reduction with ultrasound assisted reduction. Heating during reduction was accompanied by ultrasonic waves for the desired durations. Experimental method 3 was performed with two different UAR durations i.e. 15 min and 20 min. Rest of the procedure, parameters and reagent quantities were same as mentioned in standard method (EN 14362-1). Final extracts were analyzed by GC-MS and HPLC-DAD with the same instrumental conditions and configurations mentioned in the standard method above.

ACKNOWLEDGMENTS

The authors are grateful to Dr. Hafiz Rab Nawaz, Director Leather Research Center, PCSIR, for co-operation and support throughout the work.

REFERENCES

1. M. J. Prival, S. J. Bell, V. D. Mitchell, M. D. Peiperl, V. L. Vaughan, *Mutation Research/Genetic Toxicology,* **1984**, *136*, 33-47.
2. F. Calogero, H. S. Freeman, J. F. Esancy, W. M. Whaley, B. J. Dabney, *Dyes and Pigments,* **1987**, *8*, 431-447.
3. M. Kojima, M. Degawa, Y. Hashimoto, M. Tada, *Biochemical and biophysical research communications,* **1991**, *179*, 817.
4. C. P. Hartman, G. E. Fulk, A. Andrews, *Mutation Research/Genetic Toxicology,* **1978**, *58*, 125.
5. E. Messerly, J. Fekete, D. Wade, J. Sinsheimer, *Environmental and molecular mutagenesis,* **1987**, *10*, 263.
6. H. S. Freeman, J. F. Esancy, L. D. Claxton, *Chemtech,* **1991**, *21*, 438.
7. Y. Hashimoto, H. Watanabe, M. Degawa, *Gann= Gan,* **1981**, *72*, 921.
8. B. de Campos Ventura-Camargo, M. A. Marin-Morales, *Textiles and Light Industrial Science and Technology,* **2013**, *2*, 85-103.
9. G. de Aragao Umbuzeiro, H. S. Freeman, S. H. Warren, D. P. De Oliveira, Y. Terao, T. Watanabe, L. D. Claxton, *Chemosphere,* **2005**, *60*, 55-64.
10. Environment Canada/Health Canada. "Aromatic Azo- and Benzidine-based substances", Screening assessment report, **2012**, pp. 3-6.
11. BSI. Colorants - Methods for determination of certain aromatic amines. BS EN 14362-1, E (Annex F). The British Standards Institution, **2012**.
12. ISO. Chemical tests for the determination of certain azo colorants in dyed leathers. ISO/DIS 17234-1/IUC 20-1. International organization for standards, **2012**.
13. BSI. Textiles - Methods for determination of certain aromatic amines derived from azo colorants. BS EN 14362-1, E. The British Standards Institution, **2012**.
14. R. D. Voyksner, R. Straub, J. T. Keever, H. S. Freeman, H. Whei-Neen, *Environmental science & technology,* **1993**, *27*, 1665-1672.
15. A. Puntener, D. Mausezahl, C. Page, *Journal of the Society of Leather Technologists and Chemists,* **1993**, *77*, 1.
16. A. G. Pindar, H. M. Tinsley, *Analyst,* **1984**, *109*, 1101-1102.
17. R. F. Straub, R. D. Voyksner, J. T. Keever, *Analytical Chemistry,* **1993**, *65*, 2131-2136.
18. D. Muralidharan, V. S. Rao, *Journal of the Society of Leather Technologists and Chemists,* **1994**, *78*, 139-41.
19. F. Planelles, E. Verdu, D. Campello, N. Grane, J. Santiago, *Journal of the Society of Leather Technologists and Chemists,* **1998**, *82*, 45-52.
20. M. C. Garrigós, F. Reche, M. L. Marin, A. Jiménez, *Journal of Chromatography A,* **2002**, *976*, 309-317.
21. M. Mościpan, M. Zarębska, R. Kulesza, *Chemik,* **2016**, *70*, 135-143.
22. F. Parolin, U. M. Nascimento, E. B. Azevedo, *Environmental technology,* **2013**, *34*, 1247-1253.
23. G. Tezcanli-Güyer, N. H. Ince, I. A. Alaton, *Coloration technology,* **2003**, *119*, 292-296.

24. G. Tezcanli-Guyer, N. H. Ince, *Ultrasonics Sonochemistry,* **2003**, *10*, 235-240.
25. A. S. Özen, V. Aviyente, G. Tezcanli-Güyer, N. H. Ince, *The Journal of Physical Chemistry A,* **2005**, *109*, 3506-3516.
26. L. H. Keith, L. U. Gron, J. L. Young, *Chemical reviews,* **2007**, *107*, 2695-2708.
27. M. de la Guardia, S. Garrigues, "Handbook of green analytical chemistry", Wiley Online Library, **2012**, chapter 7, pp. 117.
28. A. S. Özen, V. Aviyente, G. Tezcanli-Güyer and N. H. Ince, *The Journal of Physical Chemistry A,* **2005**, *109*, 3506-3516.
29. M. Işık, D. T. Sponza, *Journal of International Environmental Application & Science,* **2006**, *1*, 1-26.
30. G. C. Santos, C. R. Corso, *Water, Air, & Soil Pollution,* **2014**, *225*, 2026.
31. P. Suwannawong, S. Khammuang, R. Sarnthima, *Journal of Biochemical Technology,* **2010**, *2*, 182-186.
32. W. Hailei, L. Ping, L. Guosheng, L. Xin, Y. Jianming, *Enzyme and Microbial Technology,* **2010**, *47*, 37-43.
33. C. I. Pearce, R. Christie, C. Boothman, H. von Canstein, J. T. Guthrie, J. R. Lloyd, *Biotechnology and bioengineering,* **2006**, *95*, 692-703.
34. A. Assadi, R. Nateghi, G. R. Bonyadinejad, M. M. Amin, *International Journal of Environmental Health Engineering,* **2012**, *1*, 1-5.
35. I. Gültekin, G. Tezcanli-Güyer, N. H. Ince, *Ultrasonics sonochemistry,* **2009**, *16*, 577-581.
36. N. H. Ince, G. Tezcanlí, *Dyes and Pigments,* **2001**, *49*, 145-153.
37. Z. Eren, N. H. Ince, F. N. Acar, *Journal of Advanced Oxidation Technologies,* **2010**, *13*, 206-211.
38. G. Tezcanli-Güyer, N. H. Ince, *Ultrasonics,* **2004**, *42*, 603-609.
39. M. Q. Cai, X. Q. Wei, Z. J. Song, M. C. Jin, *Ultrasonics sonochemistry,* **2015**, *22*, 167-173.
40. S. K. Sharma, "Green Chemistry for dyes removal from waste water: research trends and applications", John Wiley & Sons, **2015**.
41. L.-H. Ahlström, C. S. Eskilsson, E. Björklund, *Trends in Analytical Chemistry,* **2005**, *24*, 49-56.
42. M. Cai, M. Jin, L. K. Weavers, *Ultrasonics sonochemistry,* **2011**, *18*, 1068-1076.
43. B. P. Vellanki, B. Batchelor, A. Abdel-Wahab, *Environmental engineering science,* **2013**, *30*, 264-271.
44. A. H. Gemeay, *Dyes and pigments,* **2002**, *54*, 201-212.
45. M. de la Guardia, S. Garrigues, "Handbook of green analytical chemistry". 1st ed., John Wiley & Sons, Pondicherry, **2012**.
46. N. H. Ince, G. Tezcanli-Güyer, *Ultrasonics,* **2004**, *42*, 591-596.
47. A. S. Özen, V. Aviyente, R. A. Klein, *The Journal of Physical Chemistry A,* **2003**, *107*, 4898-4907.
48. J. Oakes, P. Gratton, *Journal of the Chemical Society, Perkin Transactions 2,* **1998**, 1857-1864.
49. R. Singla, F. Grieser, M. Ashokkumar, *Ultrasonics sonochemistry,* **2009**, *16*, 28-34.
50. J. Mendham, R. Denney, J. Barnes, M. Thomas, "Vogel's Quantitative Chemical Analysis", Pearson Education Ltd., Singapore, **2000**, pp. 768-769.

STUDIA UBB CHEMIA, LXIII, 1, 2018 (p. 177-188)
(RECOMMENDED CITATION)
DOI:10.24193/subbchem.2018.1.13

C-C CHEMOKINE RECEPTOR TYPE 3 INHIBITORS: BIOACTIVITY PREDICTION USING LOCAL VERTEX INVARIANTS BASED ON THERMAL CONDUCTIVITY LAYER MATRIX

CLAUDIU N. LUNGU*

ABSTRACT. A series of compounds with known inhibitory activity for C-C chemokine receptor type 3 (CCR_3) was considered in order to build a predictive model useful in further development of novel CCR_3 inhibitors. Model was built using topological descriptors (Cluj indices included) and multiple linear regression. Principal component analysis was applied in order to enhance the model. Errors were taken into consideration and discussed. Finally, vertex invariants based on thermal conductivity layer matrix proved to be a valuable tool in bioactivity prediction of CCR_3 inhibitors.

Keywords: *Topological descriptors; QSAR; Regeression model; CCR3 inhibitors.*

INTRODUCTION

C-C chemokine receptor type 3 (CCR_3), recently designated cluster for differentiating CD193, is highly expressed in eosinophils [1]. Its function is the accumulation and activation of eosinophils at the site of an immune stimulus (allergy, parasitic infection, etc.). A chemokine inhibitor will prohibit this proinflammatory effect. A series of broad spectrum chemokine inhibitors (BSCI) were designed. Remarkably, peptide 3'', a dodecapeptide section of chemokine (C-C-motif) ligand 2 (CCL2) was proven to be a functional inhibitor of many chemokines [2]. The crucial peptide sequence responsible for its

* *Department of Chemistry, Faculty of Chemistry and Chemical Engineering, Babes-Bolyai University, 400028 Cluj, Romania. E-mail: lunguclaudiu5555@gmail.com.*

effect was identified as the tripeptide AcNH-Trp-Val-Gln-OH. Peptide mimetics were fashioned mainly a range of 3-acylaminoglutarimides, with low nM BSCI potencies [3]. A particular interest exists for cyclic peptide NR58-3.14. CCR_3 was shown to inhibit HIV replication [4]. In this respect, there is an entry co-receptor for HIV-1. This gene receptor and other chemokine receptors genes form a cluster on chromosomal region 3p21 [5]. A number of small molecules with inhibitor effect on CCR_3 (expressed as IC50, nM) were studied. In this work, a prediction model based on computed data regarding molecules that act as inhibitors of CCR_3 was carried out, in order to be used as a tool for further development of these compounds.

RESULTS AND DISCUSSION

A set of 41 compounds with inhibitory effect on CCR_3 was selected from PubChem (Table 1), on which topological indices [6], encoding fragmental topo-chemical information [7-9], were computed by means of layer matrices [11-14]. The fragmental properties were chosen the mass M and thermal conductivity Tc (Table 2).

In order to select the descriptors for model building, a monovariate correlation between each descriptor and the dependent variable (IC_{50}) was performed: X[LM[Tc]] has r^2=0.335 followed by C[LM[Tc]] r^2=0.240 and C[LM[Mass]] r^2=0.203. The other descriptors have r^2 values below 0.1. A multiple regression model [13] was computed using all mass and thermal conductivity descriptors. Dependent variable was chosen IC_{50}. Pearson correlation (r) retrieved was r=0.632, with r^2=0.399, Spearman rank correlation (p)=0.673, cross validated squared (q^2) =0.399, y=0.399x+12.11. Based on PCA, principal components (PC) 1-8 for variables listed in Table 2 were computed. Results are shown in Table 3.

In order to build a model using descriptors listed in Table 1 and PC showed in Table 3, a multi-variate correlation between target variable and descriptors was performed. Conclusive results are shown in Table 4.

A model using correlation (entry 5) (Table 4) was built with IC_{50} (nM) as dependent variable. This solution was chosen mainly because of its correlation with the target variable (r^2=0.999) and the reduced number of descriptors (4). The plot of correlation between predicted IC_{50}p and IC_{50}o experimentally determined (observed) is shown in Fig. 1. In Table 5 descriptors contribution to the model is listed. Model equation is y=0.029+0.998*IC_{50}o. Person correlation square (r^2)=0.998,Speareman rank correlation(p)=0.931, Cross validated square (q^2)=0.998.

Table 1. Compounds (in Smiles) used in building of the model, $IC_{50}o$ (observed), $IC_{50}p$ (predicted)

No	Compound	$IC_{50}o$	$IC_{50}p$
1	ON(=O)C(=CC=1)C=CC=1CC(C(OC)=O)NC(=O)C=2C=CC=C3C=CC=CC=23	5.000	4.987
2	FC(=CC=1)C=CC=1CC(CC2)CCN2CC(C3)NCCN3C(=O)NC(C=4)=CC=CC=4OC	30.000	29.986
3	FC(=CC=1)C=CC=1CC(CC2)CCN2CC(C3)CCCN3C(=O)NC(C=4)=CC=CC=4OC	50.000	50.006
4	O=C(NC=1C=C(C=CC=1)C(C)=O)NCCCN(C(C(CCCC)O)C2)CCC2CC3=CC=CC=C3	80.000	80.016
5	ClC(=CC=1)C=CC=1CC(CC2)CCN2CCCNC(=O)NC(=C3)C=CC=C3C#N	20.000	20.051
6	O=C(NC=1C=C(C=CC=1)C(C)=O)NCCCN(C(C(CC)O)C2)CCC2CC3=CC=CC=C3	8.000	7.981
7	FC(=CC=1)C=CC=1CC(CC2)CCN2CCCNC(=O)NC(C=3)=CC=CC=3C#N	80.000	80.053
8	FC(=CC=1)C=CC=1CC(CC2)CCN2CC(C3)OCCN3C(=O)NC(C=4)=CC=CC=4OC	50.000	49.996
9	O=C(NC=1C=C(C=CC=1)C(C)=O)NCCCN(C(CCC)C2)CCC2CC3=CC=CC=C3	100.000	100.017
10	ClC(C=C1)=CC=C1CC(C2)CC3CCC2N3CC(C(C)O)NC(=O)NC(C=4)=CC(OC)=C(OC)C=4OC	8.200	8.192
11	ClC(C=C21)=CC=C2OC3=CC=C(Cl)C=C3C1C(=O)NC(CC4)CCN4(CC)CC=5CCCCCCC=5	0.580	0.652
12	ClC(C=C1)=CC=C1CC(C2)CC3CCC2N3CC(C(C)O)NC(=O)NC(C=4)=CC=CC=4S(=O)(=O)C	12.000	11.963
13	ClC(C=C1)=CC=C1CC(C2)CC3CCC2N3CC(C)NC(=O)NC(C=4)=CC(OC)=C(OC)C=4OC	11.000	11.003
14	ClC(C=C1)=CC=C1CC(C2)CC3CCC2N3CC(C)NC(=O)NC(C=4)=CC=CC=4S(=O)(=O)C	65.000	64.980
15	FC(=CC=1)C=CC=1CC(C2)CC3CCC2N3CCCNC(=O)NC(C=4)=CC=CC=4C(=O)C	47.000	46.957
16	FC(C=C1)=CC=C1CC(C2)CCCN2CC3CCCCC3NC(=O)NC(C=4)=CC=CC=4C(=O)C	0.364	0.347
17	ClC=1C=CC=C(S2)C=1N=C2NC(=O)NC3CCCCC3CN(C4)CCCC4CC=5C=CC(F)=CC=5	0.090	0.084
18	FC(=CC=1)C=CC=1CC(C2)CCCN2CC3CCCCC3NC(=O)NC=4C=CC=CC=4C	100.000	99.998
19	FC(=CC=1)C=CC=1NC(=O)NC2CCCCC2CN(C3)CCCC3CC=4C=CC(F)=CC=4	5.000	5.004
20	BrC(=CC=1)C=CC=1NC(=O)NC2CCCCC2CN(C3)CCCC3CC=4C=CC(F)=CC=4	50.000	49.967
21	FC(=C1)C(C)=CC=C1NC(=O)NC2CCCCC2CN(C3)CCCC3CC=4C=CC(F)=CC=4	35.000	34.963
22	FC(=CC=1)C=CC=1CC2CCCCN2NC(=O)NC(C=3)=CC=CC=3C(=O)C	2.600	2.564
23	FC(=CC=1)C=CC=1CC(CC2)CCN2CC3=C(C(NC)=O)C=CC=C3NC(=O)NC(=C4)C=CC=C4C(=O)C	30.000	29.987
24	FC(=CC=1)C=CC=1CC(C2)CCCN2CC3CCCCC3NC(=O)NC=4C=CC=CC=4	17.000	16.946
25	FC(C=C1)=CC=C1CC(C2)CCCN2CC3CCCCC3NC(=O)NC(=CC=4)C=CC=4OC	1.000	0.996
26	FC(=CC=1)C=CC=1CC(C2)CCCN2CC3CCCCC3NC(=O)NC(C=4)=CC=CC=4N5N=NN=C5C	1.400	1.334
27	FC(C(=C1)C(C)=O)=CC=C1NC(=O)NC2CCCCC2CN(C3)CCCC3CC=4C=CC(F)=CC=4	0.015	-0.017
28	FC(=CC=1)C=CC=1CC(C2)CCCN2CC3CCCCC3NC(=O)NC4=CC=C5NN=CC5=C4	0.045	0.053
29	FC(=CC=1)C=CC=1CC(C2)CCCN2CC3CCCCC3NC(=O)NC(=C4)C=C(C=5N(C)N=NN=5)C=C4C6=NN=NN6C	0.042	0.009
30	FC(=CC=1)C=CC=1CC(C2)CCCN2CC3CCCCC3NC(=O)NC(S4)=NC(C)=C4C(=O)C	0.030	0.071
31	FC(C=C1)=CC=C1CC(C2)CCCN2CC3CCCCC3NC(=O)NC(C=C4)=CC=C4C5=NN=NN5C	0.700	0.667
32	FC(=CC=1)C=CC=1CC(C2)CCCN2CC3CCCCC3NC(=O)NC4=CC=C5NC=CC5=C4	0.400	0.364
33	FC(=CC=1)C=CC=1CC(C2)CCCN2CC3CCCCC3NC(=O)NC(C=C4(C#N))CC=C4N5C=CC=N5	4.000	4.049
34	FC(=CC=1)C=CC=1CC(C2)CCCN2CC3CCCCC3NC(=O)NC=4C=CC=CC=4OC	1.400	1.394
35	FC(C=C1)=CC=C1CC(C2)CCCN2CC3CCCCC3NC(=O)NC(=C4)C=C(C(C)=O)C=C4C(=O)C	0.007	0.049
36	FC(=CC=1)C=CC=1CC(C2)CCCN2CCCNC(=O)NC(C=3)=CC=CC=3C(=O)C	2.500	2.509
37	FC(=CC=1)C=CC=1CC(C2)CCCN2CC3CCCCC3NC(=O)NC(C=4)=CC=CC=4C5=NN=NN5C	0.010	-0.003
38	FC(=CC=1)C=CC=1CC(C2)CCCN2CC3CCN(C(C)=O)CC3NC(=O)NC(S4)=NC(C)=C4C(=O)C	7.000	7.054
39	FC(C=C1)=CC=C1CC(C2)CCCN2CC3CS(=O)(=O)CC3NC(=O)NC(S4)=NC(C)=C4C(=O)C	0.900	0.987
40	FC(=CC=1)C=CC=1CC(C2)CCCN2CC3CNCCC3NC(=O)NC(S4)=NC(C)=C4C(=O)C	0.100	0.150
41	FC(=CC=1)C=CC=1CC(C2)CCCN2CC3CCNCC3NC(=O)NC(S4)=NC(C)=C4C(=O)C	0.075	0.093

Table 2. Descriptors used in building of the model: C-Centrality, X-Centrocomplexity, CS-Colum Sum, PDS-Product Distance Sum, LM-Layer matrix, [M]-Mass, [Tc]- Thermal conductivity

No.	C[LM[M]]	C[LM[Tc]]	CS[LM[M]]	CS[LM[Tc]]	PDS[LM[TM[M]]	PDS[LM[Tc]]	X[LM[M]].10^{-3}	X[LM[Tc]].10
1	2.193	2.698	10080	758.572	55964	4036.730	10.212	126.836
2	1.925	2.195	13024	1032.060	93054	7345.680	10.219	125.679
3	1.925	2.192	12960	1073.330	92670	7593.310	10.219	125.585
4	2.100	2.368	15330	1309.410	114510	9889.530	10.211	125.105
5	1.720	2.011	11107	860.470	82491	6187.130	10.208	125.732
6	2.004	2.271	13662	1149.440	99072	8421.480	10.212	125.318
7	1.724	2.008	10643	860.476	77707	6187.190	10.213	125.732
8	1.924	2.195	13088	1032.060	93438	7345.680	10.219	125.679
9	1.944	2.202	12736	1114.600	92362	8172.440	10.213	124.865
10	2.203	2.508	18241	1336.520	135797	9688.480	10.212	126.324
11	2.411	2.807	17640	1393.240	117398	9161.840	1.002	126.600
12	2.160	2.493	16975	1174.060	123295	8114.060	10.219	126.623
13	2.072	2.368	16275	1219.120	121519	8844.720	10.213	126.023
14	2.031	2.352	15081	1064.390	109761	7350.250	10.220	126.310
15	1.897	2.165	12960	1073.330	95809	7822.950	10.218	126.407
16	2.115	2.419	14586	1228.130	102979	8573.730	10.217	126.139
17	2.150	2.496	16870	1219.200	122363	8690.510	1.002	127.098
18	2.088	2.403	12832	1114.60	85200	7397.140	10.219	125.827
19	2.031	2.356	13056	1073.330	88632	7108.270	10.217	126.346
20	2.019	2.351	15008	1073.360	107786	7108.560	1.002	126.346
21	2.075	2.372	13860	1149.440	95676	7833.250	10.216	126.278
22	2.013	2.420	9315	731.473	53579	4200.480	10.213	126.021
23	2.275	2.569	18354	1470.680	136021	10777.300	10.214	126.380
24	2.042	2.348	12059	1039.780	78691	6766.310	10.219	125.877
25	2.030	2.317	13761	1149.440	96222	7930.010	10.218	125.831
26	2.193	2.493	17353	1336.530	130849	9820.180	10.222	126.191
27	2.155	2.473	15680	1264.270	113277	8924.710	10.215	126.579
28	2.115	2.458	14586	1184.280	102743	8146.820	10.223	126.765
29	2.444	2.813	23607	1664.250	189543	12992.800	1.002	126.598
30	2.112	2.449	15334	1140.510	108185	7941.050	10.216	126.355
31	2.125	2.429	17353	1336.530	134811	10000.800	10.222	126.262
32	2.116	2.420	14518	1228.130	102105	8558.250	10.223	126.603
33	2.175	2.473	18202	1470.680	140565	11222.300	10.221	126.365
34	2.128	2.455	13761	1149.440	93554	7762.290	10.218	125.832
35	2.242	2.571	17353	1431.970	128555	10461.100	10.215	126.367
36	1.829	2.119	11430	928.848	82195	6612.890	10.212	125.634
37	2.193	2.519	17353	1336.530	130909	9781.480	10.222	126.263
38	2.280	2.634	18241	1288.900	131569	9199.060	10.215	126.300
39	2.175	2.543	17185	1083.870	120554	7588.320	10.222	126.867
40	2.111	2.464	15402	1096.660	108635	7650.860	10.216	126.520
41	2.111	2.452	15402	1096.660	108639	7648.280	10.216	126.520

Table 3. Principal components used in building the model.
PC 1-8 for the descriptors in Table 2

No.	PC1	PC2	PC3	PC4	PC5	PC6	PC7	PC8
1	2.008	-4.022	-0.198	-1.783	-0.018	-0.092	0.272	-0.023
2	2.162	0.629	0.040	0.459	-0.263	-0.139	-0.056	0.041
3	2.229	1.184	-0.213	0.084	-0.088	0.011	-0.055	-0.007
4	0.226	2.994	-0.303	-1.2542	-0.482	-0.029	0.097	0.045
5	3.988	0.188	-0.005	1.622	-0.060	-0.210	0.095	-0.060
6	1.188	0.991	0.545	0.408	-1.332	-0.086	-0.001	0.058
7	4.535	1.101	-0.914	0.472	0.902	0.012	0.133	-0.023
8	2.283	0.966	-0.259	0.105	0.088	-0.141	-0.052	0.039
9	2.693	2.968	-0.841	-1.116	-0.396	-0.113	0.046	0.018
10	-2.184	0.457	0.700	-0.014	0.227	-0.299	-0.101	-0.014
11	-3.772	-1.335	-2.212	-0.615	-1.150	0.369	-0.159	-0.022
12	-1.124	-0.571	0.395	-0.075	0.728	-0.455	-0.128	-0.029
13	-0.476	0.588	0.542	0.413	-0.072	-0.300	-0.050	-0.034
14	0.872	0.442	-0.504	-0.546	1.278	-0.409	-0.053	-0.047
15	1.823	0.372	-0.218	0.630	1.186	0.525	0.080	0.057
16	-0.236	-0.188	0.637	0.091	-0.429	0.341	-0.044	-0.005
17	-2.263	-1.455	-2.342	1.327	0.259	0.320	0.024	0.098
18	1.711	1.121	-1.010	-1.993	0.673	0.298	-0.040	-0.019
19	1.101	-0.967	0.336	0.242	0.001	0.288	-0.065	-0.045
20	0.202	-0.247	-3.236	0.717	0.117	-0.171	-0.124	-0.075
21	0.658	-0.065	-0.001	-0.367	0.408	0.366	-0.087	0.017
22	3.576	-2.531	-0.070	-0.629	-0.890	-0.269	0.120	0.025
23	-2.886	1.046	0.514	-0.721	0.482	0.312	-0.034	0.024
24	1.851	-0.530	0.138	-0.295	-0.631	0.206	-0.112	0.009
25	0.862	0.049	0.562	0.421	-0.755	0.126	-0.118	-0.023
26	-1.927	0.463	0.816	0.071	-0.160	-0.103	0.004	0.012
27	-1.137	-0.520	0.662	0.116	0.266	0.371	-0.002	-0.001
28	-0.447	-1.140	0.528	0.154	0.504	0.485	0.034	-0.030
29	-7.242	1.021	-1.646	0.449	-0.434	-0.440	0.259	-0.001
30	-0.277	-0.677	0.539	0.126	0.006	-0.165	-0.042	-5.680
31	-1.768	0.642	0.843	0.573	0.102	-0.055	0.091	-0.051
32	-0.446	-0.730	0.594	0.225	0.262	0.654	-0.024	0.030
33	-2.756	1.057	0.952	0.425	0.237	0.378	0.133	-0.012
34	0.421	-0.360	0.530	-0.355	-1.004	0.045	-0.062	-0.020
35	-2.595	0.330	0.902	-0.214	-0.117	0.408	0.085	-0.041
36	3.160	-0.072	0.327	1.269	-0.753	-0.116	0.060	-0.001
37	-2.015	0.306	0.823	0.041	-0.097	-0.089	0.059	-0.044
38	-2.356	-0.073	0.642	-0.701	-0.038	-0.566	-0.057	0.006
39	-1.151	-1.416	0.447	-0.045	0.883	-0.706	-0.080	0.083
40	-0.257	-1.019	0.478	0.120	0.275	-0.284	-0.004	0.021
41	-0.231	-0.998	0.481	0.158	0.286	-0.275	-0.036	0.045

Table 4. Model correlation in multi-variate regression

No.	Pearson r^2	Descriptors	Descriptors
1	0.999	6	C[LM[Mass]],PC2,PC3,PC7, PDS[LM[Tc]],X[LM[Mass]]
2	0.999	6	CS[LM[Tc]],C[LM[Mass]],PC2,PC3,PDs[LM[Tc]],X[LM[Mass]]
3	0.999	6	CS[LM[Mass]],C[LM[Mass],PC2,PC3,PDS[LM[Tc]], X[LM{Mass]]
4	0.999	5	C[LM[Mass]],PC2,PC3,PDS[LM[Tc]],X[LM[Mass]]
5	0.999	4	PC2,PC3,PDS[LM[Tc]], X[LM[Mass]]
6	0.798	3	PC2,PC3,PDS[LM[Tc]]
7	0.680	2	PC2, PDS[LM[Tc]]
8	0.627	2	CS[LM[Tc]], PC2
9	0.615	2	PC2,PDS[LM[Mass]]
10	0.371	1	PC2
11	0.172	1	PC3
12	0.074	1	PDS[LM[Mass]]

Table 5. Tolerance, VIF (value of inflation) and r^2 calculated for the descriptors used in the model

No.	Descriptors	r^2	Tolerance	VIF
1	PC2	0.777	0.222	4.485
2	PC3	0.936	0.063	15.645
3	PDS[LM[Tc]]	0.860	0.140	7.149
4	X[LM[Mass]]	0.944	0.056	17.860

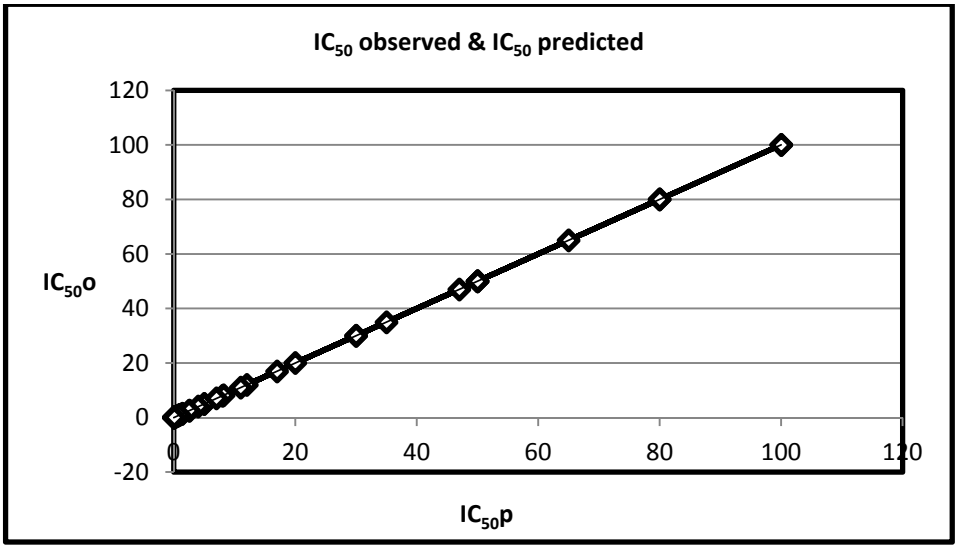

Figure 1. Scatter plot of IC_{50} observed ($IC_{50}o$) vs IC_{50} predicted ($IC_{50}p$)

The results obtained by using simple descriptors alone (without PC values) are rather modest. Best r^2 value described in literature is 0.960 on a series of 4-benzylpiperidinealkylurease CCR3 antagonist with a model obtained by using CoMFA methodology [10]. However, the cited study used a vast set of descriptors. The approach by local vertex invariants based on thermal conductivity descriptors, within Cluj descriptors, has the advantage of using a small number of descriptors which encode both topological and physico-chemical properties of a ligand. Correlation obtained supports the supposition that thermal conductivity and topological information plays a distinct role in bioactivity of these compounds. Furthermore, by using PCA, a significant increase in predictive performance of the model is obtained. Certainly, this model is not the best CCR3-interaction estimator but regardless of collinearity and multi-collinearity introduced by using PCA, the model is a good predictor of bioactivity of the studied compounds, as demonstrated below. In Table 6, standard errors are listed. Standard error is a measure of divergence of estimator value from the expected value.

Average standard deviation computed was 19.665. Percentage error and percent difference error, calculated for observed and predicted values are listed in Table 6.

Multicollinearity has no impact on the regression model and association statistics such as r^2, F ratio and p values. It also should not generally have an impact on prediction made using the overall model. Tolerance and VIF are two main tests in detecting multicollinearity. Results are represented in Tables 7 and 8.

Fig. 2 shows data dimensionality, although r^2=0.999 variations are observed. For two variables 1-100% interval is violated. In this case there is a lack of accuracy and precision.

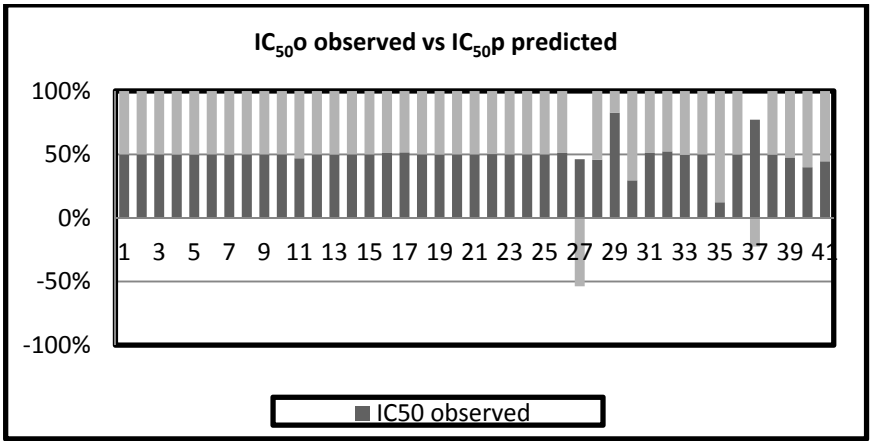

Figure 2. $IC_{50}o$ vs $IC_{50}p$ % stacked column.

Table 6. Percentage error, percent difference error, calculated for observed and predicted values

No.	$IC_{50}o$	$IC_{50}p$	%error	%difference	%error predicted	Error SD
1	5.000	4.987	0.256	0.128	0.637	15.170
2	30.000	29.986	0.045	0.022	0.113	-29.986
3	50.000	50.005	0.011	0.005	0.027	-50.005
4	80.000	80.015	0.019	0.009	0.048	-80.015
5	20.000	20.051	0.256	0.128	0.635	-20.051
6	8.000	7.980	0.240	0.120	0.596	-7.980
7	80.000	80.052	0.067	0.032	0.163	-80.052
8	50.000	49.996	0.007	0.003	0.018	-49.996
9	100.000	100.017	0.017	0.008	0.042	-100.017
10	8.200	8.191	0.099	0.049	0.246	-8.191
11	0.580	0.651	12.408	5.841	28.979	-0.651
12	12.000	11.963	0.305	0.152	0.757	-11.963
13	11.000	11.002	0.024	0.012	0.060	-11.002
14	65.000	64.980	0.030	0.015	0.075	-64.980
15	47.000	46.957	0.091	0.045	0.227	-46.957
16	0.364	0.347	4.568	2.337	11.597	-0.347
17	0.090	0.083	6.7664	3.501	17.371	-0.083
18	100.000	99.998	0.002	0.001	0.004	-99.998
19	5.000	5.004	0.082	0.041	0.205	-5.004
20	50.000	49.967	0.065	0.032	0.161	-49.967
21	35.000	34.962	0.107	0.053	0.265	-34.962
22	2.600	2.563	1.390	0.700	3.473	-2.563
23	30.000	29.987	0.043	0.021	0.106	-29.987
24	17.000	16.945	0.318	0.159	0.790	-16.945
25	1.000	0.996	0.364	0.182	0.905	-0.996
26	1.400	1.333	4.718	2.416	11.987	-1.334
27	0.015	-0.017	215.900	1357.810	6736.000	0.017
28	0.045	0.053	17.901	8.215	40.756	-0.053
29	0.042	0.008	79.458	65.918	327.016	-0.008
30	0.030	0.071	137.365	40.717	201.994	-0.071
31	0.700	0.666	4.750	2.433	12.070	-0.666
32	0.400	0.363	9.124	4.780	23.713	-0.363
33	4.000	4.048	1.215	0.604	2.996	-4.048
34	1.400	1.393	0.461	0.231	1.147	-1.393
35	0.007	0.049	604.554	75.141	372.770	-0.049
36	2.500	2.508	0.340	0.170	-0.843	-2.508
37	0.010	-0.003	129.130	182.208	903.923	0.003
38	7.000	7.054	0.773	0.385	1.910	-7.054
39	0.900	0.987	9.681	4.617	22.904	-0.987
40	0.100	0.150	50.025	20.008	99.258	-0.150
41	0.075	0.093	24.295	10.832	53.736	-0.093

Table 7. PCA and topological descriptors combined model VIF and Tolerance

Tolerance calculus: Variable	R^2	Tolerance (1-R^2)	VIF(1/Tolerance)
PDS[LM[Tc]]	0.983	0.016	62.282
C[LM[Mass]]	0.990	0.009	110.192
X[LM[Mass]]	0.988	0.011	89.015
PC2	0.967	0.032	30.700
PC3	0.983	0.016	59.234
PC4	0.973	0.026	37.813
PC7	0.323	0.676	1.478
PC8	0.005	0.994	1.005

Table 8. PCA and topological descriptors combined model validation

No	Descriptors	p	Q^2	R^2	Adjuat R^2	St error	F ratio
1	PDS[LM[Tc]], C[LM[Mass]]	0.002	0.220	0.220	0.200	2.341	11.041
2	PDS[LM[Tc]], X[LM[Mass]]	0.258	0.032	0.032	0.007	18.172	1.313
3	PDS[LM[Tc]], PC2	0.812	0.681	0.680	0.672	3.424	83.251
4	PDS[LM[Tc]], PC3	0.469	0.188	0.188	0.167	7.885	9.076
5	PDS[LM[Tc]], PC4	0.339	0.168	0.168	0.147	8.321	7.904

Random errors evaluation is represented in Fig. 3; there are no randomization errors. However, there is a violation in data dimensionality for variables 27 and 37.

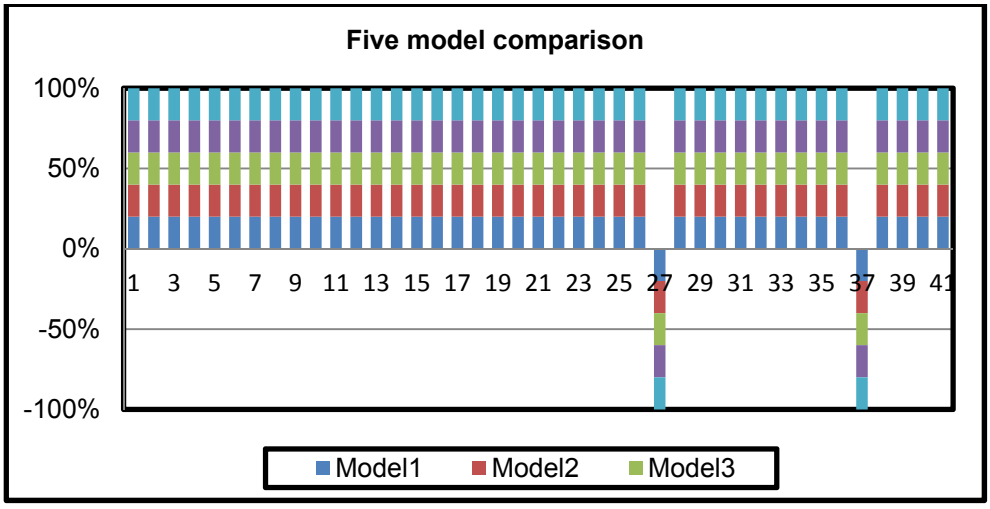

Figure 3. % stacked column plot of identical multiple regression models.

METHODS

Data set used to build the regression model was curated: 3D structures were built using Smiles formulas, compounds resulted were energetically minimized, only compounds with IC50(nM) equal or >100 nM were kept. After this process 41 compounds (Table 1) were retained. Compounds were randomly divided in a training set (21 compounds) and a test set (20 compounds). All structures were converted to "hin" format. The model was built by using TopoCluj topological descriptors. Layer matrices of two physico-chemical properties were used: mass and thermal conductivity of respective compounds (as included in data base of TopoCluj) Centrocomplexity, colum sum, product distance sum, as vertex invariants, were used to compute mass and thermal conductivity layer matrix indices. In order to increase the coefficient of correlation, principal components analysis (PCA) was performed [15]; PC 1-8 were computed. Dependent variable IC_{50} was predicted using combined PC and topological descriptors, applying the multiple linear regression method. The model was internally and externally validated. Contribution of descriptors to the model was evaluated based on variance, inflation factor (VIF) [16] and tolerance [17]; these were computed based on r^2. To find if a value is "accurate", a comparison with the acceptable value must be made; in this respect, percentage error (% error) was used. To find if a value is "precise", the average of IC_{50} predicted value was calculated. Average of the deviations was calculated to find the uncertainty. Also, VIF, Tolerance, p, q^2, r^2, adjust r^2, standard error, F ratio were computed in order to assess the model multicolinearity and validate the model.

Error analysis, in respect to observed and predicted IC_{50}, was performed using the percent error and percent difference, calculated by formulas:

$$\%\,\text{error} = 100\,\text{x}\,\frac{|(\text{value}\,2)| - |(\text{value}\,1)|}{|\,\text{value}\,2\,|}$$

$$\%\,\text{difference} = 100\,\text{x}\,\frac{|(\text{value}\,1)| - |(\text{value}\,2)|}{\frac{|(\text{value}\,1)| + |(\text{value}\,2)|}{2}}$$

where value 1 is IC_{50}o observed and value2 is IC_{50}p predicted. The two values are interchangeable due to allowance of sign neglection.

A percentage representation of predicted and observed values is used to show data dimensionality. Ideally, none predicted or observed values should pass the 1-100% limit. A perfect model has both observed and predicted values represented as same quantities (percent), i.e., 50/50%.

Randomized errors were also computed. In this respect, 5 models using same descriptors, same methods of model generation and evaluation were used. Models were compared using a stacked column plot.

CONCLUSIONS

Bioactivity prediction using local vertex invariants based on thermal conductivity layer matrix is a good methodology in predicting activity of C-C chemokine receptors type 3 inhibitors.

PCA is a valuable tool in optimizing a regression model. Accuracy and precision errors affecting data dimensionality were detected in the model. Such errors may occur even at high values of r^2. Random errors were uncommon in this type of model and were not observed.

ACKNOWLEDGMENTS

The author declares no conflict of interest.

REFERENCES

1. K.D. Dyer, K.E. Garcia-Crespo, K. E. Killoran and H. F. Rosenberg, *Journal of Immunological Methods*, **2011**, *369* (1-2), 91.
2. J. Reckless, D.J. Grainger, *Biochemical Journal* **1999**, *340* (3), 803.
3. D.J. Fox, J. Reckless, S.G. Warren, D.J. Grainger, *Journal of Medicinal Chemistry*, **2002**, *45* (2), 360.
4. D.J. Grainger, A.M. Lever, *Medicinal Chemistry,* **2005**, *2* (1), 23.
5. Entrez Gene, CCR3 chemokine (C-C motif) receptor 3.
6. H. González-Díaz, S. Vilar, L. Santana, E Uriarte, *Current Topics in Medicinal Chemistry*, **2007**, *7* (10), 1015.
7. L. Jäntschi, G. Katona, M.V. Diudea *MATCH Communications in Mathematical and Computer Chemistry* **2000**, *41*, 151.
8. P.V. Khadikar, S. Karmarkar, V.K. Agrawal, J. Singh, A. Shrivastava, I. Lukovits, M.V. Diudea, *Letters in Drug Design & Discovery*, **2005**, *2* (8), 606.
9. O.M. Minailiuc, G. Katona, M.V. Diudea, M. Strunje, A. Graovac, I. Gutman, *Croatica Chemical Acta*, **1998**, *71* (3), 473.
10. Jain V1, Pandey A, Gupta S, Mohan CG, *Journal of Molecular Modeling*, **2010**,*16* (4), 669.
11. M.V. Diudea, M. Topan, A. Graovac, *Journal Chemical Information and Computer Science,* **1994**, *34* (5), 1072.

12. M.V. Diudea, O. Ursu, *Indian Journal of Chemistry A,* **2003**, *42* (6), 1283.
13. M.V. Diudea, O.M. Minailiuc, G. Katona, I. Gutman, Szeged matrices and related numbers, *MATCH Communications in Mathematical and Computer Chemistry,* **1997**, *35*, 129.
14. M.H. Kutner, C.J. Nachtsheim, and J. Neter, “Applied Linear Regression Models”, 4th ed., McGraw-Hill/Irwin, Boston, 2004, p. 25.
15. H. Abdi, L.J. Williams, “Principal component analysis”. Wiley Interdisciplinary Reviews: Computational Statistics. **2010**, 2 (4), 433.
16. A.F. Zuur, E.N. Ieno, C.S. Elphick, *Methods in Ecology and Evolution*. **2010**, *1*, 3.
17. S. Menard, Applied Logistic Regression Analysis: Sage University Series on Quantitative Applications in the Social Sciences. Thousand Oaks, CA. Sage, 1995.

STUDIA UBB CHEMIA, LXIII, 1, 2018 (p. 189-198)
(RECOMMENDED CITATION)
DOI:10.24193/subbchem.2018.1.14

EVALUATION OF POLYCYCLIC AROMATIC HYDROCARBONS IN PORK MEAT PRODUCTS OBTAINED IN TRADITIONAL SYSTEMS IN ROMANIA

ALEXANDRA TĂBĂRAN[a], IONUŢ VLAD CORDIŞ[a,*], ANCA BECZE[b], SORIN DANIEL DAN[a], OANA REGET[a], GHEORGHE ILE[a], DANA LIANA PUSTA[a], IOAN PASCA[a], MIHAI BORZAN[a], MARIAN MIHAIU[a]

ABSTRACT. The aim of this study was to determine the polycyclic aromatic hydrocarbons (PAH) levels in the smoked meat products obtained in the traditional system in Romania. The importance of this study resides in the fact that these compounds are known to be carcinogenic and their levels should be strictly monitored so as to ensure the safety of the consumers. Until now, no study was performed in Romania that addresses this issue in the traditional pork meat products. The study was performed on 60 meat products samples (sausages, bacon, ham) taken from a certified traditional meat processing unit but also from retail units that delivered industrially processed meat products. The method used in the detection of the 15 PAHs analysed was HPLC. Our results showed that the highest percent of total PAHs is found in the traditionally obtained smoked bacon and the lowest in industrially produced pork meat sausage. None of the samples examined exceeded the limit imposed by the European legislation for benzo[a]pyrene (BaP), but the smoked bacon revealed higher values for PAH4 than the allowed limit. Following this study we suggest that a more careful attention should be paid to all factors and apply such smoking conditions that result in the lowest possible contamination with PAH in pork meat products obtained in the traditional system in Romania.

Keywords: *polycyclic aromatic hydrocarbons, traditional, industrial, smoked, product.*

[a] *Agricultural Sciences and Veterinary Medicine University, Faculty of Veterinary Medicine, 3-5 Manastur str., RO-400372, Cluj-Napoca, Romania.*
[b] *INCDO-INOE2000, Research Institute for Analytical Instrumentation, ICIA Cluj-Napoca Subsidiary, 400293 Cluj-Napoca, Romania.*
[*] *Corresponding author: lapusan_alexandra@yahoo.com; cordisionutvlad@gmail.com*

INTRODUCTION

Traditional products represent an important part of Romanian culture, having a major role in the preservation of various technologies of processing, distinctive in many regions and with many identity trade markers. At the level of the agricultural economy in Romania, traditional products account for only 2.5% of the total sales [1], while in the European countries there is a growing trend of production and consumption of these types of products [2]. Various researches have been performed on a number of traditional meat products obtained in different regions, underlining their unique flavours and nutritional benefits [3,4]. Still, it is important also to focus the studies on their biochemical particularities resulting after the traditional processing, that sometimes may affect their quality and protection of consumers.

Cured meat products are usually processed through a series of technological steps, like: salting, drying and smoking. In Romania, traditional cured meat products have the characteristic of being processed in a particular way, depending on the region, leaving them to dry and smoke for a larger amount of time and using natural wood, which defines their specific organoleptic quality and stability requirements. Previous studies have been carried out to evaluate the impact of these technological steps on the microbiological and compositional modifications [5, 6] but very few focused on the aspect of potentially toxic residues that may exceed their limits imposed by the current legislation, like the polycyclic aromatic hydrocarbons (PAHs) levels.

Polycyclic aromatic hydrocarbons (PAHs) comprise the largest class of chemical compounds known to be cancer causing agents [7]. Due to these effects they are considered to be top of the list of the most hazardous substances [8]. Smoking influences the levels of PAHs in products, and that is why the period and conditions in which this step is made holds great importance. Unfortunately, traditional products are not strictly monitored and this step evaluated only from the aspect of sensorial characteristics not also the biochemical changes that affect these functional products.

During the smoking process, hundreds of individual PAHs are formed and released during the incomplete combustion or thermal decomposition (pyrolysis) of the organic material. Among the PAHs released in the product, benzo[*a*]pyrene can be used as a specific biochemical marker for the occurrence and impact of these carcinogenic factors [9]. Thus, the European Food Safety Authority (EFSA) recommends analysis of benzo[*c*]fluorene (B*c*L) assessed to be relevant by the Joint FAO/WHO Experts Committee on Food Additives (JECFA) [10]. Recently another PAH has been the major interest for toxicological evaluations, dibenzo[*a*,*l*]pyrene, being considered to have a much stronger carcinogenic potential than benzo[*a*]pyrene [11]. In 2005, the European Commission issued a Recommendation [12] that Member States

should perform random monitoring for the presence of PAHs in foodstuffs. The Panel found that PAH4 (the sum of benzo[a]pyrene, benz[a]anthracene, benzo[b]fluoranthene and chrysene) and PAH8 (the sum of benzo[a]pyrene, benz[a]anthracene, benzo[b]fluoranthene, benzo[k]fluoranthene, benzo[ghi] perylene, chrysene, dibenz[a,h]anthracene and indeno[1,2,3-cd]pyrene) were the most suitable indicators for PAHs in food, with PAH8 not providing much added value compared to PAH4.

The estimated contribution of meat products to the overall intake of PAHs also differs between countries: from very low for the UK to 21% in USA and 27% in France, resulting in the second contributing food group after bread and cereals [13, 14].The study of PAH levels in Romania is interesting and very important in order to be able to improve the quality and safety of the traditional products that use smoking as main step in processing. Given that some traditional products are in the course of obtaining the protected designated origin trade marks (PDO), it is imperious to check the compliance with the EU regulations. These types of products are also highly consumed in Romania so any potential harmful effect is mandatory to be exposed and assessed. The most consumed smoked meat product in Romania is the pork meat sausage, which is distinguishable by a particular taste, high nutritional value and large variety of processing technologies.

The aim of this study was to investigate the contents of PAH compounds in three different meat products (pork sausage, pork ham, pork bacon) and to evaluate the effect of traditional smoking process with the industrial one.

RESULTS AND DISCUSSION

The mean PAH levels obtained at the assessment of the traditional products compared to the industrial ones are shown in table 1, 2 and 3. For each product tested the evaluation of PAH level was made from the external layer as well as from the internal one. In the case of traditional pork sausage, among the 15 PAHs investigated, 14 compounds were detected within the external layers and 7 also from the inner layers. The sum of PAH evaluated from the external layers was 80.52 μg/kg^{-1}, and from the content 3.48 μg/kg^{-1}. The quantity of benzo[*a*]pyrene (BaP) was found to be in an average 1.86 μg/kg^{-1}, a value that was relatively high compared to the industrially obtained products. When compared to the industrially obtained pork sausage, we found that the 12 PAHs values at the external surface of the products were lower (65.9 μg / kg^{-1}). From the inner part of the product, the levels of PAHs were also in a lower amount (2.25 μg/kg^{1}), as well as the BaP levels (0.45 μg/kg^{-1}).

Table 1. PAH level in the traditional sausage produced in a traditional and industrial system

No.	PAH	Traditional smoked pork sausage (μg·kg^{-1})	Industrial smoked pork sausage (μg·kg^{-1})	ANOVA
1	Naphthalene	11.8	11.54	*
2	Acenaphthene	3.23	4.14	**
3	Fluorene	<LQ	<LQ	NP
4	Phenanthrene	14.91	17.54	**
5	Anthracene	2.18	2.45	*
6	Fluoranthene	0.59	0.47	**
7	Pyrene	0.37	0.84	***
8	Benz[a]anthracene	0.04	<LQ	NP
9	Chrysene	0.18	0.26	*
10	Benzo(b)fluoranthene	8.19	9.45	**
11	Benzo(k)fluoranthene	1.16	0.84	***
12	**Benzo[*a*]pyrene**	**1.86**	**0.45**	***
13	Dibenz(a,h)anthracene	3.29	2.44	**
14	Benzo(ghi)perylene	32.66	15.48	***
15	Indeno(1,2,3cd)pyrene	LQ	<LQ	-
Total value PAHs		**80.52**	**65.98**	*

Significance, NP, not performed; * P< 0.05; ** P<0.01; *** P<0.001; Data is presented as least square mean.

The total values of PAHs are different according to the smoking technology, the statistical analysis showing significant variations between the levels of PAHs in traditional pork sausage and the industrial one. It was obvious that the traditional smoking process affects in a high amount the concentration of PAHs in the product, therefore making it from this point of view more dangerous.

The PAHs values obtained in the Romanian traditional pork meat sausages are also higher than the ones revealed in the Spanish traditional pork meat sausages [15], where the BaP levels were only 0.02 μg / kg^{-1}, much lower than the one revealed by our study (1.86 μg / kg^{-1}). Also, when analysing the PAH4 levels (the sum of benzo[a]pyrene, benz[a]anthracene, benzo[b]fluoranthene and chrysene) we revealed that the number obtained (10.27 μg / kg^{-1}) is high and very close to the limit (12 μg·kg^{-1}) imposed by the current EU legislation [9].

Table 2. PAH concentrations in traditionally and industrially produced smoked bacon

No.	PAH	Traditional smoked pork bacon (μg·kg^{-1})	Industrial smoked pork bacon (μg·kg^{-1})	ANOVA
1	Naphthalene	6.96	10.32	**
2	Acenaphthene	17,55	<LQ	NP
3	Fluorene	<LQ	<LQ	NP
4	Phenanthrene	45.93	37.79	**
5	Anthracene	1.20	0.47	*
6	Fluoranthene	3.03	1.16	**
7	Pyrene	3.15	3.65	***
8	Benz[a]anthracene	0.75	3.33	**
9	Chrysene	0.47	4.09	*
10	Benzo(b)fluoranthene	9.47	9.51	**
11	Benzo(k)fluoranthene	2.05	17.90	***
12	**Benzo[*a*]pyrene**	**1.87**	**0.32**	***
13	Dibenz(a,h)anthracene	7.63	3.84	**
14	Benzo(ghi)perylene	7.40	7.02	***
15	Indeno(1,2,3cd)pyrene	0.12	0.60	*
Total value PAHs		**107.57**	**100**	*

Significance, NP, not performed; * P< 0.05; ** P<0.01; *** P<0.001; Data is presented as least square mean.

Compared to smoked sausage, smoked bacon contains higher levels of PAHs. We revealed that the total value of the 15 PAHs in the traditional smoked bacon is 107.57 μg / kg^{-1}, much higher compared to the traditional smoked sausage (80.52 μg / kg^{-1}). The difference in PAHs levels between the two types of processing (industrial and traditional) is not so high in case of bacon (107.57 μg / kg^{-1} vs. 100 μg / kg^{-1}). Literature data are very diverse for this type of products; this fact could be explained by the different smoking technologies used. An essential role in the total content of PAHs is held by the type of wood used in smoking, quantity of oxygen, type of procedure (direct or indirect) and period [13].

All the values obtained in the analysis of PAHs concentration in the traditionally obtained smoked bacon and the industrially obtained one has shown statistically significant differences (table 2). The value of BaP in the industrially obtained smoked bacon showed a markedly lower level (0.32 μg / kg^{-1}), than in the case of traditional smoked bacon where the value is almost six time higher (1.87 μg / kg^{-1}). The maximum acceptable level for BaP in food products is 2 μg / kg^{-1}, and even though none of the samples exceeded this limit imposed, the values are very high. Even though the value of BaP in the industrial smoked bacon was relatively low compared to the traditional one, in case of PAH4 the values were much higher (17.25 μg / kg^{-1} vs. 12.56 μg / kg^{-1}). Both products exceed the limit (12 μg·kg^{-1}) imposed by the current EU legislation.

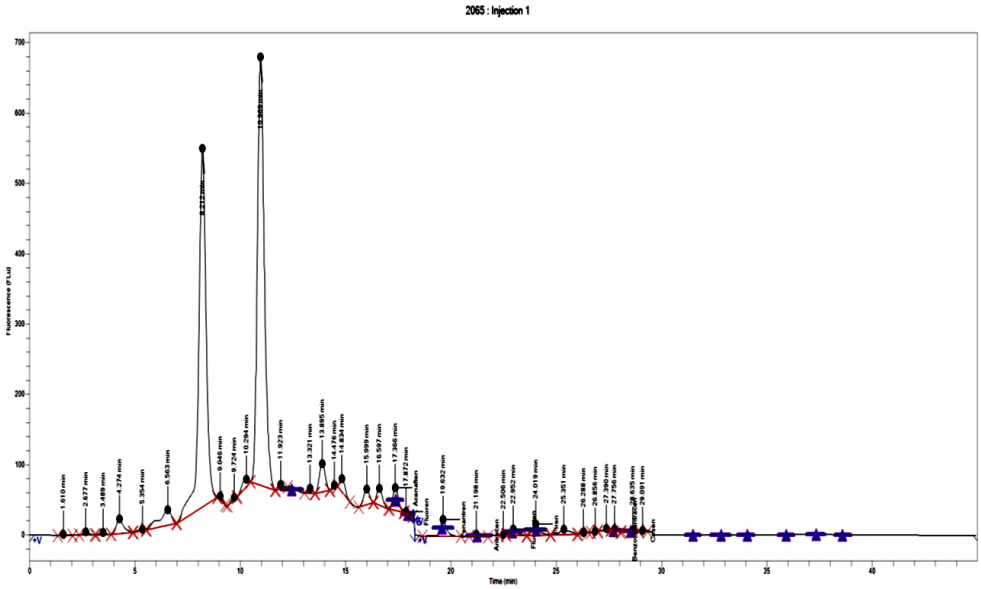

Fig. 1. Representative chromatogram obtained in a sample of traditional smoked bacon

Compared to smoked sausage and smoked bacon, pork ham contains the lowest levels of BaP (Table 3), not detectable by our method because of the low quantity (LQ). The highest level among the 15 PAHs analysed was the phenanthrene, which showed in both types of products (traditional and industrial ones) a level that exceeded 60 µg / kg^{-1}. We revealed that the total value of the 15 PAHs in the traditional smoked ham was 92.69 µg / kg^{-1}, not statistically different from the industrial one (97.15 µg / kg^{-1}).

The PAHs values determined in Romanian traditional pork meat sausage were lower than the ones reported in Portuguese traditional smoked sausage [16] but when compared to other studies made in Italy and Spain, our values were much higher [15, 17]. The content of BaP in the Romanian traditional sausage was much higher than the one revealed in "Pitina" (traditional Italian smoked sausage) (0.8 µg / kg^{-1}) [15], Serbian smoked sausage (0.24 to 0.33 µg / kg^{-1}) [8], Swedish sausage (below the limit of detection) [18]. Although the level of BaP were much higher than the other traditional products from other countries, none of the products investigated exceeded the maximum limit (2 µg / kg^{-1}) imposed by the current legislation in what concerns the BaP levels [9].

Table 3. PAH concentrations in traditionally and industrially produced smoked ham

No.	PAH	Traditional smoked ham (μg·kg^{-1})	Industrial smoked ham (μg·kg^{-1})	ANOVA
1	Naphthalene	6.66	4.41	**
2	Acenaphthene	6.30	5.07	**
3	Fluorene	16.63	18.51	NS
4	Phenanthrene	60.50	67.62	**
5	Anthracene	0.23	0.64	*
6	Fluoranthene	1.21	0.60	NS
7	Pyrene	0.94	0	NP
8	Benz[a]anthracene	0.18	<LQ	NP
9	Chrysene	<LQ	<LQ	NP
10	Benzo(b)fluoranthene	<LQ	<LQ	NP
11	Benzo(k)fluoranthene	<LQ	<LQ	NP
12	**Benzo[*a*]pyrene**	<LQ	<LQ	NP
13	Dibenz(a,h)anthracene	<LQ	<LQ	NP
14	Benzo(ghi)perylene	<LQ	<LQ	NP
15	Indeno(1,2,3cd)pyrene	<LQ	<LQ	NP
Total value PAHs		**92.69**	**97.15**	**NS**

Significance, NP, not performed; NS – no statistical significance (P>0.05); * P< 0,05; ** P<0.01; *** P<0.001; Data is presented as least square mean.

PAH4 is a more suitable indicator for the occurrence of PAHs, with a maximum allowed content in smoked meat products of 12 μg / kg^{-1} [9]. In the studied products we revealed that traditional and industrial pork meat sausage and ham do not exceeded this limit and there is no hazard concerning this aspect. In the traditionally and industrially smoked bacon the levels of PAH4 were higher than the limit imposed by the current EU legislation which constitutes a great concern regarding the safety of these products.

CONCLUSIONS

According to the results obtained in this study, Romanian sausage and ham, smoked in traditional and industrial conditions, are safe for its consumers regarding European regulation on PAHs content. In case of pork bacon produced in Romania, PAH4 levels exceed the imposed European limit and further investigation for identification of optimal smoking conditions in order to minimize levels are needed. We suggest that a more careful attention should be paid to all factors and apply such smoking conditions that result in the lowest possible contamination with PAH in pork meat products obtained in the traditional system in Romania, given the fact that in all types of products the levels of BaP were higher than in the industrially obtained ones.

EXPERIMENTAL SECTION

Sampling

The study was performed on a number of 60 meat product samples, which were taken from a certified traditional pork meat processing unit and retail units found in Salaj County. The following meat products were examined: traditional pork meat sausage (n=10), industrial pork meat sausage (n=10), traditional pork meat bacon (n=10), industrial pork meat bacon (n=10), traditional pork meat ham (n=10), industrial pork meat ham (n=10). All the samples taken were kept in their original package and at a temperature of 0-4 ˚C until their analysis in the laboratory.

The analysis of PAHs through HPLC method

The analysis of the 15 PAHs in the meat products was carried out at the Research Institute for Analyses Instrumentation Cluj-Napoca, Romania. The Perkin Elmer 200 Series High Performance Liquid Chromatograph (HPLC) with FLD detector was used to determine the following PAHs: Naphthalene, Acenaphthene, Fluorene, Phenanthrene, Anthracene, Fluoranthene, Pyrene, Benz[a]anthracene, Chrysene, Benzo[b]fluoranthene, Benzo[k]fluoranthene, Benzo[a]pyrene, Dibenz[a,h]anthracene, Benzo[ghi]perylene, Indeno[1,2,3-cd]pyrene. For sample preparation, the method described by Ojaveer and Tanner (1996) [19] was used. The extraction method used was the following one: 10 g of sample was homogenized in a blender and 50 ml of KOH solution 0.4M in ethanol and water (9:1) for saponification was added. The reaction was performed in an ultrasound bath for 30 minutes at 60˚C, after which filtration was made using a filtering paper. The obtained product was extracted twice using 15 ml cyclohexane and the supernatant was purified on a Florisil column. After this step the sample was evaporated under nitrogen flow and finally recaptured with 1 ml of acetonitrile. Before injection, the samples were filtrated again on cartridges of 0.45 µm.

For the recuperation study, a sample of meat product was taken and contaminated with a standard solution that contained all the 15 PAHs in the same proportion, dissolved in acetonitrile. Afterwards, at the 10 g of sample, 1 ml of standard solution with a concentration of 30µg/ml for each PAH was added. In parallel, a blank solution was analysed in order to calculate with accuracy the recuperation levels. In table 4, the levels of recuperation are presented.

Table 4. The recuperation level for PAH through liquid/liquid extraction from food samples

No.	PAH	Recuperation (%)
1	Naphthalene	81.2
2	Acenaphthene	75.4
3	Fluorene	73.2
4	Phenanthrene	69.8
5	Anthracene	77.9
6	Fluoranthene	73.8
7	Pyrene	71.3
8	Benz[a]anthracene	84.3
9	Chrysene	78.4
10	Benzo(b)fluoranthene	75
11	Benzo(k)fluoranthene	79.5
12	Benzo[*a*]pyrene	77.1
13	Dibenz(a,h)anthracene	75.8
14	Benzo(ghi)perylene	69.9
15	Indeno(1,2,3cd)pyrene	84.5

ACKNOWLEDGMENTS

This study has been financed by the National Council of Scientific Research of Higher Education, Romania, PN-III-P2-2.1-CI-2017-0728.

REFERENCES

1. G. Gheorghe, B.G. Nistoreanu, A. Filip, *Business and Sustainable Development,* **2013**, *XV*, 645.
2. J. Pleadin, L. Demšar, T. Polak, A. Vulić, T. Lešić T., D. Kovačević, *Meso*, **2016**, *18*, 89.
3. C. Marcos, C. Viegas, A.M. de Almeida, M.M. Guerra, *Journal of Ethnic Foods*, **2016**, *3*, 51.
4. S.A. Rather, F.A. Masoodi, R. Akhter, *Journal of Ethnic Foods*, **2016**, *3*, 246.
5. S.E. Yotsuyanagi, C.J. Contreras-Castillo, M.H. Haguiwara, M.V. Katia, A.B. Cipolli, L.S.C. Lemos, M.A. Morgano, E.A. Yamada, *Meat Science*, **2016**, *115*, 50.
6. O.A. Olaoye, *International Food Research Journal*, **2011**, *18(3),* 877.
7. P. Simko, *Journal of Chromatography,* **2002**, *B 770*, 3.
8. J. Djinovic, A. Popovic, W. Jira, *Meat Science,* **2008**, *80*, 449.
9. EC (European Comission Regulation) No. 835/2011, *Official Journal of the European Union*, **2011**, *L215*, 4.

10. EFSA, *EFSA Journal*, **2008**, *724*, 1.
11. S. Higginbotham, N.V.S. RamaKrishna, S.L. Johansson, E.G. Rogan, E.L. Cavalieri, *Carcinogenesis*, **1993**, *14*, 875.
12. EC (European Comission Regulation) No**.** 108/2005, *Official Journal of the European Union*, **2005,** *L34*, 43.
13. SCF, **2002**, http://ec.europa.eu/food/fs/sc/scf/out153_en.pdf
14. SCOOP, **2004**, http://ec.europa.eu/food/food/chemicalsafety/contaminants/scoop_3-2–12_final_report_pah_en.pdf
15. J.M Lorenzo, L. Purrinos, M.C Fontan, D. Franco, *Meat Science*, **2010**, *86(3),* 660.
16. C. Santos, A. Gomes, L. C. Roseiro, *Food Chemical Toxicolology,* **2011**, *49,* 2343.
17. G. Purcaro, S. Moret, L.S. Conte, *Meat Science*, **2009**, 81(1), 275.
18. S. Wretling, A. Eriksson, G.A. Eskhult, B. Larsson, *Journal Food Composition Analysis*, **2010**, *23*, 264.
19. H. Ojaveer, R. Tanner, *Proceedings of the Estonian Academy of Sciences Ecology*, **1996**, *6*, 136.

STUDIA UBB CHEMIA, LXIII, 1, 2018 (p. 199-214)
(RECOMMENDED CITATION)
DOI:10.24193/subbchem.2018.1.15

PULSE FLOUR BASED EMULSIONS – THE EFFECT OF OIL TYPE ON TECHNOLOGICAL AND FUNCTIONAL CHARACTERISTICS

INA VASILEAN[a], IULIANA APRODU[a], ION VASILEAN[a], LIVIA PATRAȘCU[a,*]

ABSTRACT. Three different types of whole pulse flours (broad bean, green and red lentils) were used to obtain emulsions and thereafter heat-set gels, and their properties were compared to the soy protein concentrate. The influence of different vegetable oils (sunflower, canola and palm) on emulsions and heat-set gels properties was investigated by considering the antioxidant activity and rheological characteristics. The emulsifying capacity resulted fairly similar in case of all protein sources in combination with sunflower and canola. Slightly higher emulsifying capacity was observed in case of soy-canola oil emulsion compared to soy-sunflower oil emulsion. The palm oil presented limited capacity to form emulsions. Among studied proteins sources, the highest antioxidant capacity was recorded for broad bean flour. DPPH radical scavenging activity of obtained emulsions was influenced by oil type. It was also observed that antioxidant activity was affected by the thermal treatment. Rheological measurements showed no stability for pulse flour based emulsions, samples entering directly into the transition phase towards flowing. The heat-set gels presented linear viscoelastic regions with higher yield point values in comparison to emulsions. The oil used for preparing the emulsions had a significant influence on yield point value both for emulsions and gels.

Keywords: *Emulsions, Fatty acids, Natural antioxidants, Rheology, Legumes*

INTRODUCTION

The growing interest on vegetable proteins as alternatives to animal ones is related to the nutritional benefits, agricultural aspects and biodiversity preservation. Among vegetables, the legume seeds and in particular pulses represent a rich source of proteins with significant potential to provide benefits for human health [1, 2, 3].

[a] *Universitatea Dunarea de Jos, Facultatea de Stiinta si Ingineria Alimentelor, Str. Domneasca, Nr. 111, RO-800201 Galati, Romania.*
[*] *Corresponding author: livia.patrascu@ugal.ro*

Technological processing of vegetable foods products might involve passing through an emulsified state before becoming final ready to eat products, such as pate or cake batters. Knowledge of the rheological characteristics of the emulsion state, is crucial for efficient handling the quality of the final product, because many of the sensory attributes of food emulsions like creaminess, thickness, smoothness, spreadability, pourabilty, flowability, brittleness, and hardness are directly related to their rheological properties [4].

Many studies report on the properties of vegetable emulsions containing leguminous proteins from lupine, soy, broad bean or pea as emulsifiers and stabilizers [5, 6, 7, 8, 9, 10]. When referring to emulsion based foodstuff, lipid peroxidation is one of the major concerns, and emulsifying the protein sources in their natural matrices containing bioactive compounds is an appealing alternative to synthetic antioxidants in fighting free radicals. In this respect, leguminous seeds represent important sources of natural antioxidants such as phenolic compounds like flavanols and condensed tannins, tocopherols, and vitamin C [11]. However, thermal treatment at high temperatures was reported to decrease the antioxidant properties of pulses, while increasing the amount of total available phenols [12]. On the other hand, Xu and Chang [13] stated that processing the pulse legumes through cooking decreased both antioxidant capacities and total phenolic, while Chakraborty and Bhattacharyya [14] reported increasing the antioxidant capacities for some pulses. These differences are due to different cooking methods applied in different studies for pulses treatment.

The physicochemical properties of emulsions are highly influenced by all major constituents. In particular, proteins influence both emulsion formation and stability. The ratio between polar and non-polar groups within protein structure is considered one of the major factors that modulate proteins functionality as emulsifiers. Also, the properties of the oil phase influence the texture and spreadability of the final products [15]. The ratio between linear saturated fatty acids and branched unsaturated fatty acids in oils was reported to mainly determine the performances of the oils in stabilizing the emulsion structure [4]. However there is limited knowledge regarding the effect of oil nature on the physicochemical characteristics of the emulsion based gels. To the best of our knowledge there is no scientific data on proteins emulsifying capacity as a function of oil type.

On the other hand, there is the increasing interest for minimally processed products with short ingredient list and high nutritional functionality [16, 17]. In line with the FAO mission of increasing the awareness on the importance of developing sustainable food production based on pulses, and also considering the new trends in human nutrition the present study was focused on minimally refined flours from red and green lentils and broad

beans for substituting the highly processed forms of the soy bean. The aim of the study was to emphasize the effect of different oil types on antioxidant activity and rheological characteristics of pulses flour based emulsions and thermally induced gels. Three frequently used food grade oils were tested, namely sunflower, canola and palm oils.

RESULTS AND DISCUSSION

Emulsifying capacity

The emulsifying capacity of the pulse flours was estimated as volume of oil required for emulsion break down due to phase inversion, and was compared to the soy protein concentrate (Figure 1) which is commonly used in a large variety of food products due to the good emulsifying properties.

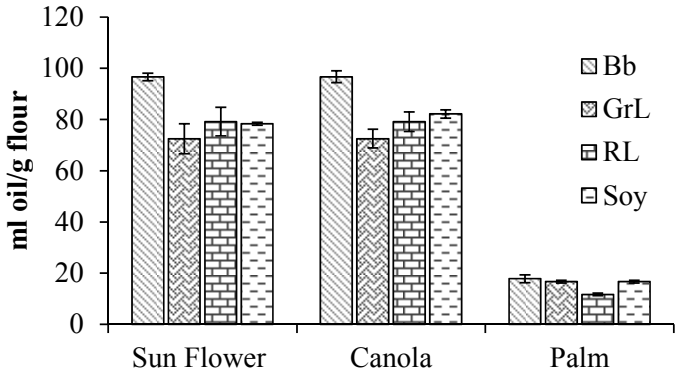

Figure 1. The influence of selected oils on emulsifying capacity of proteins

The emulsifying capacity of proteins is influenced by the molecular structure of the compounds prevailing in the composition of the oils, and in particular by the ratio between saturated and unsaturated fatty acids [4]. The fatty acids composition of the oils considered in the study is given in Table 1. As one can see, canola oil presented the least percentage of saturated fatty acids, with the ratio of saturated and unsaturated acids of 1:13.38, followed by sunflower oil with the ratio of 1:9. Palm oil had the highest quantity of saturated fatty acids with a ratio of saturated and unsaturated acids of 1:1.3.

Regardless of the protein source, the emulsifying capacity resulted fairly similar in case of emulsions prepared with sunflower and canola oils ($p>0.05$), with slightly higher values in case of soy-canola oil emulsion compared to

soy-sunflower oil emulsion. All investigated protein sources displayed limited capacity to form emulsions in combination with palm oil (Figure 1). The limited capacity of the protein derivatives to form emulsions with palm oil might be due to fat destabilization as a consequence of crystallization phenomena. Moreover, in case of the palm oil based emulsions the consistency of the system during the entire period of emulsification was observed to be significantly lower compared to sunflower or canola oil where thick emulsions were obtained before the breakdown.

Table 1. Oils composition in saturated acids according to label

Oil type	**Declared composition**
Sunflower	Lipids – 97 % from which saturated – 10.1% monounsaturated – 83.6% polyunsaturated – 3.9%
Canola	Lipids – 92 % from which saturated – 6.4% monounsaturated – 58.7% polyunsaturated – 26.9%
Palm	Lipids – 100 % from which saturated – 43% monounsaturated – 45% polyunsaturated – 12%

Available scientific reports indicate that protein emulsions with 10 to 20 wt% palm oil concentrations were passed through a high-pressure valve homogenizer in order to reduce droplet size and to assure thus emulsion stability [22, 20].

Emulsions stability

Emulsions instability and break down is known to be dictated by many physicochemical processes. Several studies indicate different mechanisms leading to emulsion destabilization, such as Ostwald ripening, creaming, gravitational sedimentation and flocculation, spontaneous coalescence and coalescence under stress [26, 22].

The stability of the investigated emulsions over 24 hours of storage at 10°C is presented in Figure 2. The destabilization of the emulsions with droplet sizes larger than a few microns mainly occurs due to creaming and sedimentation phenomena. According to our results the stability of the emulsions was mainly influenced by the protein sources rather than the nature of oil. As one can see the most stable formulations were those based on soy protein concentrate with no separated phases. In case of broad bean based emulsions, only the sample prepared with palm oil separated a liquid

phase. Regardless of the oil used for preparing the emulsions, all lentils flour based samples separated liquid and/or foam phases. However, the lowest stability with 2 - 2.5 cm^3 of total separated phase was observed in case of the red lentils based emulsions (Figure 2).

Radical scavenging activity

Because different classes of antioxidants respond to different analytical methods, three types of assays were used in order to cover both hydrogen atom transfer mechanism (ABTS radical scavenging method) and electron transfer mechanism (DPPH radical scavenging assay and total phenols) [27].

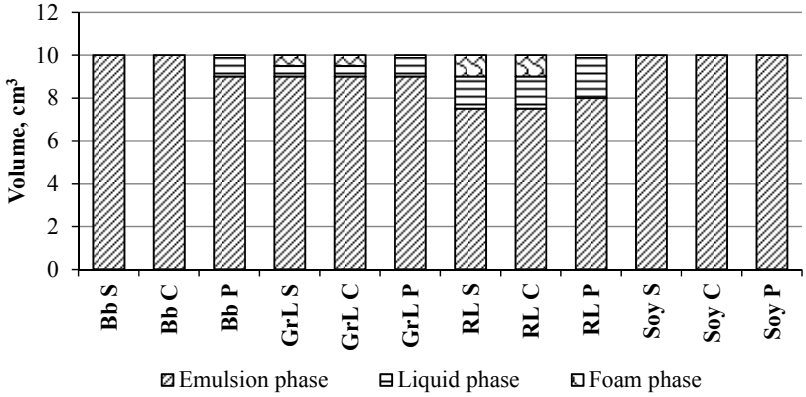

Figure 2. Stability of the emulsions prepared with broad bean (*Bb*), red lentils (*RL*) or green lentils (*GrL*) flours and sun flower (*S*), canola (*C*) or palm (*P*) oil after 24 h of storage at 10°C

The antioxidant properties were determined for pulses flours, derived emulsions and heat-set gels, and were compared to the soy protein concentrate (Table 2).

Table 2. Proximal composition and antioxidant capacity of protein derivatives used in the present study

	Broad bean flour	Green Lentil flour	Red Lentil flour	Soy Protein Concentrate
Moisture, %	9.76±0.05	11.51±0.04	8.49±0.12	9.52±0.09
Total protein, %	21.61±0.00	21.59±0.21	21.81±0.09	74.28±0.47
Total phenolics, FA mg/g	8.31±0.15	5.15±0.02	3.44±0.01	7.18±0.01
EC50 of DPPH, mg	10.26±0.03	12.55±0.00	28.92±0.01	25.72±0.00
TEAC, µmol Trolox/g	11.01±0.11	9.07±0.01	3.93±0.01	4.88±0.01

Total phenolic content is highly important, as the phenolic compounds were reported to be related with many health benefits and also were found responsible for most of the antioxidant properties of the methanolic extracts of pulse seeds [28]. In addition, Elias et al. [29] reported that proteins can act as antioxidants in food products, through multiple mechanisms such as inactivation of reactive oxygen species, scavenging free radicals, chelation of prooxidative transition metals, reduction of hydroperoxides, and alteration of the physical properties of food systems.

The highest total phenolic content was obtained for the broad bean flour, followed by soy protein concentrate, green lentil and red lentil (Table 2). Higher phenolic content for green lentil in comparison to red lentil was also reported by Amarowicz et al. [30, 31]. The high content of polyphenols in the broad bean flour can be explained by the presence of insoluble fiber content (hulls) that are known to concentrate most polyphenols of the bean seeds. Antioxidant activity in terms of EC50 of DPPH and TEAC presented a similar trend to total phenolic content in case of pulse flours. The highest DPPH radical scavenging activity was recorded for broad bean flour while for red lentil flour was registered the lowest activity. Despite the high content of total phenols, the DPPH radical scavenging activity and TEAC of the soy protein concentrate was fairly low. The antioxidant activity of the soy protein derivatives is mainly due to polyphenolic compounds like isoflavones (genistein and daidzein) [32], chlorogenic acid isomers, caffeic acid and ferulic acid [33]. However, soybean isoflavones and their glycosides were found to be no effective in scavenging the DPPH free radicals [34, 32].

The antioxidant properties of emulsions and gels were correlated with data obtained for the corresponding protein sources (Table 3). Thus trend of the antioxidant potentials of the emulsions and gels resulted as follows: red lentil < soy < green lentil < broad bean. As expected, the type of oil used to prepare the emulsions had no significant effect on the total phenolic content ($p>0.05$). In case of the DPPH antioxidant activity significant differences were obtained between groups defined based on the oil nature ($p<0.05$), both for emulsions and gels. The highest DPPH radical scavenging activity was obtained in case of samples prepared with sun flower oil, followed by those with palm and canola oils. Thermal treatment determined a significant decrease of DPPH radical scavenging activity in case of all gel samples ($p<0.05$). As a general trend TEAC antioxidant activity presented no significant differences after thermal treatment ($p>0.05$), with slight differences only in case on broad bean based emulsions and gels.

Rheological behavior

Rheological behaviour of the tested food grade oils is presented in Figure 3 as viscosity and shear stress responses to the applied shear rate.

Canola and sunflower oils presented Newtonian behavior, while palm oil showed a shear thinning behavior with a yield stress of 25.64 Pa and a slightly visible thixotropy area of 1040 Pa/s (determined with Hershel-Bulkley equation).

Table 3. Antioxidant capacity of obtained emulsions and heat-set gels

Samples		Total phenolics, FA mg/g	EC50 of DPPH, mg	TEAC, µmol Trolox/g
Emulsions	Soy+Sunflower	2.16±0.01	227.68±0.01	0.67±0.01
	Soy+Canola	2.14±0.01	205.28±0.01	1.16±0.01
	Soy+Palm	2.14±0.01	212.30±0.01	1.08±0.01
	Broad bean+ Sunflower	2.33±0.01	43.64±0.01	2.68±0.01
	Broad bean+Canola	2.30±0.01	47.10±0.01	2.62±0.01
	Broad bean+Palm	2.31±0.01	46.58±0.01	2.51±0.01
	Green Lentil+ Sunflower	0.83±0.01	78.85±0.01	1.79±0.01
	Green Lentil+Canola	0.81±0.01	82.64±0.01	1.53±0.01
	Green Lentil+Palm	0.81±0.01	79.22±0.01	2.13±0.01
	Red Lentil+ Sunflower	0.55±0.01	396.55±0.01	1.20±0.01
	Red Lentil+Canola	0.53±0.01	516.62±0.01	0.78±0.01
	Red Lentil+Palm	0.55±0.01	451.90±0.01	0.97±0.01
Gels	Soy+ Sunflower	2.72±0.01	127.67±0.01	1.14±0.01
	Soy+Canola	2.69±0.01	147.52±0.01	1.73±0.01
	Soy+Palm	2.71±0.01	135.47±0.01	1.62±0.01
	Broad bean+ Sunflower	2.99±0.01	40.93±0.01	3.11±0.01
	Broad bean+Canola	2.97±0.01	42.83±0.01	3.71±0.01
	Broad bean+Palm	2.98±0.01	41.72±0.01	3.41±0.01
	Green Lentil+ Sunflower	0.99±0.01	61.07±0.01	1.62±0.01
	Green Lentil+Canola	0.96±0.01	64.20±0.01	2.38±0.01
	Green Lentil+Palm	0.98±0.01	63.78±0.01	2.13±0.01
	Red Lentil+ Sunflower	0.78±0.01	213.27±0.01	0.81±0.01
	Red Lentil+Canola	0.78±0.01	247.55±0.01	0.85±0.01
	Red Lentil+Palm	0.76±0.01	231.23±0.01	0.96±0.01

When studying palm oil rheological behavior as influenced by crystallization, Tarabukina et al. [35] identified the 17-22°C range as the onset of crystallization process. At room temperature, palm oil is a semi-solid material

with rheological properties depending on the amount, size and tri-dimensional organization of its fat crystal network [35]. Viscosity values resulted fairly similar for sunflower and canola oils ($p>0.05$), and significantly different compared to the palm oil. Our results comply with the observation of Santos et al. [36], who reported a Newtonian behavior for different edible oils, through which sunflower and rape seed, at temperatures ranging between 10 and 80°C.

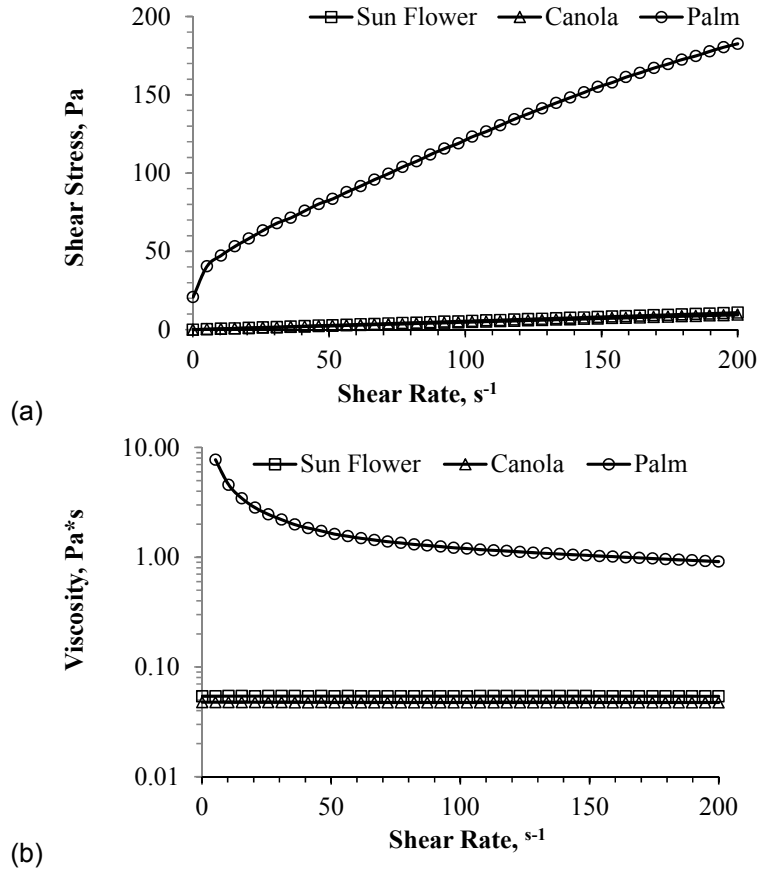

Figure 3. Evolution of shear stress (a) and viscosity (b) of selected vegetable oils under forced flow conditions

Rheological behavior of the obtained emulsions was studied at 20°C in low amplitude oscillatory conditions, by increasing the strain values from 0.01 to 100% at a constant frequency of 1 Hz. Emulsions obtained from broad bean (Figure 4a) and lentil flour (Figure 4 b and c) presented no stability no

LVR was registered), displaying even from the beginning of the tested strain interval a behavior specific to the transition phase, when particles just start moving. Soy protein emulsions prepared with sunflower and canola oils presented limited structure stability, with LVR up to a critical strain of 1%, while emulsion obtained with palm oil resisted only up to ~ 0.5% strain. In all studied protein sources the highest G` values were obtained for the emulsions prepared with palm oil. The G` and G`` values were significantly influenced by the flour type. The lowest G` and G`` values, ranging from 1 to 3 Pa, were obtained for red lentils based emulsions, followed by green lentils and broad bean. The emulsions based on soy protein concentrate presented the highest G` and G`` values, revealing a strong solid like behavior with G` values up to 5000 Pa, and the lowest delta values of ~ 9° in the linear viscoelastic region (data not presented).

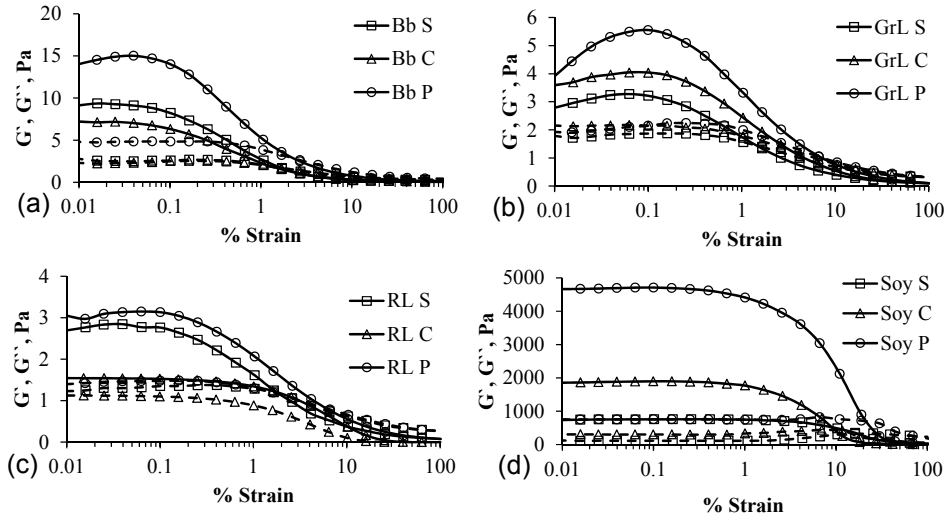

Figure 4. Rheological behavior, under strain sweep, of the emulsions based on broad bean flour (a), red lentils flour (b), green lentils flour (c) and soy protein concentrate (d). Emulsions were prepared with sunflower (*S*), canola (*C*) or palm (*P*) oils. Full lines stand for G`, dashed lines stand for G``; *Bb* - broad bean flour, *RL* - red lentils flour, *GrL* - green lentils flour

The proper beginning of flow, also known as the yield point, was determined as the strain value at G`/G`` crossover as represented in Table 4. In case of most proteins sources the canola oil based samples had the earliest beginning of flow, followed by sunflower and palm oils. When discussing the influence of the protein source on the yield point, generally the lowest values were obtained in case of broad bean based emulsions, followed by lentils and soy protein derivative.

The heat-set gels presented similar viscoelastic characteristics for the three investigated pulse flours, with strong solid like behaviors as can be seen in Figure 5.

Table 4. Yield point of pulse flour based emulsions and gels determined as the strain value (%) at G`/G`` crossover

	Sample	Sunflower Oil	Canola Oil	Palm Oil
Emulsions	Soy	15.52±0.98%	9.28±0.05	25.31±1.12
	Broadbean	2.13±0.15%	1.33±0.78	2.68±0.10
	Green Lentil	1.65±1.02%	3.15±0.22	8.38±0.06
	Red Lentil	4.13±1.17%	4.05±0.84	6.61±0.43
Gels	Soy	22.21±0.66%	22.51±1.54	22.49±1.34
	Broadbean	33.50±1.83%	35.95±2.02	17.38±0.80
	Green Lentil	40.00±1.68%	18.44±0.70	10.61±0.04
	Red Lentil	31.99±0.31%	34.72±0.64	33.17±0.51

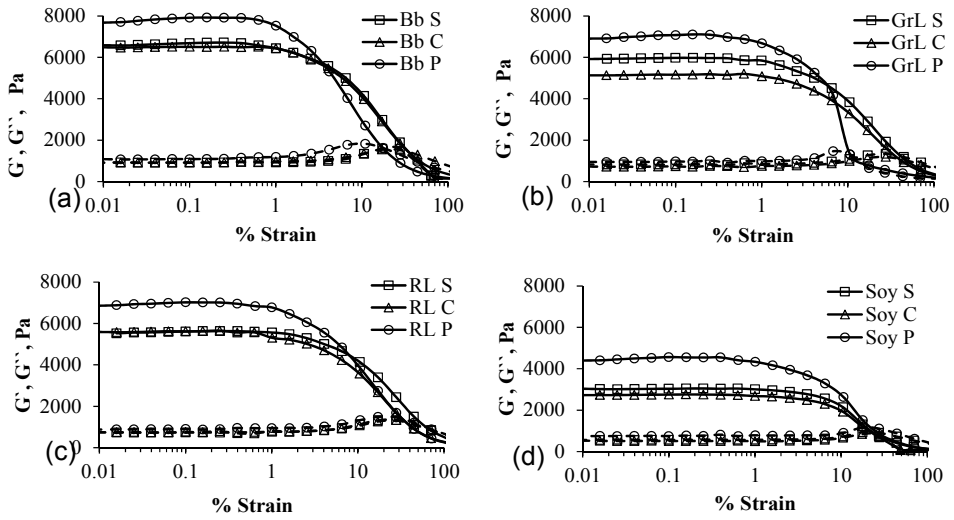

Figure 5. Rheological behavior of obtained heat –set gels under strain sweep (broad bean (*Bb*), red lentils (*RL*), green lentils (*GrL*) flours, sun flower (*S*), canola (*C*), palm (*P*)). Full lines stand for G` and dashed lines stand for G``

The high G` values in case of pulse flour based gels are explained by the presence of polysaccharides and fibers [18], but also by the protein unfolding during thermal treatment that favored the development of a stable entangled network [37]. Lower G` values were obtained in case of soy protein based gels in comparison to emulsions. It seems that at pH values higher than 5 the thermal treatment softens the structure of the soy proteins gels, due to the decreased number of protein molecules involved in establishing the network [38]. In case of all studied gels the structure remained unchanged up to strain values of 1%, marking the end of the linear viscoelastic region. The yield point values of the gels appeared at significantly higher strain values compared to the emulsions. A particular behavior was observed for gels obtained with palm oil. In case of emulsions the samples with palm oil presented the highest G`/G`` crossover strain value, whereas after gel formation higher yield point values were determined for samples prepared with sunflower and canola (Table 4). No influence of oils on yield point of soy protein based gels was noticed.

CONCLUSIONS

The emulsifying capacity of the flours obtained from broad beans, green and red lentils is comparable to the soy protein concentrate. Regardless of the protein source, no significant difference in terms of emulsifying capacity and emulsions properties were found between samples prepared with sunflower and canola oils. All studied protein sources presented limited capacity to form emulsions in combination with palm oil which could be given by fat destabilization due to crystallization phenomena. The stability of the emulsions varied significantly with protein source and the oil type. The antioxidant activity of emulsions and heat-set gels was significantly influenced by the protein source. Rheometric measurements showed that sunflower and canola oils are Newtonian fluids, while palm oil behaved as a thixotropic fluid. Moreover, a strong solid like behavior was observed for the palm oil containing emulsions. Even if the rheological tests performed on emulsions indicated the significant influence of both protein sources and oil type, after the thermal treatment no important differences were found between samples prepared with different oils. Finally it can be stated that, given the high content of saturated fatty acids, the palm oil alone is not suitable for obtaining stable emulsions and further heat-set gels, while oils with high ratios of saturated *vs*. unsaturated acids ratio presented similar technological and functional characteristics.

EXPERIMENTAL SECTION

Materials

Three different pulses, namely broad beans (*Vicia faba*), red and green lentils (*Lens culinaris*) purchased from a local store (Galati, Romania), were considered in the study. The pulse flours were obtained at laboratory scale as specified by Patrascu et al. [18]. Proximal composition of obtained samples is presented in Table 1. Because the majority of foodstuff that implies the use of vegetable proteins is based on soy protein derivatives (concentrates and isolates), a soy protein concentrate (Ubimedia S.R.L., Galati, Romania) was used as control.

Three different food grade refined vegetable oils were considered for the investigations: bottled sunflower (produced in Romania), canola (produced in Romania) and palm (produced in Malaysia) oils purchased from a local supermarket (Galati, Romania). All materials were stored in dark conditions at room temperature until use.

All chemicals used in the experiments were of analytical grade. The reagents 1,1-diphenyl-2-picrylhydrazyl (DPPH), 6-hydroxy-2,5,7,8-tetramethyl-chroman-2-carboxylic acid (Trolox), 2,2-azinobis(3-ethylbenzothiazoline-6-sulfonic acid) diammonium salt (ABTS) and ferulic acid were purchased from Sigma Aldrich Chemie GmbH (Taufkirchen, Germany), while Folin Ciocalteu reagent was purchased from Merck and Co., Inc. (New York, USA).

Proximate composition

The physicochemical composition of the obtained pulse flours was determined using the following methods: the moisture content through the AACC 44-51 method (AACC International, 2000); the protein content using the semimicro-Kjeldahl method (Raypa Trade, R. Espinar, S.L., Barcelona, Spain).

Emulsifying capacity

In order to assess the emulsifying capacity of pulse flours and soy protein concentrate as a function of selected oils the method proposed by Ionescu et al. [19] was used. First suspensions of 6% (w/v) concentration were prepared in 0.2M phosphate buffer of pH 7. The oil was progressively added to the suspensions, using a laboratory burette, under continuous stirring with a 650W Philips blender, until the inversion point of the emulsion was observed. The emulsifying capacity was reported as ml of oil/g flour. In the case of palm oil, a preliminary melting was performed through storage for 24 h at 40°C. In order to prevent crystallization a similar palm oil preparation for emulsion formation was applied by Pongsawatmanit et al. [20].

Emulsion preparation

Suspensions were first prepared by adding 65 ml of tap water to 15 g of pulse flour under continuous manual stirring. The concentration of the pulse flour suspensions was established by first determining the least gelling concentration using the method described by Ogunwolu et al. [21]. A volume of 20 ml of oil was then added to the homogenous mixture while mixing the ingredients at 1500 rpm with a Philips RH13 vertical mixer for 5 minutes.

It is commonly accepted that a true emulsion consists of two phases, oil and water, with the dispersed droplet size between 0.1 and 100 μm. Taking into account that the protein derivatives used in the present study had particles size lower than 500 μm, we consider that the obtained system is an O/W emulsified protein dispersion. Anyway, for convenience the term *emulsion* will be further used in the paper.

Emulsion stability

The stability of the emulsions over 24 h of storage at 10°C was determined by filling a known quantity of emulsion (10 ml) into laboratory tubes and measuring phase separation. In agreement with the method of Thanasukarn et al. [22] with modifications, the separated layers were visually estimated at the end of the resting period. In our study the following phases were considered: “emulsion phase” which is a layer similar to the initial emulsion, “liquid phase” an intermediate white watery layer with little traces of free oil, and “foam phase” a dense and more opaque phase separated on the top of the emulsion.

Heat-set emulsion gels

Fresh emulsions were poured into glass containers, hermetically sealed with food grade metal caps and thermally treated in a water bath (JSWB-06T, JSR) by increasing the temperature with ~1.5°C/min until 90°C, where was maintained for 30 minutes. The obtained products had a paté like structure, and were further termed gels. All samples were stored at 10±1°C for further analysis.

Radical scavenging activity

In order to investigate the antioxidant activity of obtained emulsions, gels and flours, first a methanol extraction of active compounds was carried. The extraction of the active compounds from pulse flours, emulsions and gels responsible for the antioxidant activity was performed by mixing 1 g of sample with 10 mL of 80% aqueous methanol solution, followed by stirring for 2 h at room temperature using a magnetic stirrer at 300 rpm and centrifugation at 9,690×g for 10 minutes.

Determination of total phenolic contents

The concentration of total phenolic compounds was determined using the Folin-Ciocalteu method proposed by Deng et al. [23] with slight modification. A volume of 0.2 ml of extract solution was mixed with 1.5 mL Folin-Ciocalteu reagent, previously diluted with water 1:10, v/v. The mixture was kept at room temperature for 10 min, and then 1.5 mL of 60 g/L sodium carbonate was added. After 90 min of reaction at room temperature, absorbance was read at 725 nm. Acidified methanol was used as blank. Results were expressed as mg ferulic acid equivalents (FAE)/g sample.

DPPH-radical scavenging assay

Volumes of 0.1 mL extracts were added to 3.9 mL DPPH in methanol solution of 6×10^{-5} mol. A control sample containing the same volume of solvent in place of extract was used to measure the maximum DPPH absorbance. After a resting period of 30 min in dark conditions the absorbance was recorded at 515 nm. The DPPH radical scavenging activity was expressed as EC50 values after the method of Anagnostopoulou *et al*. [24].

Antioxidant activity by ABTS radical cation decolorization assay

ABTS assay was based on the slightly modified method of Re *et al.* [25]. ABTS radical cation ($ABTS^{\cdot+}$) was obtained by reacting 7 mM ABTS solution with 2.45 mM potassium persulphate and allowing the mixture to stand in the dark at room temperature for 12-16 h before use. The $ABTS^{\cdot+}$ stock solution was then diluted with ethanol to an absorbance of 0.70 ± 0.02 at 734 nm. After addition of 20 µL of sample to 1.48 mL of diluted $ABTS^{\cdot+}$ solution, absorbance was measured after exactly six min. The antioxidant activity was expressed as micromoles of Trolox equivalent antioxidant capacity (TEAC) per gram of sample.

Rheological tests

Rheological characterization of oils, emulsions and gels was performed by using a control-stress Rheometer (AR2000ex, TA Instruments), equipped with a Peltier jacket temperature control system. A cup and conical cylinder geometry assembly was used, with the bob diameter of 28 mm and 42 mm in length.

Rheological characteristics of considered oils were studied at 20°C under forced flow conditions, by submitting samples to a stepped flow test. Shear rate was increased from 0.1 to 200 s^{-1} and then decreased back to 0.1 s^{-1}. Results were plotted as the shear stress response/viscosity *vs.* shear rate, in order to determine the hysteresis formed by the destructured - restructured material. The thixotropic behavior was estimated as the decreasing viscosity under increasing shear rate. When appropriate (namely in the case of palm oil),

data were analyzed with Herschel-Bulkley equation: $\sigma = \sigma_y + \eta \times \dot{Y}^n$, where σ = shear stress (Pa); σ_y = yield stress (Pa); η = viscosity (Pa·s); $\dot{Y}$ = shear rate (s^{-1}); n = rate index, also known as flow behavior index (dimensionless).

Rheological properties of emulsions and gels were analyzed under oscillatory flow in small amplitude conditions, by performing a strain sweep test under increasing strain from 0 to 100%, with an oscillation frequency of 1 Hz. The linear elastic region and the beginning of flow were determined as described by Patrascu et al. [18].

Statistical analysis

Statistical analysis was performed using Microsoft Excel Software. The data were subjected to ANOVA Single Factor, considering a significance level of 95%. Each experiment was carried out in duplicate and the results were reported as mean values.

ACKNOWLEDGEMENTS

This work was supported by a grant of the Romanian National Authority for Scientific Research and Innovation, CNCS – UEFISCDI, project number PN-II-RU-TE-2014-4-0618.

REFERENCES

1. E. Makri, E. Papalamprou, G. Doxastakis, *Food Hydrocolloids,* **2005**, *19*, 583.
2. C. Bassett, J. Boye, R. Tyler, B.D. Omah, *Food Research International*, **2010**, *43*, 397.
3. K. Crépon, P. Marget, C. Peyronnet, B. Carrouée, P. Arese, G. Duc, *Field Crops Research*, **2010**, *115*, 329.
4. D.J. McClements, "Food emulsions: principles, practices, and techniques", CRC Press, **2004**, chapter 1.
5. A. Raymundo, J.M. Franco, J. Empis, I. Sousa, *Journal of the American Oil Chemists' Society*, **2002**, *79*, 783.
6. W. Jang, A. Nikolov, D.T. Wasan, K. Chen, B. Campbell, *Industrial and Engineering Chemistry Research*, **2005**, *44*, 4855.
7. R.R. Roesch, M. Corredig, *Journal of Food Science-Chicago*, **2002**, *67*, 2837.
8. F. Donsì, B. Senatore, Q. Huang, G. Ferrari, *Journal of Agricultural and Food Chemistry*, **2010**, *58*, 10653.
9. A.C. Karaca, N. Low, M. Nickerson, *Food Research International*, **2011**, *44*, 2742.
10. Y. Ladjal-Ettoumi, H. Boudries, M. Chibane, A. Romero, *Food Biophysics*, **2016**, *11*, 43.
11. R. Amarowicz, R. B. Pegg, *European Journal of Lipid Science and Technology*, **2008**, *110*, 865.
12. H. Han, B.K. Baik, *International Journal of Food Science and Technology*, **2008**, *43*, 1971.
13. B.J. Xu, S.K.C. Chang, *Journal of Food Science*, **2008**, *73*, H19.

14. A. Chakraborty, S. Bhattacharya, *Journal of Applied Pharmaceutical Science*, **2014**, *4*, 65.
15. D.P. Moran, "Fats in Food Products", Springer US, **1994**, chapter 5.
16. R.K. Keservani, R.K. Kesharwani, N. Vyas, S. Jain, R. Raghuvanshi, A.K. Sharma, *Der Pharmacia Lettre,* **2010**, *2*,106.
17. I. Goldberg, "Functional Foods: Designer foods, Pharmafoods, Nutraceuticals" Springer Science and Business Media, **2012**.
18. L. Patrascu, I. Banu, I. Vasilean, I. Aprodu, *Food Science and Technology International,* **2017**, *9(1)*,67.
19. A. Ionescu, I. Aprodu, M. Zara, G. Gurau, *The Annals of the University Dunarea de Jos of Galati–Food Technology*, 2009, *32(1)*, 9.
20. R. Pongsawatmanit, T. Harnsilawat, D. J. McClements, *Colloids and Surfaces A: Physicochemical and Engineering Aspects*, **2006**, *287*, 59.
21. S.O. Ogunwolu, F.O. Henshaw, H.P. Mock, A. Santros, S.O. Awonorin, *Food Chemistry*, **2009**, *115*, 852.
22. P. Thanasukarn, R. Pongsawatmanit, D.J. McClements, *Food Hydrocolloids*, **2004**, *18*, 1033.
23. G.F. Deng, X. Lin, X.R. Xu, L.L. Gao, J.F. Xie, H.B. Li, *Journal of Functional Foods*, **2013**, *5*, 260.
24. M.A. Anagnostopoulou, P. Kefalas, V.P. Papageorgiou, A.N. Assimopoulou, D. Boskou, *Food Chemistry*, **2006**, *94*,19.
25. R. Re, N. Pellegrini, A. Proteggente, A. Pannala, M. Yang, C. Rice-Evans, *Free radical biology and medicine*, **1999**, *26*, 1231.
26. D. Langevin, S. Poteau, I. Hénaut, J.F. Argillier, *Oil and Gas Science and Technology*, **2004**, *59*, 511.
27. E. Shalaby, S. Shanab, *African Journal of Pharmacy and Pharmacology,* **2013**, *7*, 528.
28. B.A. Cevallos-Casals, L. Cisneros-Zevallos, *Food Chemistry*, **2010**, *119*, 1485.
29. R.J. Elias, S.S. Kellerby, E.A. Decker, *Critical reviews in food science and nutrition,* **2008**, 48, 430.
30. R. Amarowicz, I. Estrella, T. Hernández, M. Dueñas, A. Troszynska, A. Kosinska, *International Journal of Molecular Sciences*, **2009**, *10*, 5513.
31. R. Amarowicz, I. Estrella, T. Hernández, S. Robredo, A. Troszyńska, A. Kosińska, R. B. Pegg, *Food Chemistry*, **2010**, *121*, 705.
32. C.H. Lee, L. Yang, J.Z. Xu, S.Y.V. Yeung, Y. Huang, Z.Y. Chen, *Food Chemistry*, **2005**, *90*, 735.
33. D.E. Pratt, P.M. Birac, *Journal of Food Science,* **1979**, 44, 1720.
34. J.H. Mitchell, P.T. Gardner, D.B. McPhail, P.C. Morrice, A.R. Collins, G.G. Duthie, *Archives of Biochemistry and Biophysics*, **1998**, *360*, 142.
35. E. Tarabukina, F. Jego, J.M. Haudin, P. Navard, E. Peuvrel-Disdier, *Journal of Food Science*, **2009**, *74*, E405.
36. J. Santos, I. Santos, M. Conceição, S. Porto, M.F.S.A. Trindade, A. Souza, A. Araújo, *Journal of thermal analysis and calorimetry*, **2004**, *75*, 419.
37. A. Raymundo, J. Franco, C. Gallegos, J. Empis, L. Sousa, *Nahrung-Food*, **1998**, *42*, 220.
38. J.M. Renkema, H. Gruppen, T. Van Vliet, *Journal of Agricultural and Food Chemistry*, **2002**, *50*, 6064.

STUDIA UBB CHEMIA, LXIII, 1, 2018 (P. 215-237)
(RECOMMENDED CITATION)
DOI:10.24193/SUBBCHEM.2018.1.16

CALCIUM HYDROXYAPATITE SUPPORTED COBALT CATALYSTS FOR ETHANOL STEAM REFORMING: EFFECT OF THE INCORPORATION METHOD OF ACTIVE PHASE

JUSTYNA DOBOSZ[a], SYLWIA HULL[b], MIROSŁAW ZAWADZKI[a,*]

ABSTRACT. Cobalt catalysts supported on calcium hydroxyapatite ($Ca_{10}(PO_4)_6(OH)_2$, HAp) and modified with cerium ions were prepared in two different ways: direct microwave-assisted hydrothermal synthesis or incipient wetness impregnation method and characterized by XRD, TEM, SEM/EDS, FT-IR and Raman spectroscopy, N_2 adsorption–desorption, TPD–NH_3, TPR–H_2 and XPS. The results indicate that Ca^{2+} ions in the hydroxyapatite lattice are substituted by Co^{2+} and Ce^{3+} under hydrothermal conditions while cobalt and cerium species are formed on the HAp surface during support impregnation. Catalytic activity of samples was tested for hydrogen production via ethanol steam reforming (SRE), and it was found that the highest hydrogen yield (over 3,5 mol H_2/mol C_2H_5OH) and the best distribution of products were obtained for the catalyst prepared by the incipient wetness impregnation method. For this catalyst, Co species formed on the HAp surface was easier reducible than Co^{2+} ions located in the HAp crystal lattice, and surface was characterized by lower acidity.

Keywords: *Cobalt Catalysts, Hydroxyapatite, Hydrothermal Synthesis, Ethanol Steam Reforming*.

INTRODUCTION

Hydrogen is defined as the energy carrier of the future due to its the highest energy content per unit of weight (120,7 kJ/g) [1]. Additionally, it burns cleanly, without pollutants emission such as SO_x, NO_x, CO or volatile

[a] *Institute of Low Temperature and Structure Research, Department of Nanomaterials Chemistry and Catalysis, Polish Academy of Sciences, PO Box 1410, 50–950 Wrocław, Poland.*
[b] *Wrocław University of Technology, Division of Chemistry and Technology Fuels, Gdańska 7/9, 50 - 344 Wrocław, Poland.*
[*] *Corresponding author: m.zawadzki@int.pan.wroc.pl*

organic compounds (VOC). Nowadays, approximately 95% of hydrogen is produced through the steam reforming of natural gas [2]. However, the depletion of fossil fuel resources and growing environmental problem tend to seek a new method of hydrogen production. The steam reforming of ethanol (SRE) is considered to be a promising approach for obtaining H_2 from an environmentally friendly and renewable energy source. In addition to typical features of bio-based fuels (for example CO_2 neutrality), ethanol can be produced by fermentation of biomass such as sugar cane, corn, and their waste material. Moreover, it is characterized by relatively high hydrogen content, easy storage, safe handling, wide availability and significant lower toxicity than methanol [3]. Theoretically, this method of hydrogen production assumes the formation of only two products: hydrogen and carbon dioxide, according to the reaction (1):

$$C_2H_5OH + 3H_2O \rightarrow 2CO_2 + 6H_2 \qquad \Delta H_{298} = 174 \text{ kJ mol}^{-1} \qquad (1)$$

However, in practice selectivity toward H_2 can be governed by a number of other reactions with the formation of several intermediates and by-products [4-5]. The main pathways include the following reactions:

$$C_2H_5OH \rightarrow CO + CH_4 + H_2 \quad \text{(ethanol decomposition)} \qquad (2)$$
$$C_2H_5OH + H_2O \rightarrow 2CO + 4H_2 \quad \text{(incomplete reforming)} \qquad (3)$$
$$CO + H_2O \leftrightarrow CO_2 + H_2 \quad \text{(water – gas shift, WGS)} \qquad (4)$$
$$C_2H_5OH \rightarrow CH_3CHO + H_2 \quad \text{(dehydrogenation)} \qquad (5)$$
$$C_2H_5OH \leftrightarrow C_2H_4 + H_2O \quad \text{(dehydration)} \qquad (6)$$
$$CO + 3H_2 \leftrightarrow CH_4 + H_2O \quad \text{(methanation)} \qquad (7)$$
$$2CO \leftrightarrow C + CO_2 \quad \text{(Boudouard reaction)} \qquad (8)$$
$$2C_2H_5OH \rightarrow CH_3COCH_3 + CO + 3H_2 \quad \text{(ethanol decomposition)} \qquad (9)$$

The occurrence of particular reaction during SRE process depends on the nature of catalysts used and the reaction conditions [5].

Catalysts utilize in SRE could be divided into three groups: noble metal catalysts, base metal catalysts and oxide catalysts [6]. Noble metal catalysts (Rh, Ru, Pd, Pt or Ir based) exhibit high hydrogen yield and ethanol conversion [7]. In comparison to the base metal catalysts, the noble metal catalysts show a higher catalytic activity [8] for steam reforming of ethanol but are very expensive. Non-noble metal catalysts based on Co, Cu or Ni also exhibit good catalytic performance for hydrogen production [9-12] and are less expensive alternative. Among them, especially cobalt-based materials are reported as catalysts ensuring a high conversion of ethanol and selectivity to hydrogen as well as good products distribution due to their capacity for

C–C bond cleavage [9-10]. However, cobalt catalysts can be easily deactivated by carbon deposition or sintering. To prevent against deactivation process, cerium ions are used. Ceria, in fact, limits ethanol dehydration to ethylene (a well-known coke precursor), contributes to water gas shift reaction, due to its excellent oxygen mobility, promotes the gasification/oxidation of deposited carbon as soon it forms [13]. Nevertheless, to improve the performances of these catalysts, a suitable support and its convenient preparation method should be used.

Several compounds have been studied as supports or host of Co based catalysts [14]. Co supported on Al_2O_3, ZrO_2 and TiO_2 were studied by Song et al. [15] and they found that Co/ZrO_2 showed the best dispersion and the best catalytic activity in SRE. Over the 10wt%Co/ZrO_2 catalyst, using water to ethanol molar ratio of 10:1 and GHSV=5000 h^{-1}, a total conversion and yield of 5.5 mol H_2/mol EtOH were obtained at 550 ^oC. In the study conducted by Batista et al. [16], Co/Al_2O_3 (8.6 wt%), Co/SiO_2 (7.8 wt%), and Co/MgO (18 wt%) were examined for hydrogen production via SRE process. The authors reported that all catalysts showed high catalytic activity (>90% ethanol conversion) and selectivity to hydrogen (about 70%). However, the catalysts deactivation by coke formation after 9 h time-on-stream was detected. Llorca et al. [17] prepared Co catalysts with several supports (ZnO, MgO, Al_2O_3, SiO_2, TiO_2, V_2O_5, La_2O_3, CeO_2 and Sm_2O_3) and found that Co/ZnO catalyst showed the best catalytic performances. This catalyst showed total conversion and over 40% of H_2 selectivity at 450 ^oC. Hydrotalcites have been also studied as supports of Co catalysts. Contreras et al. [18] demonstrate that addition of tungsten to the hydrotalcite produced great catalytic stability and high H_2 selectivity The addition of 1wt%W to the hydrotalcite caused an H_2 selectivity of 70% at 450 ^oC after 6 h. Lin et al. [19] observed a synergistic effect of ZrO_2 and CeO_2 to promote high ethanol conversion when $CeZrO_4$ was used as a support of Co catalyst. The $Co/CeZrO_4$ catalysts showed higher catalytic performance (to produce H_2) than Co/ZrO_2 as a result of methanation suppression. Banach et al. [20] prepared another trimetalic $Co/ZnO-Al_2O_3$ catalyst and found that alumina stabilized zinc oxide support. Among studied catalysts, 24wt%Co/ZnO+5wt%Al_2O_3 was the best for SRE process. Wang et al. [21] reported that Co_3O_4-CeO_2 catalysts were very active and selective for SRE. It was also shown by Ma et al. [22] that the presence of Co_3O_4 phase increased the reactivity toward H_2 production in Zn-doped $LaCoO_3$ catalysts. Most of these Co-based catalysts were prepared by coprecipitation and incipient wetness impregnation method, and only some of them by complexing-citrate or hydrothermal method. Apart from the nature of the support used, the synthesis conditions are also important parameters determining the activity and stability of Co-based catalyst. Kaddouri and Mazzocchia [23] reported that cobalt supported alumina and silica catalysts

prepared by different methods (impregnation, sol-gel and combination of both), exhibited various surface area, surface composition and metal dispersion. These distinct physicochemical properties resulted in an apparent difference in H_2 selectivity and products distribution. Therefore, the selection of proper support for cobalt catalyst and the methods of catalysts preparation significantly affect the activity of catalysts during SRE process.

Calcium hydroxyapatite ($Ca_{10}(PO4)_6(OH)_2$, HAp) is an inorganic compound used as biomaterial, chromatographic absorbent and catalyst [24-26]. In the field of catalysis, HAp is attractive material due to its thermal stability over a wide range of temperature, acid – base properties, high porosity, mesoporous structure and adsorption capacity [27-28]. The hydroxyapatite was found as useful catalysts support for the decomposition of methane [29], removal of oxygenated volatile organic compounds [30] and propane oxidation [31]. HAp was also investigated in reactions for hydrogen production such as glycerol steam reforming [32] and hydrolysis of sodium borohydride [33].

In the literature, several methods of nanosize hydroxyapatite synthesis have been described, for example: precipitation [30], sol – gel [34], hydrothermal reactions [35], microemulsion [36] and soft solution freezing method [37]. Among them, the hydrothermal method is one of the most interesting techniques used for the synthesis of nonoscale materials due to its simplicity, low energy consumption and good environmental aspects. It is reported as a route for obtaining well-dispersed, homogenous products with controlled shapes, sizes and structures [38]. Moreover, a combination of hydrothermal synthesis and microwave radiation reduces significantly reaction time essential to receive the proper crystal structure.

In our previous paper [39] we studied the effect of the HAp preparation method on the properties of cobalt/cerium catalysts used for SRE process. The aim of the present work was to examine the properties of these systems, including their catalytic behavior in SRE, where active metal phase was incorporated in different ways: by direct microwave-hydrothermal synthesis or incipient wetness impregnation method.

RESULTS AND DISCUSSION

XRD characterization

The phase composition and crystal structure of the studied catalysts were evaluated by XRD method and diffractogram patterns are presented in Fig. 1. XRD measurements reveal that all synthesized materials have a well–formed hexagonal hydroxyapatite structure crystallized in $P6_3/m$ space group (PDF No 09-0432). However, the substitution as well as the impregnation

with cobalt and cerium ions causes the appearance of additional peaks in the diffraction patterns. After the substitution, small peaks corresponding to cerium phosphate (PDF No. 04-0632) are observed. It indicates that only a part of Ce^{3+} ions was incorporated into the HAp crystal structure whereas the other cerium ions form a $CePO_4$ phase. Formation of $CePO_4$ on the surface of calcium hydroxyapatite substituted with cerium ions was suggested by Yasukawa et al. [40]. They reported that only 1 at% of cerium ions can be incorporated into the HAp structure. Increase of cerium content results in the formation of $CePO_4$ on the hydroxyapatite surface. In case of the impregnation sample, the cerium ions formed a cerium dioxide phase (PDF No. 02-1306) on the support surface. The XRD pattern of the catalyst prepared by impregnation method also shows the peak at 37° ascribed to Co_3O_4 phase (PDF No. 01-1152).

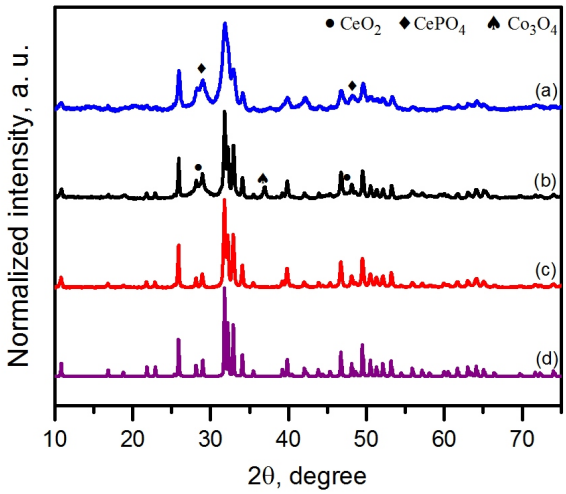

Fig. 1. XRD patterns of (a) 5Co10Ce:HAp, (b) 5Co10Ce/HAp, (c) HAp and (d) standard diffraction pattern of HAp (PDF No. 09-0432).

The unit cell parameters were calculated on the basis of peaks at around 26°, 34° and 53°, which do not overlap with any peaks of additional phases. Results (Table 1) show that lattice constants of 5Co10Ce:HAp decrease after introduction of cobalt and cerium ions due to the substitution of Ca^{2+} ions (ionic radius: 0,100 nm) by smaller Co^{2+} (ionic radius: 0,0078 nm). The ionic radius of Ce^{3+} (0,101 nm) is comparable with ionic radius of Ca^{2+} and has a slight impact on unit cell parameters.

Table 1. Unit cell parameters and values of mean crystallite size.

Sample	Cell parameters, Å			Cell volume, Å^3	Mean crystallite size, nm
	a	b	c		
HAp	9.424	9.424	6.882	529.28	35
5Co10Ce:HAp	9.421	9.421	6.867	527.81	23
5Co10Ce/HAp	9.423	9.423	6.881	529.15	35

The mean crystallite sizes were calculated from XRD patterns by using the Scherrer equation (Table 1). It should be noticed that the substitution with cobalt ions strongly affects the mean crystallite sizes of calcium hydroxyapatite. The introduction of cobalt cations into the HAp structure induces a reduction of crystallite size from 35 nm to 23 nm. For 5Co10Ce/HAp sample, the mean crystallite size is the same as for the support.

Electron microscopy analysis

TEM and SEM images of the samples are shown in Fig. 2. Electron microscopy analysis reveals a rod – like structure and nanoscale size of hydroxyapatite particles. The average length and width of pure hydroxyapatite particles are 87 nm and 28 nm, respectively (Fig. 2a).

The presence of cobalt and cerium ions leads to slight changes in the shape of HAp particles but their size is visible lower for substituted sample. Moreover, the small and spherical particles are additionally observed (Fig. 2b,c). Based on the HRTEM and SEAD images (not shown), these particles are ascribed to the cerium phosphate (Fig. 2b) or dioxide (Fig. 2c) and cobalt oxide with spinel structure. Particle sizes of cerium phases and cobalt oxide are about 10 nm and 20 nm, respectively.

Analysis of SEM images (Fig. 2d,e,f) showed that the catalysts exhibit slightly different textures depending on the preparation method. The 5Co10Ce/HAp sample is characterized by elongated grains and presented a similar morphology with pure HAp sample, whereas the 5Co10Ce:HAp material exhibits an irregular shape of particles. Various morphologies of the studied catalysts may be associated with position of cobalt and cerium ions. In substituted samples, Ca^{2+} ions were partially replaced by Co^{2+} and Ce^{3+} ions. Substitution of calcium ions by smaller cobalt ions changes the lattice parameters thus the shape of grains. In the catalyst prepared by incipient wetness impregnation method the active species are located on the support surface and no apparent changes of the initial morphology of support is detected.

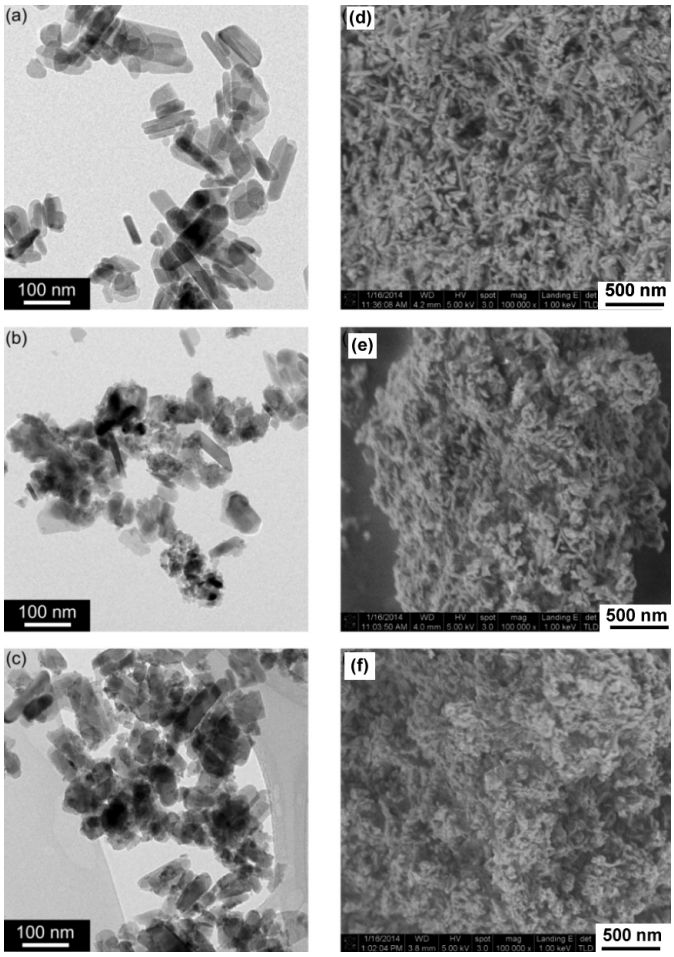

Fig. 2. Electron microscopy images of (a, d) HAp, (b, e) 5Co10Ce:HAp and (c, f) 5Co10Ce/HAp.

Chemical composition of prepared samples was analysed by the EDS measurements. As shown in Table 2, the cobalt and cerium contents are in good agreement with expected ones for 5Co10Ce:HAp catalyst. For 5Co10Ce/HAp sample, results of EDS analysis showed that cobalt and cerium contents were slightly lower than targeted ones.

To determine the pore structure and the specific surface area of the HAp samples, the N_2 adsorption – desorption isotherms method was used. According to IUPAC classification, N_2 adsorption – desorption isotherms correspond to a combination of Type II and Type IV isotherms with H3 hysteresis loop in the relative pressure (p/p_0) range of 0.8-1.0, as shown in

Fig. 3. The obvious hysteresis loop is typical for materials with interparticle mesoporosity [41]. The presence of mesopores was substantiated by BJH differential pore volume plot (*inset* to Fig. 3) indicating that most of pores are in the range 5–40 nm. It can also be noticed that HAp and 5Co10Ce/HAp sample exhibit narrow pore-size distribution with maximum at 24 nm whereas 5Co10Ce:HAp sample shows a little broader distribution of pore diameter with maximum at 20 nm.

Table 2. Results of EDS, physical sorption and TPD-NH_3 measurements.

Sample	Chemical composition, wt%		Total acidity, mmol/g·10^{-2}	Specific surface area, m^2/g	Pore volume, m^3/g
	Co	Ce			
HAp	-	-	5.51	53.13	0.34
5Co10Ce:HAp	5.09	10.04	20.71	88.62	0.37
5Co10Ce/HAp	4.64	9.65	11.99	42.19	0.20

Physical sorption

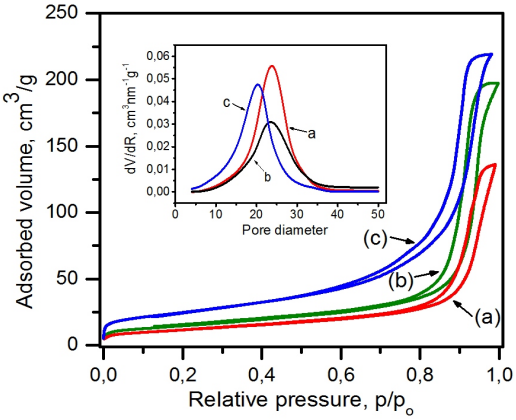

Fig. 3. N_2 adsorption - desorption isotherms of (a) HAp, (b) 5Co10Ce/Hap, (c) 5Co10Ce:HAp and corresponding pore size distributions as *inlet.*

The specific surface area and pore volume of studied catalysts are summarized in Table 2. It can be noticed that the catalyst prepared by the microwave-assisted hydrothermal method, in which the calcium ions were substituted with cobalt and cerium ions exhibits a higher specific surface area than the pure HAp. As was shown on TEM image (Fig. 2b), substituted

HAp is characterized by smaller particle size in comparison to HAp, which can cause an increase in the surface area. On the other hand, the presence of $CePO_4$ nanoparticles on the HAp surface (Fig. 2b) can also increase the specific surface area. Additionally, the 5Co10Ce:HAp exhibits a higher surface area then 5Co10Ce/HAp catalyst. According to XRD pattern (Fig. 1b), on the surface of the impregnated catalyst Co_3O_4 and CeO_2 phases are present. These phases could increase the surface area. However, the 5Co 10Ce/HAp catalyst exhibits the lower pore volume than pure HAp. It indicates that the Co_3O_4 and CeO_2 particles are placed into the pore of the support and as a result decrease the surface area.

FT – IR spectra

FT – IR spectra of the studied HAp samples, shown in Fig. 4, confirm the formation of hydroxyapatite structure in all samples and contain characteristic absorption bands of HAp originating from hydroxyl and phosphate groups. The vibrational modes of PO_4^{3-} tetrahedral apatite`s structure are clearly observed at around at 480 cm^{-1} (v_2), 565, 601 cm^{-1} (v_4), 962 cm^{-1} (v_1) and 1033, 1090 cm^{-1} (v_3) while sharp bands, detected at around 633 cm^{-1} (v_1) and 3572 cm^{-1} (v_1) correspond to bending and stretching mode of the hydroxyl groups in the channels of the structure [28]. Besides typical bands of HAp, a broad band in

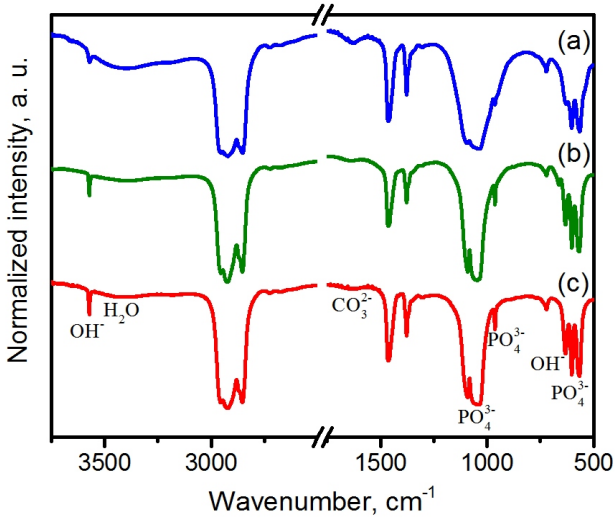

Fig. 4. FT-IR spectra of (a) 5Co10Ce:HAp, (b) 5Co10Ce/HAp and (c) HAp.

the region around 3100 – 3550 cm^{-1} (v_1) and weak band at around 1641 cm^{-1} are observed. The first band is associated with the H – bonding between the adsorbed water and hydroxyl ions in the hydroxyapatite structure [42], whereas the second is attributed to the vibration group of CO_3^{2-}. The presence of this band suggests the insignificant amount of carbonate substitution due to adsorption of CO_2 from atmosphere [24-25]. For all materials, the FT – IR spectra also contain bands at 719, 1385 and 1464 cm^{-1} assigned to nujol that was used during measurements.

The incorporation of Co ions into HAp structure leads to the decrease in the intensity of the structural OH^- peaks at 633 cm^{-1} and 3572 cm^{-1}. The decrease of intensity might be caused by the dehydroxylation attributable to cobalt substitution in the HAp lattice [43-44]. It is worth noting that the replacement of Ca^{2+} ions by Co^{2+} ions affects the width of the band originating from PO_4^{3-} groups (v_1). The band broadening can be ascribed to a decrease of sample crystallinity [45].

The FT-IR spectra of HAp and 5Co10Ce/HAp show that cobalt impregnation do not cause any significant change in bands shape and intensity. Nevertheless, 5Co10Ce/HAp spectrum contains one additional band at 667 cm^{-1}, which corresponds to the stretching vibration of the metal-oxygen bond and confirms the formation of Co_3O_4 [46]. It is in agreement with result obtained from XRD analysis and TEM images.

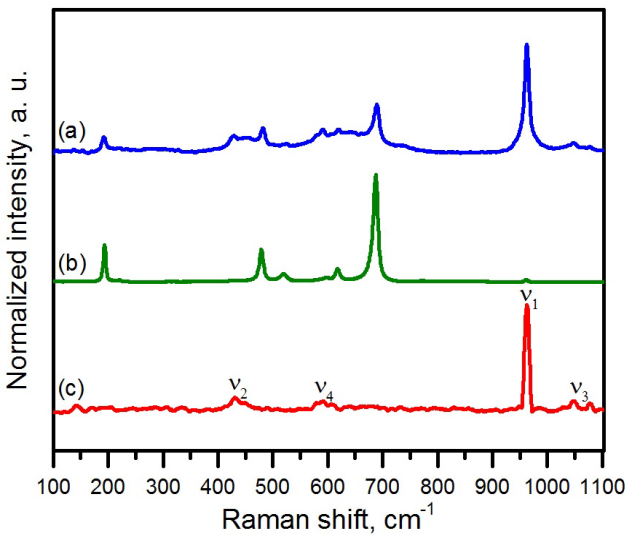

Fig. 5. Raman spectra of (a) 5Co10Ce:HAp, (b) 5Co10Ce/HAp and (c) HAp.

Raman spectra

Figure 5 shows Raman spectra of hydroxyapatite promoted with cobalt and cerium ions. Results obtained for "pure" hydroxyapatite show typical bands of phosphate group [30, 35, 45]. The strongest band at 963 cm^{-1} is assigned to the symmetric modes (v_1) of PO_4 group. Other bands observed at around 433, 600, 1047 and 1080 cm^{-1} correspond to bending vibration (v_2, v_4) and asymmetric stretching vibration (v_3) of phosphate ions. The modes of PO_4 are observed for the promoted samples, too. However, the spectrum of 5Co10Ce/HAp displays very weak bands of PO_4 group due to the presence of additional strong peaks (at 194, 482, 622 and 691 cm^{-1}) of Co_3O_4 [30, 46]. It should be noted that the vibrational modes of Co_3O_4 are also seen in the spectrum of 5Co10Ce:HAp. It suggests that part of cobalt ions did not substitute the calcium ions into HAp structure forming Co_3O_4 on hydroxyapatite surface. Moreover, for 5Co10Ce:HAp sample, the peak broadening at 963 cm^{-1} (compared to HAp) can be noticed. The peak broadness is related to the replacement of Ca^{2+} ions by Co^{2+} ions in the HAp lattice [35].

Acid – base properties

To characterize the acid surface properties of the catalysts, the temperature-programmed desorption of NH_3 was used. As can be seen from Table 2, pure HAp exhibits the lowest total acidity among studied samples. After calcium hydroxyapatite promotion with cobalt and cerium ions, the surface acidity increases in the following order: 5Co10Ce:HAp > 5Co 10Ce/HAp > HAp.

TPR – H_2

Results of TPR - H_2 measurements are presented in Table 3 and Fig. 6. For 5Co 10Ce:HAp (Fig. 6a), two reduction regions are observed, the first one at low temperature range (below 500 ^oC) and the second one at high temperature range (above 500 ^oC). The H_2 consumption below 500 °C can be ascribed to the reduction of Co species, which are located on the HAp surface. The reduction taking place above 500 ^oC corresponds to the reduction of cobalt ions, which substituted the calcium ions in HAp structure. In case of

Table 3. H_2 consumption of Co and Ce promoted HAp catalysts.

Sample	Peak temperature, ^oC				H_2 consumption, mol/g 10^3			
	(I)	(II)	(III)	(IV)	(I)	(II)	(III)	(IV)
5Co10Ce:HAp	355		657	783	0.364		0.691	0.035
5Co10Ce/HAp	314	373	-	-	0.382	1.013	-	-

5Co10Ce/HAp (Fig. 6b) sample, the TPR profile contains two distinct reduction peaks at temperature below 500°C. These peaks are ascribed to Co_3O_4 reduction. Cobalt oxide (Co_3O_4) is reduced in the following two steps [3, 9, 30]:

$$Co_3O_4 + H_2 \rightarrow 3CoO + H_2O \quad (10)$$

$$CoO + H_2 \rightarrow Co + H_2O \quad (11)$$

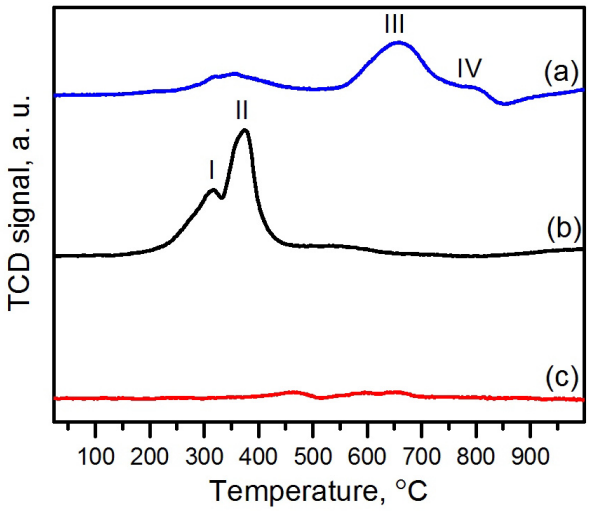

Fig. 6. TPR – H_2 profiles of (a) 5Co10Ce:HAp, (b) 5Co10Ce/HAp and (c) HAp.

According to the above reaction equations, the H_2 consumption ratio of second peak to the first one should be as 3:1. Table 3 shows that this ratio is lower than 3. It suggests, that some of cobalt ions could be incorporated into the hydroxyapatite structure in 5Co10Ce/HAp sample. Although, one cannot exclude the possibility of ceria reduction in this region. TPR - H_2 results show also that pure HAp (Fig. 6c) was not reduced in the temperature range studied, which is in line with literature data [29-32].

XPS measurements

XPS measurements were performed in order to determine the surface oxidation state of cobalt and cerium in the samples. XPS spectrum in the Co 2p region of the 5Co10Ce:HAp catalyst (Fig. 7a) show peak at

782,1 eV that is assigned to the Co $2p_{3/2}$ of $Co2^{+}$ located at the Ca^{2+} position in the hydroxyapatite structure, along with apparent satellite peak at 786,8 eV. The satellite peak can be ascribed to the shake-up excitation of the high-spin Co^{2+} ions [47]. As was suggested by K. Elkabouss et al. [28] the intense satellite peak as well as the binding energy of Co $2p_{3/2}$ peak corresponds well with Co^{2+} oxidation state. For 5Co 10Ce/HAp, the Co $2p_{3/2}$ peak is observed at 780,1 eV (Fig. 7b) what is slightly lower than for the 5Co10Ce:HAp sample but it is in agreement with literature data for Co_3O_4 spinel [28, 48].

Ce3d regions of catalysts are presented in Fig. 7c, d. XPS spectrum of 5Co10Ce:HAp catalyst (Fig. 7c) contains the two peaks at around 883,7 eV and 901,4 eV. These peaks correspond to the spin – orbit split Ce $3d_{5/2}$ and Ce $3d_{3/2}$, respectively [49-50]. Both peaks have the satellite structure. Their satellites are observed at 885,6 eV and 904,5, respectively. The spectrum is characteristic to Ce^{3+} oxidation state and match well to XPS spectra reported in the literature for $CePO_4$ [49-50].

The Ce3d region of 5Co10Ce/HAp (Fig. 7d) is different from that observed for the 5Co10Ce:HAp. Six peaks corresponding to three pairs of spin – orbit doublets can be identified. The peaks at around 882 eV and 900,5 eV are the $3d_{5/2}$ and $3d_{3/2}$, respectively [48]. The spin – orbit splitting between these peaks is about 18 eV. The peaks at 887,9 eV and 898,2 eV are the satellites associated to the $3d_{5/2}$, whereas the highest binding energy peaks (at 906,5 eV and 916,3 eV) are the satellite peaks connected with the $3d_{3/2}$ [38]. The peak located at 916,3 eV is typical to Ce^{4+} [49-50].

The XPS spectra confirmed the results of XRD measurements and TEM images about the cobalt and cerium compounds formed on hydroxyapatite surface. As was shown before, on the HAp surface, Co_3O_4 and CeO_2 are observed for 5Co10Ce/HAp and $CePO_4$ for 5Co10Ce:HAp. Therefore, the formed compounds are strongly depended on the promotion method.

Additionally, the XPS spectra can give some information about acid – base properties. According to K.E. Elkabouss et al. [28] the binding energy of O1s is sensitive to the change of sample basicity. The authors noticed that the binding energy of O1s change from about 529 eV (for the most basic oxide) to 533 eV (for the most acid oxide). Binging energy of O1s (not shown) for 5Co10Ce:HAp is higher than for 5Co10Ce/HAp indicates that the sample prepared by the incipient wetness method is more basic than the sample obtained by microwave – assisted method. This result is in good agreement with the TPD - NH_3 measurements.

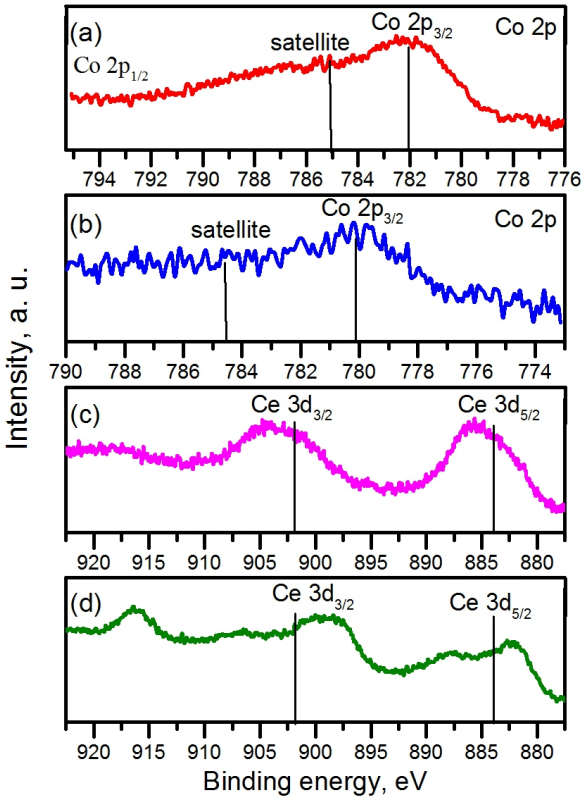

Fig. 7. XPS spectra of the Co 2p region for (a) 5Co10Ce:HAp, (b) 5Co10Ce/HAp and Ce 3d regions for (c) 5Co10Ce:HAp, (d) for 5Co10Ce/HAp.

Catalysts performance

Catalytic activity of the samples was evaluated in SRE to determine ethanol conversion, hydrogen yield and distribution of reaction products during 6 hours at 450°C with a constant ethanol/water ratio (1:6). First, catalytic performance of HAp was examined and results are shown in Fig. 8. The pure HAp exhibits the low catalytic activity for SRE in terms of ethanol conversion and hydrogen yield as well as products distribution. The pure HAp shows only 8% of ethanol conversion and 6% of hydrogen produced in the last hour of process. Moreover, the main products formed over HAp catalyst were acetaldehyde and carbon monoxide (Fig. 8b). High amount of these compounds in reaction products suggests that the major reaction takes place over this sample is dehydrogenation (reaction 5).

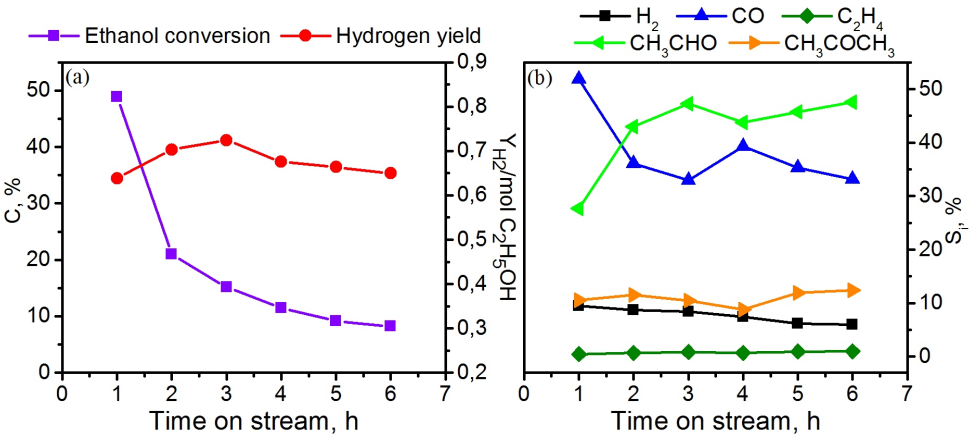

Fig. 8. (a) Ethanol conversion, hydrogen yield and (b) products distribution as a function of reaction time over HAp.

Ethanol dehydrogenation occurs on the base centres of the catalysts, which correspond with TPD – NH_3 measurements (Table 2). Results obtained for HAp showed that the surface acidity of HAp is the lowest among the studied samples. Fig. 8b also shows that carbon dioxide is not formed over HAp. It points out that the steam reforming reaction (reaction 1) does not occur at all.

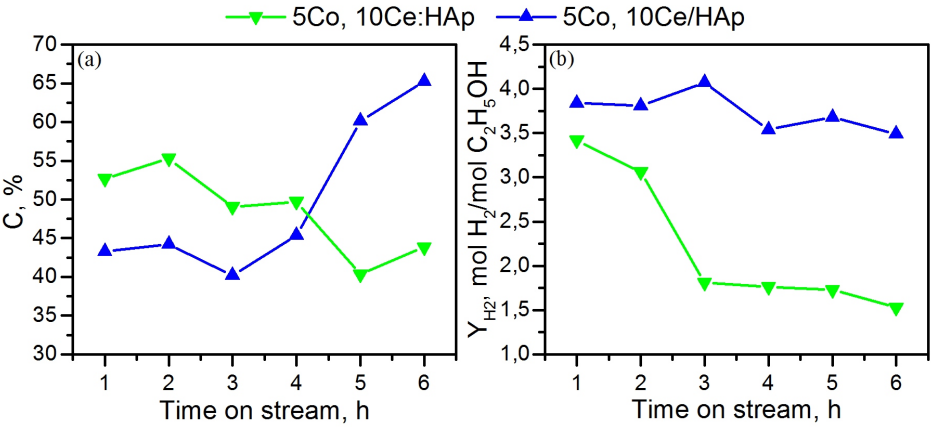

Fig. 9. (a) Ethanol conversion and (b) hydrogen yield as a function of reaction time over HAp promoted with cobalt and cerium ions.

The catalytic performance of hydroxyapatite promoted with cobalt and cerium ions in the ethanol steam reforming process was determined under the same conditions as for the pure HAp. Fig. 9 presents the ethanol conversion and hydrogen yield results as a function of reaction time for 5Co10Ce:HAp and 5Co10Ce/HAp catalysts. Analysis of the obtained data indicates that the promotion of calcium hydroxyapatite with cerium and cobalt ions improves both the conversion of ethanol and hydrogen yield. Studied catalysts demonstrate a comparably high conversion in the range of 40% to 65%. However, the ethanol conversion decreases with time on stream for 5Co10Ce:HAp, whereas for 5Co10Ce/HAp increases after 3 hours of the test. It can be explained by different acidity of the studied catalysts. TPD – NH_3 measurements (Table 2) show that the 5Co10Ce:HAp have more acid centres on surface in comparison to 5Co10Ce/HAp catalyst. Additionally, these catalysts are characterized by different reduction properties, which can also have the impact on catalytic activity. As was shown from TPR profiles, the catalyst prepared by incipient wetness impregnation method is reduced at lower temperature than the 5Co10Ce:HAp. Co_3O_4 on the surface of 5Co10Ce/HAp catalyst is reduced to CoO and metallic Co under reaction conditions. It means that amounts of CoO and metallic Co increase during the test what can improve the conversion of ethanol as well as ensure a high hydrogen yield (more than 3,5 mol H_2/mol C_2H_5OH). It should be noticed that reduction is a necessary step to achieve a high catalytic activity as was already suggested by Byram et. al. [3]. Moreover, the results of Tuti and Pepe studies [51] indicate that activation of cobalt catalysts under reaction conditions, milder with respect to the reduction pre-treatment in H_2, would be responsible of lesser metallic active phase sintering. As a consequence, higher hydrogen yield over no activated in pure H_2 catalysts can be obtained. In the 5Co10Ce:HAp sample, the cobalt ions are located in calcium hydroxyapatite structure. Therefore, in comparison with 5Co10Ce/HAp, the 5Co10Ce:HAp sample contains hard to reduce cobalt species and only little is reduced to metallic Co. As a result, the ethanol conversion can decrease with time on stream. The reduction properties of 5Co10Ce:HAp can also effect on H_2 yield that decrease during the ethanol steam reforming, too.

Products distributions as a function of reaction time are presented in Fig. 10. Reaction products contain seven compounds: H_2 (hydrogen), CO_2 (carbon dioxide), CO (carbon monoxide), CH_4 (methane), C_2H_4 (ethylene), CH_3CHO (acetaldehyde) and CH_3COCH_3 (acetone). The presence of these products indicates that both acid and basic sites are active in the ethanol steam reforming process. However, a slight amount of ethylene (produced on acid sites) allows to assume that the basic sites are more active in this process.

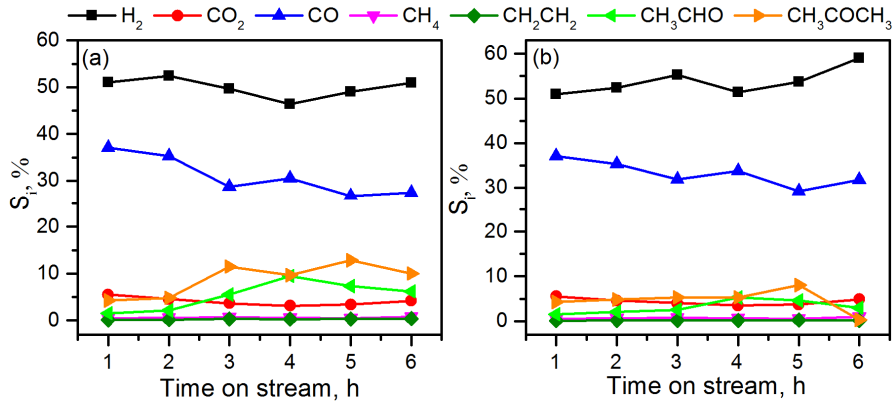

Fig. 10. Products distribution as a function of reaction time over (a) 5Co10Ce:HAp and (b) 5Co10Ce/HAp.

It should be noticed that hydrogen is the main component of the reaction product for both promoted with cobalt and cerium ions HAp catalysts (Fig. 9). At the same time, these catalysts form higher amount of carbon monoxide than carbon dioxide. It suggests that the reaction pathway favoured by these catalysts is incomplete ethanol steam reforming to hydrogen and carbon monoxide (reaction 3). As can be seen from Fig. 10, the share of CO in reaction products decreases with time on stream what would suggest the proceeding of water gas – shift reaction (WGS, reaction 4) or catalytic methanation. However, there is on increase in CO_2 or CH_4 at the same time. Generally, the WGS reaction is a significant stage for ethanol steam reforming process due to the conversion of CO to CO_2 and H_2 through reaction with steam. Carbon monoxide has an adverse effect upon catalytic activity because it can poison the catalysts (reaction 8) and that's why the reforming of ethanol is carried out in the presence of steam, which reduce the formation of carbon monoxide [12].

Compared with 5Co10Ce/HAp, for 5Co10Ce:HAp the increase of acetone and acetaldehyde was observed. It can be a result of dehydrogenation process (reaction 2) or ethanol decomposition to acetone, carbon monoxide and hydrogen. On the other hands, the acetone can be formed over 5Co10Ce:HAp catalyst from acetaldehyde by using the cerium oxide. According to Nishiguchi et. al. [6] the acetone is obtained from acetaldehyde via three sequential steps: dehydrogenation of ethanol to acetaldehyde, aldol condensation and aldol reaction with lattice oxygen on CeO_2.

Fig. 10 reveals that the catalyst prepared by incipient wetness impregnation method ensures a better distribution of products than the catalyst obtained by substitution of calcium ions by cobalt and cerium ions.

The 5Co10Ce/HAp ensures a higher amount of hydrogen that slightly increases during the test. Moreover, this catalyst exhibits a lower share of acetone and acetaldehyde in reaction products. Similar results' concerning the preparation method was reported by Wang et al. [52]. They studied the cobalt catalysts supported on ceria, prepared by coprecipitation and impregnation methods, and found that the presence of easily reducible Co_3O_4 on the ceria surface leads to a higher catalytic activity. Over 10%Co_3O_4/CeO_2 catalyst, ethanol conversion was close to 100% and H_2 selectivity was about 70% at 450 ^oC. Effect of the preparation method on cobalt catalysts applied to SRE process was also studied by Garcia and Assaf [53]. The authors pointed out that both the support synthesis method (solvothermal or precipitation) and the way of cobalt incorporation (impregnation or deposition-precipitation) were essential for obtaining efficient catalyst for the hydrogen production. Although ethanol conversion was superior of 99% at 600 ^oC for all catalysts, catalysts prepared by deposition-precipitation method presented the greater hydrogen yield. It was suggested that better catalytic performance of Co catalysts, due to the appropriate synthesis technique, could be attributed to the improved metal phase dispersion, enhanced metal-support interaction and increased metal-support interface [54]. Additionally, in this paper the influence of the incorporation method of active phase on the acid-base properties of the catalysts was emphasized. It is known that catalyst acidity is one of the main factors determining the catalytic properties for hydrogen production via SRE process.

CONCLUSIONS

Calcium hydroxyapatites promoted with cobalt and cerium ions show promising catalytic activity for hydrogen production via ethanol steam reforming. Promotion with cobalt and cerium ions significantly improves the ethanol conversion, hydrogen yield and products distribution for HAp catalysts. It was found that the catalytic performance depends on the preparation method in terms of the acid-base and reduction properties. The catalyst obtained by the incipient wetness impregnation method exhibits a higher hydrogen yield (more than 3,5 mol H_2/mol C_2H_5OH) and increasing ethanol conversion with time on stream, which can be a result of easier reduction of cobalt species and lower surface acidity. Over these catalysts, mainly the ethanol steam reforming to hydrogen and carbon monoxide was observed. Further research over calcium hydroxyapatite promoted with higher cobalt loadings and other active ions will be conducted.

EXPERIMENTAL SECTION

Catalysts preparation

Direct Microwave-assisted hydrothermal synthesis

As precursors, $(NH_4)_2HPO_4$ (POCH), $Ca(NO_3)_2{\cdot}4H_2O$ (POCH), $Co(NO_3)_2{\cdot}6H_2O$ (POCH) and $Ce(NO_3)_3{\cdot}6H_2O$ (ACROS) were used. All reagents were separately dissolved in distilled water. Afterwards, $(NH_4)_2HPO_4$) solution was added to the solution containing an appropriate amount of $Ca(NO_3)_2{\cdot}4H_2O$, $Ce(NO_3)_3{\cdot}6H_2O$ and $Co(NO_3)_2{\cdot}6H_2O$ under vigorous stirring. The suspension was precipitated by adding drop-by-drop 25% solution of ammonia (POCH) until the pH attained 10,5. Then, the as-prepared precipitate was transferred into Teflon vessel and placed into a microwave autoclave for 1 h at 200˚C. After hydrothermal treatment, the product was filtered and washed with distilled water and ethanol (POCH) several times. Finally, the obtained powder was dried at 80˚C overnight and calcined at 500˚C for 3 h under atmospheric conditions. Calcium hydroxyapatite substituted with cobalt and cerium ions obtained in this way was denoted as 5Co10Ce:HAp (5 and 10 correspond to the expected mass percentage in the sample). Pure calcium hydroxyapatite (without Co and Ce ions) was also obtained by the above-mentioned method.

Incipient wetness impregnation method

Pure HAp sample (prepared by the microwave-assisted hydrothermal method) was impregnated using aqueous solution of $Co(NO_3)_2{\cdot}6H_2O$ and $Ce(NO_3)_3{\cdot}6H_2O$. After cobalt and cerium ions incorporation, the sample was dried at 30˚C for 24 h and calcined in air at 500˚C for 3 h. As a result, catalyst with 5 wt% Co and 10 wt% Ce was obtained. Impregnated sample was denoted as 5Co10Ce/HAp.

Catalysts characterization

The structure of catalysts was analyzed by X-Ray powder diffraction method (XRD) using an X'PertPro HighScore Plus (PANalytical Ltd.) diffractometer with a Ni-filtered CuKα radiation (1,54060Å) from 10˚ to 80˚. The crystalline phase was identified by comparison with PDF standard. Unit cell parameters were refined by the least-squares method with the aid of X'Pert HighScore Plus program. The Scherrer formula was used to calculate the mean crystallite size of studied catalysts.

Electron microscopy was used to characterize the morphology of the prepared samples. The TEM images were performed using Philips CM-20 Super-Twin transmission electron microscope operating at 200 kV with 0,25 nm resolution. The SEM images were acquired by FESEM FEI Nova NanoSEM 230 scanning electron microscopy. EDS (Energy Dispersive X-Ray Spectroscopy) was employed to determine the surface chemical composition of the prepared samples. EDS measurements were performed using SEM equipped with EDAX spectrometer.

The surface area and pore volume were measured by the N_2 adsorption/ desorption isotherms at liquid nitrogen temperature, using Sorptometic 1990. Before the measurement the catalyst was degassed at 200°C for 2 h under vacuum. The Brunauer-Emmett-Teller (BET) method was used to calculate the specific surface area while Barret-Joyner-Halenda (BJH) for pore size and volume analysis.

Fourier Transform Infrared spectra (FT - IR) were collected with a Bruker IFS-88 spectrometer equipped with a FRA-106 (laser Nd:YAG, 1064 nm) over the range of wavenumber 4000 – 50 cm^{-1}.

Raman spectra were measured with a Renishaw InVia Raman spectrometer equipped with a diode laser (830 nm), confocal DM 2500 Leica optical microscope and thermoelectrically Ren Cam CDD detector.

Hydrogen temperature-programmed reduction (TPR-H_2) measurements were carried out in an AutoChem II 2920 analyzer equipped with a thermal conductivity detector (TCD). Sample was placed in U-shaped quartz reactor and heated from room temperature to 1000°C (heating rate 5°C/min). A mixture 5 vol% hydrogen in argon (50 ml/min) was used as a gas carrier at the flow rate of 50 ml/min. Hydrogen consumption was evaluated using the CuO standard.

X-ray Photoelectron spectra (XPS) were collected on a XPS, UHV spectrometer SPECS equipped with a dual Al/Mg X-ray source and PHOIBOS 100 analyzer. Data analysis was performed using SPECLAB Software. Line of background was calculated by Shirley methods. The carbon C 1s 284,8 eV line was used as reference.

Surface acidity was determined by temperature-programmed desorption of ammonia (TPD – NH_3). Sample (mesh 0,2 – 0,4 mm) was placed in the reactor and heated (heating rate 10°C/min) in argon stream (30 ml/min) up to 550°C, for the removal of adsorbed contaminants. Next, the sample was cooled down to 180°C and then the adsorption of ammonia was conducted. Then, physically adsorbed ammonia was removed by stream of argon. Finally, the catalyst was heated from 180°C to 550°C in stream of argon and amount of ammonia desorbed was determined by TCD detector.

Activity test

Catalytic performance tests for SRE process were carried out in a fixed bed quartz tubular reactor (8 mm diameter) over the catalyst sample (particle size between 0,45 – 0,75 Tyler mesh) heated in a nitrogen stream (22 ml/min) at 450˚C. The temperature was measured by using thermocouple placed over the catalytic bed. The aqueous ethanol solution with water to ethanol molar ratio 6:1 was delivered into the reactor through a pump (Perkin Elmer). The mixture of $EtOH+H_2O$ was vaporized in heater before introduction on the catalyst bed. The gas hourly space velocity (GHSV) was maintained at 26000 h^{-1}. The analysis of the reagents and reaction products was made by using a gas chromatograph (with a flame ionization detector (FID) and TCD detector) equipped with two packed columns filling Poropak Q and type S of active carbon.

The catalytic performance was characterized by ethanol conversion (denoted as *C*), hydrogen yield (denoted as Y_{H2}) and products distribution (denoted as S_i). They were calculated according to the Eqs. (12)-(14):

$$C = (N_{C2H5OH(IN)} - N_{C2H5OH(OUT)})/N_{C2H5OH(IN)}\ 100\% \quad (12)$$

$$Y_{H2} = N_{H2}/(6 \cdot N_{C2H5OH(IN)})\ 100\% \quad (13)$$

$$S_I = X_I/\Sigma_I X_I\ 100\% \quad (14)$$

where $N_{C2H5OH(in)}$ – moles of inlet ethanol, $N_{C2H5OH(out)}$ – moles of outlet ethanol, N_{H2} – moles of hydrogen produced, X_i – mole of i product in gaseous products of SRE.

ACKNOWLEDGEMENTS

The authors are thankful MSc E. Bukowska for XRD data, MSc L. Krajczyk for TEM studies, Prof. J. Baran for FT – IR measurements and Dr. M. Ptak for Raman data.

REFERENCES

1. A. Kumar, R. Prasad, Y.C. Sharma, *International Journal of Environmental Research*, **2014**, *4*, 203.
2. C.D. Dave, K.K. Pant, *Renewable Energy*, **2011**, *36*, 3195.
3. B. Bayram, I.I. Soykal, D. von Deak, J.T. Miller, U.S. Ozkan, *Journal of Catalysis*, **2011**, *284*, 77.

4. H. Muroyama, R. Nakase, T. Matsui, K. Eguchi, *International Journal of Hydrogen Energy*, **2010**, *35*, 1575.
5. C.C.R.S. Rossi, C.G. Alonso, O.A.C. Antunes, R. Guirardello, L. Cardozo-Filho, *International Journal of Hydrogen Energy,* **2009**, *34*, 323.
6. T. Nishiguchi, T. Matsumoto, H. Kanai, K. Utani, Y. Matsumura, W.-J. Shen, S. Imamura, *Applied Catalysis A-General*, **2005**, *279*, 273.
7. D.K. Liguras, D.I. Kondarides, X.E. Verykios, *Applied Catalysis B- Environmental*, **2003**, *43*, 345.
8. A.G.M. da Silva, P.A. Robles-Dutenhefner, A. Dias, H.V. Fajardo, A.S.P. Lovón, J.J. Lovón-Quintana, G.P. Valenca, *Journal of Sol-Gel Science and Technology*, **2013**, *67*, 273.
9. A.F. Lucredio, J.D.A. Bellido, A. Zawadzki, E.M. Assaf, *Fuel*, **2011**, *90*, 1424.
10. P.V. Snytnikov, S.D. Badmaev, G.G. Volkova, D.I. Potemkin, V.D. Belyaev, M.M. Zaryanova, *Hydrogen Energy,* **2012**, *37*(21), 16388.
11. A. N. Fatsikostas, X. E. Verykios, *Journal of Catalysis,* **2004**, *225*, 439.
12. R.C. Cerritos, R.F. Ramírez, A.F.A. Alvarado, J.M.M. Rosales, T.V. García, G. Esquivel, *Industrial & Engineering Chemistry Research*, **2011**, *50*, 2576.
13. T. Hou, S. Zhang, T. Xu, W. Cai, *Chemical Engineering Journal,* **2014**, *255*, 149.
14. J.L. Contreras, J. Salmones, J.A. Colin-Luna, L. Nuno, B. Quintana, I. Cordova, B. Zeifert, C. Tapia, G.A. Fuentes, *International Journal of Hydrogen Energy*, **2014**, *39*, 18835.
15. H. Song, L. Zhang, R.B. Watson, D. Braden, U.S. Ozkan, *Catalysis Today*, **2007**, *129*, 346.
16. M.S. Batista, R.K.S. Santos, E.M. Assaf, E.A. Ticianelli, *Journal of Power Sources*, **2003**, *124*, 99.
17. J. Llorca, N. Homes, J. Sales, P. Ramirez de la Piscina, *Journal of Catalysis*, **2002**, *209*, 306.
18. J.L. Contreras, J. Salomones, L.A. Garcia, A. Ponce, B. Zeifert, G.A. Fuentes, *Journal of New Materials for Electrochemical Systems*, **2008**, *11*(2), 109.
19. S.S.Y. Lin, D.H. Kim, S.Y. Ha, *Catalysis Letters*, **2008**, *122*(3-4), 295.
20. B. Banach, A. MacHocki, P. Rybak, A. Denis, W. Grzegorczyk, W. Gac, *Catalysis Today,* **2011**, *176*(1), 28.
21. H. Wang, J.L. Ye, Y. Liu, Y.D. Li, Y.N. Qin, *Catalysis Today*, **2007**, *129*, 305.
22. F. Ma, W. Chu, L. Huang, X. Yu, Y. Wu, *Chinese Journal of Catalysis*, **2011**, *32*, 970.
23. A. Kaddouri, C. Mazzocchia, *Catalysis Communications,* **2004**, *5*, 339.
24. K. Agrawal, G. Singh, D. Puri, S. Prakash, *Journal of Minerals and Materials Characterization and Engineering*, **2011**, *10*, 727.
25. P.K. Tank, K.S. Chudasama, V.S. Thaker, M.J. Joshi, *Journal of Nano-particle Research*, **2013**, *15*, 1644.
26. R.-B. Suen, S.-C. Lin, W.-H. Hsu, *Journal of Chromatography A*, **2004**, *1048*, 31.
27. S. Ogo, A. Onda, K. Yanagisawa, *Applied Catalysis A-General,* **2008**, *348*, 129.
28. K. Elkabouss, M. Kacimi, M. Ziyad, S. Ammar, F. Bozon-Verduraz, *Journal of Catalysis,* **2004**, *226*, 16.
29. J. Ashok, N. Kumar, M. Subrahmanyam, A. Venugopal, *Catalysis Letters*, **2007**, *121*, 283.

30. B. Aellach, A. Ezzamarty, J. Leglise, C. Lamonier, J. F. Lamonier, *Catalysis Letters*, **2010**, *135*, 197.
31. S. Sugiyama, T. Shono, D. Makino, T. Moriga, H. Hayashi, *Journal of Catalysis,* **2003**, *214*, 8.
32. L. Hakim, Z. Yaakob, M. Ismail, W.R.W. Daud, R. Sari, *Chemical Papers,* **2013**, *67*, 703.
33. M. Rakap, S. Özkar, *Catalysis Today*, **2012**, *183*, 17.
34. Y. Han, S. Li, X. Wang, X. Chen, *Materials Research Bulletin*, **2004**, *39*, 25.
35. Z. Stojanović, L. Veselinović, S. Marković, N. Ignjatović, D. Uskoković, *Materials and Manufacturing Processes*, **2009**, *24*, 1096.
36. G.C. Koumoulidis, A.P. Katsoulidis, A.K. Ladavos, P.J. Pomonis, C.C. Trapalis, A.T. Sdoukos, T.C. Vaimakis, *Journal of Colloid and Interface Science*, **2003**, *259*, 254.
37. D. Gopi, S. Nithiya, L. Kavitha, J. M. F. Ferreira, *Bulletin of Materials* Science*,* **2012**, *35*, 1195.
38. W. Suchanek, *Materiały Ceramiczne*, **2005**, *2*, 58.
39. J. Dobosz, S. Hull, M. Zawadzki, *Polish Journal of Chemical Technology*, **2016**, *18*, 59.
40. Yasukawa, K. Gotoh, H. Tanaka, K. Kondori, *Colloid Surface A: Physicochemical and Engineering Aspects*, **2012**, *393*, 53.
41. P.A. Webb, C. Orr, "Analytical methods in fine particle technology"*,* Micromeritics Instrument Corporation, Norcross, Georgia, **1997**, chapter 3.
42. R.R. Sheha, *Journal of Colloid and Interface Science*, **2007**, *310*, 18.
43. S.M. Sallam, K.M. Tohami, A.M. Sallam, L.I. Abo Salem, F.A. Mohamed, *J. Biophysical Chemistry*, **2012**, *3*, 278.
44. N. Devi Ravi, R. Balu, T.S. Sampath Kumar, *Journal of the American Ceramic Society,* **2012**, *95*, 2700.
45. V. Aina, G. Lusvardi, B. Annaz, I.R. Gibson, F.E. Imrie, G. Malavasi, L. Menabue, G. Cerrato, G. Martra, *Journal of Materials* Science*: Materials in Medicine*, **2013**, *529-530*, 88.
46. S. Farhadi, K. Pourzare, S. Sadeghinejad, *Journal of Nanostructure in Chemistry*, **2013**, *3*, 1.
47. E. Kramer, E. Itzkowitz, M. Wei, *Ceramics International*, **2014**, *40*, 13480.
48. L. Xue, C. Zhang, H. He, Y. Teraoka, *Applied Catalysis B-Environmental,* **2007**, *75*,167.
49. R. Asuvathraman, K.I. Gnanasekar, P.C. Clinsha, T.R. Ravindran, K.V. Govindan Kutty, *Ceramics International*, **2015**, *41*, 3731.
50. E. Bêche, P. Charvin, D. Perarnau, S. Abanades, G. Flamant, *Surface and Interface Analysis,* **2008**, *40*, 264.
51. S. Tuti, F. Pepe, *Catalysis Letters*, **2008**, *122*, 196.
52. H. Wang, J.L. Ye, Y. Liu, Y.D. Li, Y.N. Qin, *Catalysis Today*, **2007**, *129*, 305.
53. S.R. Garcia, J.M. Assaf, *Modern Research in Catalysis*, **2012**, *1*, 52.
54. S. Song, B. Tan, U.S. Ozkan, *Catalysis Letters*, **2009**, *132*, 422.

STUDIA UBB CHEMIA, LXIII, 1, 2018 (p. 239-254)
(RECOMMENDED CITATION)
DOI:10.24193/subbchem.2018.1.17

HEAT TRANSFER CHARACTERISTICS OF NANOFLUID FLOW AROUND A ROTATING CYLINDER

KHELILI YACINE[a*], ALLALI ABDERAZZAK[a], BOUAKKAZ RAFIK[b]

ABSTRACT. The forced convective flow and heat transfer of nanofluids past a rotating cylinder placed in a uniform cross stream is investigated numerically. The computations are carried out at a representative Reynolds number (Re) of 200. The dimensionless cylinder rotation rate (α) is varied between 0 and 6. The range of nanoparticle volume fractions (φ) considered is $0 \leq \varphi \leq 5\%$. Two-dimensional and unsteady mass continuity, momentum, and energy equations have been discretized using finite volume method. SIMPLE algorithm has been applied for solving the pressure linked equations. The effect of rotation rates (α) on fluid flow and heat transfer were investigated numerically. In addition, time-averaged (lift and drag coefficients and Nusselt number) results were obtained and compared with the literature data. A good agreement was obtained for both the local and averaged values.

Keywords: *unsteady flow, nanofluid, volume fraction, Reynolds number, finite volume, circular cylinder.*

INTRODUCTION

The classical problem of viscous incompressible flow over a circular cylinder confined in a channel is one of the most widely studied problems in computational fluid dynamics (CFD). This type of flow problems frequently arise in various engineering fields. Because of its popularity, a plethora of numerical, theoretical and experimental results are available for this problem in the literature.

[a] *Aircraft Laboratory, Department of Mechanical Engineering, Univ. Blida 1, Algeria*
[b] *Department of Mechanical Engineering, Univ. Constantine 1, Algeria*
** Corresponding author: khliliyacine1@gmail.com.*

Ingham and Tang [1] carried out numerical simulations for two-dimensional steady flow, extending their previous research work to *Re* = 60 and 100 for $0 \leq \alpha \leq 1$. Another numerical attempt at *Re* = 200 was reported by Chen *et al*. [2]. An explicit pseudo-spectral technique was adopted for resolving the fundamental equations. According to their results, when $\alpha = 3.25$ more than one vortex is shed downstream. Kang [3] also has contributed significant work to this research area. Sequential numerical simulations at *Re* equal to 40, 60, 100 and 160 in the range of $0 \leq \alpha \leq 2.5$ were performed. It was observed that at $60 \leq Re \leq 160$ the maximum value of a, which favors flow instability, varies logarithmically when plotted against *Re*. Zdravkovich [4], has compiled almost all the experimental, analytical and numerical simulation data on flow past cylinders,

In the study of wake dynamics, bluff body rotation has always drawn considerable attention largely due to its effects on boundary layer separation and the Magnus effect. Increase in the lift magnitude more than classic Prandtl's limit due to increase in rotation rate of the circular cylinder was proposed by Glauart [5]. For the similar flow configuration, Kang and Choi [6], followed with the numerical solution of the unsteady governing equations in the primitive variables velocity and pressure for flows with *Re* = 60, 100 and 160 with $0 = \alpha = 2.5$. Their results showed that vortex shedding vanishes when α increases beyond a critical value which follows a logarithmic dependence on the Reynolds number (e.g., the critical dimensionless rotation rate $\alpha = 1.9$ for *Re* = 160). Later, the work of (Mittal & Kumar, [7]) performed a comprehensive numerical investigation by fixing a moderate value of *Re* = 200 while considering a wide interval for the dimensionless rotation rate of $0 \leq \alpha \leq 5$. They used the finite-element method to solve the unsteady incompressible Navier–Stokes equations in two-dimensions for the primitive variables velocity and pressure.

In the work of Nemati *et al*. [8], the laminar flow and heat transfer from a rotating circular cylinder with uniform planar shear was investigated, where the free stream velocity varies linearly across the cylinder using Multi-Relaxation-Time (MRT) LBM. Recently, the convective heat transfer from a rotating cylinder with inline oscillation was studied by Nobari *et al.* [9] at *Re* numbers of 100, 200, and 300. Different rotational speeds of the cylinder (0 - 2.5) are considered at various oscillating amplitudes and frequencies with three different *Pr* numbers of 0.7, 6, and 20.

Paramane *et al*. [10] investigated numerically the forced convection heat transfer across a rotating circular cylinder in the 2-D laminar regime. They concluded that the rotation can be used as a drag reduction and heat transfer suppression technique. Subsequently, Paramane *et al*. [11], studied numerically the free stream flow and forced convection heat transfer across a rotating cylinder, dissipating heat flux for Reynolds numbers of 20 - 160 and

a Prandtl number of 0.7. Their results show that, at higher rotational velocity, the Nusselt number is almost independent of Reynolds number and the thermal boundary conditions.

Experimental measurements of the flow past a rotating cylinder were performed by Barnes [12]. At low rotation rates to determine the value at which shedding is suppressed for Reynolds numbers between 50 and 65. The vortex shedding behind a rotating cylinder disappears when α is increased above the value of 2 is showed by Stojkovic et al [13].

Despite a number of studies on convective heat transfer of nanofluids reported in the literature, investigation of mixed convective flow and heat transfer past a rotating circular cylinder employing nanofluid as the operating medium has largely been ignored. However, this problem has important applications in designing several heat transfer devices used in modern industry. Al though few studies on forced and mixed convective heat transfer of nanofluids past circular ([15-18]) and square ([19-20]) cylinders have recently been reported, a systematic study addressing this extremely significant issue is yet to be found in the literature.

In the present work, we have simulated the forced convective flow and heat transfer of nanofluids past a rotating circular cylinder in cross flow using a finite volume method. Water-based nanofluids containing various volume-fractions of copper (*Cu*) nanoparticles are used. Computations are carried out at a representative Reynolds number of 200. Dimensionless rotation rates are considered in the range, $0 \leq \alpha \leq 6$. One of the objectives of the present investigation is to find out the effect of nanoparticle agglomeration on the vortex dynamics and heat transfer for various rotational speeds.

1. PROBLEM STATEMENT AND MATHEMATICAL FORMULATION

Consider the two-dimensional, laminar flow of an incompressible Newtonian fluid with a uniform inlet velocity U_∞ and temperature, T_∞ across an infinitely long (in z-direction) circular. To convert the physical problem into a computational equivalent, a circular cylinder of diameter D is placed concentrically in a circular domain of diameter D_∞ as shown in Fig. 1. The radius of the enveloping circular domain is chosen to be sufficiently large in order to minimize the boundary effects. The surface of the solid cylinder is maintained at a constant wall temperature, T_w. The thermo-physical properties (viscosity, density, heat capacity and thermal conductivity) of the streaming liquid are assumed to be independent of the temperature and the viscous dissipation effects in the energy equation are neglected in this study.

1.1. Governing equations

The flow and heat transfer phenomena are governed by the continuity, Navier–Stokes and thermal energy equations written in their dimensionless forms, as follows.

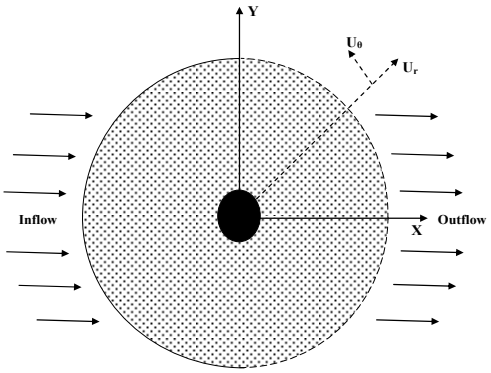

Fig. 1. Schematic of computational domain and coordinate system

Continuity Equation:

$$\frac{\partial U_r}{\partial r} + \frac{U_r}{r} + \frac{1}{r}\frac{\partial U_\theta}{\partial \theta} = 0 \tag{1}$$

θ-Momentum Equation:

$$\frac{\partial U_\theta}{\partial t} + \left(\vec{V}.\vec{\nabla}\right)U_\theta + \frac{U_r U_\theta}{r^*} = -\frac{\rho_f}{\rho_{nf} r}\frac{\partial P}{\partial \theta} + \frac{2}{v_f Re}\frac{\mu_{nf}}{\rho_{nf}}\left(\nabla^2 U_\theta + \frac{2}{r^2}\frac{\partial U_r}{\partial \theta} - \frac{U_\theta}{r^2}\right) \tag{2}$$

r-Momentum Equation:

$$\frac{\partial U_r}{\partial t} + \left(\vec{V}.\vec{\nabla}\right)U_r - \frac{{U_\theta}^2}{r} = -\frac{\rho_f}{\rho_{nf}}\frac{\partial P}{\partial r} + \frac{2}{v_f Re}\frac{\mu_{nf}}{\rho_{nf}}\left(\nabla^2 U_r - \frac{2}{r^2}\frac{\partial U_\theta}{\partial \theta} - \frac{U_r}{r^2}\right) \tag{3}$$

Energy Equation:

$$\frac{\partial T}{\partial t} + \left(\vec{V}.\vec{\nabla}\right)T = \frac{k_f}{k_{nf}}\frac{(\rho C_p)_{nf}}{(\rho C_p)_f}\frac{2}{RePr} \times (\nabla^2 T) \tag{4}$$

With $\nabla^2 = \frac{\partial^2}{\partial r^{*2}} + \frac{1}{r^*}\frac{\partial}{\partial r^*} + \frac{1}{r^{*2}}\frac{\partial^2}{\partial \theta^{*2}} + \frac{\partial^2}{\partial z^{*2}}$

1.2. Thermal properties of nanofluid

The density of nanofluids at different volume concentrations and temperatures are obtained from the literature. The nanofluids density calculated with the equation from Pak and Cho [21].

$$\rho_{nf} = (1-\varphi)\rho_{f+}\varphi\rho_p \tag{5}$$

For typical nanofluids with nano particles of volume fraction less than 1%, a variation of less than 5% in the fluid density is expected.

Specific heat: The specific heat of a nanofluid can be calculated by using energy balance as:

$$(\rho C_p)_{nf} = (1-\varphi)(\rho C_p)_f + \varphi(\rho C_p)_p \tag{6}$$

Where, φ is the nano particle volume fraction and is given as:

$$\varphi = \frac{Volume\ of\ nanoparticles}{Total\ volume\ of\ solution} \tag{7}$$

The Eqs. (5) and (6) were introduced by *Buongiorno* [22].

The Brownian motion has a significant impact on the effective thermal conductivity. Koo and Kleinstreuer [20] proposed that the effective thermal conductivity is composed of the particle's conventional static part and a Brownian motion part. This 2-component thermal conductivity model takes into account the effects of particle size, particle volume fraction, and temperature.

$$k_{nf} = k_{static} + k_{Brownian} \tag{8}$$

$$\frac{k_{static}}{k_f} = \frac{k_p + 2k_f - 2(k_f - k_p)\varphi}{k_p + 2k_f + (k_f + k_p)\varphi} \tag{9}$$

$$k_{Brownian} = 5 \times 10^4 \beta\varphi\rho_f C_{p.f} \sqrt{\frac{kT}{2\rho_p d_p} f(T,\varphi)} \tag{10}$$

Where k = 1.3809×10^{-23} J/k is the Boltzmann constant, and β is given as:

$$\beta = 8.4407(100\varphi)^{-1.07304} \tag{11}$$

and $f(T,\varphi)$ is given as :

$$f(T,\varphi) = (2.8217 \times 10^{-2}\varphi + 3.917 \times 10^{-3})\left(\frac{T}{T_0}\right)$$
$$(-3.0669 \times 10^{-2}\varphi - 3.91123 \times 10^{-3}) \tag{12}$$

The effective dynamic viscosity for the nano-fluid could be calculated by the following equations (Corcione [23]):

$$\mu_{nf} = \frac{\mu_f}{\left(1 - 34.87\left(d_p/d_f\right)^{-0.3} \times \varphi^{1.03}\right)} \tag{13}$$

$$d_f = \left(\frac{6M}{N\pi\rho_{f0}}\right)^{1/3} \tag{14}$$

where d_p and d_f represented the mean diameter of the nanoparticles and equivalent diameter of a base fluid molecule, respectively; M represented the molecular weight; N represented the Avogadro number = 6.0229 10^{23} mol^{-1} ; and ρ_{f0} is the density of the base fluid found at Temperature = 293 K.

1.3. Boundary conditions

According to Fig. 1 the governing Eqs. (1) – (4) are subjected to the following boundary conditions:

Inlet boundary ($r = R_\infty = 150R,\ -\pi/2 \le \theta \le \pi/2$) :

$$U_\theta = 0,\ U_r = 1,\ T = 0 \tag{15}$$

Outlet boundary ($r = R_\infty = 150R,\ \pi/2 \le \theta \le -\pi/2$) :

$$\frac{\partial U_\theta}{\partial r} = 0, \qquad \frac{\partial U_r}{\partial r} = 0, \qquad \frac{\partial T}{\partial r} = 0 \tag{16}$$

Cylinder wall boundary ($r = R$, $0 \le \theta \le 2\pi$) :

$$U_\theta = -\alpha sin\theta\ ,\ U_r = -\alpha cos\theta,\ T = 1 \tag{17}$$

1.4. Auxiliary equations

- The wall pressure coefficient, C_P, may be defined as the following:

$$Cp = \frac{P - P_0 + 0.5\rho U_\infty^2}{0.5\rho U_\infty^2} \tag{18}$$

Where, P_0 is the pressure at the front stagnation point.

- In the time-periodic flow regime, there is also a net force acting on the cylinder in the lateral direction and this is expressed in terms of a lift coefficient C_L, defined as follows:

$$C_L = \frac{F_L}{0.5\rho D U_\infty^2} \tag{19}$$

Where F_L is the lift force acting on the cylinder per unit length. The lift force also has two components, shear and pressure. These components are represented by two dimensionless parameters known as the pressure lift coefficient (C_{LF}) and friction lift coefficient (C_{LP}).

- non-dimensional rotation rate:

$$\alpha = \frac{\Omega D}{2U_\infty} \tag{20}$$

- The local Nusselt number of the nanofluid, based on cylinder diameter is defined as:

$$Nu = -\left[\frac{\partial T}{\partial n}\right]_{along\ the\ cylinder\ surface} \tag{21}$$

- Surface averaged Nusselt number of fully developed thermal boundary layer is defined as:

$$Nu_{ave} = \frac{1}{s}\int_s Nuds \tag{22}$$

1.5. Grid generation

In the present meshing scheme, cylinder with a diameter D resides in the center of the chosen computational domain. Outer boundary of the domain is circular with diameter D_∞ from the center of the cylinder, Fig. 1. Number of node points along the cylinder circumference and along the normal direction is represented by 'N' and 'M' respectively. We use M = 360 nodes stretched along the radial direction and N = 120 equispaced nodes around the circumferential direction. The wall normal distance of the first internal grid point is maintained at Δr = 0.0001D , required for adequate resolution of the sharp near wall gradients of the flow variables.

1.6. Numerical Method

The governing equations mentioned in previous section are discretized based on finite volume approach. The governing equations are integrated over a staggered grid arrangement. A pressure correction based iterative algorithm, SIMPLE is used to solve the pressure linked equations. Central difference scheme is used to discretize the diffusion terms whereas a combination of upwind and central difference is adopted for discretizing the convection terms.

The thermos-physical properties of the fluid and the nanoparticle, copper, are listed in Table 1.

Table1. Thermophysical properties of nanoparticle and base fluids

	k [W/mK]	ρ [Kg/m^3]	$\mu\ 10^{-3}$ [Kg/ms]	C_p [J/kgK]
Water	0.613	997.1	1.003	4179.0
Cu	400	8933.0	…..	385.0

2. RESULTS AND DISCUSSION

2.1. Validation of results

In order to validate our numerical solution, estimated results for pressure coefficients around a circular cylinder are compared with the available data in the literature. Fig. 2 compares the pressure coefficient C_p obtained in the present research with those from reference [7]. It is clear that the results are in very good agreement with previous studies.

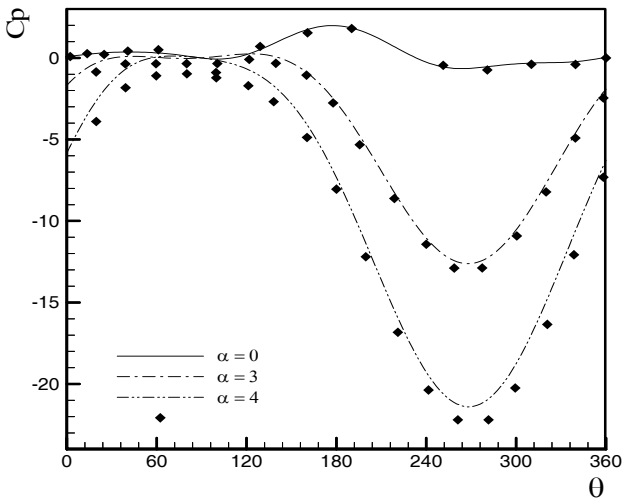

Fig. 2. Comparison results for pressure coefficient around surface of cylinder for various values of α at *Re* = 200 with Mittal and Kumar [7]

In the fig. 2 the stagnation pressure coefficient reduces from 1 as α increases. At α = 2 when a closed streamline circulating around the cylinder can be observed, it becomes less than zero. For $\alpha \geq 2$, the pressure coefficient is negative everywhere on the cylinder rotation on the flow.

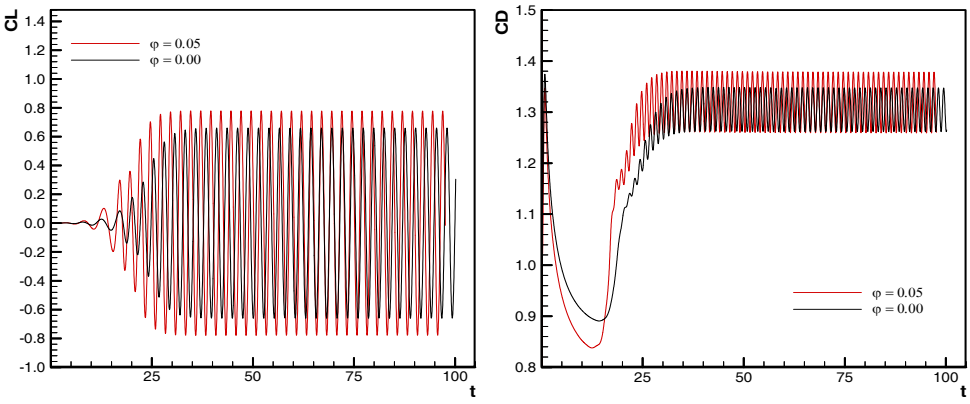

Fig. 3. Temporal evolution of lift and drag coefficients for laminar flow past a circular cylinder at *Re* = 200

Fig. 3 shows the temporal evolution of the lift and drag coefficients computed for Reynolds number *Re* = 200. The differences observed between the base fluid and nanofluid. The magnitude of the maximum lift coefficient and the mean drag coefficient are, in general, observed to be less for the base fluid.

Structure of flow field

The time histories of the lift coefficient for the base fluid flow past a rotating cylinder for various values of α at *Re* = 200 is presented in Figures 4 and 5. The phase diagrams of C_L and C_D are shown in Figure 6. For $0 \leq \alpha \leq 1.9$ a Von Karman street is seen in the wake behind the cylinder, it achieves a steady state for $\alpha > 1.90$. An increase in the rotation rate is accompanied by an increased upward deflection of the wake and a reduction in its lateral width. At α = 1.91 the vortex shedding ceases and the flow achieves a steady state. It is seen that the flow remains steady for $1.91 \leq \alpha \leq 4.35$. However, the flow is unstable again for $4.34 \leq \alpha \leq 4.75$. Beyond $\alpha > 4.75$ the flow is steady, but multiple solutions are observed.

But in case of nanofluid (Figure 5) the flow is unstable again for $4.34 \leq \alpha \leq 4.65$. Beyond $\alpha > 4.65$ the flow is steady.

Table 2 summarizes the basic integral parameters (Strouhal number *St*, lift coefficient C_L, and average Nusselt number), computed in the present study for tow values of the volume fraction of nanoparticles.

Table 2. Value of Strouhal number, mean lift coefficients and average Nusselt number with α and φ

α	*St*	C_L (0%)	*Nuav* (0%)	C_L (5%)	*Nuav* (5%)
0	0.183	0.00	17.55	0.00	19.75
0.5	0.184	-0.58	17.03	-1.74	19.42
1	0.184	-1.83	15.99	-3.24	18.47
1.5	0.187	-3.24	13.27	-4.62	15.03
1.9	0.177	-4.81	10.87	-6.99	13.01
2.5	----	-7.62	9.38	-7.62	11.24
3	----	-10.34	9.18	-10.37	11.12
3.5	----	-13.65	9.48	-13.74	11.55
4	----	-17.59	9.49	-17.73	11.51
4.35	0.039	-20.32	8.89	-20.33	10.69
4.5	0.027	-23.71	6.50	-23.73	6.62
4.7	0.021	-24.98	4.39	-24.99	4.94
5	----	-27.07	3.98	-27.08	4.26
5.5	----	-30.59	3.16	-30.61	3.59
6	----	-34.05	2.82	-34.05	3.21

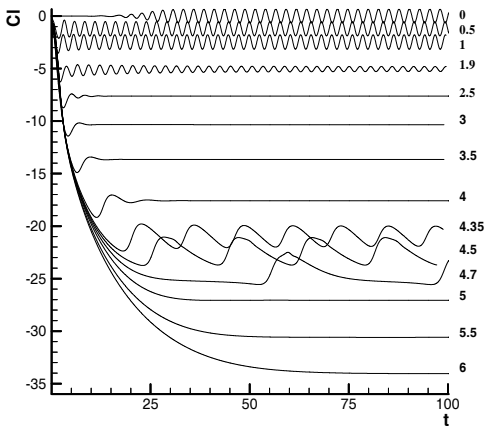

Fig. 4. Temporal evolution of lift coefficients for laminar flow past a rotating circular cylinder at Re = 200 (φ = 0 %)

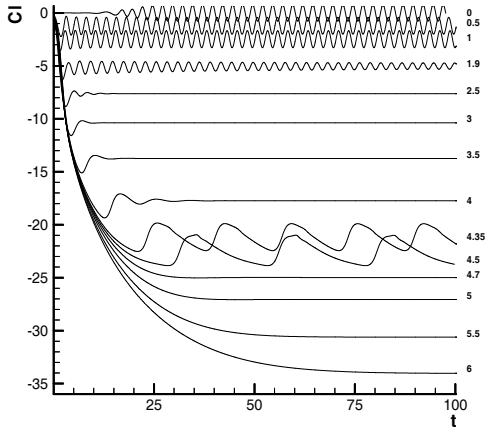

Fig. 5. Temporal evolution of lift coefficients for laminar flow past a rotating circular cylinder at Re = 200 (φ = 5 %)

It is evident from Fig. 6 that mean lift and drag coefficient have strong dependence on increasing or decreasing the values of cylinder rotation. Phase diagrams correspond to α show limit cycle, representing a complete periodicity in the flow, whereas for α = 0 a limit cycle is not discerned, showing double loop. It is clearly seen from Fig. 6 that the limit cycle collapses to a point at α = 2.

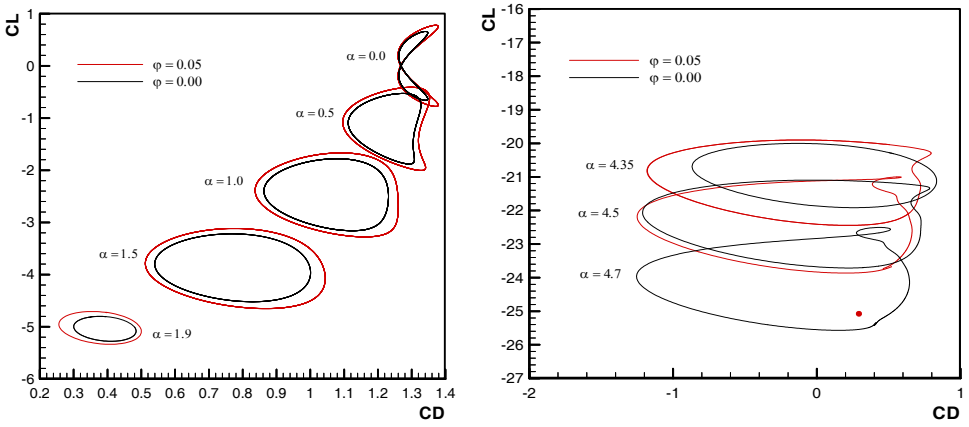

Fig. 6. Phase diagrams of C_L and C_D for various values of α for Re = 200

This is the situation of steady flow showing steady asymmetric recirculatory streamlines. In all other cases (α < 2 and 4.34 ≤ α ≤ 4.75) for bas fluid and (α < 2 and 4.34 ≤ α ≤ 4.65) for nanofluid a periodic vortex shedding with the formation of fluctuating stream lines and the transverse diffusion between shear layers originating from the top and bottom half of the cylinder shoulder is observed.

Fig. 7 shows the variation of Strouhal number for various rotation rate α. The Strouhal number ($St = fD/U$) of vortex shedding is practically constant and decreases as a function of α before the first bifurcation, and is very low in the second mode interval.

Fig. 8 shows the stagnation point for various rotation rates α. (red line present the first stagnation points and green line present the second stagnation points). It can be observed that for the case when α < 3, there are two apparent stagnation points. The first is attributed to the collision of the rotating boundary layer with the free-stream flow, while the second to the creation of a strong vortex downstream of the cylinder, which is formed due to the strong vorticity gradient between the free-stream layer and the rotating fluid, moving upstream and towards the top of the cylinder. As the dimensionless rotational rate increases, the upstream stagnation point moves

downstream until α = 4. The downstream vortex begins to contract and fully collapses at α = 4. For greater α the flow becomes swirling with a single stagnation point, which moves towards the outer region of the free-stream flow.

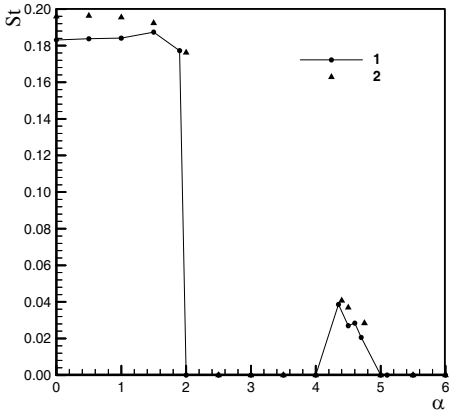

Fig. 7. Variation of Strouhal number with increasing rotation rate α.
1– present study, 2– results of [12].

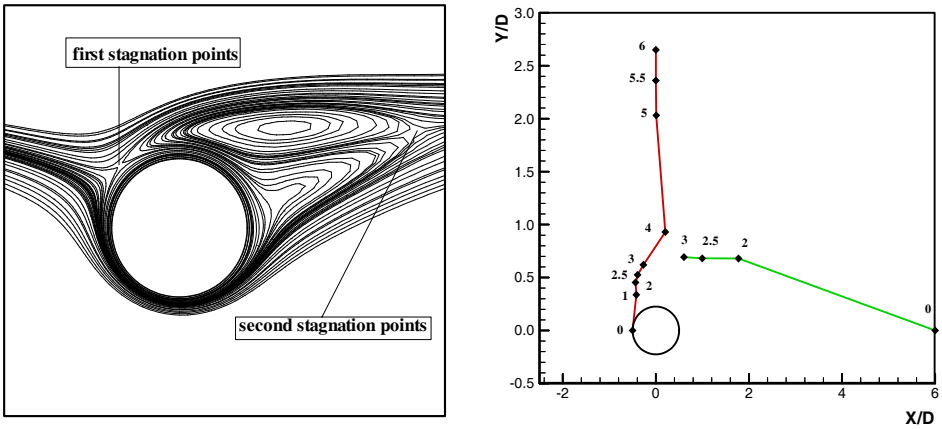

Fig. 8. Variation of stagnation point with increasing rotation rate α

Heat transfer

A comparison between local Nusselt numbers along the cylinder for values of rotation rates α was show in Fig. 9. It can be seen that Nusselt number decrease with increase in values of rotation rates α.

Variation of average Nusselt number for different values of rotation rates α is shown in Figure 10. For various rotation rates α and solid fraction, to understand the suppression of heat transfer. It can be seen from this Figure that the suppression increases with increasing α, having a value of 65.18 % for Re = 200 at α = 6. Thus, cylinder rotation can be used not only for controlling flow but also as an efficient heat transfer suppression technique.

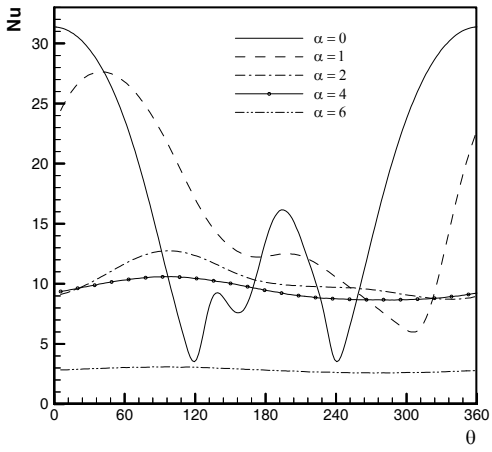

Fig 9. Variation of local Nusselt number on cylinder surface with various rotation rate α

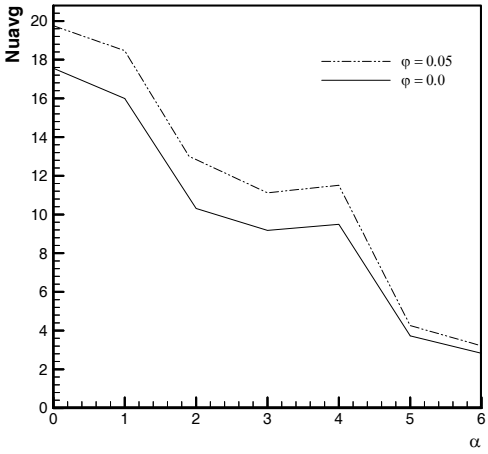

Fig. 10. Variation of average Nusselt number on the wall of cylinder versus various rotation rate α

The contours of positive and negative vorticity are presented in Figure 11. The positive vorticity is generated mostly in the lower half of the surface of the cylinder while the negative vorticity is generated mostly in the upper half.

Fig. 11 illustrated the streamlines, vorticity and isotherm contours around the cylinder, for Reynolds numbers of 200. Here, the contours of base fluid and nanofluid are shown for comparison. Where red lines are used for nanofluid and black solid lines are used for base fluid. This figure indicated that the magnitude of the maximum negative velocity in recirculation zone is increased by any increment in solid concentration and Reynolds number. In the base fluid the strength of the vorticity is increased comparison with the nanofluid.

For the temperature distribution contours, it can be observed, in increasing the value of the rotation rate, the maximum density of isotherms shifts from front surface towards the bottom surface of the rotating cylinder. It is also observed that isotherms shifts in the direction of rotation of the cylinder and becomes almost vertical at higher values of the rotation rate. The temperature distributions presented by way of isotherms can be used to interpret the variation in the local and average heat transfer characteristics with rotation rate.

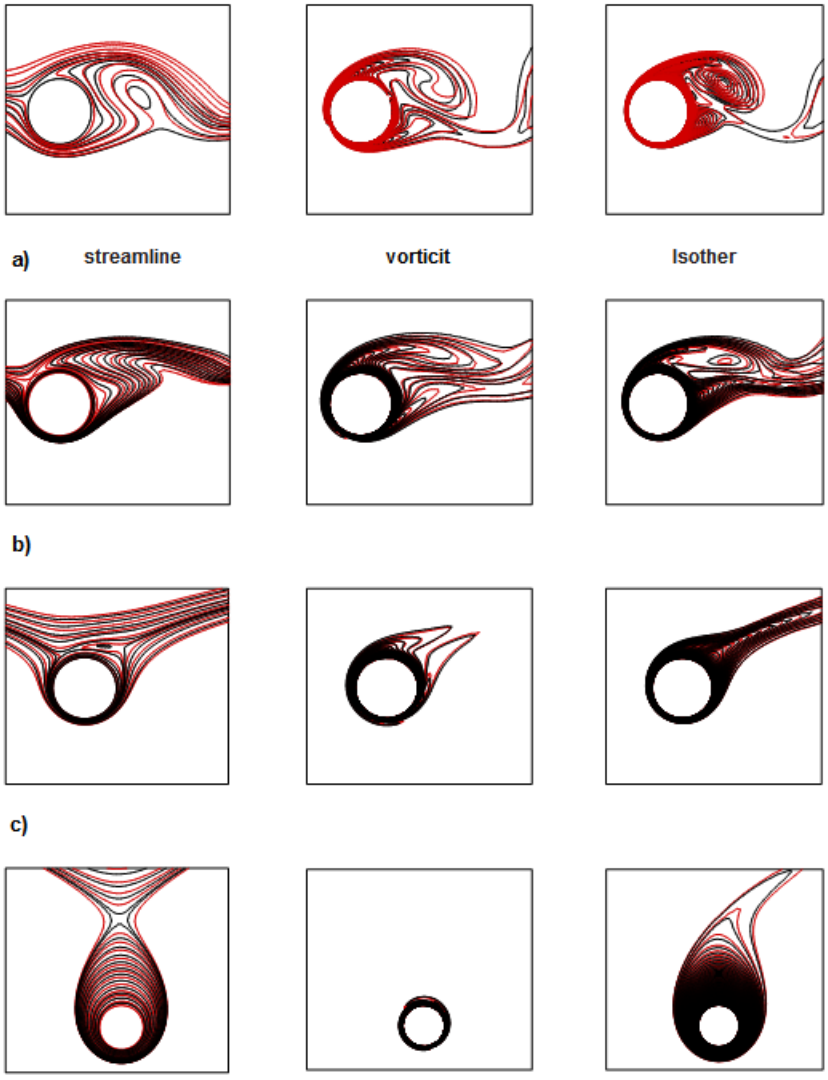

Figure 11. The streamlines, vorticity and isotherm contours around the cylinder, at: a) $\alpha = 1$, b) $\alpha = 1.9$, c) $\alpha = 3$, d) $\alpha = 6$ (nanofluid (plotted by red solid lines) and base fluid (plotted by black solid lines))

For the temperature distribution contours, it can be concluded that the temperature contours are steeper in the near-wake region with increasing Reynolds number. This signifies that higher Reynolds number sets a higher temperature gradient, leading to an enhanced heat transfer from the cylinder.

Thus, due to higher temperature gradient, temperature contours are much denser near the front surface of the cylinder. It can also be seen that the nanofluid show higher heat transfer rate from the cylinder than base fluid.

CONCLUSION

Unsteady laminar flow behind a rotating circular cylinder, has been subjected to numerous experimental and computational studies. In this work, the flow over and heat transfer from a circular cylinder immersed in Newtonian fluids has been studied numerically. The flow transition map found by earlier researchers is shown here for a rotation rates. The von Karman vortex street disappears when the rotation rate of the cylinder increases to $\alpha = 2$. This is due to the weakening of the shear layers associated with flow in the wake. A second shedding mode is observed in the range of $4.34 \leq \alpha \leq 4.75$, characterized by the shedding of one counterclockwise vortex from the upper part of the cylinder. The core of the instability is identified in the advection of the positive vorticity of the base flow from the low–rear part of the cylinder to the stagnation point where it accumulates and is then shed. The average Nusselt number is found to decrease with increasing rotation rate. Heat transfer suppression due to rotation increases with increasing rotation rate.

In this article, the point of investigation was to evaluate the effect of nano-particle on convective heat transfer and flow characteristics. The significant observations made on the forced convection around a circular cylinder are summarized as follows:

1) The vorticity, pressure coefficient, recirculation length are increased by the addition of nanoparticles into base fluid.

2) The Local Nusselt number, average Nusselt number and heat transfer coefficient of a nanofluid is augmented by increasing the volume fraction of nanoparticles.

3) Temperature gradient at the cylinder surface along normal direction drops with increase in nano particle concentration. However there is an increase in the thermal conductivity of nanofluid, thus leading to increase in Nusselt number.

REFERENCES

1. D.B. Ingham, T.Tang, *J. Comput. Phys*., **1990**, *87*, 91–107.
2. Y.M. Chen, Y.R. Ou, A. J. Pearlstein, *J. Fluid Mech*., **1993**, *253*, 449–484.
3. S. Kang, *Phys. Fluids*, **2006**, *18*, 047106-1–047106-12.
4. M. Zdravkovich, Flow Around Circular Cylinders, vol. 1, *Oxford Science Publication*, **1997**
5. M.B. Glauert, *Proceedings Royal Society London A*, **1957**, *242*, 108–115.
6. S. Kang and H. Choi, *Physics of Fluids*, **1999**, *11*, 3312-3320.
7. S. Mittal and B. Kumar, *Journal of Fluid Mechanics*, **2003**, *476,* 303-334.
8. H. Nemati, M. Farhady, K. Sedighi, and E. Fattahi, *Thermal Sci*., **2010**, *3*, No. 3, 859–878.
9. M.R.H. Nobari and J. Ghazanfarian, *Thermal Sci*., **2010**, *49*, No. 10, 2026–2036.
10. S.B. Paramane, Sharma, A., *Int. J. Heat and Mass Transf*., **2009**, *52*, 3205-3216.
11. S.B. Paramane, A. Sharma, *Int. J. Heat Mass Transf*., **2010**, *53*, 4672-4683.
12. F.H. Barnes, *J. Phys. D: Appl. Phys*. **2000**, *33*, 141–144.
13. D. Stojkovic, P. Schon, M. Breuer and F. Durst, *Phys. Fluids*, **2002**, *14*, 3160–3178.
14. E. Abu-Nada, K. Ziyad, M. Saleh, Y. Ali, *J. Heat Transfer*, **2008**, *130*, 084505-1-4.
15. S. Sarkar, S. Ganguly, G. Biswas, *Int. J. Heat Mass Transfer* **2012**, *55*, 4783–99.
16. M.S. Valipour, A. Z. Ghadi, *Int. Commun. Heat Mass Transfer* **2011**, *38*: 1296–304.
17. S. Sarkar, S. Ganguly, A. Dalal, *ASME-Heat Transfer*, **2014**, *136*: 062501-1-10.
18. S. Sarkar, S. Ganguly, A. Dalal, *ASME-J. Heat Transfe*r **2012**, *134*: 122501-1-8.
19. R. El Akoury, M. Braza, R. Perrin, Harran, G. and Horau, Y., *J. Fluid Mech*., **2008**, *607*, 1-11.
20. J. Koo and C. Kleinstreuer, *Int Commun Heat Mass Transf*., **2005**, *32*, 1111–1119.
21. B.C. Pak and Cho Y.I., *Exp. Heat Transf*., **1998**, *11*, 151 - 170.
22. J. Buongiorno, *ASME J. Heat Transfer*, **2006**, *128*, 240-250.
23. M. Corcione, *Int. J. Therm. Sci*., **2010**, 49 1536 - 1546.